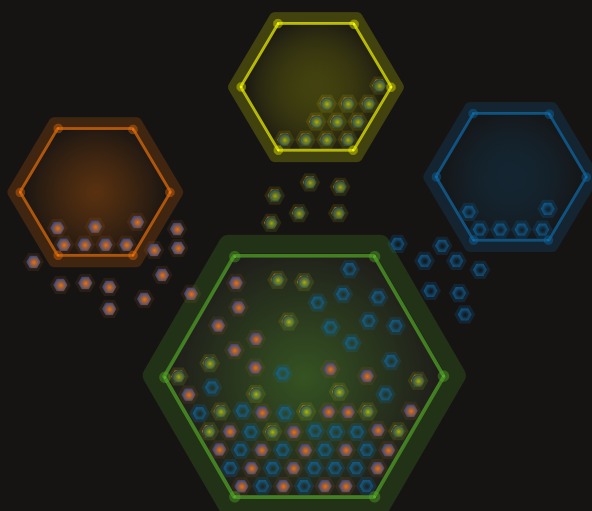


CENTRE FOR ENERGY RESEARCH
HUNGARIAN ACADEMY OF SCIENCES



PROGRESS REPORT ON RESEARCH ACTIVITIES

2016

HUNGARIAN ACADEMY OF SCIENCES
CENTRE FOR ENERGY RESEARCH

29-33 KONKOLY-THEGE MIKLÓS ÚT

1121 BUDAPEST, HUNGARY

PROGRESS REPORT
ON RESEARCH ACTIVITIES
IN 2016

DEAR READER,

Welcome to the 2016 yearbook published by the MTA Centre for Energy Research (MTA EK), summarizing the scientific results of its three institutions and highlights in 2016. This booklet provides a summary of the research personals and equipment of departments and research groups working in the Centre.

The year 2016 was very successful in terms of awarded grants and new opportunities. Research in nuclear safety is supported by the National Nuclear Research Project within the frame of the Hungarian Sustainable Nuclear Technology Platform is continued. A new research project was awarded by the National Research, Development and Research Office (NKFIH) in the field of safety of nuclear fuel cladding. Hungary became a member of the European Space Agency (ESA) and MTA EK was awarded by ESA to develop Cosmic Radiation and Magnetic Field (RadMag) Instruments for the RADCUBE Mission.

One of the “Lendület” (Momentum) research groups of MTA EK MFA was awarded with outstanding qualification. The other excellent Momentum group, the NanoFab2D research group successfully applied for an ERC starting grant.

The Budapest Neutron Centre (BNC) become a member of the Central European Research Infrastructure Consortium (CERIC ERIC). The BNC researchers take part in various EU funded projects such as IPERION, E-RIHS, BrightnESS and CHANDA. The Centre is involved in the preparation of the European Spallation Source project aimed at constructing the new neutron source facility in Sweden. Member countries are invited to contribute on an *in-kind* basis, and the expenditures of the participating Institutions in Hungary are compensated from the membership fee of the country.

In the year 2016, MTA EK signed a formal Collaboration Agreement with the Joint Research Centre of the European Commission in the field of nuclear safety and security. The International Atomic Energy Agency designated MTA EK as the first Collaboration Centre in Nuclear Forensics.

Ákos Horváth
Director General
horvath.akos@energia.mta.hu

CONTENTS

Dear Reader,.....	2
Contents	3
Mission Statement of MTA Centre for Energy Research	7
Scientific Advisory Board of the MTA Centre for Energy Research	7
Organization Structure of the MTA Centre for Energy Research	8
Quality Management	9
Budapest Research Reactor	10
Environmental Protection Service	12
I. EU SUPPORTED RESEARCH ACTIVITIES.....	13
SINE2020 Project - Industry Consultancy.....	14
Budapest Neutron Centre NMI3 - A Successful European Collaboration for Science.....	15
Benchmarking of the Reactor Physics Computer Codes Used for ALLEGRO Calculations in European Projects (ESNII+ and VINCO)	16
BrightnESS- WP6: Collaboration, Communication and Dissemination.....	17
Participation in the EU ESNII Plus Project.....	18
Participation in the EU SAFEST Project	19
Participation in CONCERT-European Joint Programme for the Integration of Radiation Protection Research....	20
Update on VV Bolometer Design and Analysis	21
AGE-60 EU Project.....	22
Elaboration of Database and MPH Volumes within the WPMAT EDDI Project.....	23
Transnational Access within the EC H2020 IPERION CH Project	24
Goal Oriented Training Programme of European Fusion Development Agreement - RADEFF GOT	25
II. RESEARCH AND DEVELOPMENT RELATED TO NUCLEAR POWER PLANTS	26
Hungarian Nuclear Research Program	27
The ALLEGRO Project	28
Selection of Fuel for the ALLEGRO Reactor	29
Development and Verification of the SP3 Method Applied in the KIKO3DMG Code.....	30
Modelling and Investigations of Multi-Physics Phenomena by the KARATE-1200 and the FRAPTRAN-TRABCO Coupled Code Systems.....	31
Super-VVER Reactor Research	32
Neutron Transport Calculations of Fuel Assemblies to be Applied in the New Paks Units	33
Modelling the Transport of Radionuclides in Surface Water	34
Calculation of Unprotected Transients in Fast Spectrum GEN-IV Reactors	35
Implementation of Pin Power Reconstruction into the KIKO3D Code.....	36
Validation of the KARATE Code System Against the Latest Operational Data and Startup Measurements	37
Estimation of the Uncertainties of the Power and the Burnup at Nodal and Pin-Wise Levels by the Statistical Version of KARATE Code System	38
Using HZP States of Paks NPP for the Validation of Burnup Credit Calculations, Consideration of the Uncertainty of Isotopic Composition.....	39
Application of Discontinuity Factors and Group Constants Generated by SERPENT in the KIKO3DMG Code ..	40
Investigation of Optical, Acoustic and Thermoelectric Properties of Zirconium Claddings	41
Advanced Models for Future Structural Integrity Calculations	42
Irradiation of P91 Material	44
Introduction of New Fuel Types to Thermal Power Plants: MOX and REMIX Fuel	45
A Review and Simulations of Experiments Regarding New Fuel Types	46
CODEX-LOCA Experiments.....	47
Simulation of Leaking Fuel Rods With the RING Code.....	48
Axial Distribution of Radioactive Isotopes in a Leaking Fuel Rod.....	49
Participation in the OECD SCIP III Project	50
Preliminary Mandrel Tests with Zr Cladding Samples	51
High-Temperature Corrosion Model of E110G - a Code Development for TRANSURANUS.....	52
New Possibilities for Modelling of the Up- and Down- Load in the FUROM 2.1.1 Version and Validation.....	53
On-line Measurement of the Burst of Cladding Tubes in a High Temperature Setup	55
E110G Material Neutron Irradiation, Post Irradiated and Heat Treated E110 Material Mechanical Properties Examination.....	56

Re-Evaluation of Surveillance Specimens of Paks NPP	58
Adaptation of Version 2.0 of the Code FRAPTRAN to VVER Fuel.....	59
The Effect of Hydrogen Content on the Embrittlement of E110 and E110G Alloys.....	60
Development of a Multifunctional Compact Simulator Platform for Nuclear Reactor Simulations	61
New Communication Interfaces of the Control Rod and Reactor Power Controller Systems	62
Plant Computer Reconstruction	63
Renewing the RMR and ÁNER Systems at the Paks NPP.....	64
Reactor Noise Diagnostics Measurements at Paks NPP	65
Development of Interaction Techniques for a Virtual Control Room	66
In-Situ Investigation of VVER Steam Generator Heat Transfer Tubes by XRF Technique	67
Measurement of Chloride Contamination on Stainless Steel Surface	68
Radiological Consequences of Beyond Design-Basis Accidents	69
Sensitivity Analysis of Contamination Monitors	70
Determination of Operation Scenario of Spent Nuclear Fuels by Gamma-Spectrometry	71
Safeguards Measurements at Paks NPP	72
Analysis of Corrosion Particles originated from the primary and secondary cooling system of Paks NPP	73
III. NUCLEAR SECURITY AND DOSIMETRY	74
Developing an Improved Production Technology for the Ceramic Block of the PorTL Dosimeter System.....	75
Personal Neutron and Beta Dosimetry	76
Research&Development Activities in Space Dosimetry and Space Weather.....	77
Detection of Cosmic Radiation in Near-Earth Orbit by Active and Passive Dosimeter Systems.....	79
Effective Container Inspection at Border Control Points	80
Development of National Nuclear Forensics Library	81
Specialized Training Courses for Nuclear Forensic Purposes.....	82
Regional Training Course on Adoption of QA/QC Methods and Procedures for Inter-Comparison of Radiation Dosimetry in Radiation Facilities for Process Control.....	83
Spectrum Evaluation Algorithm for Scintillation Detectors.....	84
Organization of a Virtual Table Top Exercise (TTX) for Practice of Response to Nuclear Security Events.....	85
Basic Research on the Biophysical Effects of Low Doses of Ionising Radiation	86
Delayed Neutron Counting to Determine Nanogram Quantities of ²³⁵ U	87
IV. ENERGY AND ENVIRONMENTAL STUDIES	88
The Evaluation of the Meteorological Database of the Paks NPP	89
Suppressing Coke Formation During Dry Reforming on Sodium or Indium Promoted Nickel Catalysts	90
Characterization of Bimetallic Catalysts by ¹⁹⁷ Au Mössbauer Spectroscopy	92
Au-Containing Bimetallic Catalysts in Highly Selective Aerobic Oxidation Reactions.....	93
New Systems to Promote Water Oxidation	94
Catalytic Properties of 2D MoS ₂ Catalysts During Electrolysis of Water	95
Towards Supported FePt Ferromagnetic Nanoparticles	96
Radioactive Waste Management: New Vitrification Process and Investigation of Radionuclide Uptake	97
Vitrification - Development of Glass Matrices for High-Level Radioactive Wastes.....	98
Atomic Structure of High-Entropy Alloys	99
Preparation, Structural Studies and Optimization of Oxide Glasses for HLW Storage Applications.....	100
Possibility of Nuclear Cogeneration Development in the Region of Paks	101
Microscale X-Ray Spectrometry Investigation of Radionuclide Uptake on Argillaceous Rocks.....	102
High-Energy Ionizing Radiation Induced Decomposition of Pharmaceutical Compounds.....	103
Removal of Antibiotics and Pesticides from Wastewater Using High-energy Ionizing Radiation.....	104
Hydroxyl Radical Induced Transformation of Phenylurea Herbicides: A Theoretical Study	106
Separation of Plutonium and Lanthanides on DGA Resin by Extraction Chromatography from Human Urine - Development of a Rapid Method	107
Mathematical Modelling of Low Dose Hypersensitivity	108
Surveying Methods for Development of Renewable Energy Potential	109
V. NUCLEAR ANALYSIS	110
Gamma-Ray Strength Functions	111
Background Radiation Study for Multi-Grid Neutron Detector.....	112
Composition Measurements for Activation Study of Shielding Materials to be Applied at the European Spallation Source	113
Chemical Applications of Nuclear Analytical Methods.....	114

Applications of Prompt Gamma Activation Analysis and Other Analytical Methods in Heritage Science (Archaeometry) - Highlights.....	115
Development of Nuclear Analytical Techniques, Nuclear Data Measurements, and Related Dissemination Activities	117
Provenance Study of Lithic Raw Materials of Stone Tools Found in the Carpathian Basin – Closing Year of the OTKA K100385 Project.....	118
Separation of Lanthanides and Americium in Liquid Nuclear Waste.....	119
Non-Destructive Analysis of Metallic Samples Using PGAA and Complementary Methods.....	120
Selected Applications of Mössbauer Spectroscopy.....	121
Radiography and tomography at BRR	122
Synthesis of Carboxymethylcellulose/ Acrylic Acid Hydrogels with Superabsorbent Properties by Radiation-Initiated Crosslinking.....	123
Advanced Moderators for Intense Cold Neutron Beams in Materials Research.....	124
VI. RESEARCH AND DEVELOPMENT IN INSTITUTE OF TECHNICAL PHYSICS AND MATERIAL SCIENCES	125
Taming Defection – How We All Might Be Better Off with Certain Level of Tolerance.....	126
Flagellin Based Biomimetic Coatings: From Cell-Repellent Surfaces to Highly Adhesive Coatings	128
Moiré Superlattices in Strained Graphene-Gold Hybrid Nanostructures	130
Magnetic Phase-Transition Graphene Transistor with Tunable Spin Polarization.....	132
Oxidation of Transition Metal Dichalcogenide Monolayers	134
Determination of the STM Tip-Graphene Repulsive Forces by Comparative STM and AFM Measurements on Suspended Graphene	136
Electromagnetic and Thermal Properties of Three-Dimensional Printed Multilayered Nano-Carbon/ Poly(Lactic) Acid Structures	138
Pretreated Butterfly Wings for Tuning of Selective Vapor Sensing	140
Simulation of Magnetic Flux Distribution During Measurement of Local Thinning of Ferromagnetic Plates	142
Spectroellipsometric Detection of Silicon Substrate Damage caused by Radiofrequency Sputtering of Niobium Oxide	144
Makyoh Topography	145
Grating Coupled Optical Waveguide Interferometry Combined with In Situ Spectroscopic Ellipsometry	146
Performance Analysis of Plasmon-Enhanced Ellipsometry for Protein Adsorption Measurements	147
Optical Characterization of Columnar Porous Si Thin Films and Si Nanowires Exhibiting Large Structural Anisotropies	148
Optical Properties of Zr and ZrO ₂	149
Development of Optical Metrology Tool for In-Line Qualification of Thin Films on Large Area	150
Aggregation Kinetics and Cluster Structure of Amino-PEG Covered Gold Nanoparticles.....	151
Self-Assembly of Like-Charged Nanoparticles Into Voronoi Diagrams.....	152
Assembling Patchy Nanorods with Spheres: Limitations Imposed by Colloidal Interactions.....	153
Identification of Dewetting Stages and Preparation of Single Chain Nanoparticle Rings by Colloidal Lithography	155
Force Feedback Control System for Robin Heart Surgical Robot	157
Development of Gas Densing Microstructures	159
Effective Flow Control in Autonomous Polymer Microfluidic Systems Based on Surface Modification and Bioinspired Micropatterning.....	161
Particle Manipulation in Microfluidic Systems.....	163
Precisely Tailored Solid State Nanopores for Molecule Recognition.....	165
Silicon Microelectrodes for Infrared Neural Stimulation.....	166
Simultaneous in Vivo Recording of Local Brain Temperature and Electrophysiological Signals with a Novel Neural Probe	167
A Multimodal, SU-8 - Platinum - Polyimide Microelectrode Array for Chronic In Vivo Neurophysiology	168
Neurobiochemical Changes in the Vicinity of a Nanostructured Neural Implant.....	169
Piezoelectric Based Nanowire Sensors	170
New Approaches in the Development of Hypoallergenic Implant Material in Orthopaedics: Steps to Personalized Medicine.....	171
Mechanical Characterization and Corrosion of Protective TiC/ Amorphous C Nanocomposite Coating as Surface Thin Film.....	172
Development and Characterization of Multi-Element Doped Hydroxyapatite Coatings on Metallic Implant Materials	173

Graphene-Ceramic Composites for Tribological Application in Aqueous Environments.....	174
Improving the Tribological Performance of Ceramic Composites by a Continuous Few-Layer Graphene Tribo-Film.....	175
Developing an Improved Production Technology for the Ceramic Block of the PorTL Dosimeter System.....	176
Graphitic Films of Group III Nitrides and Group II Oxides: Platform for Fundamental Studies and Applications	177
TEM Study of the As-Deposited and Annealed Ga ₂ O ₃ Films Grown by Vapor Phase Epitaxy	178
Highly Safe GaN Metal-Oxide-Semiconductor Transistor Switch (SAFEMOST)	179
Inclusions in Si Whiskers Obtained in Metal (Ni) Induced Lateral Crystallization of Amorphous Si Thin Films.....	180
Comparative Study of Direct Current Magnetron Sputtering (DCMS) and High Power Impulse Magnetron Sputtering (HiPIMS) Processes for CN _x Thin Film Growth with Different Inert Gases.....	181
FePt Nanoparticles; Colloid Chemistry Towards Catalysts and Magnetic Recording Media.....	182
Versatile Nanopatterning Technique Using RF Plasma Etching Through Langmuir-Blodgett Films.....	183
Characterization of Defect Structure, Mechanical Properties and Stability of Electrodeposited Nanocrystalline Ni Films	184
Effect of High Efficient Attrition Milling on 316L Austenitic Steel Reinforced by Ceramic Nanoparticles.....	185
New Type Functional Alloy Films	186
Processing of Faint, Diffuse Diffraction Rings from Amorphous Materials	187
Hydrogel Film Fabrication for Biosensing	188
ZnO Nanostructure Templates as a Cost-Efficient Mass-Productible Route for the Development of Cellular Networks	189
Self-Assembled, Nanostructured Coatings for Water Oxidation by Alternating Deposition of Cu-Branched Peptide Electrocatalysts and Polyelectrolytes	190
Self-Assembly and Structure of Flagellin-Polyelectrolyte Composite Layers: Polyelectrolyte Induced Flagellar Filament Formation During the Alternating Deposition Process	191
Cell Adhesion Measurements with a Label-Free Optical Biosensor	192
Label-Free Optical Biosensor for On-Line Monitoring the Integrated Response of Human B Cells upon the Engagement of Stimulatory and Inhibitory Immune Receptors.....	193
Anisotropic Invasion and its Consequences	194
mtDNA Analysis of 174 Eurasian Populations using a New Iterative Rank-Correlation Method	195
ABBREVIATIONS	196

MISSION STATEMENT OF MTA CENTRE FOR ENERGY RESEARCH

- Research and development in the field of nuclear science and technology for facilitating the adoption and the safe use of nuclear technology in Hungary.
- To participate in international research effort aiming at the establishing a new generation of nuclear power plants and closing the fuel cycle.
- Maintaining and improving competence in nuclear science and technology, especially in the field of nuclear safety, security, health physics, nuclear and isotope chemistry.
- To guarantee the safe operation of Budapest Research Reactor (BRR), and to ensure the accessibility of the research facilities around the reactor.
- Research activities to improve nuclear analytical and imaging methods and their applications for energy and materials science.
- Perform studies in the field of environmental physics related to energy generation, renewable energies, energy storage and their impact on public health, and on environmental safety.
- Research and development in the field of low carbon energy technologies and of energy saving in industrial technologies.
- Interdisciplinary research on complex functional materials and nanometer-scale structures, exploration of physical, chemical, and biological principles, their exploitation in integrated micro- and nanosystems, and in the development of characterization techniques.
- Dissemination of the results in international programs, education and industrial research.

SCIENTIFIC ADVISORY BOARD OF THE MTA CENTRE FOR ENERGY RESEARCH

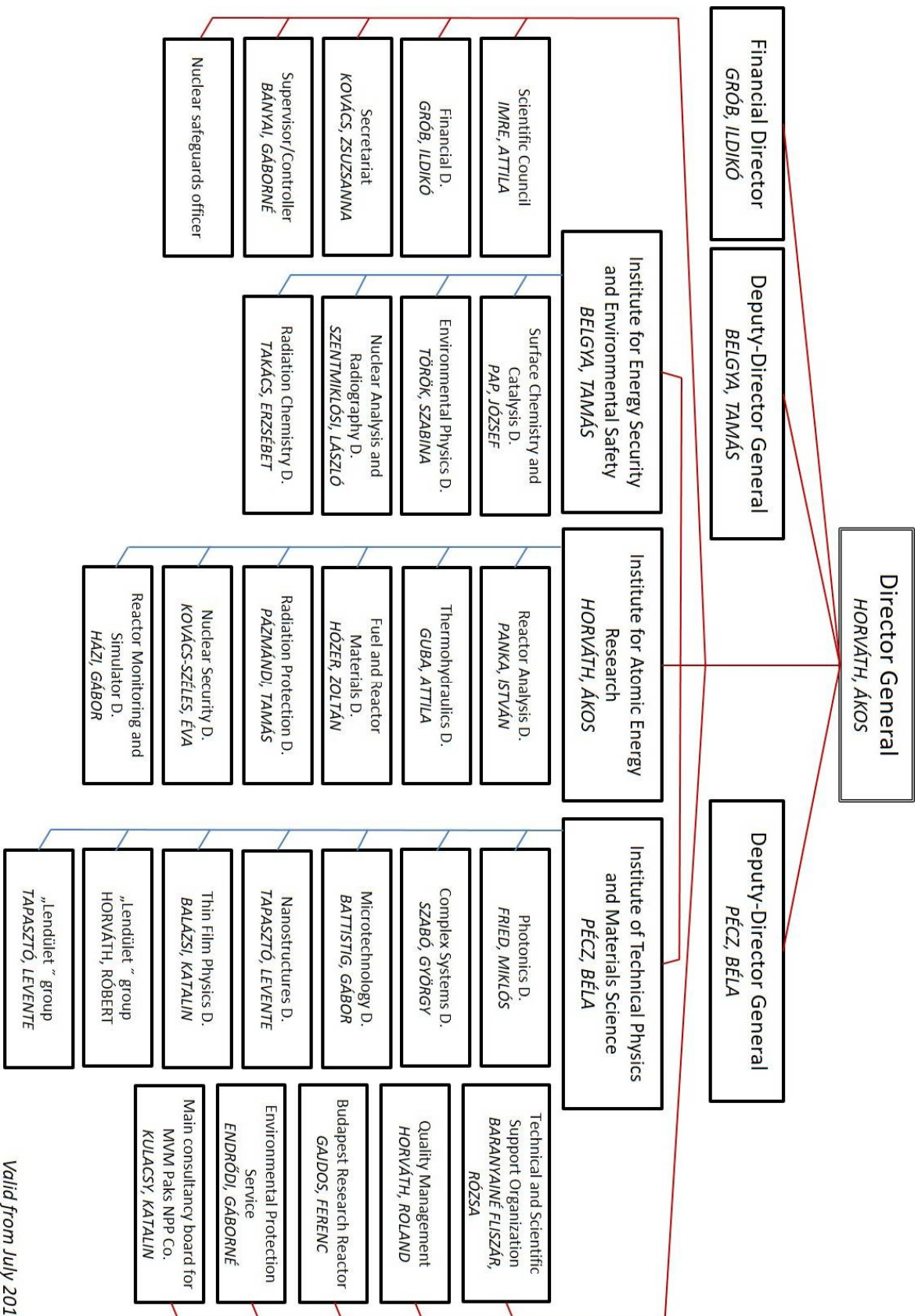
The Board consists of five Hungarian and two foreign leading scientists. The last meeting of the board took place in Budapest, April 14, 2015. The management of EK presents usually an overview of the R & D activities in the previous year as well as figures about financial data and analyses of human resources. The R&D plans for the coming year and for the near future are also presented.

The Board members usually comment the presentations and ask questions. The Board suggested in 2015 to inform the president of the MTA on the problem that the insufficient number of qualified people might cause difficulties in the nuclear field in the future, especially taking into account the need due to government decision on new NPP units. The Board members commented that the activities of the recently joined Institute for Technical Physics and Materials Science should be harmonized with those of the two other institutes within the Centre. The Board suggested also preparing a more detailed vision of the future activities and presenting it at the next meeting.

Members of the Board:

- Prof. Dr. László Keviczky (Chair), MTA Institute for Computer Techniques and Automation
- Dr. Hervé Bernard, Deputy Chairman, Centre French Alternative Energies and Atomic Energy Commission (CEA)
- Dr. Maximilian Fleischer, Head of Department of Corporate Technology, Siemens AG
- Prof. Dr. Ádám Kiss, Eötvös Loránd University
- Dr. Zoltán Homonnay, Head of Laboratory of Nuclear Chemistry, Eötvös Loránd University
- Mr. István Hamvas, Director General, Paks Nuclear Power Plant
- Dr. József Rónaky, Scientific Advisor, Hungarian Atomic Energy Authority

ORGANIZATION STRUCTURE OF THE MTA CENTRE FOR ENERGY RESEARCH



Valid from July 2016

QUALITY MANAGEMENT

In order to achieve the highest quality of research, development, design, condition monitoring and valuation, engineering, contracting and managing in design, production, implementation and inspection, the Research Centre's quality management system has been continuously upgraded by the recommendations of ISO 9001 standard since 1994. Reviewing our QM system by integral audits and management reviews, evaluating improvement opportunities, maintaining project documentation, infrastructure, supporting communication, ensuring the competence of workers the management improves the Centre's QM system. For the new organization structure our Quality Policy has been renewed. Many new employees induced a need to upgrade our QM tuition practice. We organised the work and fire safety educations. Our QM system has been certified by Hungarian Standards Institution, IQNet, and MVM Paks NPP.



Certifications by Hungarian Standards Institution, IQNet, and MVM Paks NPP



Accreditation Certificate for Environmental Protection Service, and Nuclear Security Department

BUDAPEST RESEARCH REACTOR

One of the most important strategic large scale research facilities in Hungary is the Budapest Research Reactor (BRR). It serves the needs of an extensive and diverse scientific community by supporting R&D opportunities, helping innovation and providing a strong foundation for training and education.



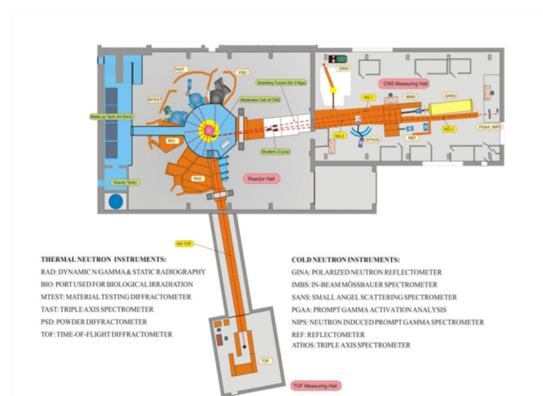
Bird's eye view of the Budapest Research Reactor

The BRR is a VVR-type reactor that uses light water as moderator and cooling fluid. The power of the reactor is 10 MW provided from low enrichment uranium fuel, and its main purposes – as established during the feasibility/functionality study – are: radioisotope production, production of thermal and cold neutron beams for research and applications in all areas, development of new functional materials and neutron activation analysis.

The core is designed to have about 10-11 reactor cycles per year, each having a cycle length of 10 days. We are committed to long-term safety and responsible operations, taking care of the wastes from the spent fuel coming from the reactor. Besides the temporary spent fuel storage pool, we also operate a long term spent fuel storage building for the physical and environmental separation between the reactor and the spent fuel storage.

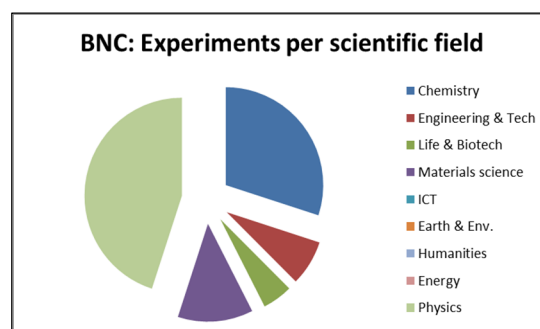


Top view of the research reactor



Layout of the BRR's facilities

The reactor is the centre of three kind of activities: e.g. research activities utilizing neutron beams, production of radioisotopes for industrial and research purposes and national and international training sessions. We are proud of our innovative flagship research topics, which are carried out with a network of neutron beam stations, including beam-lines of thermal neutrons, experiments on powder diffractometry, residual stress diffractometry, radiography, biological irradiations and beam-lines of cold neutrons for experiments on small angle neutron scattering, reflectometry, prompt gamma activation analysis and others. In accordance with recent worldwide trends, we are open to establishing new industrial relations, and supporting innovation. We aim to increase our competence on special topics, to implement new technologies and develop new materials, to promote and exploit our R&D capacity at the national and regional/international level. During the past years the BRR hosted several international schools on various technical and research topics, special trainings in the field of reactor physics, reactor operation, nuclear measurement techniques, and safety and environmental issues.



BRR is used by members of many scientific, medical, environmental and industrial communities, as well as several Hungarian Universities. Neutron beams are uniquely suited to study the structure and dynamics of materials at the atomic level. The Budapest Neutron Centre (BNC) coordinates the scientific utilization of the research reactor. Some of main research topics currently are:

- neutron scattering, used to examine samples under different conditions such as variations in vacuum or pressure, high and low temperature, and magnetic field, modelling real-world conditions.
- using neutron activation analysis, both prompt and delayed, it is possible to measure the concentration of elements in ppm and ppb levels of even small samples. Atoms in a sample are made radioactive by exposure to neutrons from the reactor. The characteristic gamma radiation each element emits can then be detected.
- neutron activation is also used to produce different radioisotopes, widely used in industry and medicine, by bombarding particular elements with neutrons so that the target nucleus has a neutron added. For example, Y-90 microspheres to treat liver cancer are produced by bombarding Y-89 with neutrons.
- testing of materials for reactors; materials are subjected to intense neutron irradiation to study induced changes. For instance, some steels become brittle, and alloys exp. high-entropy alloys, which resist embrittlement, must be used in nuclear reactors.
- production of radioisotopes for different applications.
- applied research using neutron beams (neutron radiography, exp. cooling system of refrigerator or engine system of a car, tomography of different materials and items).

The BNC provides researchers with 15 neutron instruments; 13 instruments are installed directly on the horizontal beam ports of the reactor or to the thermal and cold neutron guides, while the other 2 are placed at the vertical irradiation channels. The instruments are supported by a variety of sample environments and data analysis and visualization capabilities.

The BNC provides access to the international neutron user community through a peer-review arrangement. Local scientists assist researchers and industrial users to find the appropriate neutron techniques that meet their research needs. The various neutron scattering instruments in BNC cater to a large number of users from Europe and has grown in strength and stature over the years.

BNC is a member of the European network of neutron centres, and a partner in the EU Framework Programme projects (NMI3-II, CHANDA, IPERION, SINE2020, ESS-BrighnESS, CERIC).

BNC is strongly committed to the training of future professionals. In cooperation with Hungarian universities (Budapest University of Technology and Economics, Eötvös Loránd University, Pannon University), BNC accommodates students for laboratory practice for studying nuclear-based techniques. A specialized course was developed for geology students at the Eötvös Loránd University to introduce nuclear analytical techniques into their education. To train young scientists in neutron physics and to attract new users, BNC organizes the Central European Training School on Neutron Scattering on a regular basis. The school provides insight into neutron scattering, element analysis and imaging techniques and their applications to study the structure and dynamics of condensed matter.

The Budapest Research Reactor is open to the public. Members of the local communities and high school and university students are invited to visit regularly and learn more about the amazing nuclear science possibilities available at BRR.



Researchers working at the Budapest Research Reactor

ENVIRONMENTAL PROTECTION SERVICE

In the past year the Environmental Protection Service (EPS) operated in compliance with the pertinent laws and orders. EPS is a functional unit of MTA Centre for Energy Research (MTA EK). In accordance with our main tasks, EPS took and measured environmental samples, which were collected in the whole territory of the KFKI Campus.

In the year of 2015 we made several improvements in our laboratory equipment. We got one of our semiconductor detectors repaired which is used for measuring samples from environmental monitoring. We bought some radioactive sources and performed calibration procedures with these sources in order to make our detectors more sensitive to environmental control measurements.

EPS took part in the education of two groups of trainees of an international education course supported by the International Atomic Energy Agency (IAEA). They studied the operation of nuclear research centres and research reactors including the tasks of the environmental service.

Furthermore, we hosted two MSc students from Eötvös Loránd University of Sciences and Budapest University of Technology and Economics for their diploma thesis work.

Measurements of different type and sensitivity are performed by EPS for the analysis of radioactive materials including gamma-ray spectroscopy, selective alpha and beta counting and liquid scintillation spectrometry. We improved the measurement features of our in-vivo whole body counter; direct thyroid measurements are also available with the detector installed in the mobile laboratory.



Gáborné, Endródi
Head of Department
endrodi.gaborne@energia.mta.hu

New mobile laboratory unit



I. EU SUPPORTED RESEARCH ACTIVITIES



Call for CERIC Research
Grants now open
Deadline postponed
March 7th



SINE2020 PROJECT – INDUSTRY CONSULTANCY

Rózsa Baranyai

Sine2020 – world-class Science and Innovation with Neutrons in Europe in 2020 – is a consortium with 18 partners from 12 countries, and it is an EU funded project. The Industry Consultancy work-package of the Sine2020 project aims (i) to enhance the knowledge in industry about the neutron based analytical methods, (ii) to train the industrial researchers in the applications of neutron techniques and (iii) offer test measurements and feasibility studies to be carried out, free of charge, at European neutron research facilities.

Within the Sine2020 project the Budapest Neutron Centre (BNC) targeted those industrial sectors which are included in our nation- and region-wide activities. These industrial sectors are:

- automotive industries,
- life sciences & pharmaceutical + biomolecular developing centres,
- food industries & security requirements for food and (agricultural) feed industries,
- energy sector,
- plastics industry.

The automotive sector is one of the most significantly growing industry in Hungary. it includes car manufacturers like Mercedes, Suzuki, Audi and Opel (GM Group), Rába as a Bus & TIR Camion designer and producer, and suppliers from the small size to the large companies.

BNC's aim is to demonstrate the potential of neutron technologies to the car manufacturers and their suppliers. We decided to participate at the Automotive'16 Expo in October, 2016 as an exhibitor. This was the first occasion when BNC took part in an industrial event. We rented a stand where the neutron techniques "Neutrons in the Automotive Industry" were shown. Together with SINE2020 WP4 project we prepared some new and specialized catalogues, flyers, banners, roll-up posters and brochures. The most interesting and well recognized one is the "Neutrons for building a car" flyer (Fig. 1). It presents how neutrons can be useful for the vehicle industry.

During the 3-day event a thematic conference was organized titled "Materials Research and Testing with Neutrons for Technological Developments in the Automotive Industry". The small conference included four presentations, where the speakers introduced some R&D ideas and measuring opportunities based on research capabilities of BNC and other neutron laboratories in Europe.

Some outstanding results of the 3-day event:

- Several scientific & technical consultations were held,
- BNC was invited by two Automotive Cluster to inform directly their members about the neutron methods and analytical measurements carried out at BNC,
- A 'publication report' about the BNC's activities was published in the autopro.hu magazine.

(<http://autopro.hu/szolgalatok/Neutronvizsgalat-uttoro-technologia-a-jarmugyartas-szolgalataban/20763/>)

Sine2020 including BNC encourages the industrial users to exploit the unique features of neutrons for R&D and offers free access to the European neutron facilities for test measurements and feasibility studies. Two calls were launched last year and 17 companies expressed their interest to participate in this program. The most required techniques were the residual stress investigation and imaging / tomography.

Our goal is to continue this work, to maintain and develop new connection with the stakeholders of the automotive industry.

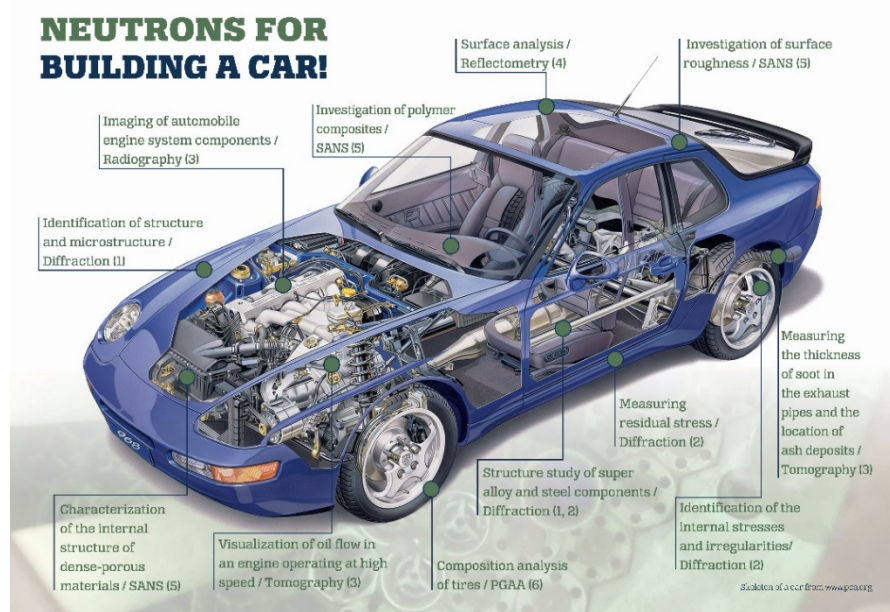


Figure 1: "Neutrons for building a car" designed by Margit Fábíán

BUDAPEST NEUTRON CENTRE NMI3 - A SUCCESSFUL EUROPEAN COLLABORATION FOR SCIENCE

Rózsa Baranyai

NMI3 was a European consortium of 18 partner organizations from 12 countries, including all major facilities in the fields of neutron scattering and muon spectroscopy (Fig. 1). The Budapest Neutron Centre took part in this collaboration from the beginning; in NMI3 FP6, NMI3 FP7 and NMI3-II FP7. The last project, the NMI3-II started in 2012 and finished in 2016. Total budget was 15.9 million EUR (EU contribution: EUR 13.3 million).

NMI3-II supported the achievements in 3 areas.

- Transnational Access Programme

The transnational access facilitated the integration of European neutron and muon research centres for efficient use of resources. It increased the mobility of scientists by offering free access to the infrastructures. The facilities provided beam time to scientists from foreign, European countries. Proposals were selected considering scientific excellence. European researchers benefitted from 10 member facilities offering access to their instruments and beam lines. Nearly half of the users came from other European countries (Fig. 2). NMI3-II attracted young scientists using neutrons first time; almost 40% of the total was new users and 23% was under the age of 30.

During the 4 years 2300 projects representing 5000 beam days were funded.

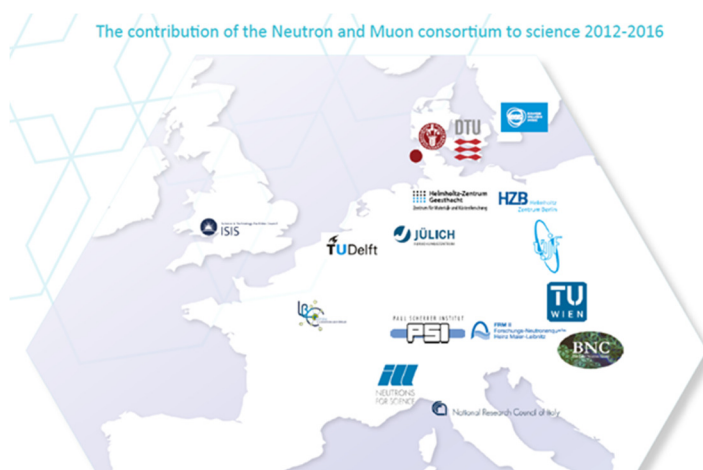


Figure 1: Members of NMI3 consortium

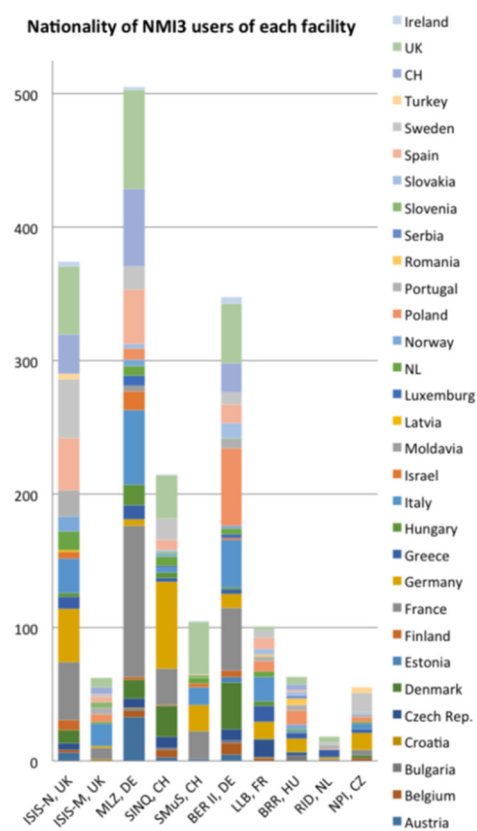


Figure 2: Nationality of NMI3 users at each facility

- Joint research activity (JRA)

NMI3-II ensured the collaborative development of new techniques, instruments, and methods to improve the service at neutron and muon centres for visiting scientists. Particular attention was paid to preparing instrumentation for the highly intensive beams of the future European Spallation Source (ESS). Into the Imaging, BNC was involved, developed innovative methods to probe structure in bulk materials, e.g. car engine. It is now possible to conduct experiments with better contrast and reconstruct 3D configurations of large arrays of nanostructures. This technique is used by experts from museums, materials science and industry.

- Networking and dissemination

15 European neutron schools were supported, e-learning platform was introduced. Now it is available at e-neutrons.org.

Neutronsources.org, muonsources.org websites were developed for the present and potential neutron and muon users. Monthly 3000 people visit these sites for information.

Prototype of integrated user access software was worked out, which harmonized the access via common procedures among facilities.

Nearly 2000 scientists supported by NMI3-II generated 210 publications in peer-reviewed journals in the fields of chemistry, engineering, life materials, information communication technology (ICT), earth & environment, humanities, energy and physics.

The NMI3-II project closed, but this successful cooperation continues within the frame of another EU funded project, SINE2020 (world class Science with Neutrons in Europe 2020), and prepares the community for the unique opportunities at the European Spallation Source.

BENCHMARKING OF THE REACTOR PHYSICS COMPUTER CODES USED FOR ALLEGRO CALCULATIONS IN EUROPEAN PROJECTS (ESNII+ AND VINCO)

Bálint Batki, András Keresztúri, István Pataki, Emese Temesvári

Objective

The same ALLEGRO 3D full core and asymptotic unit cell problems had to be solved by using a number of reactor physics codes and nuclear data libraries in order to determine their standard deviations originating altogether from the nuclear data, modelling assumptions and user effects. In the ESNII+ EU FP7 project, a reactor physics benchmark aiming at the whole core calculation with the reflectors and detailed description of the structural elements was specified. This benchmark is based on the 2009 CEA concept of the ALLEGRO core. Fixed nominal technological data at nominal reactor state (geometry, composition) were prescribed which had to be modified in specified calculation branches according to different types of the thermal expansion and control rod positions. The parameters of the point kinetic model to be applied in a system thermal hydraulic code had to be determined this way. The obtained deviations between the participants are characterizing the user effects, the modelling uncertainties and the influence of all the nuclear data differences, without the possibility of their separation because of the complexity of the benchmark problem. A conclusion could be drawn that a step by step procedure starting from a simple problem (Wigner-Seitz unit cell) is necessary if we wish to identify the reasons of the deviations. This latter benchmark was defined in the VINCO European project.

Methods

In the 3D calculation exercise organized in the frame of WP6 of ESNII+ EU project, 6 institutions – MTA EK (organizer), PSI (Paul Scherrer Institute, Suisse), AMEC (International Association for Measurement and Evaluation of Communication), NNL (National Nuclear Laboratory, UK), VUJE (Slovak Engineering Company), TU Delft (Delft University of Technology) – took part by using the KIKO3DMG, ERANOS (ECCO, VARIANT, BISTRO), WIMS, SERPENT, MONK computer codes. In the pin cell calculation exercise organized in the frame of the VINCO EU project, 4 institutions – MTA EK (organizer), VUJE, NCBJ (Polish National Centre for Nuclear Research), UJV Rez (Czech Nuclear Research Institute)– took part by using the ERANOS-ECCO, HELIOS, SERPENT, SCALE computer codes.

Results

The standard deviations were much larger than the usual ones in case of the traditional PWR reactors, especially for the reactivity coefficients. Although the standard deviations could be decreased to some extent by solving the very simple pin cell problem instead of the 3D one by eliminating the user effects, the deviations remained large due the modelling issues and because of using different nuclear data.

Remaining work

Further identification of the modelling issues and quantification of the uncertainties originating from the different nuclear data would be necessary during the coming years in the frame of a PhD study.

Related publications

- [1] A. Keresztúri, S. Pelloni, K. Mikityuk, B.A. Lindley, P. Smith, R. Gregg, M. Thomas, P. Darilek, R. Zajac, T. Chrebet, I. Z. Perkó, J.L. Kloosterman, I. Pataki, E. Temesvári and B. Batki: *ALLEGRO Core Safety Parameters, Model Uncertainties, Influence on Core Transient Estimate*, ESNII + Contract Number: 605172, Deliverable D6.1.5-1, 15/11/2016.
- [2] A. Keresztúri and E. Temesvári: *MS6 – Neutronic Benchmark Specification – part 1/2*, VINCO Grant Agreement: 662136, HORIZON 2020, October 19, 201 (2016)
- [3] E. Temesvári, A. Keresztúri, I. Pataki and Á. Tóta: *Core Safety Calculations of the Allegro Core*, Proc. of ICAPP 2016, San Francisco, USA, April 17-21, 2016, ISBN 978-0-89448-725-5. (2016)

BRIGHTNESS- WP6: COLLABORATION, COMMUNICATION AND DISSEMINATION

Margit Fábrián

Objective

The key objective of this Work Package is to strengthen the community building between members of the supply chain and stakeholders. The goal is to gain future users' trust from science and industry by means of expanding the European Spallation Source community and network. Regarding the communication, the objective is to raise awareness for ESS as the role model for managing large-scale in-kind contributions to research infrastructures. By raising awareness for ESS, the member states will be supported in their decision making process for joining other international projects which will be built in partnership. In addition, these communication measures will support the exchange of best practice among research infrastructures, which are built with a significant amount of in-kind contributions.

Scientific and public outreach

The main objective of this task is to achieve a broad dissemination of the information and communication materials and develop target group specific materials. The following activities are envisaged for the respective target groups:

Shareholders and stakeholders: they will receive the regular newsletter about the project and will be invited to project related events.

Future users: i) producing materials for use in scientific journals, ii) promotion and encouragement of publishing articles related to the achievements of the project, iii) promoting and co-branding BrightnESS at related events, workshops and conferences, iv) employing social media, v) liaising with university networks to disseminate information material about the possibilities offered by the project for students.

Industry: industry outreach will occur through the hosting, collaboration and co-branding of events targeted at industry.

Results

Budapest Neutron Centre (BNC) a partner in ESS instrumentation and in BrightnESS, BNC is involved through the Wigner Research Centre for Physics in Work Package 4 (Detectors and Moderators) and Work Package 6 (Collaboration, Communication and Dissemination.) Beside the BrightnESS contribution, both mentioned institutes are in-kind contributors to the NMX instrument at ESS: The Centre for Energy Research has a signed technical annex for the design of the shielding of the instrument and later the institute is interested in delivering the shielding; the Wigner Institute delivers the chopper system (three slow (14Hz) choppers), the design of the guide system and the design of the control system. Wigner is also interested in delivering the guide system. Besides NMX-Macromolecular Diffractometer, Wigner contributed to the proposal of Miracles backscattering instrument and also going to sign the MoU for the BIFROST (Extreme Environment Spectrometer at ESS) -it is an indirect geometry spectrometer optimised for fast measurements in the horizontal scattering plane, and allows for routine examination of the dynamic properties of small samples within controlled temperature, pressure, and magnetic and other fields.

Focus Group Meeting for potential Industrial partners; An interactive discussion followed the presentations. The moderator was László Rosta. Two main points raised by the participants during the discussion are given below: 1. methodological and professional issues and 2. financing possibilities.

Central European Training School (CETS); More than 30 students from all over Europe participated at the annual CETS at BNC in Budapest and got a unique insight into the ESS project.

Students' Awareness of Large Research Infrastructure; The survey targeted 100 students from Eötvös Loránd University and Budapest University of Technology and Economics, two leading Hungarian institutions, with top programmes in physics, chemistry, engineering and IT. The 56 students who answered the 15 questions provided information about their educational background, research field in experimental or theoretical science, awareness of existing research infrastructures and interest in ESS.

Hungarian Physics Conference held in Szeged; ESS presented for young as well as experienced scientists - the ESS representatives were also present in the talks where the timeline and research plans of the facility were presented. The interest among the young people was quite intense, but the senior scientist also expressed their interest in the further possibilities in areas such as biology, material science, soft matter and magnetic fields.

Beamline Tests Show Progress in Detector Development; A team from ESS carried out a one-week test using a beamline at the Budapest Neutron Centre (BNC) together with a team from the facility. BNC is operated jointly by Hungary's Centre for Energy Research and the Wigner Research Centre for Physics.

Remaining work

This is the first year of a three-year project; we continue the well-prepared BrightnESS WP6 schedule.

PARTICIPATION IN THE EU ESNII PLUS PROJECT

Zoltán Hózer, Nóra Vér, Péter Szabó, Emese Slonszki

Objective

The ESNII Plus project deals with the European fast reactor concepts. (ESNII stands for European Sustainable Nuclear Industrial Initiative.) The MTA EK contribution in 2016 focused on the review of research and test facilities for fast reactor designs and on the siting and project licensing for demonstrators.

Methods

International reviews were carried out with the partner organizations inside of the project. An interim meeting was held in Budapest on 22nd March 2016 in order to review the status of deliverables and the actions necessary for their finalization.

Results

Two deliverables were produced with the following main conclusions:

- A total of current European seven research reactors are identified, that are operational, have a high flux of $>1.0 \cdot 10^{14}$ n(cm²s) and have material testing capabilities and experience. Additionally, three reactors are described that are either under construction, or planned for the near term (≈ 10 year). To fully assess the irradiation capabilities, 15 other irradiation facilities are described from outside of Europe. In Europe, no reactor with a fully representative spectrum exists. Outside of Europe, there are three fast-flux test reactors, and two full-scale (sodium) fast-flux reactors. For material research, the high fast flux is essential to test and qualify the materials.
- It was concluded that in case of demonstrators using a GenIV system technology, the innovative character of this rather complex installation requires careful consideration from the start of the licensing process. A preparation (pre-licensing) phase seems to be the best approach, and engagement of early discussions with national regulator in case of innovative design seems to be the best recommendation. This will allow for an important part of licensing to be solved by the time the licensing process for a particular nuclear GenIV installation starts.

Remaining work

The review of Experimental facilities dedicated to ESNII concepts will be completed in 2017.

Related publications

- [1] S. Knol, Z. Hózer, N. Vér, E. Slonszki, A. Prybyszewska, D. de Bruyn, L. Belovsky, R. Stainsby, P. Agostini and C. Latge: *Qualification and testing infrastructure for irradiation programme*, ESNII Plus Deliverable 321 (2016)
- [2] M. Nitoi, J-M. Carrere, Z. Hózer, L. Burgazzi, D. Gugiu, M. Farcasiu and M. Constantin: *Siting and licensing requirements for GenIV demonstrators*, ESNII Plus Deliverable 321 (2016)

PARTICIPATION IN THE EU SAFEST PROJECT

Zoltán Hózer, Imre Nagy, Nóra Vér, Mihály Kunstár, Róbert Farkas, Katalin Kulacsy

Objective

A new CODEX experiment will be carried out in the framework the EU SAFEST project. The main objective in 2016 was the specification of the test conditions.

Methods

In order to discuss the main aspects of test planning and main conditions of new CODEX (COre Degradation EXperiment) test with air ingress, an expert meeting was held in Budapest on 14-15th June 2016 with the participation of eleven organisations.

Results

According to specification of CODEX-AIT-3 test, the reference scenario will be a reactor accident with melt-through of the bottom head and penetration of air+steam mixture from the reactor cavity into the reactor vessel. The experiment will simulate the high temperature interactions of peripheral fuel assemblies in air+steam atmosphere. Slow cool-down will be applied to provide information on bundle state before quench.

The main phases of the CODEX-AIT-3 test will be as follows (Fig. 1):

- I. Technological heat-up will be performed in argon atmosphere with stabilisation of temperature at 500 °C.
- II. Pre-oxidation in steam atmosphere will be carried out between 500-1100 °C. The pre-oxidation phase will start with temperature increase from 500 °C to 1100 °C with 3600 s duration, with the aim of keeping 0.167 K/s temperature increase rate. The target temperature will be reached electric power increase. The 1100 °C maximum temperature will be stabilised and pre-oxidation will be continued for 1800 s. The steam flowrate must be high enough to avoid steam starvation. The maximum oxide scale will be close to 100 µm according to the E110G oxidation kinetics correlations recently published by MTA EK.
- III. The atmosphere will be switched from steam to air+steam with argon carrier gas. The temperature of air+steam mixture will be about 600 °C. The flowrates should be selected so that steam and oxygen starvation took place in the bundle. The duration of this phase should be about 1 hour and the maximum temperature should be 1600 °C. It is expected that the x and y flowrates indicated in Fig. 1 will be determined on the basis of pre-test calculations. The power will be increased to reach the high temperature.
- IV. Slow cool-down will be performed in high argon flow by switching off power and stopping air+steam supply.

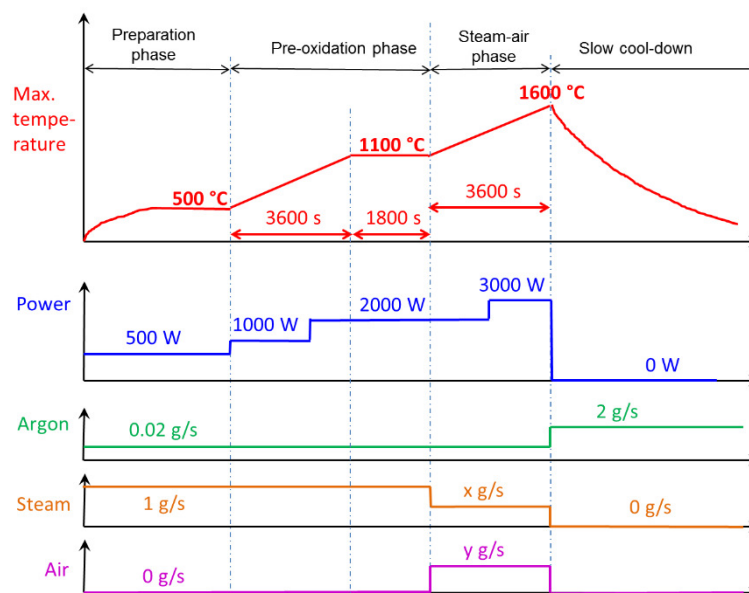


Figure 1: Main phases of CODEX-AIT-3 test

Remaining work

The CODEX-AIT-3 experiment with an electrically heated 7-rod bundle will be performed in 2017.

Related publication

- [1] Z. Hózer, I. Nagy, M. Kunstár, R. Farkas, N. Vér, and K. Kulacsy: *Specification of CODEX air ingress test in the framework of the EU SAFEST project*, MTA EK-FRL-2016-448-1-1-M0, in Hungarian (2016)

PARTICIPATION IN CONCERT–EUROPEAN JOINT PROGRAMME FOR THE INTEGRATION OF RADIATION PROTECTION RESEARCH

Balázs G. Madas, Imre Balásházy

Objective

The objective of this project is to integrate radiation protection research in the European Union, including the research priorities of five European platforms (MELODI for low dose research, EURADOS for radiation dosimetry, ALLIANCE for radioecology, NERIS for emergency preparedness, and EURAMED for radiation protection in medicine) and participating countries, the use of infrastructures and education and training (E&T).

Methods

One method for integration is to define synergistic research priorities and provide funding for projects which address these priorities. The priorities are first defined by the five platforms, then the program managers of the different countries can add suggestions. Workshops with representatives of the different platforms are organized in order to find synergies between their priorities. The first CONCERT Call was announced in 2016.

In order to increase the visibility of infrastructures for radiation protection research, a monthly newsletter about these infrastructures and a searchable database of them were established. The next task is to increment these databases. There is also funding for training activities in order to increase knowledge transfer between European researchers and attract young scientists to radiation protection research by providing them high quality courses.

Results

We participated in the update of the MELODI Strategic Research Agenda [1], and in the definition of priorities for the second CONCERT Call. For the first CONCERT Call, twelve proposals were submitted. MTA EK was involved in two consortia, one of them (CONFIDENCE) was selected for funding.

MTA EK had to present ideas how an Action plan can be prepared in order to increment infrastructure databases. The Biological Irradiation Facility at the research reactor was presented in April 2016 in the newsletter.

In the work package for Education and Training, we started to prepare electronic surveys for the evaluation of training courses. It reduces significantly the administrative tasks of the course organizers and the work package leaders.

Remaining work

The CONCERT project ends in 2020. The most important task for us in 2017 is the elaboration of the action plan for incrementing databases. Besides this we will be involved in updating the MELODI Strategic Research Agenda, in the preparation of a joint roadmap of the platforms including stakeholder involvement. The preparation of electronic surveys continues in 2017.

Related publication

- [1] M. Kreuzer, D. Averbeck, I. Balásházy, S. Bouffler, E. Cardis, J-R. Jourdain, M. Harms-Ringdahl, S. Pazzaglia, F. Zölzer, A. Ottolenghi and L. Sabatier: *Strategic Research Agenda of the Multidisciplinary European Low Dose Initiative (MELODI)* (2016)

UPDATE ON VV BOLOMETER DESIGN AND ANALYSIS

Levente Tatár

Objective

Bolometers play an important role in the ITER (International Thermonuclear Reactor) fusion device, as these will be used for tomographic reconstruction of the plasma radiative power. MTA EK participates in bolometer-related work in an international consortium led by IPP Garching, which does main design work and sensor development. The main task of MTA EK is thermo-mechanical analysis.

Bolometers are located in highly demanding environment (high vacuum, high neutron, gamma, plasma flux, electromagnetic forces, etc.). Detailed thermo-mechanical fatigue analysis will assure that peak stresses and temperatures appearing in the bolometer cameras and the structures to which these are attached are within acceptable limits.

There will be three fundamentally different types of bolometers: bolometers mounted on the vacuum vessel (VV), bolometers mounted on the divertor cassettes and bolometers mounted in the port plugs (PP).

During 2016 activity was mainly focused on VV bolometers. Specific to VV bolometers is that these are attached to bosses welded to the VV and see through a gap between adjacent blanket modules. The intended design for VV bolometers makes them replaceable for a few times during ITER lifetime. To facilitate replacement, the VV bolometers are separated into two distinct parts: a platform attached to the VV and the camera body. (Figure 1)

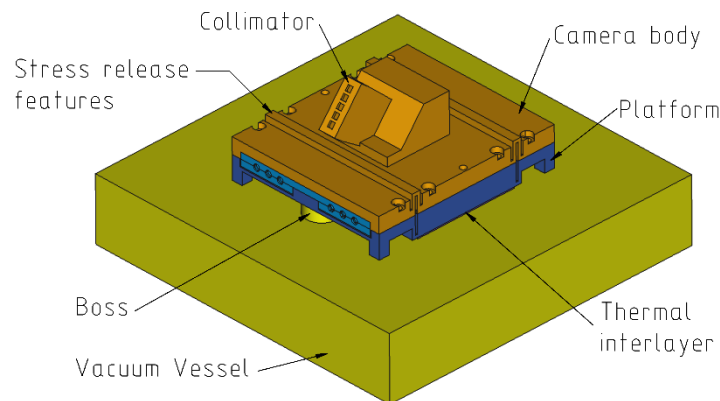


Figure 1: VV camera version

Methods

The basic design made by IPP Garching was transferred to MTA EK as a STEP file which served as base for finite element (FE) mesh. As candidate materials for bolometer camera housing (platform and camera body) TZM and CuCr1Zr are considered. Material properties for each material were collected and separate analyses were done with these materials.

For the analysis of bolometer cameras, thermal boundary conditions are very important. The incoming heat consists of neutron and gamma heating, plasma radiation, ECH (Electron-Cyclotron Heating) stray radiation, while cooling of the camera body is mainly done by contact heat transfer towards the VV, which is in turn water cooled. Due to heat expansion and EM (electromagnetic) forces high stresses will develop in the bolometer camera and in the bosses welded to the VV.

In the initial FE models EM forces were not considered, only heat expansion.

Results

During the thermal analysis the importance of heat transfer towards the VV became obvious. Good heat transfer can be assured by a soft, compliant thermal interlayer. Candidate materials for thermal interlayer are Papyex® (graphite based) and Cu foil or Cu mesh based sheets. An external contract has been placed for qualification of interlayer materials.

It turned out that in case of TZM as housing material peak temperatures may be too high, but for CuCr1Zr temperatures can be kept within acceptable limits. For initial versions of the model stresses were unacceptably high, for successive variants stresses could be greatly reduced, however still remain above acceptable limits. To reduce stresses, compliant structures "stress release features" are essential. In 2016 these stress release features were "joggles" like those seen in Figure 1.

Remaining work

The optimal solution could not be reached yet. During 2016 a preliminary EM analysis has shown that very high EM forces are to be expected. This means that joggles as stress release features may not be as effective as required, so in 2017 we started new computations considering a completely different kind of stress release features.

Related publications

- [1] H. Meister et al: *Current status of the design of the ITER bolometer diagnostic*, Fusion Engineering and Design / 29th Symposium on Fusion Technology (SOFT 2016)

AGE-60 EU PROJECT

Ferenc Gillemot, Márta Horváth, Attila Kovács, Ildikó Szenthe

Objective

The purpose of the AGE-60 project is to collect reactor material ageing information required for long term operation (60 years or beyond). Due to the limited financial support, no new research is planned within the project, only re-evaluation of the existing research and surveillance data is conducted. ÚJV, Řež, (Czech Republic) and MTA EK collected the VVER data [1]. The goal of the work was to elaborate new trend curves and evaluate new information on radiation and thermal ageing of the VVER-440 pressure vessel materials. Parallel with the use of VVER data, the western European partners are working with the data of the other European pressurized water reactors.

Methods

The original surveillance data, extended surveillance results and existing research knowledge were collected. Since most of the extended surveillance data is the result of recent activity, the data collection from several different sources is a very time consuming task. The original surveillance program of a VVER-440 unit contains 216 Charpy, 216 fracture mechanical and 72 tensile specimens, large number of dosimetry foils and temperature monitors. The extended surveillance programs nearly double the data amount. The testing and evaluation of them were made at different times. Data of 18 VVER-440 units (mostly operated within the EU) have been collected and evaluated. New ageing trend curves were elaborated using this large amount of data. Parallel with this, our group worked on the VVER materials and another group made similar collection and evaluation of other PWR units operating within Europe. The two groups supported the work of each other, and participated in the evaluation of all results.

Results

A new, updated radiation and thermal ageing database on the surveillance results of the reactor vessels operating within the EU was elaborated and evaluated. Ageing trend curves for the reactors in EU were elaborated. Their use will enhance the reactor safety and support the life extension. One piece of the interesting new information is shown in Fig 1. The ratio between the dpa dose rate and fluence integrated over 1 MeV shows linear correlation, however the slopes of the lines are slightly different in the case of the USA units, French PWR-s and the VVER-s. The reason is that the water gaps between the core and the vessel wall are different, resulting in different spectra.

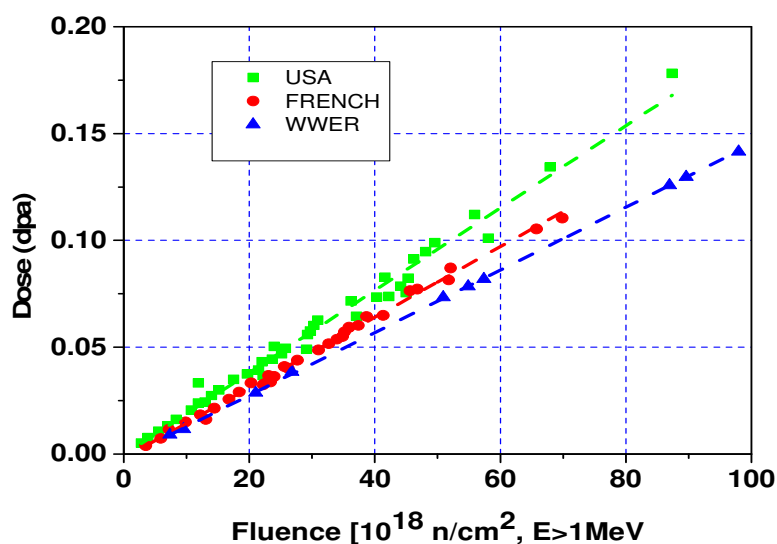


Figure 1: Ratios of dose to fluence in different reactor types

Remaining work

The AGE -60 project started in 2015 and terminated in 2016. The database prepared within the project will most probably be used or re-evaluated several times in the future in the frame of other national and international projects dealing with reactor vessel materials ageing.

Related publication

- [1] F. Gillemot, M. Horváth, A. Kovács and I. Szenthe: *Participation in the AGE-60 EU project*, Progress report 2015, Centre for Energy Research of the Hungarian Academy of Sciences

ELABORATION OF DATABASE AND MPH VOLUMES WITHIN THE WPMAT EDDI PROJECT

Ferenc Gillemot, Ildikó Szenthe, Attila Kovács

Objective

The purpose of the WPMAT project is to collect existing knowledge and produce new information on the properties of recently developed materials for the future DEMO fusion reactor. Within the project our task is to elaborate a material's database and material property handbooks (MPH). MPH should include chapters on all material properties, usable for the designer-engineers. The first volume prepared summarizes the properties of Eurofer. Eurofer is a heat resisting 9% chromium ferrite-martensitic steel with reduced activation. The next volume will deal with the properties of functional (dielectric and optical) materials.

Methods

Data collection templates had been elaborated for all selected material types. Data were collected from existing databases, literature, WPMAT research reports and templates filled by the project participants. The collected data go into the database after they have been checked and verified. After careful evaluation, the results are provided to the designers in diagrams and table format. The MPH provide information on the as received and aged (irradiated, thermal aged, fatigued, etc.) material properties. Finally, the MPH is referred and extended by the project partners.

Results

The volume on Eurofer is ready, the functional materials' volume is under construction. Figures 1 and 2 show two instances of the Eurofer mechanical properties from the MPH. Fig. 1 includes the average yield strength of the Eurofer 97 after different irradiations as a function of the testing temperature. Fig. 2 shows the scatter of the Master curve testing of Eurofer 97 made by different laboratories.

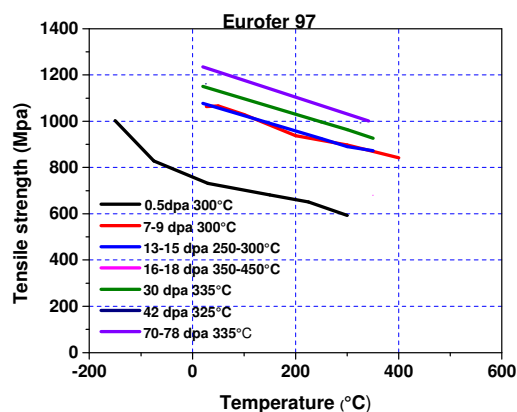


Figure 1: Tensile strength of irradiated Eurofer

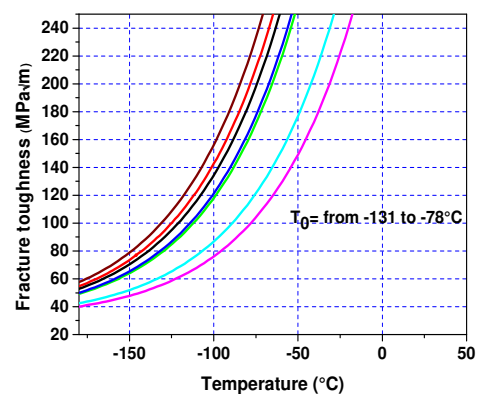


Figure 2: Master curve scatter on Eurofer

The MPH summarizes all the available information on the Eurofer 97 in three sections:

- Section 1. General information, Chemical Composition
- Section 2. Mechanical properties: yield strength, tensile strength, elongation, reduction of area, Young's modulus, Poisson's ratio, Charpy impact energy, fracture toughness, fatigue, fatigue crack growth rate, creep, swelling, ratchetting
- Section 3. Physical properties: density, linear thermal expansion, thermal conductivity, thermal diffusivity, specific heat, melting temperature, electrical resistivity, magnetic saturation, remnant magnetization, coercive field

Remaining work

New volumes are planned on other special materials important for the DEMO fusion reactor. The existing volumes will be periodically upgraded if new information will be available. The list of properties can be extended according to the new requirements of the DEMO designer group.

TRANSNATIONAL ACCESS WITHIN THE EC H2020 IPERION CH PROJECT

Zsolt Kasztovszky, László Szentmiklósi, Zoltán Kis, Ildikó Harsányi, Adél Len, Katalin Bajnok, György Káli, Imre Kovács, Zoltán Szőkefalvi-Nagy, László Rosta

Objective

Within the IPERION CH, transnational access is offered to European experts of heritage science, to perform experiments at the instruments of the Budapest Neutron Centre (BNC). In most short-term projects, compositional and structural data are obtained using predominantly non-destructive methods, from which information regarding provenance, condition, genuineness of the objects are concluded.

Methods

In the frame of the transnational access, Prompt Gamma Activation Analysis (PGAA), Instrumental Neutron Activation Analysis, Neutron Radiography, Time of Flight Neutron Diffraction, Small Angle Neutron Scattering and complementary PIXE can be used for few-days long experiments.

Results

Highlight 1: Search of Fingerprints in Archaeometallurgy: elemental composition study of three gold filigree fragments from an ancient Italian processional Cross

Aim of the project was to study a processional cross, coming from the abbey of Chiaravalle (close to Milan, Italy) and dated to the 13th century to verify the use of amalgam technique (mix of Au and Hg) over a silver sample. The amounts of Hg, Ag, Au and Cu measured by PGAA characterized the raw material that was used for production of the cross and confirmed the use of amalgam technique.



Figure 1: Photo of the three filigrees that were analysed by PGAA, milli-beam PIXE and XRF

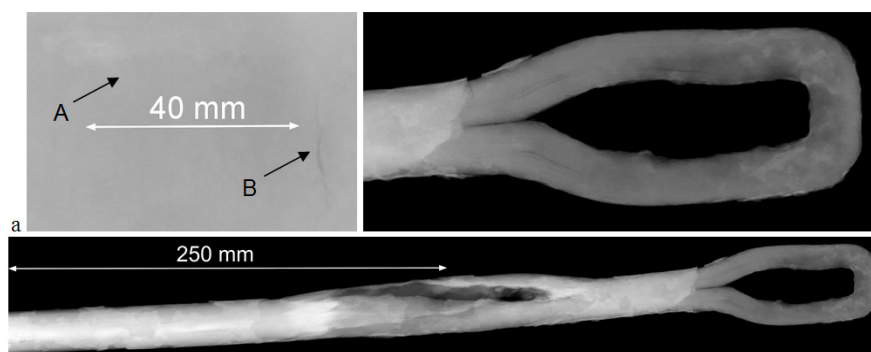


Figure 2: (a) Two defects of the large iron slab are shown by arrows (A and B). (b) The elongated cracks in the material of the long rod are well recognizable. (c) The image of the long rod created as by a mosaic of overlapping tiles shows a damaged part and gives some hints about the fabrication technique.

Highlight 2: Neutron Imaging of a failed 1400s wrought iron tie rod from Milan Cathedral

The aims were deeper material characterization and identification of local defects in the tie rods of the Milan cathedral. Former metallographic and hardness tests revealed extremely heterogeneous structure of the rods. Cracks and voids were possible to identify. Based on the Neutron Radiography studies at the RAD station of the BNC, the corroded parts are separated from each other showing how they were originally assembled. It gives some hints about the fabrication technique, and the way how other rods could principally be attacked by corrosion. The peelable layers visible to the naked eye and neutron imaging are a mixture of corrosion products and painting materials.

Remaining work

Further research proposals for Transnational Access in Heritage Research are expected within the IPERION CH project.

Related publication

- [1] V. Szilágyi, Z. Kis and L. Szentmiklósi: Neutron imaging for archaeometry / A neutronos képképzés archeometriai alkalmazása, *Archeometriai Műhely*, XIII/3, 1 (2016)

GOAL ORIENTED TRAINING PROGRAMME OF EUROPEAN FUSION DEVELOPMENT AGREEMENT - RADEFF GOT

László Szentmiklósi, Ákos Horváth

Objective

The objective of European Fusion Development Agreement (EFDA) Goal Oriented Training Programme is the involvement of early stage researchers in a structured training programme in the field of fusion energy research. We trained two fellows to work safely with activated objects.

Methods

Theoretical training, hands-on experiments, calculations, computer simulations.

Results

MTA EK hosted two trainees and provided expertise for preparation of samples for fission-reactor irradiation, dpa (displacement per atom) calculation, neutron spectrum calculation, nuclear heat calculations, and the mechanical design of the irradiation rig. In addition, the trainees became acquainted with in-situ testing techniques of small components and devices as well as with analytical techniques such as gamma spectroscopy, neutron activation analysis, and dosimetry. The main advantage of this training opportunity is the availability of the diverse experimental facilities at the Budapest Research Reactor. The two trainees, Benjamin Kaiser of the Karlsruhe Institut für Technologie (KIT) and Mickael Payet of Commissariat à l'Énergie Atomique et aux Énergies Alternatives (CEA), were hosted at the Nuclear Analysis and Radiography Department of the Centre for Energy Research. Mickael Payet attended the training between 1-4 March 2016, whereas Benjamin Kaiser stayed from the 1st to the 24th of March 2016.

First, the fundamentals of health physics, radiation safety and radiation protection guidelines were illustrated, followed by a visit to several experimental stations, the control room and the Budapest Research Reactor (BRR) itself. These illustrated with a hands-on experience the good working practice and safety aspects of the every-day work in a radiation environment. Further, specialized experimental facilities for prompt-gamma activation analysis, neutron imaging, instrumental neutron activation analysis, and gamma spectrometry were presented in details and the trainees had a chance to experience the setup of an experiment, the data collection as well as the interpretation of the results. A comprehensive presentation about the BAGIRA irradiation facility and the related sample preparation was made.

The theoretical aspects of the training included the dpa calculations with ions and neutrons, the characterization of the neutron field in a fission reactor's irradiation position, the calculation of the radioactivity induced by neutron bombardment, as well as the use of EASY-2003 and Fispack software, a code for calculating isotope inventories and decay heat followed by the irradiation. Finally, the Monte Carlo calculation technique was shown on some examples from our working practice.



Figure 1: Benjamin Kaiser (first row, to the left) and the team of the NAA laboratory carry out irradiations with the pneumatic rabbit system of the Budapest Research Reactor on 10 March 2016.

Related publication

- [1] L. Szentmiklósi and Á. Horváth: *Report on the Goal Oriented Training Programme EFDA WORKPROGRAMME 2012 WP12-GOT-RadEff*, MTA EK-NAL-2016-329-1-1-M0 (26.05.2016)



II. RESEARCH AND DEVELOPMENT RELATED TO NUCLEAR POWER PLANTS



HUNGARIAN NUCLEAR RESEARCH PROGRAM

Árpád Farkas

Objective

The Hungarian Nuclear Research Program (2014-2018) is a research and development project funded by the National Research, Development and Innovation Office (project identifier: VKSZ_14-1-2015-0021; homepage: vksz14.kfki.hu). The participants of the consortium project are: Centre for Energy Research, Hungarian Academy of Sciences (MTA EK, as coordinator), Budapest University of Technology and Economics (BME), Hungarian Academy of Sciences Institute for Nuclear Research (MTA ATOMKI), National Public Health Institute (OKI) and Nuclear Safety Research Institute Ltd (NUBIKI). The main goals of the project are to conduct high level research on the technologies supporting the long-term and safe use of atomic energy and to maintain and extend the Hungarian nuclear professional knowledge. One of the main efforts of the project is oriented towards providing technical and scientific background for the safe operation of the existing blocks of Paks NPP and preparing for the installation of the new reactors. State-of-the-art research on the safe disposal of spent fuel and development of novel approaches to study different aspects of new generation reactors are also organic parts of the project. Elaboration of the mid-term strategic plans of the Hungarian nuclear research infrastructure is also in focus within this complex research program.

Results

In 2016 a comprehensive study on the Budapest Research Reactor (BRR) located in the KFKI Campus (Csillebérc, Budapest) and the Nuclear Training Reactor of the Institute of Nuclear Techniques (Budapest University of Technology and Economics) has been elaborated. The study presents the history and status of the two reactors and proposes measures for their maintenance in the future. The study has also been submitted to Hungarian decision makers. One of the most outstanding research results of the project in 2016 is related to the planning, modelling and safety analysis of ALLEGRO fourth generation gas cooled demonstration reactor. These results are in focus also because of their importance in relation to the key objectives of the V4G4 excellence centre. For the same reason, important results were obtained also in the field of measurement and modelling of thermo-mechanical characteristics and aging of reactor materials, development of numerical models of physico-chemical processes in the reactors, multiphysics simulations, measurement and modelling of the emissions of NPPs and concerning health effects of low doses of ionizing radiations.

Remaining work

The remaining tasks of the ongoing project will be completed until the end of 2018.

Related publications

- [1] G. Mayer, R. Nagy and I. Nagy: *An experimental study on critical heat flux in vertical annulus under low flow and low pressure conditions*, Nuclear Engineering and Design **310**, 461-469 (2016)
- [2] B. G. Madas: *Radon exposure and the definition of low doses – the problem of spatial dose distribution*, Health Physics **111**, 47-51 (2016)
- [3] T. Belgya, J. Gadó, F. Gajdos, L. Szentmiklósi, L. Rosta, I. Vidovszky, Sz. Czifrus, S. Fehér, I. Szalóki, M. Szieberth and É. Zsolnay: *Visions and plans concerning the future of Budapest Research Reactor and the Nuclear Training Reactor*. Available at: http://vksz14.kfki.hu/report/BKR_BME_NTI_jovojere_vonatkozó_elkepzések.pdf (2016)

THE ALLEGRO PROJECT

János Gadó

Objective

Corresponding to the European initiative on launching research in the field of Generation IV nuclear reactors, the nuclear research institutes of the Visegrád 4 countries and the French CEA started a co-operation on the development of the Gas Cooled Fast Reactor demonstration reactor ALLEGRO in 2010. The final objective of the co-operation is to build up and operate this reactor but the construction has to be preceded by a long period of research and development related to various technological issues and the design of the reactor has to be prepared in several steps. ALLEGRO can start operation not earlier than in 2030.

Methods

The ALLEGRO Project Preparatory Phase was launched by the consortium of the nuclear research institutes of the Visegrad 4 countries (V4G4) in 2015. The French CEA joined V4G4 at the beginning of 2017. The participating research organisations and their domestic partners receive research funding from national and European projects. In Hungary, the National Nuclear Research Program (NNKP) finances the ALLEGRO related activities by the end of 2018.

In the preparatory phase of the ALLEGRO Project (2015-2025), the conceptual design will be elaborated and the necessary research-development-qualification tasks will be executed. During the design of ALLEGRO the usual design methods will be applied. A pre-conceptual design is being elaborated based on the existing CEA 2009 Design. A series of important additions and modifications are foreseen which will guarantee the safety level expected from Generation IV nuclear reactors. These additions and modifications cover the re-definition of reactor power and maximum power density, the automated start-up of the Decay Heat Removal System, nitrogen injection to ensure natural circulation and also severe accident management measures.

After 2018 the conceptual design will be elaborated (by 2025) which will be the basis of submitting the construction license application. Elaboration of the detailed design, construction, commissioning and operation will be a task of a new consortium.

Results

The design tasks of ALLEGRO are listed in the Design and Safety Roadmap. MTA EK and its Hungarian partners (NUBIKI Ltd., BME NTI and AEMI Ltd.) cover several items of this Roadmap. In 2016 several research reports were prepared by these organisations in the framework of the Hungarian National Nuclear Research Program. The reports prepared by MTA EK are related to reactor physical, thermal-hydraulic, fuel behaviour and I&C issues. They are mentioned in other parts of this Progress Report. Several general and topical reports were prepared also by Hungarian and foreign experts (e.g. summary reports on safety requirements and objectives and on connections between design and safety).

A summary report on the ALLEGRO Project will be presented at the IAEA FR17 conference [1]. Reports on the safety requirements and objectives and on the connections between design and safety are almost finalized.

Remaining work

As mentioned above, the Preparatory Phase of the ALLEGRO Project requires efforts for several years. The application for financing by the Hungarian National Nuclear Research Program beyond 2018 is under preparation.

Related publication

- [1] L. Bělovský, J. Gadó, B. Hatala, A. Vasile and G. Wrochna: *The ALLEGRO Experimental Gas Cooled Fast Reactor Project*, IAEA-CN-245-96, IAEA FR17 Conference, Yekaterinburg, June 2017

SELECTION OF FUEL FOR THE ALLEGRO REACTOR

Zoltán Hózer, Anna Pintér Csordás, Emese Slonszki

Objective

One of the most important items to be prepared in the pre-conceptual design phase of ALLEGRO reactor is the core design. Oxide fuel with stainless steel cladding will be applied in the first core of gas cooled fast reactor ALLEGRO. The review of international experience of using stainless steel clad fuel was the first objective of this work

The final core of gas cooled fast reactor will be composed of ceramic fuel operated at high temperature. The primary candidate for cladding of refractory fuel is the SiC. The second objective of this work was the collection of available data and information on SiC claddings.

The third objective was comparison of MOX (Mixed Oxide) and UOX (Uranium dioxide) fuel for ALLEGRO conditions.

Methods

Literature reviews were performed in co-operation with the partners of V4G4 Centre of Excellence.

Results

The past SFR (Sodium cooled Fast Reactor) experience shows that there is a strong need for transient fuel behaviour simulation in order to predict fuel failure in the ALLEGRO reactor. Cladding failure in fast reactors can be caused by several phenomena, which cannot be simulated by thermal hydraulic or reactor physics codes, but should be taken into account – on the basis of SFR data – in design and in further analyses.

It was proposed to modify the currently used cladding temperature criteria for ALLEGRO reactor and to introduce fuel enthalpy limits for RIA analyses. The proposed limits can be used in thermal hydraulic and reactor physics calculations.

It was proved by a detailed literature review that among others chemical purity, crystallinity and stoichiometry are very important properties of the SiC ceramic fibres and matrices. During development of various types of SiC composites, three generations of SiC fibres were developed. Only the generation III SiC fibres are appropriate for using in nuclear industry. The mechanical properties of these materials are generally very advantageous especially below about 40 dpa. Further development will be necessary to make radiation resistant joints. It would be advisable to carry out separate effect tests to study some of the above mentioned properties of SiCf/SiC. Radiation stability of SiCf/SiC against very high doses (200 dpa) has to be proved.

The on-going feasibility studies indicate that both MOX and UOX fuel could be used in the first core of the ALLEGRO reactor. Beyond the physical possibility, several other aspects must be taken into account during the selection of fuel type. In our review the available information on a MOX type (ASTRID) and a UOX type (BN-600) was collected. The main items of information about the two fuel types are summarized in Table 1.

	ASTRID	BN-600
Pellet	MOX	UOX
Cladding	AIM1	ChS-68CW
Operational experience	Decades of operation in Phénix and Superphénix reactors	Decades of operation in BN-350 and BN-600 reactors
Fuel examination after base irradiation	Irradiation in Osiris, Rapsodie, Phénix and Superphénix reactors	Irradiation in BOR-60, BN-350 and BN-600 reactors
Testing in transient conditions	Large number of tests in the Cabri reactor	No test data available in open literature
Fuel production	Not in production today	Continuous production in Electrostal

Table 1: Comparison of MOX and UOX fuel

Remaining work

The fuel development and qualification will be continued in the next years.

Related publications

- [1] Z. Hózer: *ALLEGRO fuel related acceptance criteria*, MTA EK-FRL-2016-218-1-1-M0, in Hungarian (2016)
- [2] E. Slonszki and Z. Hózer: *On the selection of fuel for the first core of ALLEGRO gas cooled fast reactor*, MTA EK-FRL-2016-218-1-2-M0, in Hungarian (2016)
- [3] A. Pintér Csordás: *SiCf/SiC Cladding Material*, MTA EK-FRL-2016-219-1-1-M0, in Hungarian (2016)

DEVELOPMENT AND VERIFICATION OF THE SP3 METHOD APPLIED IN THE KIKO3DMG CODE

István Pataki, András Keresztúri, Emese Temesvári

Objective

Recent NPPs (Nuclear Power Plants) are based on large size reactors utilizing the fission process mostly in the thermal energy region. The neutrons originating from the fission at high energy must be scattered several times to slow down to the thermal energy region which equalizes the impact of the anisotropy of the scattering processes in the fast region. Additionally, the scattering processes in the thermal energy region are already less anisotropic. Consequently, the diffusion approximation, which supposes the linear anisotropy of the flux and neglects the anisotropy of the scattering, can assure satisfactory accuracy. However, in case of the foreseen Gen-IV (Generation IV) fast spectrum reactors the mentioned advantageous physical processes cannot be utilized, namely the fission neutrons can induce further fissions in the fast energy region before very few collisions or even subsequently. Additionally, the active core height is much smaller in these reactor types due to thermal hydraulic reasons and – because the cross sections in the fast energy region are smaller –, the axial reflectors can also be reached by the neutrons very easily. Consequently, in fast spectrum reactors strong anisotropy prevails in the axial direction which is especially enhanced in the gas cooled fast reactors where the coolant density is very small. In order to remedy this problem, further terms of the Legendre components of the flux must be taken into account as it is done for example in case of the P3 approximation, where 0, 1, 2 and 3 order terms are modelled. The KIKO3DMG program had to be improved also in this direction but with some simplifying approximations which could cause that the original equation of the scalar (isotropic) flux had to be supplemented only by one additional equation involving the second order Legendre component, too. This approach is called as SP3 (Simplified P3) approximation.

Methods

The implementation of the SP3 algorithm in the nodal codes is not straightforward, it is depending on the concrete method of the original nodal approach. The theory and the implementation in KIKO3DMG (new flowchart and the related subroutines, their organization) had to be elaborated, programmed and verified.

Results

The new option was verified by calculated the 3D ALLEGRO benchmark based on the 2009 CEA concept. The following quantities were calculated in diffusion and SP3 approach by using 9 and 17 energy groups:

- Reactivity at withdrawn control rods
- Reactivity effect of the working control rods at nominal state
- Reactivity effect of the working and shut down control rods at nominal state
- Effective delayed neutron fraction
- Doppler constant
- Void effect
- Fuel expansion reactivity coefficient between 900 K and 1500 K
- Diagrid expansion reactivity for 400 K increase
- Radial power peaking factor
- Axial power peaking factor

Reasonable results with noticeable changes depending on the above approximations and energy groups were obtained.

Remaining work

There is no remaining work.

Related publication

- [1] A. Keresztúri, I. Pataki and E. Temesvári: *Development and application of the SP3 method for the ALLEGRO core calculations, ECCO solution of a simplified benchmark, VKSZ_14-1-2015-0021/MTA-EK-RAL-2016-207 report, in Hungarian (2016)*

MODELLING AND INVESTIGATIONS OF MULTI-PHYSICS PHENOMENA BY THE KARATE-1200 AND THE FRAPTRAN-TRABCO COUPLED CODE SYSTEMS

István Panka, György Hegyi, András Keresztúri, Csaba Maráczy, Emese Temesvári

Objective

To model and investigate of multi-physics phenomena in a best-estimate manner, tight coupling between the different disciplines – like reactor physics, thermal hydraulics and fuel behaviour – is essential. On the other hand, the efficient survey of the uncertainties can only be assessed by using multi-physics approaches. In 2016, our goal was to develop and verify a new, improved fine mesh coupled reactor-physics/thermal hydraulics code system. The improved model is named KARATE-1200 code system which is intended to be used for the calculations of the three-dimensional power and burnup distributions of the new VVER-1200 Units at Paks. Another task was the investigations of the uncertainties of a rod ejection transient in a PWR reactor at hot channel level using the coupled FRAPTRAN-TRABCO (Fuel Rod Analysis Program Transient - Hot channel program code) system.

Methods

Concerning the KARATE-1200 code system the following developments were carried out regarding the new Units at Paks. The different calculation levels (cell, pin and node) were connected through parameterized few group cross section libraries prepared by the MULTICELL code. The methodologies of the global and fine mesh calculations (GLOBUS1200 and SADR1200 modules) were elaborated regarding the new units. To take into account the cross flows between assemblies, sub-channel wise full core COBRA thermal hydraulics model was developed and coupled to the global and fine mesh reactor physics. In the course of the survey of the uncertainties of the rod ejection transient, the OECD NEA WGFS RIA (Reactivity Initiated Accident) benchmark, Phase II was applied.

Results

The verification of the KARATE-1200 code system was successfully performed by the solution of the “MIDICORE” benchmark defined in the frame of the AER (“Atomic Energy Research”) collaboration. In order to show the applicability of the new KARATE-1200 code system, further three-dimensional test problems were successfully calculated during the burnup. The elaborated hybrid, coarse and fine mesh, full core COBRA model is demonstrated in Fig. 1. In order to check the safety limits of the VVER-1200 cores, it was pointed out, that the elaborated model is able to calculate the maximal sub channel temperatures for the VVER-1200 reactors during the core design calculations. In case of the RIA benchmark it was pointed out that the thermal and mainly the mechanical parameters have a considerable uncertainty in case of fast RIA transients. The obtained results can be applied for the planning of experiments and the evaluation of the results of safety analyses.

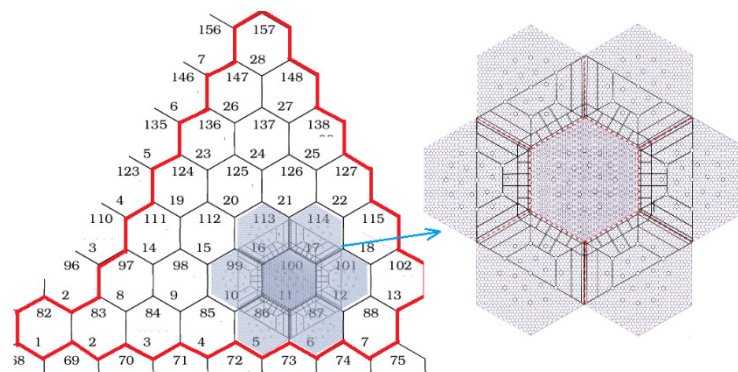


Figure 1: Hybrid COBRA model of assembly No. 100 applied in the coupled KARATE-1200 code system

Remaining work

Development of modelling of further multi-physics phenomena is to be continued.

Related publications

- [1] Gy. Hegyi, A. Keresztúri, Cs. Maráczy, I. Panka and E. Temesvári: *Coupled fine mesh reactor physics/thermal hydraulics code system to the calculations of the new units at Paks*, MTA-EK-RAL-2015-252/1-M0, in Hungarian (2016)
- [2] Gy. Hegyi, G. Hordósy, A. Keresztúri, Cs. Maráczy, I. Panka and E. Temesvári: *Comprehensive solution of the „MIDICORE” Benchmark by the KARATE and MCNP code system*, Proceedings of the twenty-sixth Symposium of AER, Helsinki, Finland, 10-14 October, (2016)
- [3] I. Panka and A. Keresztúri: *Investigations of the uncertainties of a rod ejection transient at hot channel level by multi-physics methods*, MTA-EK-RAL-2015-212-01-01/M0, VKSZ_14-1-2015-0021, in Hungarian (2015)

SUPER-VVER REACTOR RESEARCH

Csaba Maráczy, György Hegyi, István Pataki, András Szabó

Objective

Super-VVER reactor is a term for two reactor concepts which are developments of the VVER-1000 reactors and with revolutionary design can achieve better fuel utilization and higher thermodynamic efficiency. The concept „evolutionary Super-VVER” uses spectral shift to achieve higher conversion rate and fuel burnup; studies of the power distribution of fuel assemblies with different spatial enrichment by the SCALE program system were planned for this year. The single circuit supercritical pressure Gen-IV VVER (VVER-SCP) enables the coupling of a higher efficiency thermodynamic cycle, and is promising in the aspect of closed fuel cycle and final disposal of weapon grade plutonium stockpile. The cross section generation of fuel assemblies and the assessment of the applicable nodal codes were intended in the first year of research.

Methods

- SCALE neutron transport program system to optimize fuel assemblies of the evolutionary reactor.
- MULTICELL deterministic neutron transport code to generate cross sections for the supercritical reactor.
- KIKO3DMG nodal code to calculate the VVER-SCP core.

Results

In case of the evolutionary Super-VVER reactor, in order to reduce the intra-assembly power peaking factor, radial and axial enrichment zoning was proposed. The peaking factors decreased substantially. Fuel assembly neutron transport calculations of the Supercritical VVER-SCP with MOX fuel revealed the presence of hard neutron spectrum. Studying the applicable number of energy groups revealed that the usual 2 group approximation of water cooled reactors leads to high error in fuel assembly power prediction (See Figures 1-2). In the future the multigroup KIKO3DMG nodal code will be used for the studies.

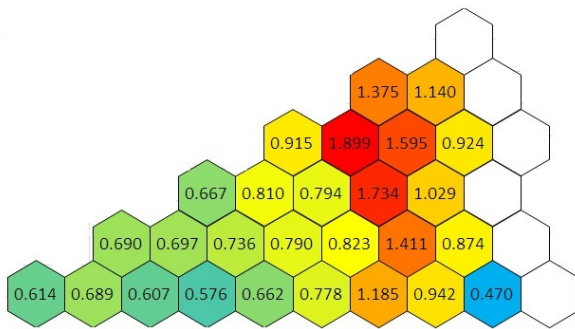


Figure 1: Radial power distribution of VVER-SCP using 2 energy groups

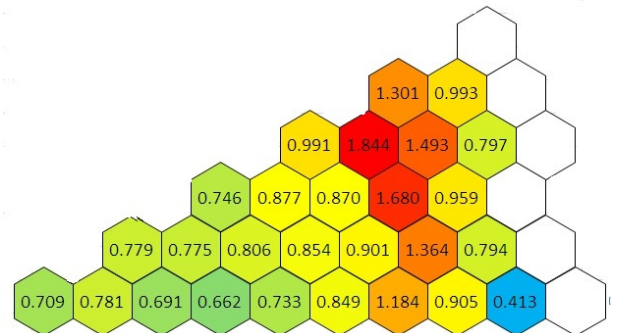


Figure 2: Radial power distribution of VVER-SCP using 6 energy groups

Remaining work

The project lasts more years, the development of tools for VVER-SCP analysis and their application will be continued.

Related publications

- [1] A. Szabó, Cs. Maráczy, Gy. Hegyi and I. Pataki: *On the Super-VVER Reactors*, 15th Nuclear Technology Symposium, Paks, 8-9 December 2016, in Hungarian (2016)
- [2] Gy. Hegyi, Cs. Maráczy, I. Pataki and A. Szabó: *Study on the Evolutionary Super-VVER and the Supercritical VVER-SCP Reactors*, MTA EK RAL-2016-210-01-01-M0, in Hungarian (2016)

NEUTRON TRANSPORT CALCULATIONS OF FUEL ASSEMBLIES TO BE APPLIED IN THE NEW PAKS UNITS

Csaba Maráczy, Gábor Hordósy

Objective

The general objective of the project is the development of the elements of a code system for the alternative solution of core design and safety analysis of the new Paks units. This year, the specific aim was to improve and apply methods for the generation of diffusion type group constants. For the fuel assembly calculations of the new Paks units the MULTICELL deterministic neutron transport code was envisaged, which has been already successfully applied in the case of VVER-440 reactors. Unlike VVER-440 reactors, in the VVER-1200 fuel assemblies the control rod cluster type reactivity regulation is used (Figure 1). The control rods strongly perturb the flux distribution. For enhancing the perturbation prediction of the exceptionally fast MULTICELL code, the infrequent application of high accuracy Monte Carlo calculations providing flux correction terms was aimed this year.

Methods

- Deterministic neutron transport and isotopic inventory calculations with the MULTICELL code.
- Monte Carlo neutron transport calculations with the MCNP code.
- Off-line coupling of the above codes.

Results

The off-line coupled MULTICELL-MCNP code was verified by high number of MCNP calculations covering different types of fuel assemblies, burnup and technological states. The multiplication factors and the pin wise normalized power distributions (k_k) were compared. We found a good agreement. In Figure 2 the statistical evaluation of the k_k differences is illustrated. The code system was applied for the generation of a cross section library with wide technological parameter range. More than 160 000 transport calculations were needed for this task.

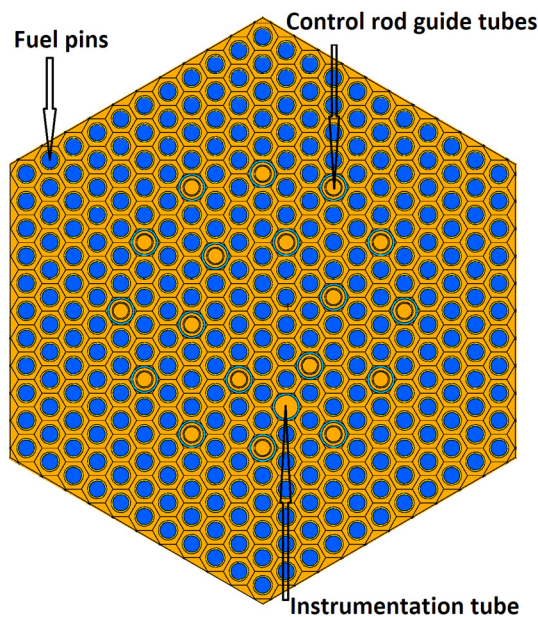


Figure 1: MCNP fuel assembly model

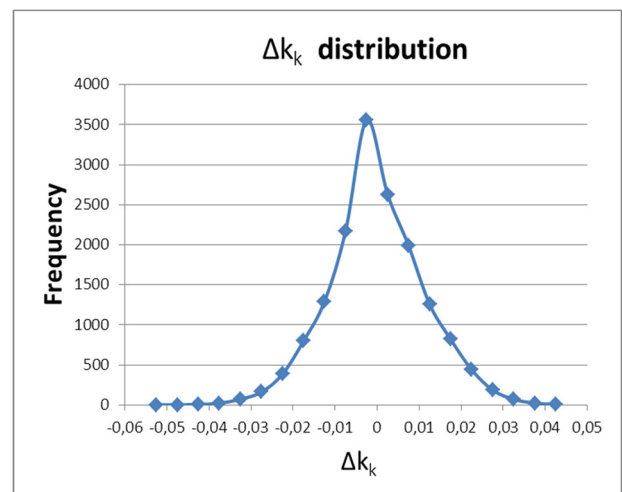


Figure 2: Distribution of k_k differences between MULTICELL and MCNP

Remaining work

No work remained in this field, but the project lasts 3 years with development and testing of further elements of the code system.

Related publication

- [1] Cs. Maráczy and G. Hordósy: *Deterministic Neutron Transport Calculations of Fuel Assemblies to be Applied in the New Paks Units with Monte Carlo Based Verification*, MTA EK RAL-2015-211-01-01-M0, in Hungarian (2016)

MODELLING THE TRANSPORT OF RADIONUCLIDES IN SURFACE WATER

Barbara Brockhauser, Sándor Deme, Tamás Pázmándi, Péter Szántó

Objective

To determine the environmental radiation burden of a possible liquid radioactive emission from the Paks Nuclear Power Plant, the radionuclide transport in the Danube must be considered, therefore, modelling the migration of radioactive materials in surface water after an accidental release is crucial. The objective of this 4-year work is to create a dynamic transport model that gives more accurate results than the currently used conservative one. To achieve this goal, realistic parameters are required to describe the local geological and hydrological properties of the river and the habits of the population to get parameter dependent dose conversions factors [Sv/Bq] for different age groups and exposure pathways.

Methods

To be able to describe the transport in detail, local site specific geological and hydrological parameters of the Danube are needed. These parameters include the local shape of the river's cross-section, the water level dependent flow rate, the flow velocity and also the local sediment data. With these data, the conversions of the general transport equations to site specific ones were made and the structure of the transport model was set. In an ideal case, the shape of the river's cross section could be characterized with one general shape (e.g. parabolic or trapezoid), but in real life, the cross sectional area was needed to be split into several different shapes (Fig. 1). Therefore, with different water levels, different equations were required to calculate the hydrological parameters.

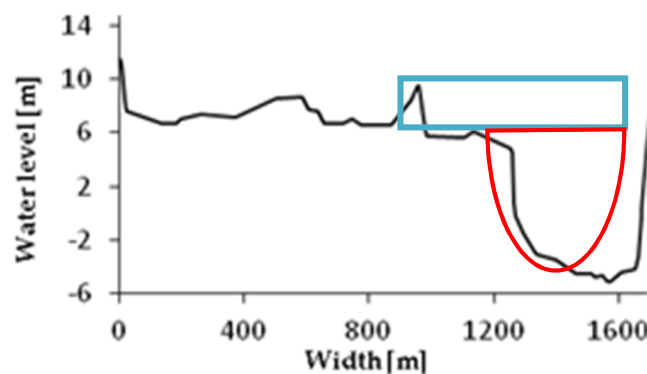


Figure 1: Shape of the river cross sectional area

Some approximations were made when calculating the mean flow velocity (u), because of the irregular shapes of the river bed terraces. Two basic equations (Eq. 1, Eq. 2) were tested for the mean water velocity calculation:

$$u = \frac{Q}{A} \quad (1)$$

$$u_{Manning} = \frac{1}{n} \left(\frac{A}{W_p} \right)^{2/3} \sqrt{S} \quad (2)$$

where Q is the flow rate [m^3/s], A is the cross section area [m^2], W_p is the wetted perimeter [m], S is the slope of the channel [m/m], and n is the Manning Roughness coefficient, which is 0,025 for the Danube.

Results

The used models and input data for the calculation were finalized and the algorithm of the program was developed.

Remaining work

This was the second part of a 4-year project. Further stage of the work consists of calculating the doses due to external and internal pathways. Field studies will be conducted for obtaining more accurate data about the habits of population living near the Paks Nuclear Power Plant, which will be used for the determination of dose conversion factor for dose calculations.

Related publication

- [1] B. Brockhauser, S. Deme, T. Pázmándi and P. Szántó: *Modelling the transport of radionuclides in the Danube under Paks: A site specific transport model*, EK-SVL-2016-225-01-01-00, in Hungarian (2016)

CALCULATION OF UNPROTECTED TRANSIENTS IN FAST SPECTRUM GEN-IV REACTORS

Bálint Batki, András Keresztúri, István Panka, István Pataki

Objective

The final goal in the future is to provide our three-dimensional neutron kinetic model, the KIKO3DMG code with group constants which are to be parameterized according to the temperature and corresponding thermal expansion effects. This 3D model will be used for the simulations of unprotected transients where the mentioned feedback effects play determining role, especially in case of fast spectrum reactors. The reported study is a preparation for this upcoming task and, correspondingly, the importance and the sensitivities of various reactivity feedback effects in two fast spectrum reactor types had to be investigated to support the answer how detailed parameterizations of the group constants concerning the different effects are necessary.

Methods

The SERPENT Monte Carlo and the ATHLET thermal hydraulic code were used for the ALLEGRO GFR (Gas Cooled Fast Reactor) demonstrator and for a 3600 MW_{th} power SFR (Sodium-cooled Fast Reactor). Fuel pellet, coolant, cladding and the wrapper temperature reactivity coefficients were determined by SERPENT. The evolving maximum fuel, cladding and coolant temperatures were determined by using the ATHLET system thermal hydraulic code with its built-in point kinetics.

Results

Spatially independent reactivity coefficients related to the active core were determined for the ALLEGRO gas cooled demonstrator and for a sodium-cooled fast reactor – specified in an OECD NEA (Nuclear Energy Agency) cooperation - with the SERPENT Monte Carlo code. Using ATHLET thermal hydraulic code with its point kinetics, transient simulations were performed for two types of unprotected transients (ULOF [Unprotected Loss of Flow] and UTOP [Unprotected Transient of Overpower]) with temperature dependent Doppler and constant coolant, fuel, cladding and wrapper expansion coefficients. The sensitivities of the fuel and cladding temperature maxima due to the individual reactivity coefficients were determined and compared also for the two reactor types. The Doppler effect proved to be the most important in case of both reactor types, followed by the fuel expansion effect. Coolant and cladding expansions have more significant impacts in case of ULOF than in case of UTOP. Considering the SFR, positive overall reactivity feedback can occur due to the coolant and the cladding reactivity effects.

Remaining work

There is no remaining work.

Related publications

- [1] B. Batki, I. Pataki, A. Keresztúri and I. Panka: *Reactivity effect impacts on the time evolution of the transients of fast spectrum reactors*, MTA-EK-RAL-2015-209 / VKSZ_14-1-2015-0021 report, in Hungarian (2016)
- [2] B. Batki, I. Pataki, A. Keresztúri and I. Panka: *Analyses of unprotected transients in GFR (ALLEGRO) and SFR reactors supporting the group constant generation methodology*, IAEA-CN-245-109 FR17, submitted FR17 conference paper. (2016)
- [3] B. Batki, I. Pataki, A. Keresztúri and I. Panka: *Investigations of transients in GFR and SFR reactors*, in Hungarian, 15th Symposium of the Hungarian Nuclear Society, Paks, December 8-9, (2016)

IMPLEMENTATION OF PIN POWER RECONSTRUCTION INTO THE KIKO3D CODE

István Panka, András Keresztúri, Csaba Maráczy, Emese Temesvári

Objective

It is well known that two VVER-1200 type reactor units will be constructed in Hungary at Paks. The fuel assemblies of the new reactors will be much larger and geometrically more complex than those applied in the existing VVER-440 units. There is an important difference between the two reactor types concerning the mechanical reactivity control system. In the VVER-440 reactors absorber assemblies are used while absorber rods will be implemented for the enhanced reactors. Through some guide tubes these absorber rods can be inserted into the assemblies directly, resulting in a large perturbation on the neutron flux distribution. This effect is especially important during rod movement (e.g. control rod ejection) transients because in this case the pin-wise neutron flux distribution is changing in space and time. In order to calculate these transients in a best-estimate manner, a pin-wise model is needed. Additionally, the feedback effects play an important role during Reactivity Initiated Accidents (RIAs), as well. Consequently, a thermal-hydraulic model of the core and of the fuel assemblies of the new units is also necessary.

Methods

In order to establish a pin-wise model during a RIA transient the so called pin power reconstruction method was applied. During the implementation of this technique, our own developed reactor physical codes were applied. The nodal reactor dynamic code KIKO3D was coupled with the pin-wise SADR1200 module of KARATE-1200 code system. Additionally, the KIKO3D code was coupled with a special version of the COBRA thermal-hydraulic code, as well. The assembly-wise COBRA model was supplied with relevant geometrical data.

Results

The elaborated new code system was tested by an asymmetric control rod ejection transient starting from the nominal power of the considered VVER-1200 reactor. For this purpose, an active core containing Gd doped fuel rods with fresh fuel assemblies was set up and modelled in the KIKO3D code. It was found that the obtained new results are logical and can be well interpreted. As an example, Fig. 1 shows the maximum values of pin-wise radial peaking factors ("Kk") in the assembly containing the ejected rods at different axial levels during the transient. It can be stated that maximum values of "Kk" are considerably changing during the control rod ejection.

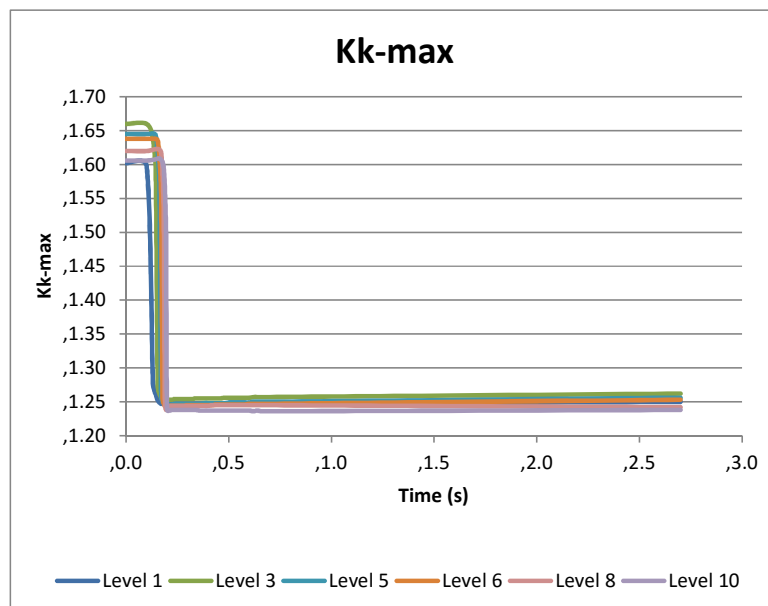


Figure 1: The maximal pin-wise radial peaking factors (Kk) in the assembly containing the ejected rods at different axial levels depending on time

Remaining work

The investigations should be supplemented by hot channel and fuel behaviour calculations.

Related publication

- [1] A. Keresztúri, Cs. Maráczy, I. Panka and E. Temesvári: *Development of the KIKO3D and COBRA codes for the calculations of some specific transients of the new units at Paks*, MTA MTA-EK-RAL-2015-291/1-M0, in Hungarian (2016)

VALIDATION OF THE KARATE CODE SYSTEM AGAINST THE LATEST OPERATIONAL DATA AND STARTUP MEASUREMENTS

István Panka, György Hegyi, Lajos Korpás

Objective

In the last decades, KARATE-440 was elaborated and developed continuously to calculate VVER-440 reactor cores by coupled neutron physical - thermal hydraulics models. The main goal of the calculations is the core reload design, however, certain safety analyses amenable to a static code can also be analysed by KARATE-440. The program serves economic core reload design so that the limitations demanded by the safety analysis should be observed. The latter function is utilized for the periodic independent check of the Paks NPP core design. On the other hand, in the last years several modifications of the VVER fuel construction and the corresponding core design aiming at more economic fuel utilization - like for example Gd doped fuel and 15-month fuel cycles - were introduced by Paks NPP which made further development of the models necessary. Having regard to the above situation, continuous validation from year to year against the latest operational and start-up measurements is indispensable for the establishment of the uncertainties and the margins for the calculated safety related frame parameters. In 2016, the cycles of Paks NPP realized in 2015 were used for the validation.

Methods

Model validation, comparison of the calculated and measured data.

Results

The following parameters were used for the validation:

- core burnup dependent radial peaking factors based on the assembly-wise in-core temperature rises,
- core burnup dependent operational critical boron concentrations,
- critical boron concentrations measured at the Minimum Controllable Power,
- moderator temperature reactivity coefficients measured at the start-up procedure,
- integral and differential efficiencies of the control rod groups.

According to the validation results, there are no significant changes of the deviations from the measurements as compared to the earlier cycles. As an example, Fig. 1 shows the comparison of the measured and calculated differential control rod group worth for Unit 3 using high enriched Gd doped fuel. The deviation is about 10 %, which is in the range of the measurement scattering.

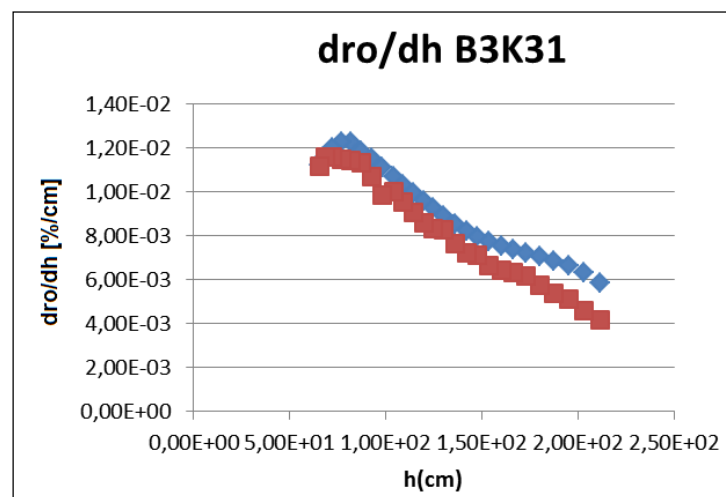


Figure 1: Measured (lower curve) and calculated differential control rod worth for Cycle 31 of Unit 3 depending on the control rod axial position ("h")

Remaining work

Continuous validation of the KARATE code system against measurements.

Related publication

- [1] Gy. Hegyi, L. Korpás and I. Panka: *Comparison of the KARATE 5.0 results with the measurements and C-PORCA calculations for the cycles of Paks NPP realized in 2015*, MTA-EK-RAL-2016-706/1-M0, in Hungarian (2016)

ESTIMATION OF THE UNCERTAINTIES OF THE POWER AND THE BURNUP AT NODAL AND PIN-WISE LEVELS BY THE STATISTICAL VERSION OF KARATE CODE SYSTEM

István Panka, György Hegyi, Csaba Maráczy, Emese Temesvári

Objective

The safe and at the same time economically competitive utilization of the recent and future nuclear installations can only be based on well-established reserves, “margins” responsible for the correctly evaluated uncertainties, which must be applied both for the normal operation and the accidental conditions. That is the reason of the increasing demand from nuclear research, industry and regulation for best estimate predictions provided with their confidence bounds. In order to support the well-validated evaluation of safety-related margins, the “statistical version” of the KARATE code system has to be developed. The improved code system can also be useful for the uncertainty evaluation of other, directly not measured parameters such as the power peaking factors of the fuel assemblies and pins. The final goal is to reduce the safety margins of the so called “frame parameters”, as far as possible.

Methods

Concerning the statistical method, basically an uncertainty propagation method was applied. At the first step, a sampling procedure for the selected isotopes and cross sections, and also for other relevant data (technological data, reactor power) is performed many times, and subsequently, the elaborated statistical methodology is applied. Finally, one can get the estimated standard deviations and /or correlations matrices for selected target parameters.

Results

In 2016, the uncertainties of an equilibrium cycle of Paks NPP were investigated. It was found that the assembly-wise power peaking factor has a considerable uncertainty due to the basic cross section uncertainties as it is demonstrated in Fig. 1. However, this uncertainty is greatly reducing during the burnup. Similar uncertainties were observed at pin-wise level, although it was pointed out that the uncertainties are considerably changing axially. Concerning the burnup, it was concluded that the uncertainties of the technological data are more important than the uncertainties of the basic cross sections due to burnup and refuelling. In case of the multiplication factor, the basic cross section uncertainties are dominant.

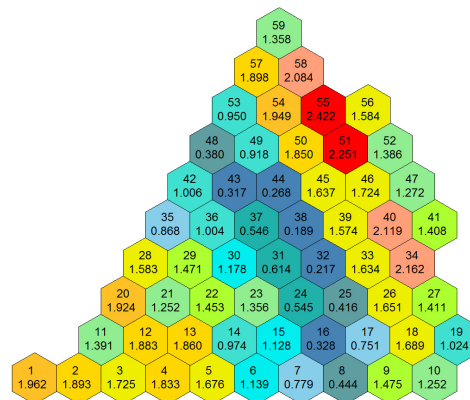


Figure 1: Relative standard deviations of the assembly-wise power peaking factor at beginning of cycle [%]

Remaining work

The planned work has been completed, although the treatment of the uncertainties of some technological data should be improved in the future.

Related publications

- [1] Gy. Hegyi, Cs. Maráczy and I. Panka: *Estimation of the uncertainties of the quantities related to the effective multiplication factor and the start-up measurements during the burnup by using the statistical version of the KARATE code system*, MTA EK-RAL-2015-988/2-M0, in Hungarian (2016)
- [2] I. Panka, Gy. Hegyi, Cs. Maráczy and E. Temesvári: *Some uncertainty results obtained by the statistical version of the KARATE code system*, in Hungarian, Proceedings of the twenty-sixth Symposium of AER, Helsinki, Finland, 10-14 October, 2016 (2016)
- [3] Gy. Hegyi, Cs. Maráczy, I. Panka and E. Temesvári: *Development of the statistical version of KARATE code system at pin-wise level, demonstration of the applicability by large number of runs*, MTA EK-RAL-2016-904/1-M0, in Hungarian (2016)
- [4] Gy. Hegyi, Cs. Maráczy, I. Panka and E. Temesvári: *Estimation of the uncertainties of the power and the burnup at pin-wise level by the statistical version of KARATE code system*, MTA EK-RAL-2016-904/2-M0, in Hungarian (2016)

USING HZP STATES OF PAKS NPP FOR THE VALIDATION OF BURNUP CREDIT CALCULATIONS, CONSIDERATION OF THE UNCERTAINTY OF ISOTOPIC COMPOSITION

István Panka, György Hegyi, Gábor Hordósy, Csaba Maráczy

Objective

The subcriticality analysis of a spent fuel storage facility is strongly influenced by the uncertainty of the calculated multiplication factor (k_{eff}) due to the uncertainties of nuclear cross section data. Traditionally, this uncertainty was determined from comparison of calculated and measured k_{eff} values for a number of critical experiments.

This approach can easily be applied to cases with fresh fuel, because there are a number of publicly available critical experiments with fuel enrichment, moderator, geometry etc. similar to the storage facilities. However, when burnup credit is applied in the subcriticality analysis i.e. the change of reactivity due to the change of composition with burnup is considered, the problem arises that there are no published critical experiments where the fuel composition is similar to the composition of the spent fuel.

A possible solution is to determine the discussed uncertainty by calculation using the covariance data of the cross sections and use the HZP (Hot Zero Power) states of operated NPP's for checking the calculations. In this case, an additional task is to assess how representative the considered HZP states are for the storage facility in connection with the fuel composition. The work was started in 2015, recently the most important task has been the consideration of the uncertainty of isotopic composition.

Methods

Concerning the statistical method, a Monte-Carlo type, sampling based methodology was used. At the first step, a sampling procedure for the selected isotopes and cross sections is performed many times, and subsequently, the elaborated statistical methodology is applied. Finally, one can get the estimated standard deviations or the results can be evaluated using the Wilks' method in case of small sampled values. In the latter case, the calculations can usually be characterized by tolerance intervals with 95%/95% probabilities.

Results

In 2016, the elaborated full core MCNP model was improved. First, real HZP states of Paks NPP were calculated by the new model. These results correspond to the so called best-estimate calculation. After that, the elaborated statistical methodology based on the Wilks' method and on the determination of the estimated standard deviation was applied to determine the uncertainties of the effective multiplication factors. The composition of the fuel was taken from the calculation results obtained from the statistical version of KARATE code system, which means that the effect of uncertainties of the compositions was also taken into account in this study.

In connection with the effective multiplication factor, several HZP states were successfully investigated, the results are demonstrated in Table 1 for a given HZP state. It can be concluded that the "full" uncertainty (σ) of the multiplication factor is about 0.7%, and the differences between measurements and calculations are covered by the obtained uncertainties with a high confidence.

Table 1: Uncertainties (σ values) of the effective multiplication factor for a given HZP state

Source of uncertainty	σ
Criticality calculation, basic isotopes	4.94E-03
Criticality calculation, every isotope	6.05E-03
Criticality calculation, every isotope + technological uncertainty	6.23E-03
Criticality calculation+ isotope composition, every isotopes + technological uncertainty	6.88E-03

Remaining work

There is no remaining work scheduled for 2016, although the researches should be continued by investigating the recently applied Gd doped fuels.

Related publication

- [1] Gy. Hegyi, G. Hordósy, Cs. Maráczy and I. Panka: *Using HZP states for the validation of burnup credit calculations, Part 2*, MTA-EK-RAL-2016-906/M0, in Hungarian (2016)

APPLICATION OF DISCONTINUITY FACTORS AND GROUP CONSTANTS GENERATED BY SERPENT IN THE KIKO3DMG CODE

Bálint Batki, András Keresztúri, István Pataki

Objective

The DF ("Discontinuity Factor") methodology is introduced worldwide in order to compensate the error of the homogenization used in the usual nodal methods, namely the shortcomings originated from the following characteristics and issues.

- In case of the nodal methods, the reactor is represented by homogenized regions, nodes (e.g. assemblies subdivided by axial layers), while really a pin wise heterogeneous structure of the neutron flux is prevailing.
- In the nodal methods, inside the nodes the fluxes (the analytical trial functions) are assumed to be smooth, additionally their continuity on the node boundaries is applied.
- On the other hand, really, the continuity of the real flux with its heterogeneous structure should be required.

Consequently, the measure of the discontinuity of the smooth nodal solutions is to be determined and required to assure the continuity of the real flux.

Methods

The SERPENT Monte Carlo code was used to provide the nodal code KIKO3DMG with DFs or/and DF related quantities. In KIKO3DMG, the unknowns are the scalar flux integrals on the node boundaries. This feature – together with the SERPENT fluxes and currents – made KIKO3DMG especially applicable to investigate the effectiveness of the DF concept. The average node-boundary wise net currents and scalar fluxes – provided also by SERPENT – allow preparing DFs for any nodal method, for example also for the KIKO3DMG nodal method. The VVER-440 full core benchmark was used to investigate the effectiveness of the concept. For this benchmark, other Monte Carlo result calculated by the MCNP Monte Carlo code is also available.

Results

- Considerable difference was obtained between the SERPENT and MCNP „reference solutions”, nevertheless the SERPENT results were regarded as a new reference because of the necessity of using consistent data.
- Noticeable improvement was obtained by using the spectrum dependent SERPENT homogenized group constants for the fuel regions instead of the asymptotic ones.
- Considerable improvement of the boundary fluxes could be achieved by applying DF methodology, but the appropriate DF values proved nodal method dependent.
- The DF improvement could be effective also for the node wise power distribution only in case of applying an additional local improvement factor („VF”), which is the ratio of the average transport boundary flux to the volumetric one.
- The solution based on the asymptotic group constants could not be improved by the DF methodology.

Remaining work

The investigations are to be repeated to the other VVER full core benchmarks.

Related publication

- [1] A. Keresztúri, I. Pataki and B. Batki: *Preparing discontinuity factors and their application in a nodal code*, MTA EK-RAL-2016-907-01/01 report, in Hungarian (2016)

INVESTIGATION OF OPTICAL, ACOUSTIC AND THERMOELECTRIC PROPERTIES OF ZIRCONIUM CLADDINGS

Péter Petrik, Tivadar Lohner, Benjamin Kalas, Emil Agócs, Richárd Nagy, Tamás Novotny, Erzsébet Perez-Feró, Zoltán Hózer, László Dózsa, János Ferencz, Gábor Pető

Objective

The main objective of the performed studies was the characterisation of optical, elastic, acoustics and thermoelectric properties of Zr cladding of nuclear fuel with the introduction of new measurement techniques. The evaluation of the applicability of the applied methods for the estimation of H content and degree of oxidation of Zr was another goal of the project.

Methods

Cladding tubes were prepared from original Zr cladding provided by the Russian fuel supplier. Part of the measurements was performed with as-received materials. Several samples were oxidised in high temperature steam to produce different degrees of oxidation. Hydrogen charging was applied in a high temperature furnace in order to prepare samples with different hydrogen contents. Optical and X-ray measurements were made using a Woollam M-2000DI rotating compensator spectroscopic ellipsometer and an ESA 105 (Stalib Instruments Ltd.) XPS equipment. Acoustic resonances were measured in ambient atmosphere applying varying frequency excitation in the 1 kHz-10 kHz range. Thermoelectric voltage was measured between tungsten tips kept at approximately 30 ± 5 °C and 220 ± 20 °C temperatures. The measurement can be used to measure the H content with a few micron spatial resolution.

Results

The optical study showed that the tubes can be measured using our commercial ellipsometer when applying focussing with proper alignment. We determined the optical properties and compositions (Fig. 2) of both the surface oxide and the bulk Zr material that can be used as references in further studies. These data and the developed models were used to measure the oxide thickness as a function of the annealing temperature.

Acoustic measurements show that the effect of H content on the resonance frequencies is comparable to the effect of applied annealing and scatter of the physical size parameters of the Zr tubes. The loss introduced by the fixing, by the excitation and by the detector elements dominate the loss of the measured resonances.

Thermoelectric measurements show clear effect of hydrogen content on the thermovoltage. The effect of the oxide layer on the Zr tube is detected by using 10 Ohm and 100 Ohm load resistances. The surface oxide has to be removed by some standard method for better interpretation of the results in further experiments.



Figure 1: Zr cladding oxidised at 600 °C for 60 s

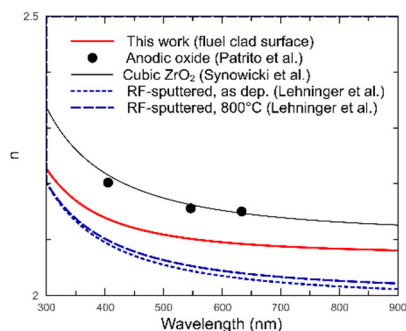


Figure 2: Refractive index of ZrO₂ from the multi-sample evaluation compared to literature references [1]

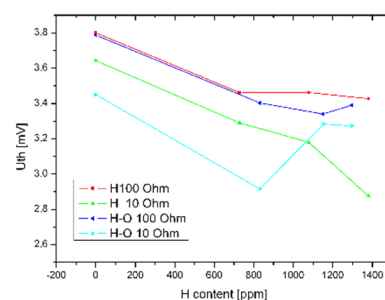


Figure 3: Thermoelectric voltage measured using 10 and 100 Ohm load resistances in H charged Zr cladding samples [2]

Remaining work

The planned work has been completed. It is intended to use the developed methods for the characterisation of samples from experiments simulating normal operational and accident conditions in a NPP.

Related publications

- [1] P. Petrik, A. Sulyok, T. Novotny, E. Perez-Feró, B. Kalas, E. Agócs, T. Lohner, D. Lehninger, L. Khomenkova, R. Nagy, J. Heitmann, M. Menyhard and Z. Hózer: *Optical properties of Zr and ZrO₂*, Applied Surface Science, Available online 21 December 2016, <http://doi.org/10.1016/j.apsusc.2016.11.072>
- [2] L. Dózsa: *Acoustic and thermoelectric investigations with zirconium cladding*, MTA EK-FRL-2016-123-1-1-M0, in Hungarian (2016)

ADVANCED MODELS FOR FUTURE STRUCTURAL INTEGRITY CALCULATIONS

Tamás Fekete, Dániel Antók, Levente Tatár

Objective

Structural Integrity (SI) refers to a branch of engineering science that studies engineering/ (building) structures, focusing on the ageing of structural materials and their defective character. SI has a crucial role in designing safe structures that work in various conditions without catastrophic damage such as brittle fracture, tearing or collapsing. Methodologies based on the Structural Integrity concept include evaluating cases of normal operation conditions as well as accidental situations that have previously occurred or are likely to occur (at or) above a certain risk level, in order to prevent failures of a structure until the end of its service lifetime.

The Reactor Pressure Vessels (RPVs) are the critical components of a nuclear power plant (NPP), as they limit the lifespan of power plants the most. RPVs have large cross-sections (e.g. VVER-440 V213: 149 mm wall thickness with 3800 mm diameter); they work at elevated temperatures ($\approx 270 - 290$ °C) and high pressure(s) (≈ 12.2 MPa). The most important function of the RPV is maintaining constant pressure and temperature conditions that are necessary for controlled power generation during operation. It is also responsible for heating up and cooling down the reactor and, in case of emergency, for cooling down the core and preventing the release of radioactive materials into the containment. The most relevant ageing mechanisms in the structural materials of an RPV are: (1) neutron irradiation assisted ageing, (2) fatigue and (3). thermal ageing. The evaluation of the SI of long term operating RPVs requires adequate knowledge of thermo-mechanical constitutive behaviour (i.e. stress-strain characteristics) and the fracture mechanics properties of their structural materials in various aged states.

The SI of fuel rod cladding tubes is another very important branch of the nuclear reactor technology. Their fast fracture could cause unacceptable release of radioactive products into the coolant liquid of the primary circuit, so these cladding tubes are also safety relevant points.

Today, there is a growing demand for simulation models that have better predictive capabilities than the generally applied engineering models. This requires the application of more physically based, more complex, nonlinear models for future SI analyses of safety-critical NPP components. All physical systems in the real world are inherently nonlinear. One of the most difficult tasks of an analyst is to decide whether a nonlinear analysis is really needed, and if so, exactly where, and to what degree.

During SI analyses, the ultimate nonlinear behaviour of a component can be considered as a result of synergistic effects of four nonlinear 'basic' mechanisms: 1) change in the geometry of the component (large deformations occurring at least locally); 2) elastic-plastic or elastic-viscous-plastic material behaviour; 3) change of relevant material parameters along the temperature-path; 4) change of relevant material parameters during operation. Because of the inherent nonlinear character of each problem, the effects of the four basic mechanisms cannot in general be entirely separated from each other, so the interactions between these 'basic' mechanisms make the development of a methodology for nonlinear SI problems a challenging research topic.

The treatment of kinematics taking into account geometric nonlinearity is considered more applicable, as from a physical point of view, the nonlinear theory permits the consideration of increased generality and deeper insight afforded by the finite deformation theory. Complex material models are needed to describe connected material phenomena more precisely wherein strains can be inevitably large. A new modelling framework needs more advanced methods for the evaluation of material tests.

The final objective of the research program is to develop a unified, coherent analysis methodology and advanced models for future nonlinear SI calculations of various safety relevant systems of NPP units.

The main research directions of the program are formulated as follows:

- Large deformation models for analyses of engineering structures;
- Complex material models for thermo-mechanical problems;
- Advanced assessment methods for evaluations of material tests;
- Long-time ageing of RPV structural materials.

Methods

A systematic literature overview has been conducted in the theoretical project in order to collect state-of-the art theoretical and simulation methods that seem promising for further development of them, and seem ideal for applications in future industrial projects. In the modelling part, numerical models are being developed for special research problems first. These models will further be developed for industrial purposes.

Results

In the modelling part of the project, a calculation methodology that simulates the ballooning tests of fuel cladding tubes (Fig. 1. a) has been developed based on a geometrically and materially nonlinear formulation of the problem. Large deformation plasticity theory was applied to model the effects of geometrical and material nonlinearities that are present in the system during calculations. The flow curves of structural materials are being developed from tensile test results. Numerical calculations were performed using the MSC Marc FEM code. During the process, a parametric study was conducted to assess the influence of geometrical imperfections and material inhomogeneities on the test results, because –based on theoretical considerations– it was expected that even small geometrical imperfections or material inhomogeneities can have strong effects on the final state, more specifically the geometry and stress-strain state of the test piece.

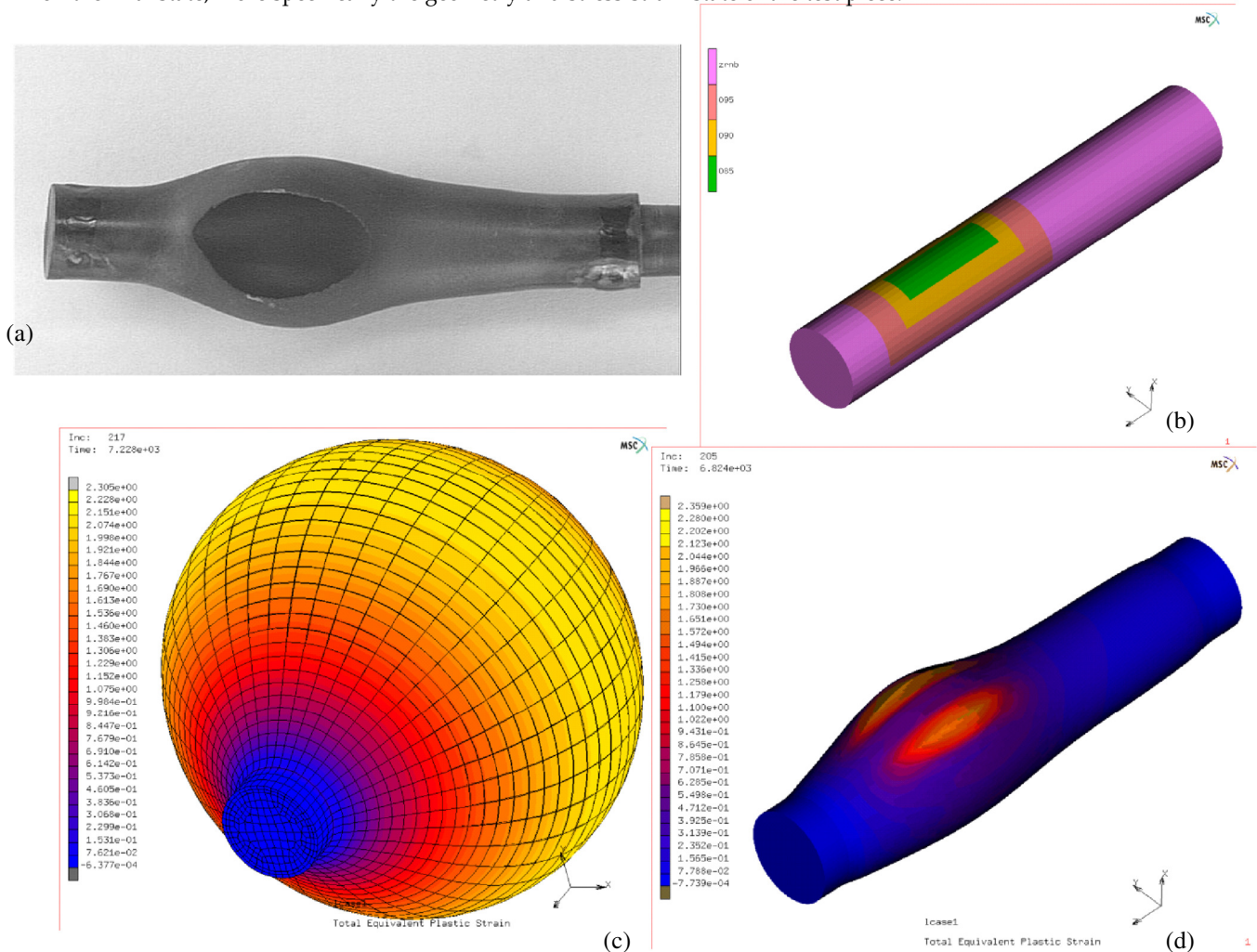


Figure 1: A fuel cladding tube piece after the ballooning test (a), FEM model of the tube with initial material inhomogeneity (b), results of a simulation performed on a materially homogeneous model (c), and on a materially inhomogeneous model (d)

The 3D finite element models of the ballooning specimens have been tested. The simulations have been performed on a geometrically perfect tube, in case of a materially homogeneous model and in case of a model with assumed material inhomogeneity (Fig. 1. b). The calculation results are presented in Fig 1. (c) and (d). It can easily be seen that in case of perfectly homogeneous material properties distribution, the initially axial-symmetric shape of the specimen remains axial-symmetric, and the strain field (plastic strain field) also preserves this symmetry (Fig. 1. c). In case of a specimen having inhomogeneous material property distribution, the final shape and the (plastic) strain field evolves into a nonsymmetrical 3D structure (Fig. 1. d). Comparing the calculated shapes with the experimental result depicted in Fig. 1. a, it can be concluded that the tested ballooning specimen most likely had some initial material inhomogeneity. Based on the improved theoretical and numerical results, it can be stated that more complex models help deeper understanding of the events occurring during material tests as well as contribute to the development of more advanced models for future SI calculations.

Remaining work

Further models in frame of the above depicted research directions are in research phase.

IRRADIATION OF P91 MATERIAL

Levente Tatár, Attila Kovács, Gábor Uri, Ildikó Szenthe, Dániel Antók

Objective

Grade P91 (also known as T91) is a ferritic-martensitic (9% chromium, 1% molybdenum) steel micro-alloyed with vanadium. Used in fossil-fuelled power plants, due to its excellent elevated-temperature strength and creep behaviour up to 580 - 600 °C, this steel is a candidate material for future generation IV reactors.

To be allowed to use it as structural material in nuclear reactors, it has to be proved that the properties of P91 material can withstand the concomitant damaging effect of high temperature and high neutron radiation for a long period of time. Of particular interest is studying and quantifying the change of fracture toughness after high temperature irradiation.

Methods

From the P91 steel piece received in the framework of the MATTER EU FP7 project, 3-point bending samples were manufactured. The specimens were precracked taking into account the strict prescriptions of the ASTM E-1921 standard. Neutron activation calculations were done prior to the test. Pre-calculations have shown that due to high activation no more than three irradiation campaigns (30 days) can be performed in order to be able to do the tests in our lab within an acceptable timeframe.

The samples were irradiated in the Budapest Research Reactor (BRR) in the Bagira3 gas-cooled irradiation rig for three campaigns. The Bagira3 rig had a detachable target holder divided into six levels with a capacity of 6 Charpy size specimens at each level. Temperatures were continuously monitored at each level of the target-holder. Cooling was assured by a He-N₂ gas mixture, while adjustments of the temperature profile was done by individual electrical heating at each level (see Fig. 1). The P91 specimens were situated at levels 1 and 2 of the target holder together with dosimetry foils.

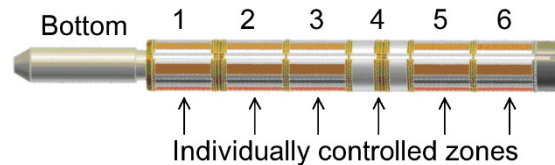


Figure 1: Target holder of the Bagira3 irradiation rig.

This rig was an upgrade of the Bagira1 and Bagira2 irradiation rigs. The operating temperature range of the Bagira1 and Bagira2 irradiation rigs has been increased from 200-350 °C to 150-650 °C. This was made possible by partial replacement of the Al structure of the rig to Ti-based structure. Due to the fact that the vertical channel in which the Bagira3 rig was placed was in a peripheral location of the active zone of the BRR, the target of the Bagira3 irradiation rig was slowly rotated by a stepper motor. Unfortunately, the Bagira3 irradiation rig is not in service any more as the irradiation channel got other uses.

Results

By controlling the electrical heating of the individual zones, the irradiation temperatures were kept at approximately 550 °C. As an example, the temperatures from the third irradiation campaign are presented (Fig. 2).

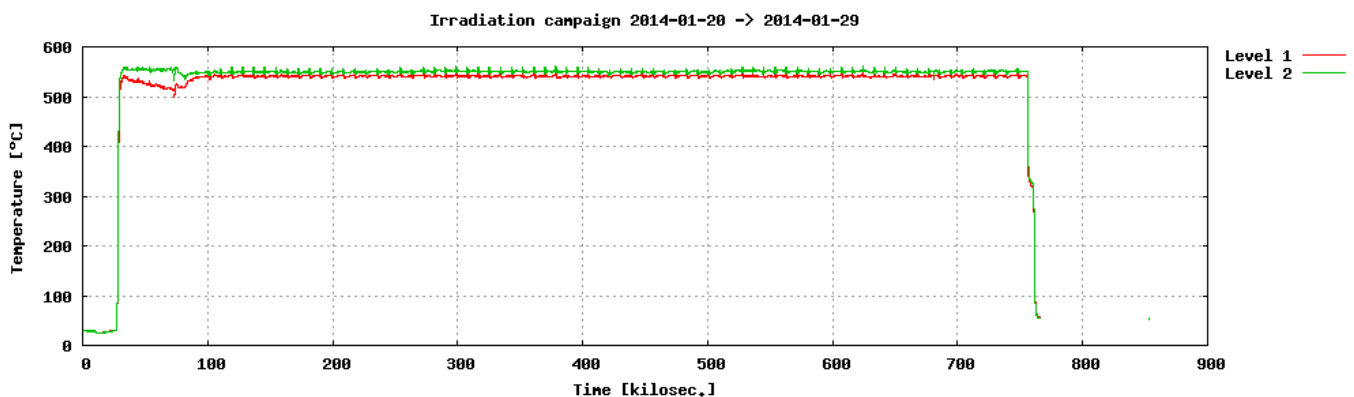


Figure 2: Time-temperature diagram for the third irradiation campaign.

Based on post-irradiation examination of dosimetry foils 0.05 dpa radiation damage could be estimated.

Remaining work

Initially the three-point bending tests were scheduled for 2016, however, the activity of the specimens did not permit the effectuation of the tests so these are postponed for 2017.

INTRODUCTION OF NEW FUEL TYPES TO THERMAL POWER PLANTS: MOX AND REMIX FUEL

Emese Slonszki, Attila Nagy

Objective

This work aims to show the advantages and disadvantages of using reprocessed fuel, MOX (Mixed OXide) and REMIX (REgenerated MIXture of U-Pu oxides), in current and future thermal reactors against UO_2 fuel.

Methods

We summarized the main aspects and requirements of storage and handling of MOX and uranium fuel assemblies; compared behaviour of high burnup MOX and UO_2 fuels during normal operation and reactivity-initiated accident; studied characterization of fast breeder and thermal MOX fuel and, finally, evaluated the differences between MOX and REMIX fuel based on literature data.

Results

The helium gas release was high for the MOX fuel, while it was low for UO_2 fuel. Fission gas release as irradiation behaviours too, which affected the integrity of fuel, have shown slight differences in MOX fuel compared to UO_2 fuel, while the swelling of MOX pellet, the oxidation of cladding inner surface and heat conduction were very similar over 60 MWd/kgHM burnup and during normal operation.

PCMI (Pellet Cladding Mechanical Interaction) cladding failure threshold of MOX fuel depends only on the state of corrosion if the pellet-cladding interaction is due to the thermal expansion of tablets during the reactivity-initiated accident. Failure threshold of UO_2 fuel could be applied for MOX fuel too. The fission gas release of MOX fuels was higher than UO_2 fuels. The mechanical behaviour of MOX fuel is different from UO_2 fuel at high temperature, while it favours to the radial hoop strain in MOX, until it does not for the clad elongation and the creep rate increases with irradiation.

The REMIX fuel which is in fact reprocessed MOX fuel, can be reprocessed up to five times. Closed fuel cycle can be created using REMIX, furthermore, it can be used with 100% core load in current VVER-1000 reactors (from Russian: Водо-водяной энергетический реактор; transliterate as Vodo-Vodyanoi Energetichesky Reaktor; Water-Water Power Reactor). Reprocessed uranium will not be accumulated using REMIX fuel in contrary to MOX. The natural uranium consumption can be reduced using MOX or REMIX fuel that may be about 20% in case of REMIX fuel.

Based on literature data, the neutron-physical characteristics of a VVER-1000 core with a 100% load REMIX fuel, e.g. the reactivity coefficients remain within the nominal range for VVER-1000. The maximum fuel burnup in fuel assemblies and fuel elements, the maximum relative energy release in fuel assemblies and fuel elements and the linear heat rate of a fuel element do not exceed the established limits for a VVER-1000 core with uranium fuel.

Remaining work

This project has been completed.

Related publication

- [1] E. Slonszki and A. Nagy.: *Introduction of new fuel types to thermal power plants: MOX and REMIX fuel*, MTA EK-FRL-2016-274-1-1-M0, in Hungarian (2016)

A REVIEW AND SIMULATIONS OF EXPERIMENTS REGARDING NEW FUEL TYPES

Eszter Kozsda-Barsy, Emese Slonszki, Katalin Kulacsy, Attila Nagy

Objective

The Paks Nuclear Power Plant currently operates with hollow pellets. This fuel geometry has the advantage of lower maximum fuel temperature and better gas flow. For a higher performance, however, an increased amount of fuel is needed, which can be achieved e.g. by introducing solid pellets. For the first part of the project a literature review on experiments introducing solid fuel pellets was prepared. This served as a basis for simulations: an actual experiment was simulated and several specific case studies on the differences between the behaviour of solid and hollow fuel pellets were made.

Methods

The data used for the experiment simulation was taken from the Halden database, and for the case studies realistic performance curves were produced. The input files were prepared with FRAT (Fuel Rod Analysis Toolbox) and the simulations were made using the fuel performance code TRANSURANUS. The output was processed with the TRANSURANUS Input Editor.

Results

The literature review on solid and hollow-pellet fuels covered the most important experiments and studies that have been made in recent years. A Russian calculation confirmed that solid pellets were suitable for use in third generation VVER-440 fuel rods in modern fuel operation cycles. Based on the serviceability of solid fuel in a nuclear power plant and its successful tests in the Halden experiments, during which no adverse effects were experienced, VVER-440 fuel cycles seem to be feasible using solid pellets.

The simulations confirmed the results found in the literature. In the first part, two rods of the Halden IFA-681 experiments (one with solid, one with hollow pellets) were modelled, with two power histories each. Concerning the relevant parameters (such as temperature, pressure) the code approaches well the experimental data. With increasing heat rate the temperature of solid pellets rises to higher values than that of hollow pellets. The difference in the amount of fission gas released was quite large between the two pellet geometries, though no significant difference was observed in pin pressure. With the geometric characteristics of the Halden rods there was no significant difference between the solid and hollow pellets from a thermo-mechanical point of view. In the second part, Russian second- and third-generation fuel pins were modelled with three fictional power histories each. It is important to mention that the third-generation rods differ not only in the central hole, but also in the pellet outer and the cladding inner diameters. Notable thermo-mechanical behavioural differences were found only in the case of power ratings that were at the upper edge or over the commercial range (see yellow and green curves in Fig. 1, respectively). In average operational conditions the state of the different rods did not differ much. The relevant design criteria were also met in realistic cases, for example the creep of the rod does not exceed the limit for fuel deformation (Fig. 1), though there is an expected difference between solid (solid curves) and hollow (dashed curves) pellet behaviour at higher burnup.

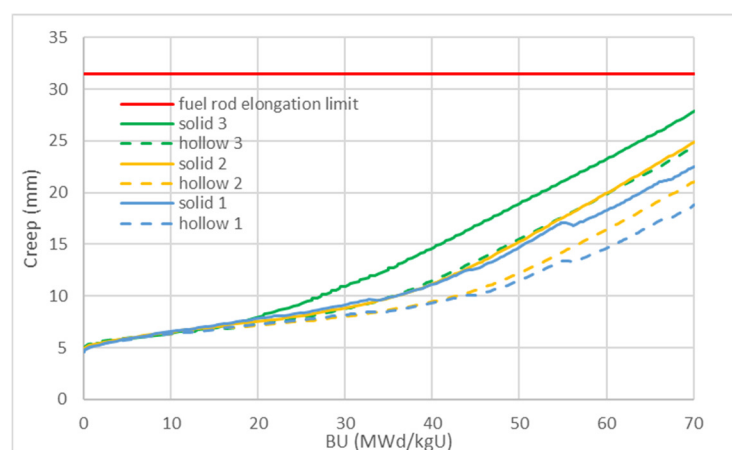


Figure 1: Simulation results on cladding elongation

Remaining work

The project was finished as planned.

CODEX-LOCA EXPERIMENTS

Zoltán Hózer, Imre Nagy, Nóra Vér, Mihály Kunstár, Róbert Farkas

Objective

The main objective of the integral tests performed in the CODEX (Core Degradation Experiment) facility was to study the behaviour of pressurized E110 and E110G claddings under high temperature LOCA (Loss of Coolant Accident) conditions.

Methods

Electrically heated 7 rod bundles were used for the simulation of LOCA events. The 7 rod bundles were composed of fuel rods with E110 and E110G cladding types. The boundary conditions of the tests were selected on the basis of reference calculations performed in the framework of the safety analyses for Paks NPP.

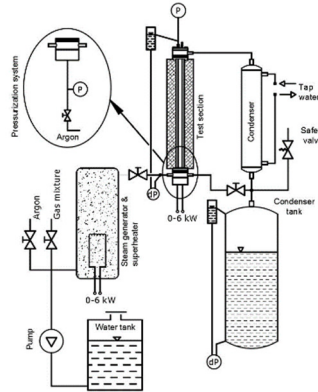


Figure 1: Main components of the CODEX facility

Two experiments were carried out: CODEX-LOCA-200B simulated a large break LOCA event starting from nominal reactor power, while in the CODEX-LOCA-E4 the reference scenario was representative for shutdown conditions.

Results

During the CODEX-LOCA-200B experiment, the maximum temperature reached 874 °C. The fuel rods did not lose their integrity. The maximum internal pressure was 14.8 bar. The oxidation was very modest due to short (200 s) dry period at high temperature.

The 1089 °C maximum temperature in the CODEX-LOCA-E4 test was measured at 400 mm position of the 600 mm long bundle. All fuel rods ballooned and burst during the transient. The long (600 s) dry period at high temperatures resulted in formation of spalling oxide scale on the E110 cladding tubes, while modest and compact oxide scale was formed on the E110G tubes. After the test, the bundle was removed from the shroud and the E110 tubes were broken. The E110G tubes kept their integrity during these conditions.

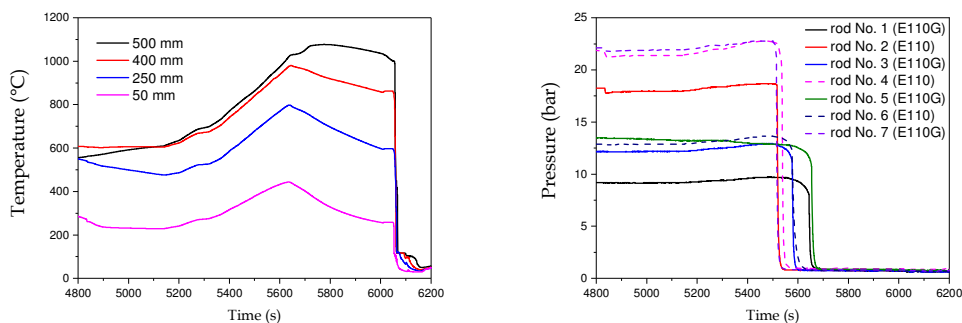


Figure 2: Temperature (left) and pressure (right) histories in the CODEX-LOCA-E4 test

Remaining work

Another CODEX test will be carried out in 2017 to simulate spent fuel pool LOCA scenario.

Related publications

- [1] I. Nagy, N. Vér, M. Kunstár, R. Farkas, P. Szabó and Z. Hózer: *Simulation of a shutdown LOCA event in the CODEX facility*, MTA EK-FRL-2016-701-1-1-M1, in Hungarian (2016)
- [2] I. Nagy, N. Vér, M. Kunstár, R. Farkas and Z. Hózer: *Simulation of 200% LOCA in the CODEX facility*, MTA EK-FRL-2016-701-1-2-M0, in Hungarian (2016)

SIMULATION OF LEAKING FUEL RODS WITH THE RING CODE

Zoltán Hózer, Péter Szabó

Objective

The original version of the RING (Release of Iodine and Noble Gases) computer code gave estimation on the number of leaking fuel rods on the basis of average power. The main objective of the present work was to provide a numerical model for the estimation of the linear heat rate of the leaking fuel rod.

Methods

Standalone testing was performed with Excel tables. When the correct algorithm was found it was built into the RING code in FORTRAN programming language. Beyond the linear heat rate iterations an additional module was built into the code to provide estimation on the burnup of the leaking rod on the basis of measured activity concentrations of two caesium isotopes. Due to the modification of the original algorithm, it was necessary to repeat the fitting of model parameters for the simulation of shut-down iodine spiking.

Results

The new version of the computer code (RING 2.0) was produced and installed into the Chemical Expert System of Paks Nuclear Power Plant.

Several series of calculations were performed using the activity concentration measurements of Paks NPP (Fig. 1). It was shown that the new code version was a useful tool for the identification of leaking fuel rods.

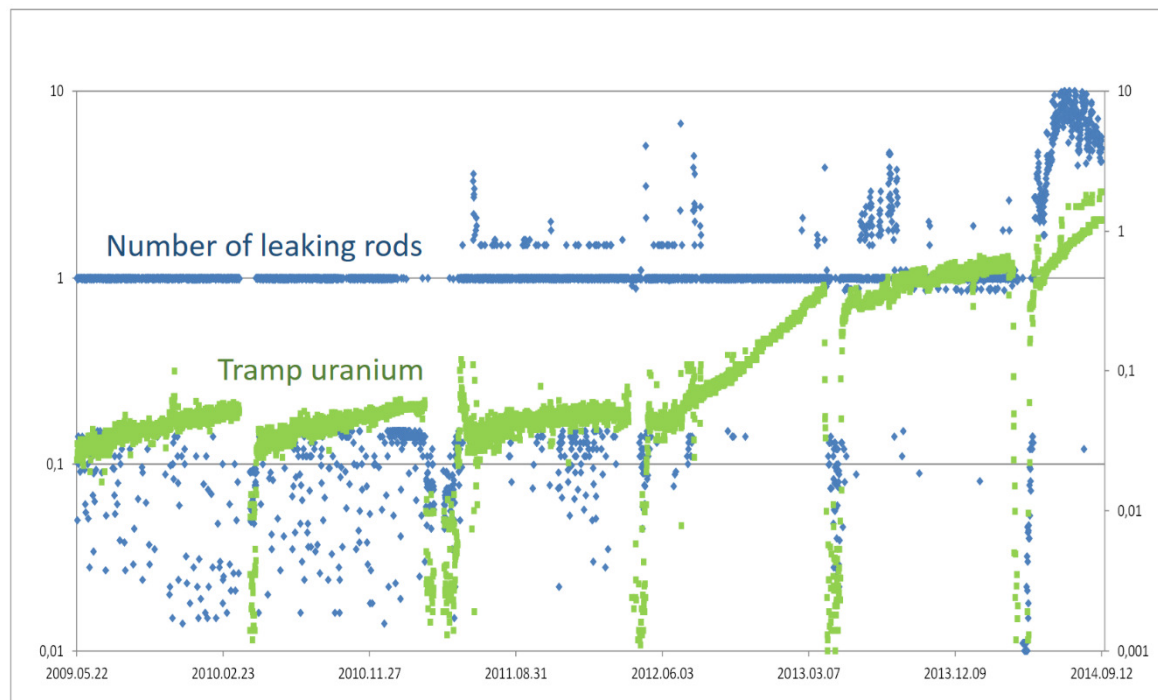


Figure 1: Estimated number of leaking fuel rods and mass of tramp uranium

Remaining work

The planned work has been completed.

Related publications

- [1] Z. Hózer and P. Szabó: *Development of numerical methods for the simulation of leaking fuel rods with different power*, MTA EK-FRL-2016-704-1-1-M0, in Hungarian (2016)
- [2] Z. Hózer: *The RING 2.0 Computer Code*, MTA EK-FRL-2016-704-1-2-M0, in Hungarian (2016)

AXIAL DISTRIBUTION OF RADIOACTIVE ISOTOPES IN A LEAKING FUEL ROD

Péter Szabó, Katalin Kulacsy, Zoltán Hózer

Objective

The TSKGO computer code was developed in order to simulate activity release from leaking fuel rods during reactor operation and different manipulations including telescope sipping examination. The original version of the code simulated the fuel rod as a single node. The main objective of the present work was to introduce a new model for the description of axial distribution of fission products in the gas volume of the leaking fuel rod.

Methods

The initial axial distribution of isotopes is calculated by the FUROM code, this distribution is representative to the intact fuel rod. The axial distribution inside of the leaking fuel rod is calculated by the TSKGO code. The transport model is based on the diffusion of atoms in the gas-steam mixture and the intensity of mass change between neighbour nodes is proportional to the difference of concentrations. The simulation includes 32 isotopes and 41 axial nodes.

Results

The first calculations with the modified models demonstrated that the axial distribution of fission products in the leaking fuel rod can be tracked and the calculated profile showed a physically correct picture (Fig. 1).

The new model allows the simulation not only of a single defect but also of multiple defects in the fuel rod. Using this approach, secondary failures of already leaking fuel rod can be simulated, too.

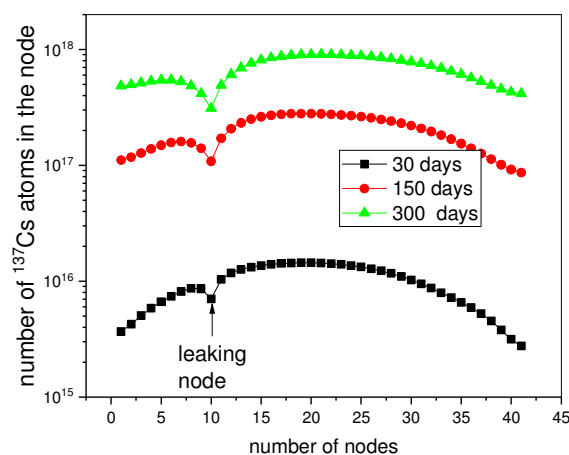


Figure 1: Axial distribution of ^{137}Cs atoms in the gap of a leaking fuel rod

Remaining work

Detailed transient model will be developed for the simulation of shut-down and start-up transients with leaking fuel rods.

Related publication

- [1] P. Szabó, K. Kulacsy and Z. Hózer: *Numerical models for the description of the axial distribution of radioactive isotopes in a leaking fuel rod*, MTA EK-FRL-2016-710-1-1-M0, in Hungarian (2016)

PARTICIPATION IN THE OECD SCIP III PROJECT

Barbara Somfai, Márton Király, Péter Szabó, Katalin Kulacsy, Zoltán Hózer

Objective

The Studsvik Cladding Integrity Project (SCIP) III was launched in 2004 with the participation of MTA EK and Paks NPP. The main objective of our participation is the collection of information on fuel behaviour phenomena in order to apply this knowledge to VVER conditions and review of the planned tests.

Methods

The experts of MTA EK regularly attend the meetings of SCIP III and review the obtained results. At the end of each year, a summary paper is produced for Paks NPP on the new results of the project. In 2015 the review focused on two specific items:

- new LOCA fragmentation tests with irradiated fuel,
- overheating tests and
- LOCA test with unirradiated fuel and axial loads.

Results

On the basis of review, the results of SCIP III project following conclusions were drawn:

- According to LOCA tests with 65-74 MWd/kgU burnup samples, fine fragmentation was not observed below 65-68 MWd/kgU. Significant pellet fragmentation took place if the fuel sample had high linear heat rate in the last cycle in the reactor. It was concluded that the structural changes in the previous cycles (e.g. formation of porous structure, fission gas accumulation, change of grain size) must be taken into account when some thresholds will be determined for fuel fragmentation. The ballooning and burst are also important aspects for the initiation of pellet fragmentation.
- The overheating tests with BWR and PWR fuel showed significant differences first of all due to different temperature histories. The PWR fuel was held at 1000 °C for 900 s, while the BWR fuel was heated up only to 700 °C. In case of PWR sample oxidation and embrittlement took place, while in case of BWR fuel only minor changes could be observed.
- The LOCA tests with axial loads showed that 400-700 N force was needed to break the sample at the end of quenching phase. The ZIRLO cladding had much better load bearing capability than that of Zircaloy-4 alloy.

Remaining work

The MTA EK experts will review the SCIP III activities by the end of the project.

Related publication

- [1] B. Somfai, M. Király, K. Kulacsy and P. Szabó: *Second series of LOCA tests in the SCIP III project, overheating tests and LOCA test with unirradiated fuel and axial loads*, MTA EK-FRL-2016-962-1-1-M0, in Hungarian (2016)

PRELIMINARY MANDREL TESTS WITH ZR CLADDING SAMPLES

Márton Király, Márta Horváth, Richárd Nagy, Tamás Novotny, Erzsébet Perez-Feró, Nóra Vér, Áron Horváth, Zoltán Hózer

Objective

In order to simulate pellet-cladding mechanical interaction, the mandrel technique will be introduced at MTA EK. In 2016 the main task was the development and optimisation of the segmented tool and the execution of some tests to demonstrate the operability of the new mandrel equipment.

Methods

First a ceramic mock-up was produced. On the basis of the first experiences the final steel segmented tool was designed and fabricated. 8 mm long cladding tubes were selected as reference size for testing. Tensile test machine with 0.5 mm/min cross head speed was used in the measurements. The load-displacement curves were recorded and evaluated.

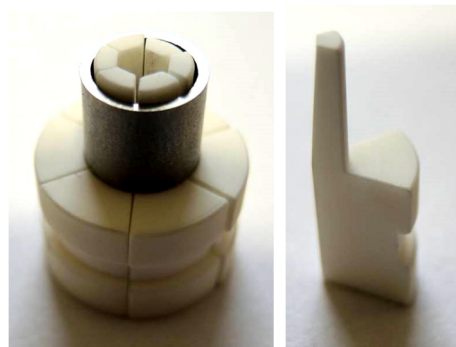


Figure 1: Ceramic mock-up of mandrel tool with 8 mm long cladding sample

Results

The first series of experiments was successfully completed with the mandrel tool. The tests were carried out at two different temperatures. Both as-received and hydrided samples were tested. The measured values of deformations were in good agreement with the results of the finite element calculations performed earlier.

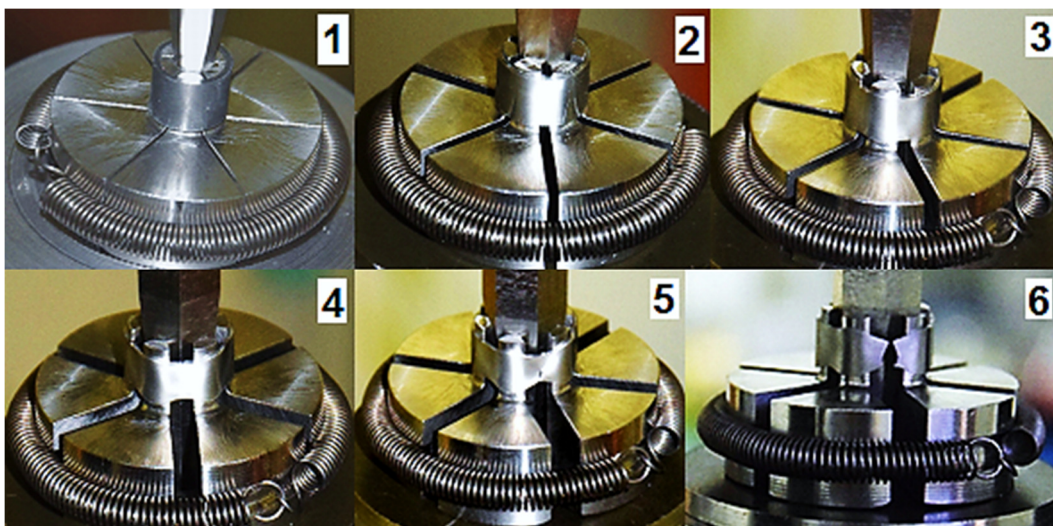


Figure 2: Steps of testing of Zr cladding tube with mandrel until complete failure

Remaining work

Large number of tests will be carried out with different cladding samples in 2017.

Related publication

- [1] M. Király, M. Horváth, R. Nagy, T. Novotny, E. Perez-Feró, N. Vér, Á. Horváth and Z. Hózer: *Preliminary mandrel tests with fuel cladding samples*, MTA EK-FRL-2016-989-1-1-M0, in Hungarian (2016)

HIGH-TEMPERATURE CORROSION MODEL OF E110G – A CODE DEVELOPMENT FOR TRANSURANUS

Eszter Kozsda-Barsy, Katalin Kulacsy

Objective

The fuel rod cladding used in the Hungarian Paks NPP is a Zirconium alloy called E110, which is quite resistant to corrosion under normal conditions. The supplier has licensed a new modification of the alloy called E110G. The new cladding has identical geometry to E110 and similar elemental composition. The main difference is in the high-temperature oxidation kinetics, which was tested during a series of experiments. The oxidation kinetics correlation of the new E110G alloy was developed at MTA EK using experimental data. The present work aims to develop a modification of the fuel behaviour simulation code TRANSURANUS with the E110G high-temperature oxidation kinetics.

Methods

The model was written into the code in Fortran 95 language. A standalone version was also made for more precise validation. Testing was done by comparing the code results to those from analytical calculations. The oxidation kinetics of E110 and E110G were compared and the two experiments were modelled for demonstration purposes.

Results

It is now possible to simulate the oxide layer thickness growth and the mass increase of the E110G cladding. The modification contains the new kinetics, is able to switch to the old low temperature corrosion model (MATPRO) and can tackle high-temperature transient oxidation which is of high importance because of the specifics of the model: the parameters of the corrosion depend on the oxidation temperature and time. As shown in an example (Figure 1), the calculations and the simulations are in good agreement. The difference between E110 and E110G in terms of corrosion was also demonstrated through the simulation.

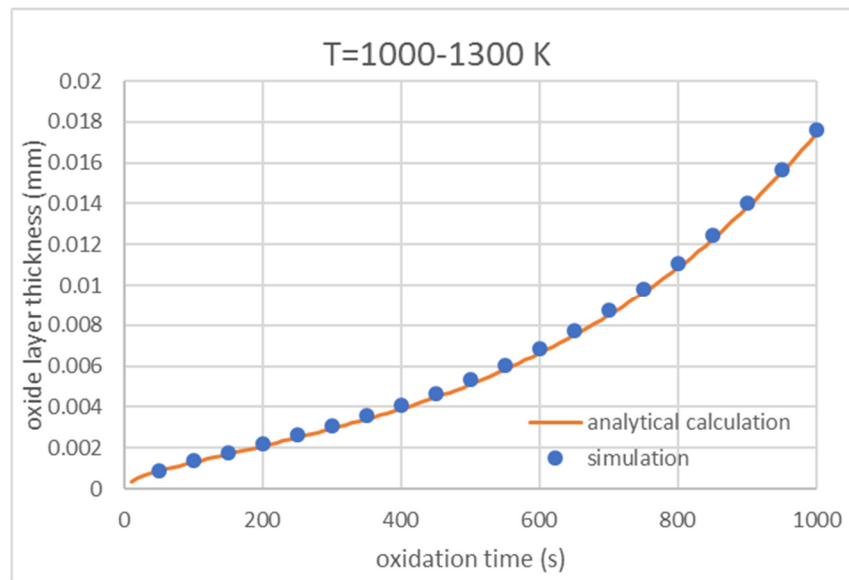


Figure 1: Oxide layer thickness growth of E110G

Remaining work

The project was finished as planned.

NEW POSSIBILITIES FOR MODELLING OF THE UP- AND DOWN-LOAD IN THE FUROM 2.1.1 VERSION AND VALIDATION

János Gadó, Ágnes Griger, Katalin Kulacsy

Objective

One of the objectives of the work was the extension of FUROM-2.1 version with some new possibilities to model automatically the normal upload and download of the reactor. Another goal was to realize a burn-up and linear heat rate dependent subdivision of the time steps. Furthermore, an extensive validation of the code based on re-calculations of many relevant experiments has been performed. The main aim was to validate the calculations of the developed FUROM 2.1.1 code version mainly for those quantities which are of the most interest from the safety point of view. The work was sponsored by MVM Paks NPP.

Methods

The validation involved the traditional methodology using simple comparison of the predictions and the measurements as well as least squares fit methods. The IFPE (International Fuel Performance Experiments) experimental data base was used as reference, which consists of a lot of integral tests of the Halden Reactor Project (HRP) and of FUMEX program. Owing to a commercial (Finnish-Hungarian-Russian) contract, normal operational data from Loviisa NPP were accessible and they were also used in FUROM validation. In some cases, the measurements were carried out on-line during irradiation, while other data were measured in post-irradiation examinations (PIE). After proper data handling and data reduction of the original raw data, FUROM-2.1.1 simulations were performed and those results were compared to the measurements.

Results

The algorithms of automatic creator of time steps during upload and download, as well as the automatic sub-divider were successfully inserted in the code.

In the validation processes the code was tested in normal operational and in transient conditions (e. g. ramp-tests) for UO₂ and gadolinia (Gd₂O₃) bearing VVER and PWR rods. In order to show the capability of the FUROM-2.1.1 simulations, results of the validation for some important target quantities are presented in Fig. 1 to Fig. 4.

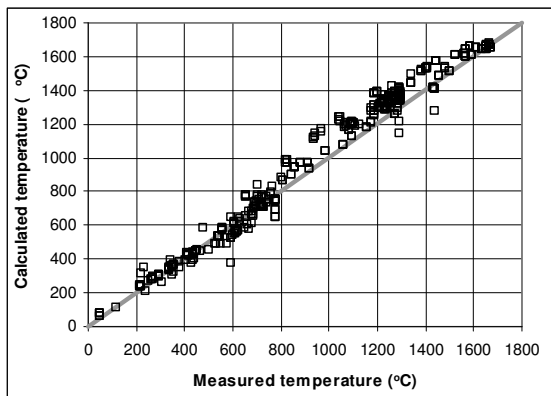


Figure 1: Comparison of T_c (SOFIT1&3 experiments)

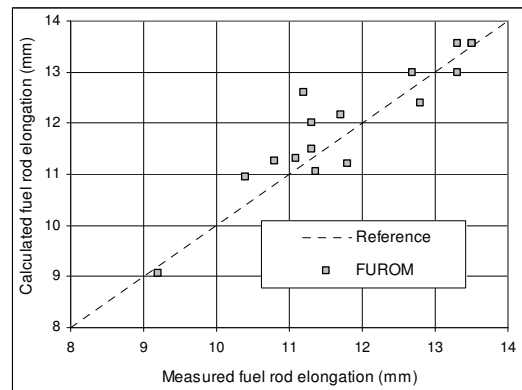


Figure 2: Comparison of elongations (KOLA experiment)

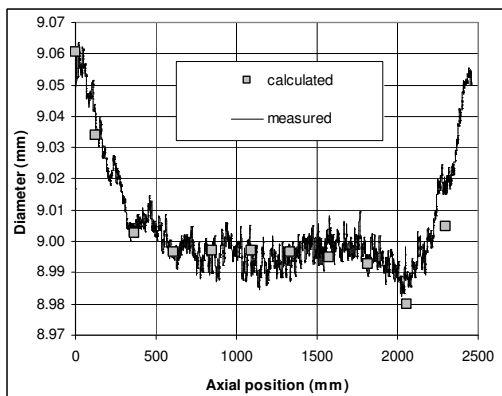


Figure 3: Comparison of cladding diameters (Loviisa)

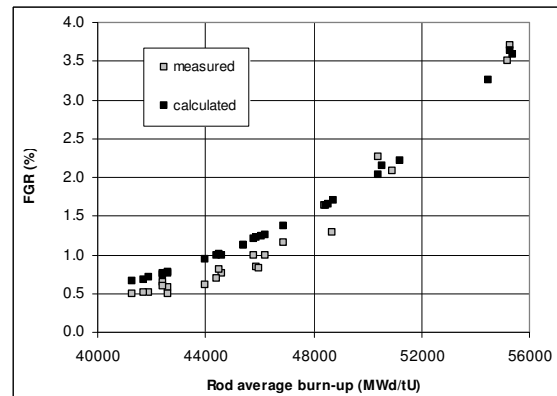


Figure 4: Comparison of FGR (KOLA experiment)

Remaining work

The validation report of FUROM-2.1.1 has been finalised, at present no further actions are needed.

Related publications

- [1] J. Gadó, Á. Griger and K. Kulacsy: *Physical models of the FUROM 2.1.1 code*, MTA EK RAL-2016-985-01-01-M0, in Hungarian (2016)
- [2] Á. Griger: *Programmer's Guide to FUROM 2.1.1*, MTA EK RAL-2016-985-01-02-M0, in Hungarian (2016)
- [3] Á. Griger: *User's Guide to FUROM 2.1.1*, MTA EK RAL-2016-985-01-03-M0, in Hungarian (2016)
- [4] Á. Griger and K. Kulacsy: *Validation of the FUROM-2.1 code*, MTA EK RAL-2016-985-01-04-M0, in Hungarian (2016)

ON-LINE MEASUREMENT OF THE BURST OF CLADDING TUBES IN A HIGH TEMPERATURE SETUP

Márton Király, Richárd Nagy, Tamás Szepesi

Objective

The purpose of the work was to visually study the ballooning and the crack propagation during the high pressure burst of different (traditional and sponge-based material) E110 fuel claddings using regular and high-speed cameras.

Methods

E110 samples were inspected under high internal argon pressures at high temperatures. For the purpose of visual inspection, a special telescope was designed and mounted onto a tube furnace in order to record the high temperature phenomena during ballooning and burst events. We performed 10 burst measurements at around 800 °C with various pressure increase rates. The appearance of non-uniform deformations was visible over 80% of the burst pressure. The regular HD camera observations revealed the kinetics of diameter change during ballooning. The crack propagation during the burst was recorded using the high-speed camera.

Results

We found that every sample has bent by approximately 5° relative to its axis. Bending happened during ballooning and was not caused by the rocket effect of the high pressure gas escaping during the burst. Every sample opened up on the convex side of the bend (Figure 1). Prior to the burst, a hot spot appeared with approximately 100 °C higher temperature at the same location where the crack propagation would initiate and it was also visible at the crack tip. The crack propagation took 0.2 ms according to our observations. Significant thinning is observed in the wall thickness of the tubes. Axial grooves have formed on the surface of the sponge-based E110 samples under tension.

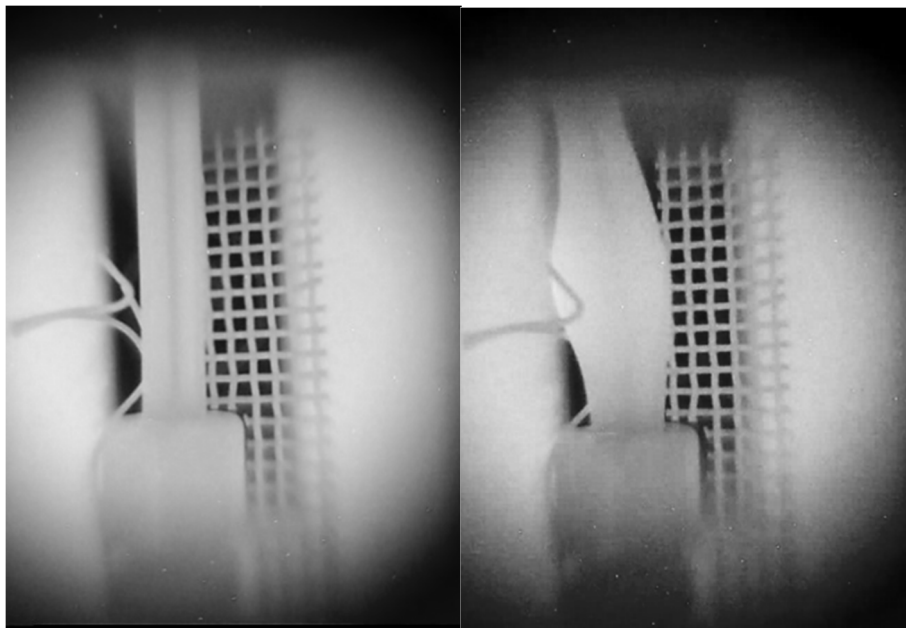


Figure 1: A welded cladding sample in the custom made tube furnace modified for this project. The picture on the left shows the sample at 5 MPa internal pressure, the right picture was taken 1/30 s before the burst.

Remaining work

Several experiments with different sample geometries, different pressurization rates and at many temperatures are planned for the following years. Some samples may contain oxides or hydrogen, or could possibly be oxidized in the furnace during the tests. This may show us the progression of the breakaway phenomenon in real time. The measurement data need to be evaluated and they have to be compared with the data from similar creep measurements of the previous years.

Related publication

- [1] M. Király, R. Nagy and T. Szepesi: *On-line Measurement of the Burst of Cladding Tubes at High Temperature*, research study, November 2016, MTA EK-FRL-2016-903-1-1-M0, in Hungarian (2016)

E110G MATERIAL NEUTRON IRRADIATION, POST IRRADIATED AND HEAT TREATED E110 MATERIAL MECHANICAL PROPERTIES EXAMINATION

Attila Kovács, Márta Horváth, Ildikó Szenthe, Ferenc Gillemot, Gábor Uri

Objective

The row material of fuel claddings for VVER type nuclear power plants is supplied by Russia. The manufacturer changed the production technology, and it will replace the present E110 material to the improved E110G. Additional investigation is needed by an independent laboratory to study the new mechanical properties of the changed fuel cladding.

Irradiation

The two received samples have the same alloying elements, but they are different in content of impurities, according to the standard (Table 1).

Table 1: Chemical composition of E110 and E110G material [1]

Element (ppm)	E110	E110G
Mg	0.5	1.5
Al	0.5	10
Si	1	35
Cr	10	30
Mn	0.1	5
Fe	45	500
Ni	15	15
Cu	0.5	5
Hf	100	10
Nb (%)	1	1
Zr (%)	99	99

The machined test specimens had been neutron irradiated in Budapest Research Reactor. The irradiation rig, called BAGIRA4 (Budapest Advanced Gas-cooled Irradiation Rig) is located in the reactor zone (Fig 1).

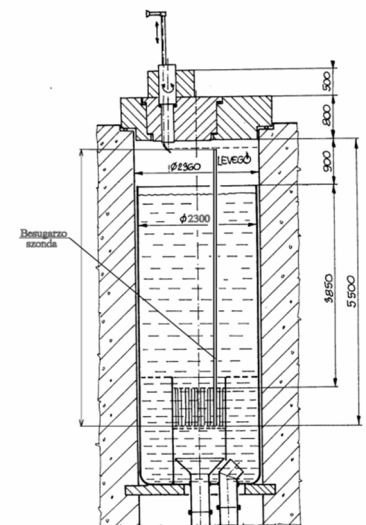


Figure 1: Budapest Research Reactor inside with Bagira

The most important technical parameters of the irradiation rig are:

- the target has in-situ temperature measuring system with 6 thermocouples
- the cooling system uses N-He gas mixture
- the PC controlled heating system in-situ adjust the requested temperature between 150 and 350 ± 5 °C

- flux: $3\text{-}6 \cdot 10^{13}$ n/cm²s, average cycle time: 240h

82 pieces E110 specimens and 82 pieces E110G specimens have been irradiated for 2395,5h at 300 °C.

Post Irradiation Examination Results

The earlier irradiated [2] E110 specimens were heat treated according to the test matrix from the operating temperature to the accidental temperature with selected time (Table 2).

Table 2: Heat treatment matrix

Temperature [°C]	Heat treatment time [h]					
	0	3	12	24	168	720
310	A				C	D
380				E	F	I
500		H	J	K		

The tensile tests on irradiated samples have been finished by using INSTRON 1195 HD at room temperature.

After analysing of the test records, we can see, that E110 material as received (not irradiated) was completely plastic, it was deformed without cracking. After irradiation, the material embrittled, the tensile strength increased, but the plastic behaviour was still valid, no significant change could be observed in elongation. Until 380 °C heat treatment there were no changes in mechanical properties, but on 500 °C the material was annealing fast.

Remaining work

The remaining work is to heat treat the irradiated and cooled E110G materials as well, and compare the results with the E110 results.

RE-EVALUATION OF SURVEILLANCE SPECIMENS OF PAKS NPP

Attila Kovács, Márta Horváth, Ildikó Szenthe, Ferenc Gillemot

Objective

The design operational lifetime of the four VVER-440 units of Paks NPP is 30 years. This operational lifetime has been extended to 50 years. The original surveillance program of the VVER-440 units has been designed in the 1970s. That time the fracture toughness was not measured. The objective of the work is to reconstitute the remnants of the surveillance specimens and evaluate the fracture toughness properties for enhanced safety analyses for long term operation.

Methods

The work started in 2015. The reconstitution technology in general remained the same as it is described in the progress report of 2015 [1], but based on the experiences of the last years the technology steps and the material testing was further developed. New computer remote controlled hardness tester has been installed into the hot laboratory. Using this equipment, the location of the heat affected zone can be determined in the weld specimens. A new shape of the notch has been developed for the reconstituted specimens, and semiconductor strain gauges have been used for pre-fatigue (see Fig. 1). The machining technology was also developed, using new type milling inserts. The software of the Instron tensile machine has been updated, the new version can make pre-fatigue, fracture toughness and J-R curve measurements without writing long programs. A high precision laser extensometer was set into work (Fig. 2). New technology and tools were developed to glue the laser reflex foils to the radioactive miniature tensile specimens. A furnace has been built for testing the miniature tensile specimens in the temperature range of -100 to 600°C. The furnace has six zones, all can be heated separately with different electronically controlled power supply units. Thermocouples measure the temperature directly at both ends of the specimens to avoid temperature differences within the specimen. The video system watching the specimens during testing got a remote controlled step motor to keep the picture sharp without going near to the radioactive specimens. Beside the development of the software and hardware systems, the laboratory staff also gain huge experience in producing and testing of radioactive reconstituted specimens.

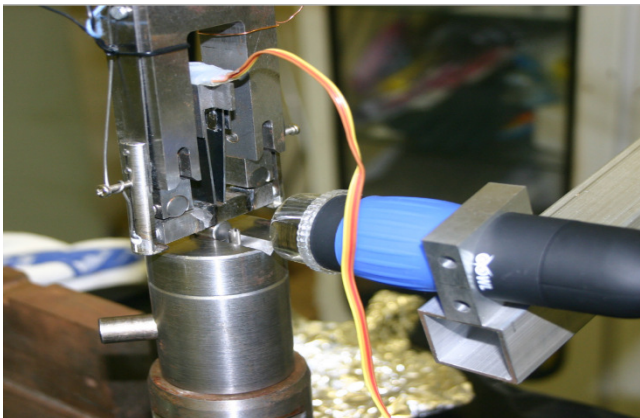


Figure 1: Pre-fatigue of the reconstituted specimens



Figure 2: Elevated temperature tensile test with laser extensometer

Results

Hundreds of the two and four years long irradiated surveillance Charpy specimens of Paks NPP have successfully been reconstituted in 2015. The ASTM1921 standard requires the length of the pre-fatigue crack to be 5 ± 0.5 mm. On the degraded surface of the old but radioactive specimens the crack length can't be measured. With the above described developments 95% of the reconstituted specimens have successfully been produced within the severe limits. Beside the fracture toughness testing tensile and J-R curve tests were also performed according to the testing plan agreed with Paks NPP. Finally, the tests have been evaluated. The results obtained on the specimens of the Unit 1 have been collected in a report. It compares the new results with those obtained during the original surveillance testing. The reconstituted specimens filled the gap of missing fracture toughness data and verified the safe extended lifetime of the unit.

Remaining work

The project will be finished in 2017. The remaining work is to reconstitute 25% of the selected specimens and to test them. According to the research plan, the Unit 1 Charpy remnants from Paks NPP should have arrived at the institute in 2015, specimens of Unit 2 and 3 in 2016 and Unit 4 in 2017. However, the specimens arrived in a mixed transport, consequently the final evaluation and the preparation of the final reports remained for 2017.

Related publication

- [1] A. Kovács, M. Horváth, I. Szenthe and F. Gillemot: *Re-evaluation of Surveillance Specimens of NPP Paks*, in Progress Report of 2015, Centre of Energy Research of the Hungarian Academy of Sciences (2015)

ADAPTATION OF VERSION 2.0 OF THE CODE FRAPTRAN TO VVER FUEL

Katalin Kulacsy

Objective

The transient fuel behaviour code FRAPTRAN developed at the Pacific Northwest National Laboratory in the US is used in the Hungarian fuel licensing procedure as confirmatory code to verify the safety analyses provided by the Russian supplier. Previous versions of the code were complemented by correlations specific to the Russian fuel, which had to be implemented in the new version as well. However, it turned out that the calculation results for the ballooning and burst behaviour of the cladding during a loss-of-coolant accident changed dramatically in the new code version due to re-coding. In the framework of the present work these parameters (the failure limits and the parameters of the equation describing plastic deformation) were re-fitted for the new code version.

Methods

Several hundred experiments were available for the fitting, including axial and ring tensile tests as well as ballooning and burst tests performed with and without axial loading. The experiments had been carried out at the predecessor of MTA EK and abroad.

The failure limits applied in the code are true tangential stress and engineering tangential strain values at burst, both depending only on temperature. The true tangential stress limit was specific to the stress state of the cladding but independent of the strain rate, all the ballooning and burst tests performed without axial loading could therefore be used to establish the new limit. On the contrary, the engineering tangential strain limit depended not only on the stress state of the cladding but also on the strain rate. Finally, the latter limit was only implemented above a temperature of 940 K and was fitted to data where the strain was greater than 20%.

After setting the failure limits the parameters of the equation describing the plastic deformation of the cladding were fitted. The squares of the deviations of the calculated burst times from the measured burst times were summed up for all the available experiments and this sum was minimised using the Levenberg-Marquardt non-linear optimisation method with the old parameters as initial values. The code was considered as a black box in the process and the dependence of the calculated burst time on small changes of the parameters was obtained by numerical differentiation implying a large number of code runs.

Results

Both burst times and burst pressures were calculated correctly using the new mechanical correlations. Figure 1 presents the results of the simulation of 50 isothermal and non-isothermal ballooning and burst tests.

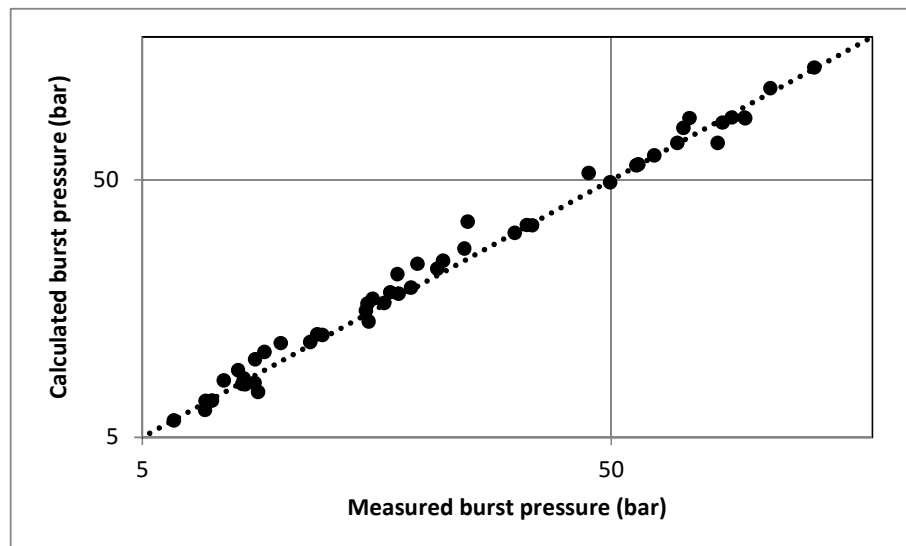


Figure 1: Results obtained with the new model

Remaining work

The work has been finished; however, a more sophisticated model will be developed in the following years.

Related publication

- [1] K. Kulacsy and M. Király: *Adaptation of the Code FRAPTRAN 2.0 to VVER Fuel Rods – Step 1*, 2017 Water Reactor Fuel Performance Meeting, September 10-14, Korea (2017)

THE EFFECT OF HYDROGEN CONTENT ON THE EMBRITTLEMENT OF E110 AND E110G ALLOYS

Tamás Novotny, Erzsébet Perez-Feró

Objective

During normal operation in light water nuclear reactors, a part of the hydrogen, which is generated by the corrosion processes and the radiolysis, is incorporated into the zirconium fuel cladding. This effect may change the mechanical properties of the cladding.

Steam oxidation experiments at high temperatures have previously indicated that oxidation is followed by hydrogen uptake. The embrittlement of zirconium alloy with hydrogen content is much faster as if the material does not absorb any hydrogen. However, these results came from the combined effect of oxidation and hydrogen uptake. In order to evaluate the separate effect of hydrogen, we aimed at carrying out hydrogen charging of metal without steam oxidation.

Methods

Hydrogen charging of the zirconium alloy can be performed by electrolysis or in hydrogen atmosphere at high temperature. The high temperature hydrogenation (mostly above 300 °C) is carried out in a closed system, in the presence of pure hydrogen gas or in inert gas atmosphere with hydrogen.

For the hydrogenation of E110 and E110G cladding samples, the latter method was chosen because the hydrogen absorption in zirconium at 300 °C is a rather slow process. Our experiments were carried out at 600 °C.

On the basis of these experiments, it is possible to verify whether the cladding is still ductile while containing the maximum permissible hydrogen (400 ppm) specified by the fuel manufacturer. To determine the ductile-to-brittle transition of the alloys, mechanical tests are required with known hydrogen content of cladding samples.

Our experimental work consisted of the following subtasks:

- Upload E110 and E110G samples (rings) with different amounts of hydrogen,
- Ring compression tests of hydrogen-containing samples,
- Measuring the substantial hydrogen content of the rings,
- Determination of the ductile-to-brittle transition of E110 and E110G alloys as a function of the hydrogen content.

Results

The experiments showed that the ductile-to-brittle transition of the E110G cladding is between 3200 ppm and 4200 ppm and for the E110 cladding at 4000 ppm.

Remaining work

The planned work has been completed.

DEVELOPMENT OF A MULTIFUNCTIONAL COMPACT SIMULATOR PLATFORM FOR NUCLEAR REACTOR SIMULATIONS

József Páles, Csaba Horváth, Tamás Fogd, Áron Vécsi, Gábor Házi

Objective

The objective of this work is to build up a compact simulator platform for the simulation of nuclear power plants. The platform has to contain all major software and technological ingredients needed to develop simulators for specific reactor types like VVER-440 or AES-1200. To demonstrate the vitality of the platform, a VVER-440 compact simulator has to be developed by using the elements of the platform.

Methods

SIMTONIA (SIMulation TOols for Nuclear Industrial Applications) [1,2] is a simulator development platform created by MTA EK a few years ago. In this work we have utilized this platform and started to develop the main components of a compact simulator of a VVER-440 type nuclear reactor.

Results

The two-phase thermohydraulics model of the six primary loops, steam generators, main steam lines etc. have been developed by SIMTONIA and coupled with a new nodal, three dimensional, two-group neutron kinetics model. The models of the major control systems like the reactor control rod system, reactor power controller, pressurizer water level controller etc. have been implemented by SIMTONIA's sequential engine and these models were also coupled with the thermohydraulics and neutron kinetics models. A touch-screen based user interface has been worked out by SIMTONIA's visual engine to mimic the control room of the nuclear power plant and to assure convenient and user friendly interface for the end users (see Fig. 1).

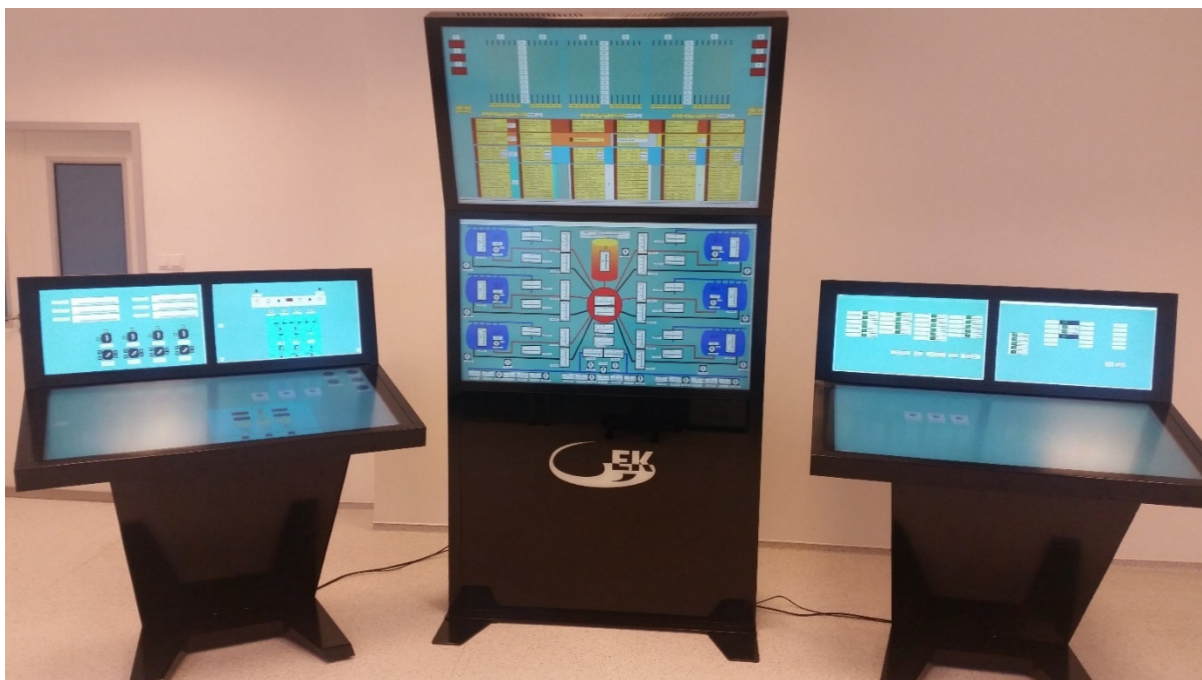


Figure 1: Touch panels of the compact simulator to mimic the control room of the power plant

Remaining work

The development of the models need to be continued in 2017, focusing on the models of I&C, electrical and single-phase thermohydraulics technological systems. The verification and validation of the compact simulator will be carried out in 2018.

Related publications

- [1] J. Páles, Á. Vécsi and G. Házi: *SIMTONIA – A framework of SIMulation TOols for Nuclear Industrial Applications*, 31st International Conference on Modelling and Simulation, May 23-26, 2017, Budapest, Hungary (2017)
- [2] J. Páles, Á. Vécsi and, G. Házi: *Nuclear Industrial Applications of SIMTONIA*, 31st International Conference on Modelling and Simulation, May 23-26, 2017, Budapest, Hungary (2017)

NEW COMMUNICATION INTERFACES OF THE CONTROL ROD AND REACTOR POWER CONTROLLER SYSTEMS

József Páles, Gábor Boleska, Gábor Házi

Objective

In 2015 Paks NPP carried out a public procurement procedure for reconstruction of the instrumentation and control of the rod control and the reactor power controller systems. SKODA JS was awarded by the end user in the procurement procedure and MTA EK as a subcontractor to SKODA JS took part in the project, among others, by implementing a new OPC UA (Open Platform Communication Unified Architecture) based communication interface between the new control rod, the VERONA core monitoring and the reactivity measurement systems.

Methods

The OPC UA, released in 2008, is a platform independent, reliable service-oriented architecture that integrates all the functionalities of the individual OPC Classic specifications into one extensible framework. It is an industrial standard used for communication between technological devices. Since Paks NPP aims to unify the communication protocols inside the plant, as they requested we have applied this protocol for the replacement of the communication between the new control rod, the VERONA core monitoring and the reactivity monitoring systems.

Results

The work has been carried out step by step:

1. Implementation of a new OPC UA stack.
2. Based on the new OPC UA stack, implementation of a new communication client for VERONA core monitoring system.
3. Based on the new OPC UA stack, implementation of a new communication client for the reactivity monitoring system.
4. Verification and validation of the new communication clients at the headquarter of Skoda JS, in Plzen.
5. Factory acceptance tests at MTA EK with the participation of the plant personnel.
6. Integration of the new communication models into the systems of the 2nd unit of Paks NPP.
7. Site acceptance tests at the plant.
8. Trial period.

The new communication models have been working successfully since the start-up of the 2nd unit (2016 December.)

Remaining work

The new communication modules have to be integrated into the systems of the 1st and 4th unit of Paks NPP in 2017, and into the 3rd unit in 2018.

Related publication

- [1] L. Varga and S. Kiss: *Modifications of VERONA core monitoring system for RCS (Rod Control System) and RPCS (Reactor Power Control System) refurbishment project, Paks NPP, 1-4 units, Basic design (2016)*

PLANT COMPUTER RECONSTRUCTION

Gergely Makai, Tamás Fogd, Gábor Boleska, József Páles, Gábor Házi

Objective

Nuclear reactor units have a so-called plant computer, which system gathers and evaluates all relevant physical parameters of the power plant. The evaluation has two levels: the first level evaluation contains simple procedures, like signal conditioning, filtering etc. and focuses on individual signal processing. In the second level, more specific operational and safety parameters are derived (e.g. operation mode of the plant, complex safety margins of the unit etc.) from a set of signals processing them together. This kind of evaluation includes complex calculations, e.g. calculation of saturation temperature at the measured reactor power, and determination of relations between measured discrete signals using complex logic sequences. In the past, this evaluation was carried out by an Excel table driven description of the evaluation algorithms at Paks NPP. Based on these tables a C source code was generated, compiled and linked to an executable file, which was run by the plant computer system.

There were several drawbacks of this approach. First, the modification of an algorithm was ponderous and time consuming. Furthermore, the resulting algorithm was not transparent for the end users, the operators, who were not able to identify easily, why a derived quantity takes its value in a certain situation.

In 2016, a refurbishment project of the old plant computer system has been started at Paks NPP and as part of this project the plant operational personnel requested the introduction of a transparent second level process evaluation procedure. MTA EK proposed to apply SIMTONIA's (simulation tools for nuclear industrial applications) sequential engine for this purpose and our proposal was awarded.

Methods

The altering of the old system to the new one included the following phases:

1. All complex calculation modules and simple logic elements used in the second level process evaluation of the old system have been implemented in a new element library of SIMTONIA.
2. The evaluation descriptor Excel tables were automatically converted to SIMTONIA logic schemes using the elements of the library.
3. SIMTONIA's sequence engine has been built into the new plant computer for second level process evaluation.
4. For each derived quantities (calculated in second level and shown in process monitoring displays), the corresponding evaluation scheme has been made available visually for the users. That is, by clicking to a displayed derived quantity, SIMTONIA's corresponding logic scheme used for evaluation appears on the process monitoring screen and the animated picture makes it transparent, how the sequential engine derived the given quantity.

Results

The new system was implemented at the full-scope simulator and in the 2nd unit of Paks NPP in 2016. After its trial period, it has been working without any problem since the end of 2016.

Remaining work

The new system has to be implemented in this year in the 1st and 4th units of the plant and in the next year in the 3rd unit.

Related publication

- [1] G. Makai and G. Boleska: *Nuclear power plant specific calculations*, Plant computer reconstruction, Detailed design (2016)

RENEWING THE RMR AND ÁNER SYSTEMS AT THE PAKS NPP

Gábor Házi, Zoltán Dezső, Sándor Kiss, Sándor Lipcsei, Miklós Ignits, Tamás Parkó, István Pósz, László Hományi

Objective

Reactivity Monitoring System (RMR, Hungarian acronym) and Refuelling Neutron Monitoring System (ÁNER, Hungarian acronym) of the Paks NPP aged and they have to be renewed. The new system is decided to be served by the same full range detectors and measurement instrumentation, i.e. the detectors and the connected instrumentation have to span the full range of neutron flux measurements from 0% to 100% of the reactor power.

Methods

In order to span the full neutron flux range, Photonis CFUL08 type detector was chosen. The same type has already been utilized by the Reactor Protection System, but its conversion unit could not handle the so-called current mode of the detector. Therefore, a new electronic interface had to be developed for the full neutron flux range and it had to be demonstrated that the interface is able to work with all three modes of the detector: impulse, Campbell (AC) and current (DC) mode. First a prototype was built and verified, calibrated at the Training Reactor of Budapest University of Technology and Economics. Then a pilot system was installed at Unit 2 of Paks NPP and trial measurements were performed. Based on the experience with these measurements, the interface was improved and final verifying measurements have been performed at Unit 3.

In order to enhance the robustness of the measurement chain, a new digital communication system (based on RS-422 interface) was developed and realized between the measuring device and its remote interface. Based on the successful test results and experiences with the pilot system, detailed system design of a six detector redundant system was prepared.

Results

The pilot system was used to make parallel measurements with the current RMR system during start-up period of a fuel cycle. It was found that the measurements with the new and the old system fit well (see Fig. 1).

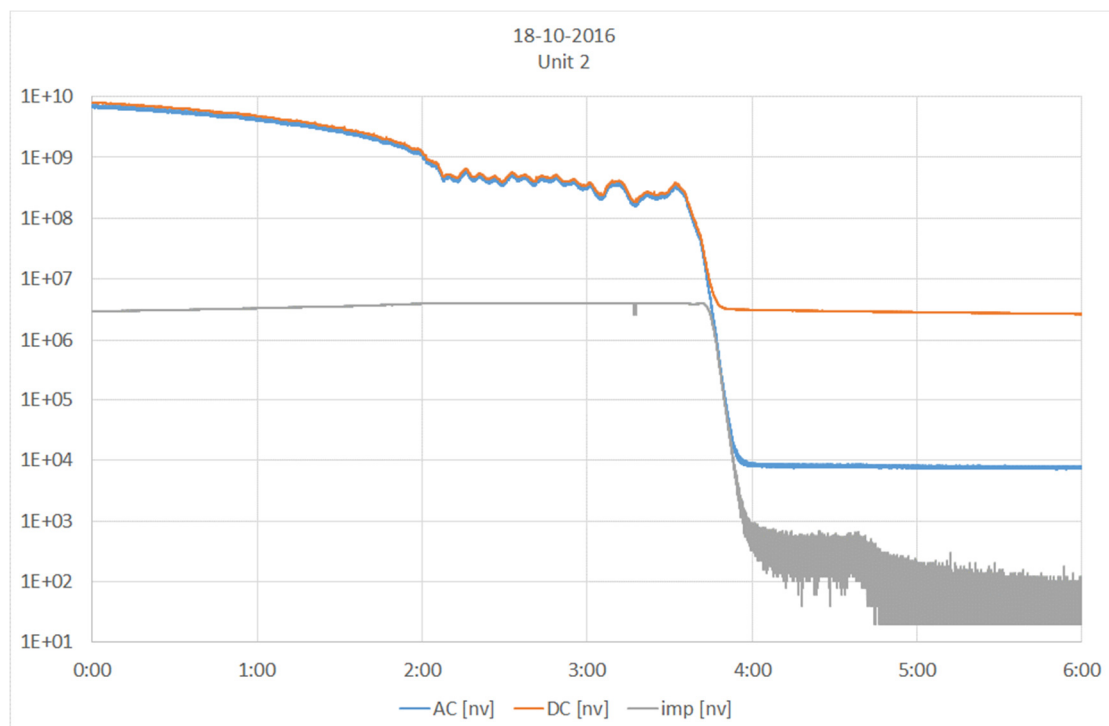


Figure 1: Measured signals with the three operation modes of the pilot system during the shutdown of Unit 2

Remaining work

Based on the experiences with the pilot system a new RMR-ÁNER system, can be built.

Related publication

- [1] S. Kiss, S. Lipcsei, G. Házi, Z. Dezső, T. Parkó, I. Pósz, M. Ignits and L. Hományi: *Developing a New Neutron Monitoring System for Paks NPP*, 25th International Conference on Nuclear Energy for New Europe, September 5-8, 2016, Portorož, Slovenia (2016)

REACTOR NOISE DIAGNOSTICS MEASUREMENTS AT PAKS NPP

Sándor Kiss, Gábor Boleska, Zoltán Dezső, Károly Krinizs, József Láz, Sándor Lipcsei

Objective

Regular reactor noise diagnostics measurements have been performed at Paks NPP since 2000. They were also continued in the present year, and the maintenance of the measurement system PAZAR was also carried out. PAZAR systems are fed by analogous signal sets of the VERONA core monitoring systems. Main part of our activity is monitoring of the coolant velocity along the fuel bundles equipped with SPND (Self Powered Neutron Detector) chains, and monitoring of vibration of the core internals.

Methods

Regular measurements were performed monthly. Long term (1 day to 2 weeks) measurements were also carried out, usually twice per month. All measurements were taken to MTA EK for further processing. The evaluation of recorded data was performed off-line by means of the evaluation software PAZAR-K. Beyond the statistical evaluation of the regularly measured noise signals, a large subset of the detector signals was continuously monitored for transients.

Electrical power supply units of the measurement system PAZAR were renewed.

Results

Noise data archive was extended with the measurements of the present year.

According to the evaluated data, the average core coolant velocity was quite stable during the year, only usual small fluctuations could be observed at all four reactor units. Distribution of coolant velocity within fuel bundles averaged over a cycle and smoothed with a spline procedure is shown in Fig. 1.

The possible vibrations of core internals also were investigated, but no such anomalies were observed in 2016. Reports were compiled for the plant from all measurements.

Files with transient events were collected and classified by events.

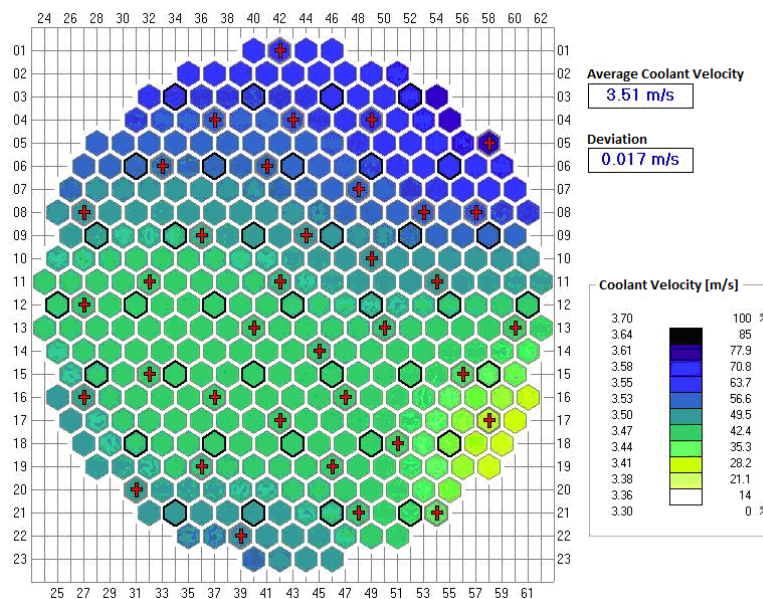


Figure 1: Distribution of average coolant velocity in Paks NPP Unit 4, Cycle 29

Remaining work

Regular noise diagnostic measurements and collection of transient events will be continued in 2017.

DEVELOPMENT OF INTERACTION TECHNIQUES FOR A VIRTUAL CONTROL ROOM

B. Katalin Szabó

Objective

Our project integrates a touchless interaction device (Leap Motion) into a virtual 3D model of the control room of the Paks Nuclear Power Plant, in order to create an experience as “real” as possible for the operators/trainees who use the simulator. For this, it is necessary to display a relatively realistic 3D representation of the user's hand.

Objectives for 2016 have been:

- Develop a rigged hand model for the Blender Game Engine (BGE)
- Drive the hand model with input from the Leap Motion hand tracking device
- Move the hand and interact with the control room devices, navigate within the control room

Methods

Developing a rigged hand model for Leap Motion means creating an armature with bones matching the hand model of Leap Motion as closely as possible and binding a hand mesh to this armature (the mesh can be regarded as a "glove" which is fitted on the armature). To make the hand model work, several programming tricks have been applied:

After rigging, the armature bones are adjusted with a script, to achieve a default position, without breaking up the rig.

The bones are driven indirectly with the input from Leap Motion: a set of simple geometric objects (not armature bones) are driven with the Leap Motion data determining their position and orientation, and the armature bones (which are connected to each other) are driven through Copy Rotation constraints from the aforementioned objects (i.e. the bones get their rotation from the rotation of the objects).

From Leap Motion, not only the position coordinates and the orientation vectors of the bones should be used, but also the so-called basis vectors which provide information about how much the bones are rotated around their own longitudinal axis (this rotation is called the "roll" of the bone). A method has been worked out to incorporate this information into the model.

All main bones of the fingers (metacarpal, proximal, intermediate and distal bones) are individually represented in the armature. The bones of the armature match the bone structure of Leap Motion's hand model. As Leap Motion has no representation for the carpal bones of the hand, and the armature's bones should be connected to each other, a simplified representation with 5 bones has been introduced, these bones connect the metacarpals with the single arm bone.

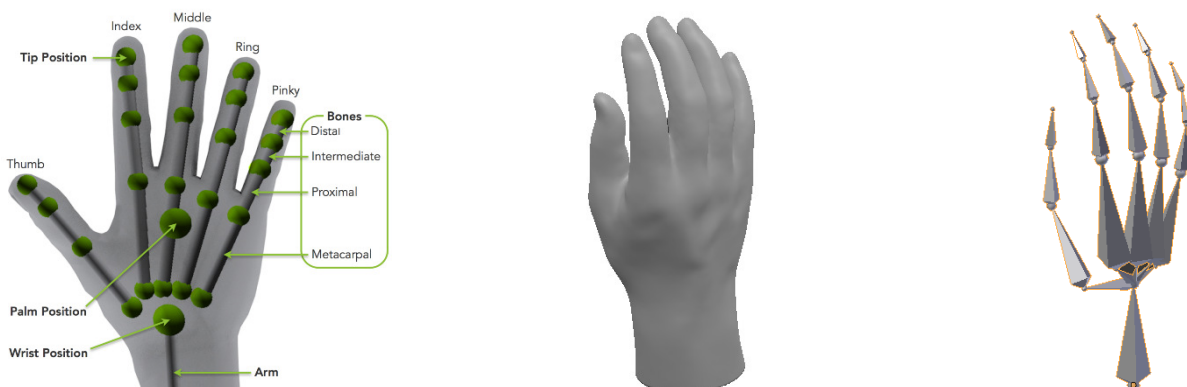


Figure 1: Leap Motion's hand model (source: leapmotion.com), a hand mesh (source: libhand.org) and the armature

Results

A new, rigged hand model has been created which is capable of following the movements of the user's hand and a demo program demonstrating this has been worked out. (To our knowledge, no one has achieved this so far for the Leap Motion – or a similar device – in the open-source BGE.) Navigation in the control room is possible in a gesture-driven way with the left hand, while the right hand is reserved for interacting with the control room devices.

Remaining work

Finish implementing the interaction with switches and pushbuttons.

Integrate Leap Motion's new, more accurate Orion API which would result in better tracking.

Integrate the Oculus Rift head-mounted display into the system.

IN-SITU INVESTIGATION OF VVER STEAM GENERATOR HEAT TRANSFER TUBES BY XRF TECHNIQUE

Zsolt Kerner, Boglárka Maróti, András Kocsonya, István Almási, Gergely Dósa, Péter Völgyesi

Objective

Heat transfer tubes of VVER 440 type nuclear power plants are made of 08H18N10T austenitic stainless steel. Knowledge of the amount of possible contaminants on the tubes' surface is necessary to evaluate the corrosion risk. Thickness of the hydrothermally grown oxide film can influence the boiling and heat transfer. A non-destructive, in-situ semi-quantitative method was developed and tested in Paks NPP.

Methods

X-ray fluorescence analysis (XRF) can give an elemental composition of the outer 10-100 μm layer of the sample. Portable analyser with appropriate shielding can be used for in-situ measurement in the opened steam generator. Diffuse gamma radiation of the activated corrosion products on the inner surface of the tubes can result in an external excitation of the detected X-ray lines over the excitation by the X-ray source of the equipment. Therefore, calibration under the internal condition of the steam generator is essential. Calibration can be done on a piece of cut-out heat transfer tube which can be analysed inside and outside of the steam generator. Some supplementary measurements were carried out in the radiation field of a caesium source.

Information depth of the XRF technique is somewhat higher than the typical thickness of the oxide layer, so contaminants (i.e. lead, silver, copper and zinc) on the surface and in the oxide layer can also be detected. Quantitation can be done based on an assumption for the depth distribution.

Outer and thicker layer of the surface oxides on the heat transfer tube is made of crucially magnetite (Fe_3O_4). From the intensity of chromium and nickel K-lines can be estimate the thickness of the oxide layer based on the absorption of X-ray photons in the magnetite. The intensity of the used lines has to be measured on a sample with same bulk composition without oxide layer. All the measurement has to be carried out strictly in the same geometry. Absorption coefficient of the magnetite in the function of the energy of the radiation is shown in Figure 1. Magnetite absorbs less the Cr-K lines than the Ni-K lines. So the evaluation of the Ni lines gives more accurate results for thin layers ($<20 \mu\text{m}$). Cr lines can be used in the 20-100 μm range.

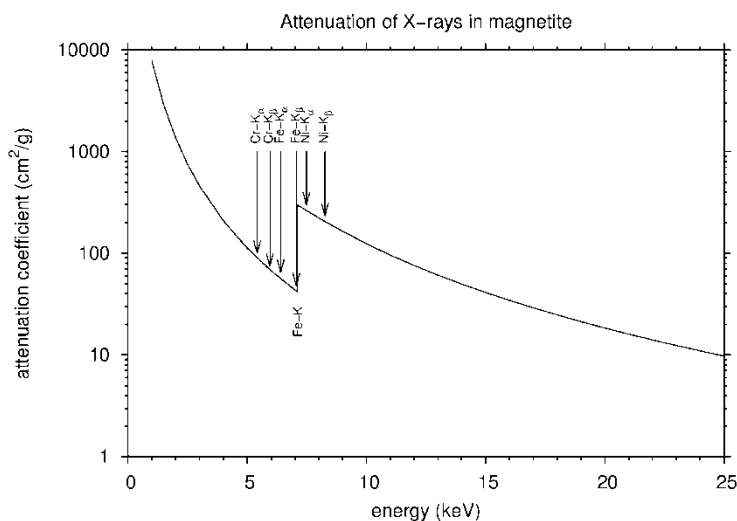


Figure 1: Attenuation coefficient of magnetite

Results

A lead shielding was fabricated for the Olympus InnovX type portable XRF analyser. In-situ measurements were carried out in four heat exchanger of Paks NPP. The effect of the external excitation was observed in the case of copper and lead. This effect is not significant in the case of the main elements of the steel. Calculated oxide thickness shows an increasing trend with the operational temperature in the measuring spot.

The described method is useful for non-destructive quick check of the thickness and composition of the heat transfer tube.

Remaining work

A comprehensive program is planned to characterize the heat transfer tubes' corrosion conditions.

MEASUREMENT OF CHLORIDE CONTAMINATION ON STAINLESS STEEL SURFACE

Zsolt Kerner

Objective

Chloride trace contamination on stainless steel surface can initialize localized corrosion. This work was dedicated to develop a method for determining 0.5-10 $\mu\text{g}/\text{cm}^2$ chloride contamination on steel coupons. This work was sponsored by MVM Paks NPP.

Methods

Chloride can be removed from the steel surface by pyrolysis in the presence of a low amount of water steam above 900 °C. It can be collected in basic solution and measured by ion chromatography. A small, electrically heated quartz tube furnace was constructed for annealing the samples with 10 cm^2 surface. High purity argon carrier gas was flown through a water-filled gas-washer, the furnace and a thin collector gas-washer filled with 20 mL 1M Suprapur® ammonia solution successively. Flow rate was optimized. The collector vessel was cooled by ice. Yield of the procedure was determined for each sample by radiotracer method, using ^{36}Cl and liquid scintillation measurement. Highest yield was obtained by the following temperature program: The furnace was heated up to 500 °C in 2 minutes, and then was heated up to 990 °C in 60 minutes. This temperature was kept for 20 minutes. Collector solution can be analysed directly by ion chromatography (IC).

The method was calibrated and tested by samples with known surface chloride concentration.

Results

Yield of chloride transfer from the steel surface to the solution was 75-99%. By dropping ^{36}Cl containing tracer solution to the sample, the yield can be measured and taken into account. Calibration curve is shown in the Figure 1. Detection limit of the method is 0.3 $\mu\text{g}/\text{cm}^2$.

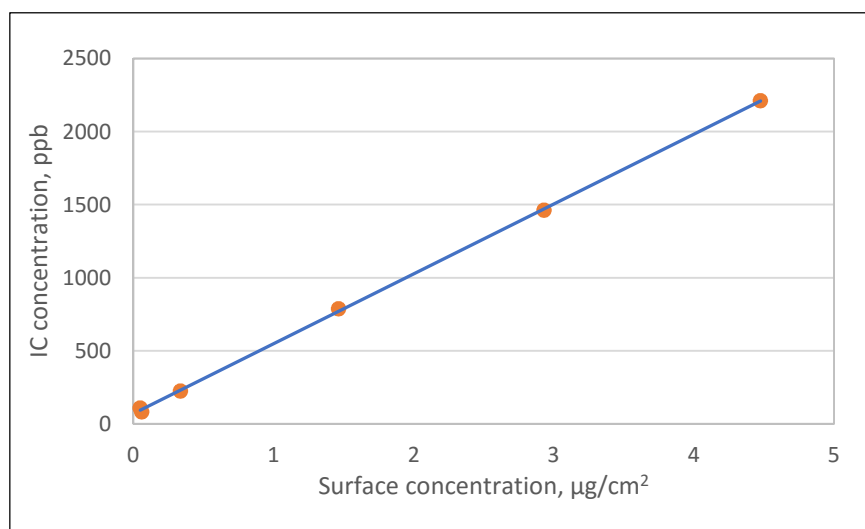


Figure 1: Calibration line

Remaining work

This work was finished.

RADIOLOGICAL CONSEQUENCES OF BEYOND DESIGN-BASIS ACCIDENTS

Sándor Deme, András László, Tamás Pázmándi, Péter Szántó

Objective

The objective of this work was the calculation of radiological consequences during one design basis accident and six cases of beyond design basis accidents for Paks Nuclear Power Plant (NPP). Our goal was to calculate activity concentrations and to assess effective dose consequences in certain rooms of the main building of the NPP and in several receptor points outside the building. Two main discharge points into the environment were considered, the main stack and the rooftop of the containment building. Each investigated scenario was combined with three possible ventilation states of the main building: two different filter system throughout the main stack, and no ventilation in the case of loss of off-site power.

Methods

The initial conditions of our Beyond Design Basis Accidents (BDBA) calculations were the best estimate results of simulations for severe accident scenarios in the containment building.

The migration of radionuclides in the main building were calculated according to the location of the rooms and the air-flow schemes. For the basis of dose calculations, isotropic distribution of contaminants was considered in the simulated rooms. Receptor points were considered in the corner and in the centre of each room.

The result of the investigation was the time dependent external gamma radiation, the inhalation dose-rates for adults and the activity concentration values for 183 environmental receptor points, for 168 hours after the initial event of the hypothetical accident with one-hour resolution. Pasquill D atmospheric stability with 5 m/s wind speed and 5 mm/s precipitation speed was considered. The spatial distribution of contaminants was calculated for five wind directions, the four cardinal and the most frequent wind direction. The atmospheric dispersion was modelled with a modified Gauss plume approach. One of the main challenges in the project was the assessment of the radiological consequences near the accidental discharge point. A simplified model, which considers the flow perturbing effect of the main building complex was used in the calculation. The irregular shape of the main building complex was replaced by a single block called effective building. The considered flow field contains a recirculating flow region with elliptical shape, where the contaminants are distributed uniformly. According to the model, the far field effect of the main building was calculated with different pairs of vertical and horizontal dispersion parameters. Therefore, the continuity of the concentration function was assured by calculating the relevant fitting parameters. The contaminants' airborne distribution, along with the dry and wet deposition on the ground were considered for the external and inhalation dose assessment.

Results

The applied model predicted that the highest concentration values occur in the recirculation region on the lee side of the main building [1]. The severest environmental impact was calculated in the scenario of a Loss of Coolant Accident with a non-functioning Emergency Cooling System. The highest total dose rate was calculated in the recirculation flow region. The spatial activity concentration distribution in the air caused by a unit release can be seen in Figure 2, while the activity deposited on the ground surface with no precipitation can be seen in Figure 3.

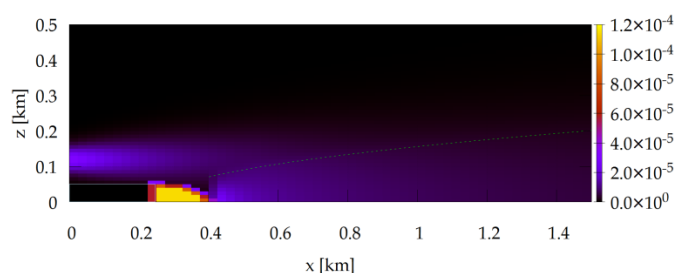


Figure 2: Cross section of dispersion near the effective building caused by unit release of contaminant.

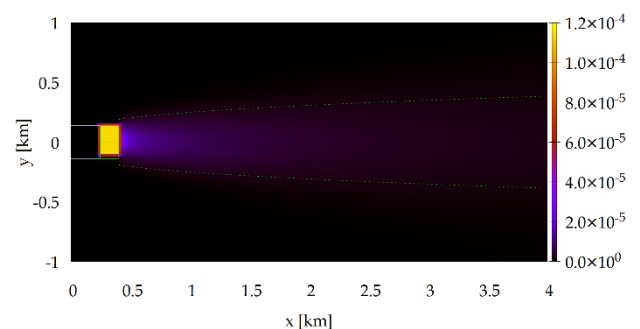


Figure 3: Viewed from above, dry deposited contaminant on the ground caused by unit release.

Remaining work

There are six other BDBA scenarios that will also be calculated in 2017 with the model used in this study. Further investigation will be conducted to determine how the main building's modifying effect on the atmospheric activity concentration can change the results of the dose assessment.

Related publication

- [1] S. Deme, A. László, T. Pázmándi and P. Szántó: *Radiological Consequences of Beyond Design-Basis Accidents*, EK-SVL-2016-994-02-01-00, in Hungarian (2016)

SENSITIVITY ANALYSIS OF CONTAMINATION MONITORS

András Kocsonya, Annamária Pántya, Tamás Pázmándi

Objectives

In order to examine the applicability of the new personal contamination monitors (Argos-5AB) for the Paks Nuclear Power Plant (NPP), calculations and measurements were made. To investigate how capable the monitors are in determining the internal contamination of gamma-emitter nuclides, measurements were conducted for isotopes ^{60}Co and ^{137}Cs with a chest phantom, and the activity intake and dose value corresponding to the alarm level of the device was calculated with simple modelling tools.

Methods

The gas flow whole body contamination monitor applies a quick two-steps measurement procedure. The monitor provides a fundamental and easily usable operation, with thorough and reliable detection of external contamination on personnel working in nuclear facilities. The monitors use a sophisticated "fast following" background trending and release-limit algorithm to provide the best possible performance in a stable or varying radiation field. The measurements were carried out in the controlled zone of Paks NPP with MIX-D chest phantom (Figure 4). It is assembled of two halves made of soft-tissue material consisting of 60 % paraffin wax, 30 % polyethylene, 6 % magnesium oxide and 4 % titanium dioxide. The ribs are real human bones and the two lung lobes are made of cork. The estimated chest wall thickness is between 2 and 3 cm, which corresponds to the chest wall thickness of an average 70 kg man. For the measurements, point sources were placed in different positions of the lung. Analysis was carried out with various chest wall thicknesses (corresponding to a 90 kg and a 100 kg man), thus, the body weight influence can be investigated. The vertical sensitivity of the detector was also studied by putting the phantom in different positions to determine the height dependence of the measurements.



Figure 4: The measurement arrangement of the MIX-D chest phantom

Results

The alert level was found to be the triple of the background, so the minimum detectable activity was determined as this alert level. The background level was 16 cps, so the alert level was suggested to be 48 cps. The efficiency of ^{60}Co measurement was 2 cps/kBq and the efficiency of ^{137}Cs measurement was 1 cps/kBq, which corresponds to 16 kBq and 32 kBq activity, respectively, assuming that the measurements were made less than 24 hours after the intake. In case of ^{60}Co , the incorporated activity was 32 kBq and the effective dose was 0.24 mSv and in case of ^{137}Cs , the incorporated activity was 124 kBq and the effective dose was 0.8 mSv.

The influence of the time of uptake was analysed for the incorporated activity and the effective dose. We calculated the activity intake and the effective dose for a hypothetical measurement of 10 kBq activity (Table 1). The time between the intake and the measurement has a significant effect in the case of ^{60}Co , as the effective dose for measurement on the 180th day is about twenty-five times higher than for the measurement on the first day, while in the case of ^{137}Cs , the ratio of the effective doses measured on the 180th and 1st day is only 4.4.

Table 1: Dose assessment data for a hypothetical activity measurement

Isotopes	Days after last intake (day)	Measured activity (kBq)	Activity intake(kBq)	Effective dose (mSv)
^{60}Co	1	10	20	0.15
	90		300	2.1
	180		487	3.5
^{137}Cs	1	10	39	0.25
	90		92	0.61
	180		162	1.1

Remaining work

The work has been completed.

Related publication

- [1] A. Kocsonya, A. Pántya and T. Pázmándi: *Sensitivity analysis of contamination monitors*, EK-SVL-2016-705-01-01-00, in Hungarian (2016)

DETERMINATION OF OPERATION SCENARIO OF SPENT NUCLEAR FUELS BY GAMMA-SPECTROMETRY

András Kocsonya

Objective

The initial nuclear material content and the irradiation scenario determine the remaining and produced nuclear materials in a nuclear fuel assembly. The correct inventory of nuclear material content is a basic requirement of international safeguards system. The nuclear material content in a spent fuel assembly cannot be measured directly by the available tools. Based on gamma-spectrometric determination of fission products, a three-year project is planned to develop a method which can determine the operation scenario of a spent nuclear fuel assembly. Our planned method is based on the numerical simulation of the production, decay and transformation of fission products in the course of the reactor operation. The input parameters describing the operation scenario can be varied and results of this calculation can be compared with experimental data. The first year of this project is devoted to develop the experimental method of determination of fission products in a spent fuel assembly.

Methods

The experimental verification of the nuclear fuel burn-up is based on the gamma-spectrometric determination of $^{134}\text{Cs}/^{137}\text{Cs}$ activity ratio for which an analysis method was developed by our department which is successfully applied since several years. As a side product of these measurements it is observed that additionally to the mentioned Cs-isotopes a set of other fission products can be detected. The half-lives of these isotopes are from 40 days to 30 years, thus they cover rather wide time-range. The basic concept of the experimental method of gamma-spectrometric determination of fission products in the spent fuel assemblies is identical with the burn-up measurements. The determination of measurable fission products, the calibration and spectra evaluation methods had to be additionally developed.

Results

First the fission products that can be measured in the circumstances of spent fuel measurements should be determined. A two-sided approach was applied. Our measured spectra are scanned and the gamma-lines are assigned to nuclides. On the other hand, the literature of fission product production is studied and the detectability of the fission products with enough fission yield were examined in our measurements. Limitation factors are the attenuation by the water between the assembly and the wall of the spent fuel storage pool, the intense continuous background and the line-overlap of different radionuclides. In the case of multi-line gamma emitters, the line recommended for analysis was selected. Due to the increasing attenuation at lower gamma-energies, not obviously the most intense line is the best choice. The possible line overlaps are discussed. Not only the fission products are considered but activation products as well which can occur in the primary loop (Table 1).

Table 1: Detectable fission products in spent fuel assemblies

nuclide	half-life	energy	branching ratio	remark
^{137}Cs	30.07 y	661.67 keV	85.1%	
^{154}Eu	8.593 y	996.26 keV	10.60%	
^{125}Sb	2.758 y	635.95 keV	11.31%	
^{134}Cs	2.065 y	795.86 keV	85.53%	
$^{110\text{m}}\text{Ag}$	249.79 d	884.68 keV	72.20%	
$^{106}\text{Ru}/^{106}\text{Rh}$	373.59 d	1050.39 keV	1.56%	
$^{144}\text{Ce}/^{144}\text{Pr}$	284.19 d	1489.16 keV	0.278%	
$^{95}\text{Zr}/^{95}\text{Nb}$	64.02 d	765.79 keV	100.0 %	
^{91}Y	58.51 d	1204.77 keV	0.30%	Detected in assemblies with <1 year cooling
^{103}Ru	39.26 d	497.08 keV	90.90%	

The key of any quantification by gamma-spectrometry is the proper efficiency calibration. In our problem the efficiency calibration is determined by three factors: the intrinsic efficiency of the detector, the attenuation of the water layer between the assembly and the detector and the self-absorption of the fuel assembly. Either the water attenuation or the self-absorption are rather significant in the circumstances of spent fuel measurements. Due to the rather wide range of activities of fuel assemblies with different burn-up and cooling time the assembly-detector distance should be varied for different assemblies.

Remaining work

The developed evaluation method is intended to be applied on spent fuel spectra measured in the previous years. The spent fuel measurements are intended to continue in the next years providing 12-15 new assemblies pro year. This way the database will be increased by future and past measurements as well.

As the next phase of the project the calculation method of fission product activities is intended to be developed which takes into consideration the supposed irradiation scenario as input parameter. The results of this calculation can be compared with the experimental results.

Related publication

- [1] A. Kocsonya: *Determining history of spent nuclear fuels by gamma-spectrometry* OAH-ABA-19/16-M, in Hungarian (2016)

SAFEGUARDS MEASUREMENTS AT PAKS NPP

István Almási, Zoltán Hlavathy, András Kocsonya, Péter Völgyesi, Gergely Dósa

Objective

- The aim was to verify the enrichment of freshly arrived fuel assemblies before they are loaded into the reactor core using a routine method developed earlier.
- IAEA and EURATOM expect the Nuclear Power Plants to be able to verify their nuclear material's inventory. For additional verification we provide an independent series of measurements with the Spent Fuel Attribute Tester (SFAT) developed earlier.

Methods

The two most intense gamma lines leaving the fuel assemblies are the 186 keV line of the ^{235}U and the 1001 keV line of the $^{234\text{m}}\text{Pa}$ which is the daughter element of the ^{238}U . Instead of I_{186}/I_{1001} intensity ratio we used only the 186 keV line intensity as the marker of the enrichment because it resulted in better accuracy during the available measuring time. At the beginning of the operation of these reactors every pin in the fuel assembly had the same enrichment (homogeneous assembly). As a result of the development of the fuel, the enhancement of the enrichment enforced to use pins with different enrichments in different positions. In addition, pins with burnable poisons were applied, too (profilised assemblies). As a consequence, the recent fuel assemblies cannot be characterised by a single number of enrichment. Different apparent enrichments can be observed from the outside and within the central hole. These apparent enrichments were determined by Monte Carlo calculation using the pin map provided by the NPP. The measured apparent enrichment was determined by comparison of the intensities and related to the calculated ones. The spectra were taken by a 95 cm³ HPGe detector from outside and a 20 mm³ CZT (Cd-Zn-Te semiconductor medium resolution) detector in the central hole.

SFAT system consists of a series of sealed tubes, a sealed and shielded detector case and a 500 mm³ CZT detector. The system was hanged above the measured assembly in the cooling pond of the power plant. The water of the pond around the tubes serves as collimator. The distance between the assembly and the detector can be preset by applying a proper number of tubes. The presence of the nuclear material can be verified indirectly by the radiation of fission products. The measured spectra are sensitive to the burn-up and cooling time of the assemblies.

Results

In 2016 we had to check profilised fresh fuel assemblies with nominal enrichment of 4.7 %. None of the assemblies displayed a value outside the double standard deviation (Fig. 1).

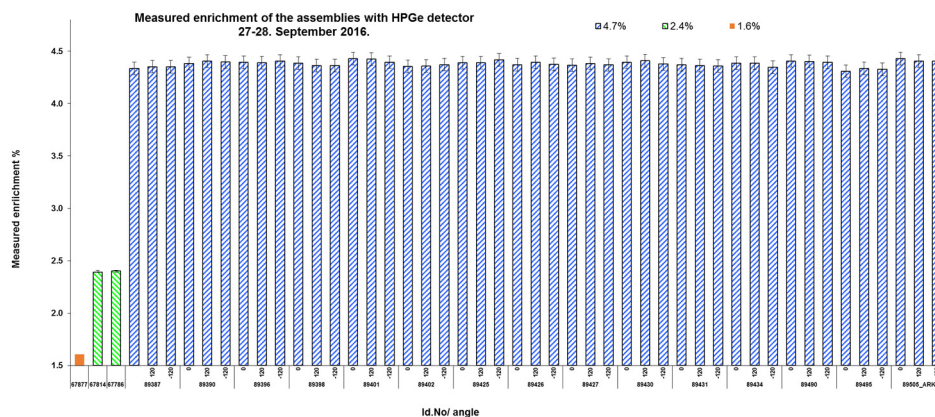


Figure 1: Apparent enrichments of fresh fuel assemblies from outside.

On a typical SFAT spectrum the presence of ^{137}Cs , ^{134}Cs and ^{60}Co can be demonstrated.

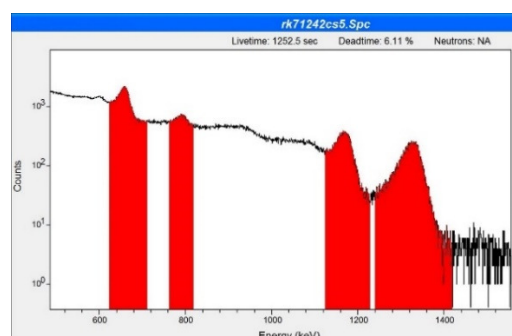


Figure 2: A typical SFAT spectrum

Remaining work

The work will continue according to the terms of the contract.

ANALYSIS OF CORROSION PARTICLES ORIGINATED FROM THE PRIMARY AND SECONDARY COOLING SYSTEM OF PAKS NPP

Éva Kovács-Széles

Objective

Between Centre for Energy Research and Paks Nuclear Power Plant (NPP) there is a research contract which specifies analysis of corrosion particles originated from the primary and secondary cooling systems of the reactors to detect the origin or source of corrosion. For determination of the nature of these particles (size, morphology, activity, elemental composition, etc.), several different techniques are used.

Methods

In this work numerous parameters of particle samples originated from the Unit No. 1 from stopping and starting period were determined using different analytical techniques: morphology by optical microscopy (OM) and scanning electron microscopy (SEM), activity by gamma-spectrometry, ^{63}Ni and ^{55}Fe content by liquid scintillation technique, corrosion products (Fe, Co, Ni, Cr, Zr, Ag) by inductively coupled plasma mass spectrometry (ICP-MS), calculation of the specific activity and the residence time of the particles in the reactor zone, analysis of the filtered particles and also the filtrates.

Results

During this work, several particles originated from the primary and secondary cooling system of Paks NPP (Unit No. 1) were investigated. Some observations from analytical data are shown hereinafter.

Following the speciation analysis, it was found: in the particles activity of Cr-51 and Zr-95 is dominant; in the solved fraction activity of Mn-54, Co-60 and Co-58 is significant; Mn-54 appears in solved form while Co-58, Co-60 and Ag-110m in different chemical forms. Variation of corrosion products in the samples in time can be seen in Fig. 1. – as an example of the results obtained.

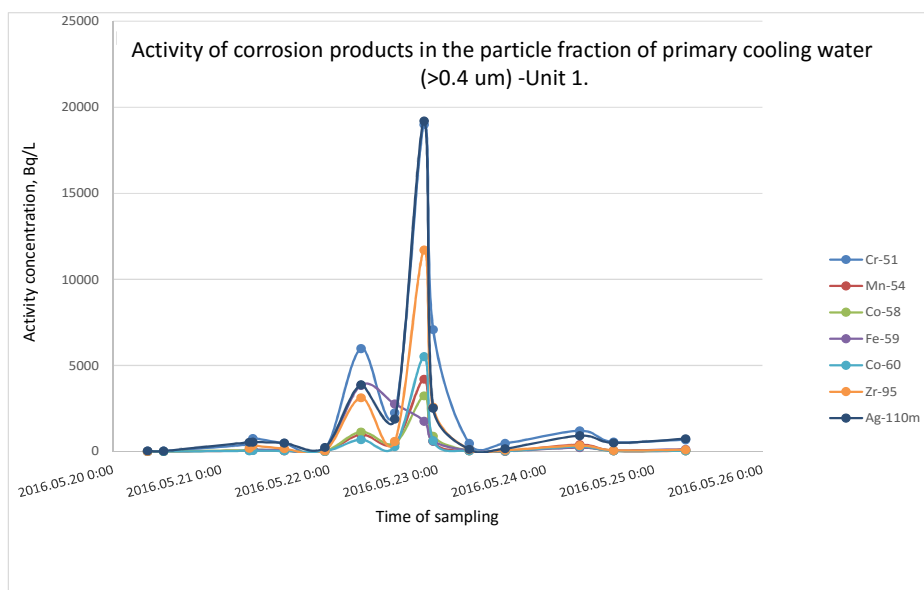


Figure 1: Activity of main corrosion products in primary cooling water

Before stopping the Unit No. 1 the total activity of corrosion products was low. After stopping the activity of particles and solved fractions significantly increased in the first few hours. During maintenance of the units the activity of the system originates from the solved components (Mn-54, Co-58, Co-60) which decreased due to the water cleaning system and elimination of active cooling water. Anomaly was found in the case of Ag-110m. The activity of this isotope increased significantly during the maintenance period. The reason of this phenomenon is unknown.

Remaining work

This work was a part of an ongoing research project for Paks Nuclear Power Plant, therefore the analysis of the particles will be continuing in the future.

Related publication

- [1] É. Kovács-Széles: *Analysis of corrosion particles originated from primary and secondary system of NPP*, research report for PAKS Zrt., MTA EK-SBL-2016-766-1-1-M0 and MTA EK-SBL-2016-766-2-1-M0, in Hungarian (2016)



III. NUCLEAR SECURITY AND DOSIMETRY



DEVELOPING AN IMPROVED PRODUCTION TECHNOLOGY FOR THE CERAMIC BLOCK OF THE PORTL DOSIMETER SYSTEM

Katalin Balázsi, Attila Hirn, István Apáthy, Csaba Balázsi, Antal Csőke, Zsolt Fogarassy, Sándor Gurbán, Tamás Pázmándi, Péter Szántó, Varga Viktor, Balázs Zábori

Objective

The portable thermoluminescent dosimeter (TLD) system PorTL consists of several dosimeter cells of compact and robust design and a light-weight battery-powered TLD reader. The TL block inside the PorTL cells consists of a ceramic plate with a miniature heater fixed on one side and a thermocouple and the $\text{Al}_2\text{O}_3:\text{C}$ TL tablet on the other side. In the collaboration of the Institute for Atomic Energy Research and the Institute for Technical Physics and Material Science, an improved production technology of the ceramic block has been developed based on attritor milling and hot isostatic pressing (HIP) using a novel Si_3N_4 ceramic/nanocomposite material. The main objective was to decrease the manufacturing lead time of the PorTL cells and to extend the lifetime of the TL block.

Methods

Activity measurements were performed on six different ceramic materials with a Berthold LB 10-Channel α - β Low-Level Counter. The $\text{Al}_2\text{O}_3:\text{C}$ TL tablet was heated in a stove at 1700°C for 3 hours in nitrogen atmosphere to check if it survives the sintering of ceramics in case the entire TL block is manufactured at once.

Results

Five of the ceramic materials tested had significant radioactive background probably due to their potassium (^{40}K) content; only the Si_3N_4 ceramic/nanocomposite material was found to be suitable for using it as the basic material of the TL block.

Since the sensitivity of $\text{Al}_2\text{O}_3:\text{C}$ TL tablet dropped significantly after heating it at 1700°C , the technology to produce the TL block was split into two: 1) production of ceramic components and 2) integration of the heater, the thermocouple, and the TL tablet into the block.

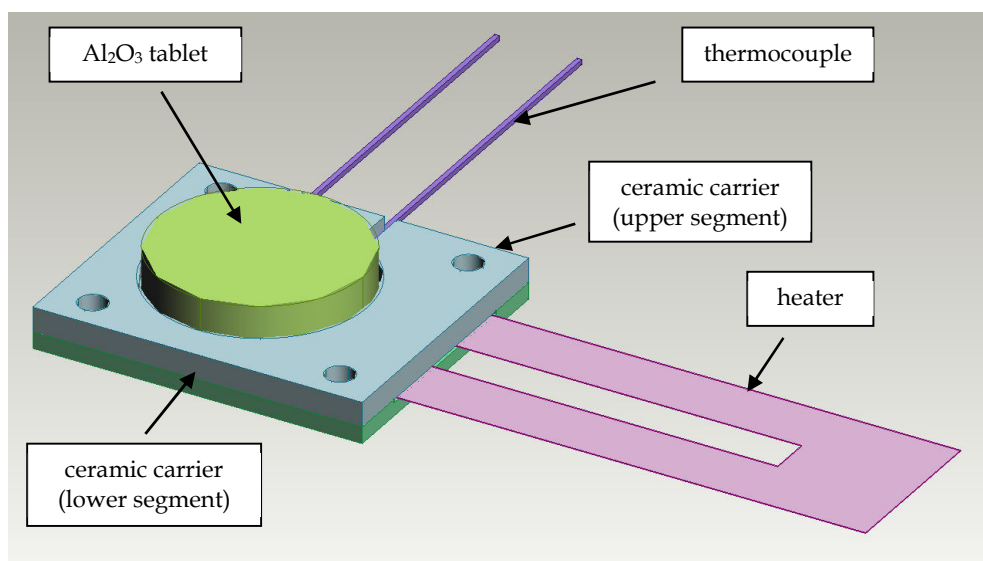


Figure 1: The novel design of the PorTL block; the ceramic plates are prepared with HIP technology

The advantages of this approach are:

- the use of Si_3N_4 material and the corresponding technology (HIP), with which the Institute for Technical Physics and Material Science has already extensive experience;
- the manufacturing of the tools needed for the production of the ceramic block is relatively simple;
- much fewer work hours required then in the case of the original technology;
- shorter manufacturing lead times.

The heater and the thermocouple are placed between two ceramic carriers (Fig. 1); the pieces are integrated by means of gluing to form one single PorTL block. The bottom carrier is indented to position the heater. The new pressing tool was manufactured and the parameters of the sintering process were optimized taking into account that very thin (0.5-0.6 mm) plates of Si_3N_4 needs to be sintered into special shape and with dedicated indentions for positioning the heater and the TL tablet.

Remaining work

Selection and testing of suitable high-temperature ceramic glues and manufacturing and testing of the prototype of the new PorTL block are in progress. The design of another version of the PorTL block with removable TL tablet got also underway.

PERSONAL NEUTRON AND BETA DOSIMETRY

Sándor Deme, József Pálfalvi, Tamás Pázmándi, Andrea Strádi, Péter Szántó

Objective

According to the Hungarian Health Governmental Decree No. 487/2015, in case of nuclear energy, the users are responsible for monitoring their workers occupationally exposed to neutron and beta radiation. These dosimetric measurements must be performed by accredited laboratories. The decree allows the users to implement calculation methods and estimated values based on monitoring results. This work is aimed at proposing an appropriate neutron dosimeter system and the related calibration process, as well as revising the necessity of separate beta dosimetry for the Paks Nuclear Power Plant (NPP).

Methods

Through a detailed review of the measurement techniques in national and international practice of personal neutron dosimetry and area monitoring complemented by organized intercomparisons of different types of dosimeters, we proposed a system and a calibration method that meets the corresponding criteria in mixed gamma-neutrons fields. The specific correction factors of ambient dose equivalent survey meters applicable at Paks NPP were calculated based on spectral data measured at a VVER-440/213 type reactor. Regarding the beta radiation, a database containing the contribution of nuclides emitting beta particles was used, to which the workers are potentially exposed during the course of maintenance works. Based on this data, the beta contribution to the effective and skin dose were calculated.

Results

Since Paks NPP and MTA EK applies the same Alnor type albedo dosimeter manufactured by RADOS, a comparative assessment of the characteristics and applicability of the system was performed and a method was proposed for the spectral survey of the radiation field inside the power plant, thus, the determination of calibration factors. The albedo dosimeter comprises of two parts: a TLD card (thermoluminescent dosimeter with two ^6LiF and two ^7LiF chips) and a holder with boron plastic filters and beta window, used for discrimination between different energies which allows the measurement of thermal neutrons that are generated by higher energy neutrons incident upon the body and then reflected back into the dosimeter. It is possible to detect the fast neutrons as well, by using nuclear track detectors (with boron converter and polyethylene radiator) along with the TLDs. Alpha particles produced by the $^{10}\text{B}(n,\alpha)^7\text{Li}$ reaction can be measured easily by optical microscope, and the dose contribution from neutrons can be calculated without any corrections, however, the evaluation is time consuming. The track detectors should be evaluated only if the neutron dose exceeds the recording-level (0.3 mSv).

By applying the Monte Carlo simulations, it was revealed that in case of "soft" neutron spectrum with high amount of backscattered neutrons, the albedo dosimeter with TLDs could overestimate the actual dose by a factor of two. This effect could be compensated with correction factors which can be calculated based on measurements using ambient dose equivalent survey meters. In our study, three types of survey meters (NE-NM2B, Berthold LB6411, Centronic) were reviewed applying neutron spectra obtained at VVER-440/213 type nuclear power plant. The calculations showed that at the power plant, the uncertainty of the dose rates are around 18% (within 95% confidence interval) compared to the calibration made at the German National Metrology Institute - Physikalisch-Technische Bundesanstalt (PTB) with ^{252}Cf . It is important to note that the actual energy spectra at Paks NPP must be investigated by Bonner Ball technique onsite in order to determine the site-specific correction factors.

The evaluation of gamma-beta ratio, the activity concentration of nuclides and energies of the emitted beta particles resulted in very low beta contribution to the skin dose. Taking into account the tissue weighting factor of the skin this would increase the effective dose from gamma radiation with 1%. In practice, the measurement errors of personal dosimeters exceed this value. By using the appropriate protective gear (equivalent to 2 mm plexi glass) during the most hazardous activities – which is the reparation works on the primary circuit – the potential exposure of the skin to beta radiation will be moderate and skin dose will be lower than the dose limit.

Remaining work

The work has been completed.

Related publication

- [1] S. Deme, J. Pálfalvi, T. Pázmándi, A. Strádi and P. Szántó: *Personal neutron and beta dosimetry*, MTA EK TFO-2016-751-05-01-M0, in Hungarian (2016)

RESEARCH&DEVELOPMENT ACTIVITIES IN SPACE DOSIMETRY AND SPACE WEATHER

Attila Hirn, István Apáthy, Antal Csőke, Sándor Deme, András Gerecs, József K. Pálfalvi, Tamás Pázmándi, Andrea Strádi, Julianna Szabó, Eszter Tóth, Balázs Zábóri

Objective

Space dosimetry and space weather activities of the research centre are concentrated in the Space Dosimetry Research Group of the Radiation Protection Department. Several dosimeter systems developed by the group operate on board the International Space Station (ISS) with the aim of providing information on the dose distribution at different locations with different shielding conditions and also personal dosimetry data during extra-vehicular activities (EVAs) and intense solar events. In parallel, different types of silicon detector telescope systems have been and are being developed for satellites on low Earth orbit. The objective of the development is to support space weather research and to provide dosimetry data and radiation history for spacecraft components. All these activities are realised in international cooperation.

Methods

The Pille space-qualified thermoluminescent dosimeter (TLD) system, developed by a predecessor (MTA KFKI AEEK) of the MTA Centre for Energy Research, provides accurate and high resolution absorbed dose data. The Pille-ISS system launched in August 2003 to the Russian segment of the ISS is operated in cooperation with the Institute for Biomedical Problems (IBMP) in Moscow in the frame of a bilateral contract. The Pille system, as part of the service dosimetry system of the Russian Segment, comprises a reader and 12 dosimeters. The Pille dosimeters located in different positions on board the ISS are read out monthly by the astronauts. Two of the dosimeters are dedicated to EVAs, as well, and the twelfth dosimeter is permanently inserted in the Pille reader and read out automatically every 90 minutes, providing high resolution dosimetry data. For on-board sensitivity analysis, from time to time, all Pille dosimeters are placed on panel No. 327 for a while, and the quasi-homogeneous radiation field at that position is used as natural radiation source. The duration of the exposure is two weeks. The correction factors for the individual dosimeters are then calculated from the results of the sensitivity measurements. Although the reader is fully operational and it performs correctly without any degradation or malfunctioning, its warranty has expired and the unit needs to be replaced. Manufacturing and assembling of the new Pille reader and eight additional dosimeters were finished in 2015. In order to demonstrate that the new units are free of manufacturing defects, workmanship errors, perceptible start of failures and any performance anomalies, acceptance tests had to be performed.

The Space Dosimetry Research Group participates in the "Dose Distribution Inside the International Space Station - 3D" (DOSIS-3D) experiment since 2012 with detector packages containing TLDs and solid state nuclear track detectors (SSNTDs) to investigate the dose contribution of the low ($< 10 \text{ keV}/\mu\text{m}$) and the high ($> 10 \text{ keV}/\mu\text{m}$) linear energy transfer (LET) cosmic radiation. The plastic detector boxes consist of two SSNTD sheets and six TLD pellets (half of them is made of ^6Li enriched MTS-6 material, the other half is ^7Li enriched MTS-7). In each phase of the experiment (one phase lasts for approximately 6 months) there are 10 single boxes and a set of 3 boxes (arranged in the 3 directions of space) located inside the European Columbus module.

The three-dimensional silicon detector telescope TRITEL-RS, developed in cooperation with BL-Electronics Ltd., was delivered to ISS in March 2013. The instrument is capable of measuring not only the absorbed dose in the cosmic radiation field, but also the LET spectrum of the charged particles and their average quality factor in three mutually orthogonal directions in order to give an estimation of the dose equivalent, too. The TRITEL Interface Unit was lost during a second delivery to ISS by the destructed Progress M-27M cargo spacecraft in April 2015 and so a new flight unit had to be manufactured and tested.

A modified, satellite version of the TRITEL three dimensional silicon detector telescope has been developed to provide measurements of the radiation environment for the European Student Earth Orbiter (ESEO) mission of the European Space Agency (ESA) Education Office. In order to be ready for the launch, first the qualification tests of the ESEO-TRITEL engineering and qualification model (EQM) had to be completed to demonstrate that the instrument design fulfils the applicable requirements including proper margins. This was followed by the manufacturing and assembling of the flight model (FM) and performing the payload FM acceptance tests.

In the frame of the General Support Technology Programme of ESA, an instrument for measuring space radiation and magnetic field parameters (RadMag) is being developed by the Space Dosimetry Research Group. The in-orbit demonstration mission is due in 2019 on board a three-unit (3U) CubeSat being developed by the Hungarian company C3S Ltd. In the study phase of the project simulation of the expected radiation field was performed with the Space Environment Information System (SPENVIS) for different orbits as well as for different solar and geomagnetic conditions. In order to simulate the expected energy deposition spectra and dose rates measured with RadMag in orbit, the Geant4 for Radiation in Space (GRAS) Monte Carlo tool was used. Trade-off analyses were also performed to address the main objective of the instrument and to meet the constraints with respect to maximum mass, dimensions, power consumption and data budget.

Results

In year 2016, approximately 6000 measurements were performed with the Pille-ISS system on board the ISS. The data obtained between March 2015 and March 2016 were evaluated, analysed, interpreted and presented at scientific conferences. The acceptance tests of the new flight model of the Pille reader were successful. Calibration of the eight new dosimeters was also

carried out with a ^{137}Cs source.

The data obtained from the DOSIS-3D TLD measurements revealed that the signal of the MTS-6 pellets is systematically higher than the MTS-7 signals, which indicates the presence of secondary neutrons, since the ^6Li isotope possesses very high cross-section for (n, α) reactions with thermal and epithermal neutrons generated by the primary cosmic rays inside the spacecraft. During the sessions no systematic differences of the neutron signals could be observed between the locations. The lowest average dose rates measured by MTS-6 detectors were observed near the maximum of the solar activity between 2014 and 2015, during the 6th session. It was also observed that the dose rate on the aft side of the Columbus module is always higher than on the forward side, presumably due to the highly directional distribution of the trapped particles in the South Atlantic anomaly region. [1]

The new Interface Unit of the TRITEL-RS experiment was manufactured and acceptance tested. The ESEO-TRITEL EQM passed the qualification tests. The FM was manufactured and calibrated at the Heavy Ion Medical Accelerator in Chiba, Japan and the acceptance tests were conducted successfully.

In the study phase of the RadMag development, measurement parameters of this complex space weather instrument have been defined and a technical study has been performed, in which it has been shown that RadMag can be realized to meet the requirements defined and within the technical limits of the 3U CubeSat mission. The brief specifications of the radiation measurements are shown in Table 1. [2]

Table 1: RadMag specifications for radiation measurements

Parameter	Value/range
particles measured	electrons, protons and heavier ions
energy range of electrons	100 keV – 8 MeV
energy range of protons	1 MeV – 150 MeV
energy range of ions	100 MeV/n – 1 GeV/n
half opening angle for proton and electron measurements	32°
half opening angle for ion measurements	44°
maximum contamination	10%
time resolution	10 s – 24 h
dose rate range	$1 \cdot 10^{-7} - 1 \cdot 10^1 \text{ Gy h}^{-1}$

Remaining work

Evaluation and interpretation of the measurement data produced by the on-board Pille-ISS and TRITEL-RS dosimeter systems, as well as maintenance of the instruments will continue. The development of new Pille dosimeters with less self-shielding will be pursued. The DOSIS-3D project is currently planned to be continued until the end of the 24th solar cycle (2018). The launch of the ESEO satellite is due in December 2017. The research group will be actively involved in the commissioning of the ESEO-TRITEL instrument and they will be responsible for the analysis and evaluation of measurement data received from TRITEL during the ESEO mission. The development of the RadMag space weather instrument enters the implementation phase, in which the technical requirements will be finalized, the technologies to be used and the final measurement concept will be selected and the detailed engineering plans will be prepared. Based on these plans, an EQM and an FM will be manufactured, which will be then subjected to thorough qualification and acceptance test procedures. In addition to that, another important task is the full calibration of the instrument, which requires the use of several radioactive sources and energetic particle accelerators.

Acknowledgements

The authors wish to acknowledge the precious help provided by the colleagues at IBMP and S. P. Korolev Rocket and Space Corporation Energia. Manufacturing and assembling of the new Pille reader and the eight additional dosimeters were funded partly by the Ministry of National Development through contract No. IKF/375/2015-NFM_SZERZ. The DOSIS-3D experiment is organized by ESA and managed by the German Aerospace Centre (DLR, Deutsches Zentrum für Luft und Raumfahrt). Participation of the research group in the latter project was funded through the Plan for European Cooperating States (PECS) contract No. 4000108464. The ESEO-TRITEL project is funded through the PECS contract No. 4000107255/12/NL/SFe. The study phase of the development of the RadMag instrument was performed in the frame of the ESA contract No. 4000117620/16/NL/LF/as.

Related publications

- [1] T. Berger, B. Przybyla, D. Matthiä, G. Reitz, S. Burmeister, J. Labrenz, P. Bilski, T. Horwacik, A. Twardak, M. Hajek, M. Fugger, C. Hofstätter, L. Sihver, J. K. Pálfalvi, J. Szabó, A. Strádi et al.: *DOSIS and DOSIS 3D: Long term dose monitoring onboard the Columbus Laboratory of the ISS*, J. Space Weather Space Clim. **6**, A39 (2016)
- [2] B. Zábori, A. Hirn, S. Deme, T. Pázmándi, Gy. Horváth, Zs. Várhegyi and I. Apáthy: *Space weather research and forecast services using CubeSats*, Proceedings of the Small Satellites, System & Services Symposium (4S) Symposium, 30 May – 3 June 2016, Valletta, Malta (2016)

DETECTION OF COSMIC RADIATION IN NEAR-EARTH ORBIT BY ACTIVE AND PASSIVE DOSIMETER SYSTEMS

Julianna Szabó, Andrea Strádi, Tamás Pázmándi, Attila Hirn, Balázs Zábori, Péter Szántó

Objective

This work was aimed at the comparative assessment of the results obtained in radiation monitoring experiments in different modules of the International Space Station (ISS) by using active and passive detectors.

Methods

Data obtained in several missions on board the ISS using two types of passive detector packages (PDPs) consisting of thermoluminescent (TL) and track detectors, and the TRITEL silicon detector telescope were re-evaluated and compared. TLDs (including the PILLE system) are the most sensitive to the particles with Linear Energy Transfer (LET, < 10 keV/μm in water), while track detectors measure in the high LET (> 10 keV/μm in water) region, both resulting in mission integrated dose. The TRITEL silicon detector telescope detects the components having LET between 0.2 keV/μm and 120 keV/μm (in water). After the revision of our previous experiments two sets of data were found to be suitable for comparison (see Table 1).

Table 1: Different missions on board the ISS involving MTA EK detectors exposed in overlapping periods

Set 1.				Set 2.			
Mission	Time frame	Module	Detector type	Mission	Time frame	Module	Detector type
DOSIS-3D/1	05/2012 – 09/2012	Columbus	TLD, track detector	DOSIS-3D/4	09/2013 – 03/2014	Columbus	TLD, track detector
DOSIS-3D/2	10/2012 – 03/2013	Columbus	TLD, track detector	SPD-10	09/2013 – 05/2014	Russian Modules	TLD, track detector
TRITEL-SURE	12/2012– 05/2013	Columbus	TLD, track detector, Si detector	TRITEL-RS2	09/2013 – 03/2014	Russian Modules	TLD, track detector
STEP	05/2012 – 05/2013	Russian Modules	TLD, track detector	PILLE	09/2013 – 03/2014	Russian Modules	TLD
PILLE	05/2012 – 05/2013	Russian Modules	TLD				

Results

It was noticeable in the case of both sets of data that the Columbus module is more shielded than the Russian Service Module, which was indicated by the lower dose of the predominant low LET components and higher amount of high LET secondary particles (generated in the walls and other materials) in Columbus. Total dose rates from both types of particles were the lowest during the end of 2012 and the beginning of 2013, when solar activity was decreasing; 285±15 μGy/day in Columbus and 345±27 μGy/day in the Service Module. The highest total dose rate was obtained in the least shielded Pirs module 508±50 μGy/day during the SPD-9 mission.

It was possible to determine the flux of cosmic ray particles in a wide LET range (between 0.2 keV/μm – 1000 keV/μm in water) by combining the data from the TRITEL-SURE PDP and the active unit. The measured fluxes in the overlapping range (12.5 – 120 keV/μm in water) were in good agreement with each other as well as with the Dosis-3D/2 PDP spectra.

In the Service Module the dose rates measured by TLDs during the SPD missions and by the PILLE system in the same time period were similar, but strongly dependent on the exact location due to different shielding configurations.

In summary it can be stated that the doses measured by different systems are in good agreement and the active measurements can be supplemented by the PDP data. The observed changes in the dose rates due to the different shielding conditions, altitude and solar activity confirm the necessity of continuous radiation monitoring on the ISS in order to understand the influence of these parameters on the radiation field inside the modules.

Remaining work

The dose assessment and the preparation of the scientific paper regarding the TRITEL-SURE project is under process. The evaluation and comparison of the regularly received data obtained by the PILLE and TRITEL systems on board the ISS will be continued as well as the passive measurements in the DOSIS-3D and SPD projects.

Related publications

- [1] A. Strádi, J. Szabó, K.O. Inozemtsev, V. V. Kushin, R. V. Tolochek, V. A. Shurshakov, I. B. Alchinova and M. Yu. Karganov: *Comparative radiation measurements in the Russian segment of the International Space Station by applying passive dosimeters*, Radiation Measurements, In Press, Corrected Proof, Available online 31 January 2017

EFFECTIVE CONTAINER INSPECTION AT BORDER CONTROL POINTS

András Kovács

Objective

Efficient non-intrusive inspection (NII) of containerised freight is increasingly critical to trade and society due to smuggling, illegal immigration and illicit trafficking of drugs, explosives, nuclear and radioactive materials, chemical and biological warfare agents and radioactively contaminated goods. Nowadays the quantity and quality of container inspection is not suitable from a societal security point of view, since no single inspection technology can effectively cope with the present challenge. A consortium has therefore been established to apply for a Horizon 2020 EU project to work out new methods and/or to improve already used ones, to help customs officials to evaluate their needs, and to design integrated solutions and optimise the container inspection by deploying comprehensive, cost-effective container NII methods and means that will more effectively protect EU sea- and land-borders. The project will also address detection and false alarm levels, throughput, health and safety issues and logistics. The project, called C-BORD (effective Container inspection at **BOR**Der control points), involving 18 technology developers, controllers and end-users (e.g. customs officials) from 9 countries (France, Germany, Italy, Hungary, Poland, Norway, The Netherlands, United Kingdom, Belgium) has been approved and started in June, 2015. The main goal of the three and a half year's long project is to try out all presently developed technologies in 3 countries addressing the requirements of big seaports (Rotterdam, The Netherlands), small seaports (Gdansk, Poland) and a land border crossing place (Röszke, Hungary). This latter one will be performed in Hungary at a non-EU land border.

Methods

The C-BORD Toolbox will include five complementary, innovative detection technologies, including improved X-rays, tagged neutron inspection system, photofission, sniffing and passive gamma and neutron detection systems. X-ray systems will be improved by combining different horizontal and vertical views as well as automatic pattern recognition. A tagged neutron inspection system will be applied in mobile units taking care of radiation protection issues. Photofission technology will be developed to detect special nuclear material (SNM) using high energy linear accelerators. Evaporation based detection technologies will also be used in mobile systems complementing X-ray imaging. Recently developed mobile and relocatable passive detection systems (e.g. radiation portal monitors) will be integrated in comprehensive NII applications.

Results

A comprehensive test campaign has been performed at the testing laboratory of MTA EK to evaluate the performance of modular mobile and relocatable detector systems designed and constructed by Symetrica Co. Ltd (Southampton, UK).

These systems involve crystal detectors, large volume PVT (Poly-vinyl toluene) instruments and He-3 free neutron detectors. Their capability to detect, categorize and identify a variety of threatening materials in masked and shielded configurations was studied extensively. Similar type vehicle based detector systems were tested with the same purpose in the mobile laboratory of MTA EK.

Beside the laboratory and open air investigations an infield validation protocol was prepared to get an approval from the Hungarian Atomic Energy Authority to assure the safe operation of the X-ray system planned to be used at the field exercise.



Remaining work

Further tests against ANSI N 42.43 standards will be performed and in 2018 an international field exercise will be carried out at a Hungarian landborder crossing place (Röszke) in the frame of the C-BORD EU project. Another task will be our participation during the in-house testing of other new technologies, like photofission and improved X-ray machine.

DEVELOPMENT OF NATIONAL NUCLEAR FORENSICS LIBRARY

Éva Kovács-Széles, László Lakosi

Objective

Illicit trafficking of nuclear and other radioactive material is a subject of serious concern due to radiological hazard to the public and the environment as well as the security risks associated with nuclear and other radioactive material out of regulatory control. Nuclear and other radioactive materials started to be smuggled across Europe following the break-up of the Soviet Union. Nuclear forensic science was born at that time to examine these materials. The aim of the investigations is to characterize the material for determination of the possible origin of it. Availability of these data characteristics, the experiences indicate that it is difficult to determine the origin and history of unknown samples without comparison of data from known samples to facilitate the identification. Therefore, establishment of databases and determination of key-parameters (signatures) for origin assessment are highly essential. MTA EK participated a Coordinated Research Project of the International Atomic Energy Agency (IAEA) which aimed the establishment of this kind of database (Library System) and to find the relevant signatures.

Methods and Samples

The project has got more aims: to analyse nuclear materials seized by the Hungarian authorities to obtain relevant signatures useful for origin assessment; statistical analysis and evaluation of the data and establishment of the library program in Hungary, to extend the analysis for sealed radioactive sources to find potential forensic signatures in this case. The following techniques, available at MTA EK, were used for this purpose: physical characterization, optical and scanning electron microscopy, gamma-spectrometry, mass spectrometry, X-ray diffraction and X-ray fluorescence, Fourier-Transformation Infrared Spectroscopy techniques. Novel methods were developed and other techniques were also tried for these purposes: Laser Induced Breakdown Spectroscopy (LIBS) and Electron Spectroscopic techniques. A database with searching function as a first prototype of a National Nuclear Forensic Library has also been developed and tested using the analytical data of the project.

Results

In the frame of the project several different nuclear materials were analysed, as well as novel types of materials as 60 laboratory chemicals and sealed radioactive sources. In the case of LIBS measurements chemometry and special statistical evaluation were also used and the results were promising. Using some parameters, samples could be separated by their type and origin. These parameters can be considered as useful signatures for origin assessment: SEM pictures (morphology study), LIBS spectra and chemometry, production date, uranium isotope composition with special emphasis on U-236 content, some key elements (e.g. V, Mg, Ga) and rare-earth profiles. In case of sealed radioactive materials PuBe sources were analysed. Relevant signatures can be the Am-241 content for determination of age of the source, as well as Pu-239 composition (type of plutonium) and homogeneity of Pu powder within the capsule. Fig 2. shows an example of the results and the Library Program.

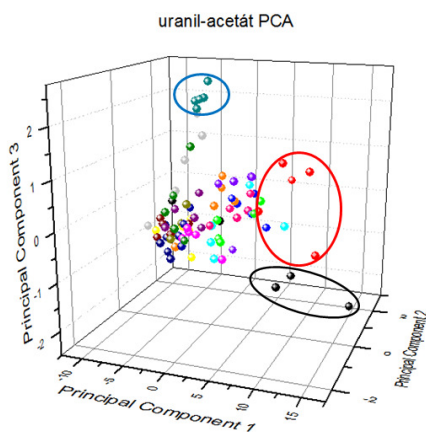


Figure 1: PCA analysis of data of different uranyl-acetate samples

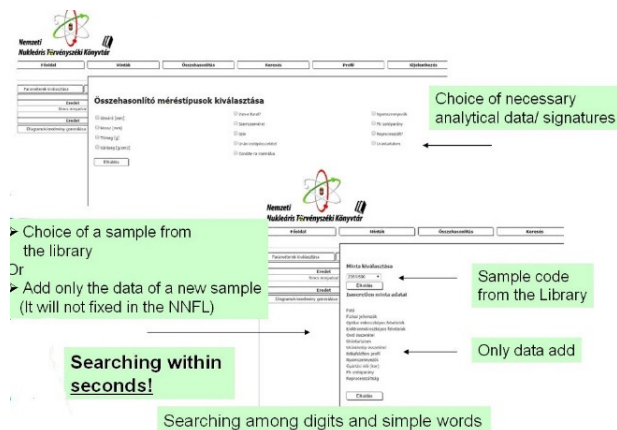


Figure 2: Searching of data-comparison function in the library system

Remaining work

Development of the Library system with extension capabilities is in progress. Further aim is the fine tuning of the Library Program with different new functions, e.g. on-line data receiving directly from the field of sample collection, as well as further searching functions (e.g. population analysis).

Related publications

- [1] É. Kovács-Széles: *Establishment of a National Nuclear Forensic Library by analysis of confiscated nuclear materials*, OAH MMT research report, OAH-NBI-ABA-20/16-M, in Hungarian (2016)
- [2] É. Kovács-Széles and L. Lakosi: *Final Report on Coordinated Research Project (IAEA-CRP: J02003) with title: „Identification of High Confidence Nuclear Forensics Signatures for the Development of National Nuclear Forensics Libraries”*, 2016

SPECIALIZED TRAINING COURSES FOR NUCLEAR FORENSIC PURPOSES

Éva Kovács-Széles

Objective

Centre for Energy Research (MTA EK) operates the only Nuclear Forensic Laboratory in Hungary which is led by the Nuclear Security Department. The task of nuclear forensics is delegated to MTA EK by a Governmental Decree (490/2015 - updated recently), following our 20-years experiences in this field. In recognition of our activity, in December 2016, the International Atomic Energy Agency (IAEA) appointed MTA EK to its Collaborating Centre for Nuclear Forensics. In the frame of this Centre, MTA EK strives to help the East-Central European Region and other IAEA member states through international training courses and special residential assignment programs. The aim of the courses is to give a comprehensive and detailed training on nuclear forensics using practically different analytical techniques as scanning electron microscopy (SEM), inductively coupled mass spectrometry (ICP-MS), gamma-spectrometry and others. More training courses were organized in 2016: an International Practical Introduction Training Course for 12 participants from different countries (Arab Emirates, Mexico, Egypt, Ecuador, Iraq, etc.) and 2 specialized practical training courses using SEM and ICP-MS techniques for 2x2 participants from Ukraine, organized by Joint Research Centre (JRC) Karlsruhe. A 3-months long Residential Assignment program was also hosted for a young scientist from Malaysia. The courses included both the theoretical background as well as a practical hands-on training with nuclear materials.

Methods - Results

The trainings contained the following elements:

1. Presentations/theoretical part
 - Basics: introduction to nuclear forensics, role and use of techniques, working principle of the different instruments, instrumentation capabilities (typical detection limits and other limitations), etc.
 - General methods and special requirements for sample preparation: e.g. radiochemistry, separation techniques
 - Evaluation, data processing and software operation: software overview, qualitative and quantitative analysis, isotope dilution and elemental analysis, elemental mapping and particle analysis (with SEM), using different certified materials
 - Quality control: certified reference materials (standards and tracers) with special focus on nuclear forensic applications, ISO-17025 laboratory quality management system
 - Introduction and demonstration of the National Nuclear Forensics Library system of MTA EK
2. Practical part
 - The trainings included the use of real instruments: a Philips SEM 505 equipped with a LINK AN 10/55S type EDS and a JEOL JSM 5600LV with an energy dispersive X-ray analyser (EDS) and a wavelength dispersive analyser (WDS), Element2 type ICP-MS instrument (Thermo Electron Corp.) and several different type gamma-spectrometers.
 - The trainings contained several analysis types for origin assessment: physical characterization, morphology study, determination of: isotopic composition, production date, impurities (trace elements), rare-earth element profiles, lead isotopic ratios, etc.

During the training the participants could get a basic and extensive knowledge about nuclear forensic and different analytical techniques as well as their special role and use for forensic purposes.



Remaining work

Further trainings in the field are under organization by IAEA. Next 1-week IAEA training course will be held in October, 2017 as well as the 3-months Residential Assignment Program for 3 participants between 1st of October and 16th of December, 2017.

REGIONAL TRAINING COURSE ON ADOPTION OF QA/QC METHODS AND PROCEDURES FOR INTER-COMPARISON OF RADIATION DOSIMETRY IN RADIATION FACILITIES FOR PROCESS CONTROL

András Kovács

Objective

Radiation processing is a worldwide technology mainly for the sterilization of medical devices, for the production of advanced polymer materials, for food irradiation and for environmental protection. The widespread application and the proper use of these technologies is one of the priority areas of both the European Union and the International Atomic Energy Agency (IAEA). In order to fulfil these tasks, the IAEA initiated regional cooperation projects also in the European region, mainly for developing countries. The Centre for Energy Research (MTA EK) operates a gamma and electron beam dosimetry laboratory aiming at our R&D in developing new dosimetry methods and procedures for radiation process control in gamma and electron beam irradiation facilities, to design new analytical instrumentation for the evaluation of dosimeter systems irradiated at these facilities, to assist Hungarian irradiation facilities in applying different process control methods and to organize international training courses for users of these technologies. In the frame of the European Regional TC Project RER 1017 "Using Advanced Radiation Technologies for Materials Processing" of the IAEA the Nuclear Security Department of MTA EK organized a training course for 13 participants from nine countries (Azerbaijan, Bulgaria, Croatia, Latvia, Portugal, Slovakia, Serbia, Turkey and Ukraine). The purpose of the training course was to provide theoretical and practical training in the field of validation and control for radiation processing providing the background for understanding the requirements of the international standards. The overall objective was to assure qualified personnel for radiation process control in Member States of the IAEA in radiation processing facilities.

Methods - Results

The training contained the following elements.

1. Presentations/theoretical part:

- Introduction to radiation processing technologies. Dosimetry principles and systems applied for quality assurance (QA) and quality control (QC). The role of dosimetry (according to the ISO Standard 11137) in validation and routine process control. Calibration of dosimetry systems, traceability, uncertainties. Influence quantities in radiation processing. Thermoluminescent dosimetry in radiation processing.
- Presentations of the participants about the role and practical application of radiation processing in their countries.
- The purpose and the practical execution of the dosimetry intercomparison programme for the RER (Regional European projects of IAEA) participating countries.
- Visit to the irradiation facilities and the research reactor of MTA EK.

2. Practical part:

- Calibration exercises using ethanol-monochlorobenzene (ECB) solution, GEX radiochromic film, Al_2O_3 thermoluminescent chip and polystyrene calorimeter dosimeter systems.
- Dose mapping and routine process control.
- Basics of dosimetry activities in installation qualification (IQ), operational qualification (OQ), performance qualification (PQ) and routine process control.



Remaining work

Further trainings in this field are to be organized both in gamma and electron beam radiation processing validation dosimetry and process control during the planned IAEA Regional TC Projects in the next (2018-2019) cycle.

SPECTRUM EVALUATION ALGORITHM FOR SCINTILLATION DETECTORS

András Kocsonya, Anna Pántya, Károly Bodor, Péter Zagyoai

Objective

Employees exposed to the risk of incorporation of radioactive materials are routinely monitored by the whole body counter of MTA EK. Due to the simple operation and high efficiency these routine screening measurements are done by scintillation detector. The currently available spectra-evaluation code requires interactive contribution of the operator. Since the vast majority of spectra contain no incorporation, the evaluation of this spectra is a time consuming and rather tedious task but it demands high attention from the operator to select spectra containing any artificial incorporation. Our aim is the development of an automatic algorithm requiring no interactive operation which supports the operator to select spectra requiring more detailed analysis.

Methods

A spectra evaluation algorithm was developed specially devoted to the spectra recorded by the scintillation detector of the whole body counter. Because of the limited measurement time of human measurements, the counting statistics of these spectra are rather poor. The background subtraction is fundamental in course of evaluation. The background is composed from gamma-lines terrestrial radionuclides including radon daughter elements (^{214}Bi , ^{214}Pb , ^{212}Pb) and the continuous Compton region. In normal cases only ^{40}K can be detected in human body. In spite of the ventilation by filtered air the radon level shows daily and seasonal variation but it depends on several environmental parameters (e.g. air pressure). Hence the variation of background cannot be predicted but it should be measured experimentally. In course of routine measurements background spectra are recorded one or two times pro day.

The aim of our algorithm is a flexible taking into consideration variation of background. The spectra to be evaluated are imported in UNA/LNA format which is compatible with the current data collection and evaluation system. The fitting algorithm is implemented in the Gnuplot code. The main routines calling the fitting algorithms are implemented in bash shell in Linux environment.

The selection of initial parameters of non-linear fitting is fundamental. An average value is derived of all model-parameters form a large set of spectra collected in similar conditions. This set is used as initial set of parameter. Due to the poor statistics non-linear fitting algorithms are tend to diverge or converge to a physically unrealistic result. To eliminate these numerical problems a four step fitting algorithm is applied:

1. Refinement of energy calibration of the spectra. The proper energy calibration is the basis of any further step, but due to the slight instability of the data processing electronics small shifts are often occurring. The energy calibration is refined by a two-point fit to the 511 keV annihilation peak and the 1461 keV peak of ^{40}K which peaks can be found in all whole body spectra.
2. Fit of linear parameters (line-intensities only) however the intensity ratio of above mentioned background nuclides are fixed at the initial value.
3. Fit the linear parameters once again, but the intensities of the individual background radionuclides become free parameters (physically the terrestrial decay series are considered independent on each other and secular equilibrium is not supposed more).
4. Fit of all parameters including non-linear parameters such as energy resolution of the detector.

The code provides the graphs of the fitted spectra and the residuals. Although the program runs automatically without interactive actions, using these graphs the correctness of fit can be checked visually by the operator. The convergence parameters are scaled according to empirical observation of several runs, which determine acceptance of the fit or draw the acceptance of the operator to the unusual case requiring more sophisticated human inspection. A few common artificial radionuclides (^{60}Co , ^{137}Cs , ^{131}I) are implemented to the numerical model, thus these common nuclides are identified and quantified automatically.

Results

Several hundred whole body spectra collected since 2013 were evaluated by the new algorithm such as two ^{65}Zn incorporation in two consecutive years. According to personal experiences the new algorithm significantly facilitated the operator's work. Using this algorithm little rather low incorporation were observed which were undiscovered by the former methods.

Remaining work

On-line connection between the data collecting computer and the computer used for evaluation would be useful. In case of interest this algorithm could be transferred to other scintillation spectrometers.

ORGANIZATION OF A VIRTUAL TABLE TOP EXERCISE (TTX) FOR PRACTICE OF RESPONSE TO NUCLEAR SECURITY EVENTS

Éva Kovács-Széles, Katalin Táló

Objective

Terrorism is a real increasing danger worldwide, nowadays. Hungary is not a typical target country for terrorists but the danger is a fact in our everyday life in Europe, therefore to be prepared for terror attacks is essential. Following the terrorist events in Brussels and Paris in 2016, the Counter Terrorism Centre brought together a Nuclear Security Working Group in Hungary with all the authorities and organizations which are responsible for response to a nuclear security event. The Working Group decided to organize exercises to improve the Hungarian system and to practice the response activities in a multiple-actor radiological situation to harmonize the activity of the responsible authorities. The first aim is the organization of a virtual Table Top Exercise (TTX), which is a good platform to discuss the present laws and regulations and to have a deep discussion and cooperation among different authorities and organizations. Secondly, the next aim would be to organize a real field exercise to practice the response activities, following the conclusions of the TTX.

The TTX is connected to the 490/2015 Governmental Decree which describes the response activities in the case of different types of nuclear security events like the case of missing, found or confiscated nuclear or other radioactive materials. This decree indicates MTA EK as the responsible expert institution for response to events connecting to nuclear materials, therefore MTA EK together with the Hungarian Atomic Energy Authority were asked by the Counter Terrorism Centre to develop a task group to organize the virtual Table Top Exercise (TTX).

Task Group

MTA EK established the TTX Task Group with the aim of the organization and implementation of the exercise. Different authorities and organizations were invited into the Task Group to help the work. The Task Group consists of 12 people from the following institutions: Hungarian Atomic Energy Authority, Hungarian Army, Counter Terrorism Centre, Hungarian Police Bomb Disposal Unit and Bureau of Investigation, Disaster Directorate, National Research Institute for Radiobiology and Radiohygiene. The main organizer is the Hungarian Atomic Energy Authority who supports MTA EK in this work.

Results

The Task Group worked out the scenarios of the virtual TTX. Besides, it developed the technical implementation of the exercise: location, construction, schedule, actors, etc. The exercise will be 3-days long with 3 different scenarios and about 50 actors with all the responsible authorities and organizations.

The picture is only an illustration for a field exercise.



Remaining work

The organization of the TTX is in progress. Implementation of the exercise is planned at the end of 2017 with all the responsible authorities. Following the conclusions of the TTX, a real field exercise is also planned in the near future.

Related publication

- [1] É. Kovács-Széles: *Organization of a virtual Table Top Exercise (TTX) for practice of response nuclear security events*, Research Report for the Hungarian Atomic Energy Authority, OAH-NBI-ABA-31/16-M, in Hungarian (2016)

BASIC RESEARCH ON THE BIOPHYSICAL EFFECTS OF LOW DOSES OF IONISING RADIATION

Imre Balásházy, Balázs G. Madas, Emese Drozsdik, Péter Fűri, Árpád Farkas, Blanka Mónika Czitrovsky, Ágnes Jókay

Objective

This year four research objectives were undertaken in the field of low dose research of ionising radiation:

- development of the stochastic lung deposition model to compute tissue and cell nucleus doses of inhaled alpha emitters along the bronchial airways,
- comparison of the radiation burden of primarily deposited and up-clearing inhaled radon progenies along the different airway generations of the bronchial airways,
- analysis of the consequences of spatial inhomogeneity of radiation burden of inhaled radon progenies [1],
- experimental investigation of the effects of low and moderate doses of ionising radiation on moth.

Methods

The stochastic lung deposition model applies Monte Carlo methods to generate the geometry of human airways and to compute deposition and clearance of inhaled aerosol particles in the whole respiratory system. The paths of alpha-tracks and absorbed energy components were determined in the mucus, the epithelium and the target cell nucleus. Based on these values the absorbed doses can be computed.

The velocity of clearance of the deposited radionuclides was supposed to be equal with the velocity of the mucus in the different airway generations.

It was also studied, how the changes in tissue architecture upon radon exposure modulate the cellular burdens.

324 eggs of a gypsy moth (*Lymantria dispar*) were irradiated with 1 Gy ^{137}Cs external gamma-radiation. A control group of 258 eggs of the same gypsy moth were not irradiated. Both the irradiated and the non-irradiated individuals were kept and developed in room temperature and under average humidity. The date of pupation and the date of hatching were measured at each of the individuals. In addition, several other parameter values were monitored during the development of the larvae, pupae and imagoes.

Results

Based on the computations, it has been stated that the alpha-burden originating from inhaled radon progenies is very inhomogeneous in the bronchial region. In this way, the necessity of the dosimetric analysis in an airway generation level is justified.

The radiation burden of the cleared-up fraction of inhaled and deeply deposited radon progenies can be commensurable or even higher than the burden of the primarily deposited particles but only in the first few large bronchial airways [2].

It was pointed out that recent exposure history of the tissue modulates its geometrical properties and thus the microscopic dose consequences of a given macroscopic exposure to radon progeny [3].

Irradiation of the eggs of gypsy moth with 1 Gy gamma radiation resulted in slight effects on the distributions of pupation time and hatching time. This means that one part of the female caterpillars originating from irradiated eggs becomes pupa later than the non-irradiated ones and, similarly, one part of the female pupae becomes moth later due to irradiation [4, 5].

Remaining work

Fractions of the cell nucleus doses due to primary deposition and mucociliary clearance will be further analysed.

Related publications

- [1] B.G. Madas: *Radon exposure and the definition of low doses - the problem of spatial dose distribution*. Health Physics **111** (1) 47-51 (2016)
- [2] P. Fűri, I. Balásházy, G. Kudela, B.G. Madas, Á. Farkas, Á. Jókay and B. Czitrovsky: *Comparison of deposited and cleared up fractions of the bronchial burdens of inhaled radon progenies*, XLI. Radiation Protection Course. 26-28 April 2016, Hajdúszoboszló, Hungary, Book of Abstracts, 35 (2016)
- [3] B.G. Madas: *Radon induced hyperplasia: effective adaptation reducing the local doses in the bronchial epithelium*, Journal of Radiological Protection **36** (3) 653-666 (2016)
- [4] B. Czitrovsky: *Examination of the effects of low and moderate dose ionising radiation on moths*, MSc diploma work. University of West Hungary (2016)
- [5] B. Czitrovsky, P. Fűri, Zs. Bálint, Á. Jókay, P. Szántó and I. Balásházy: *Gamma and neutron radiation effects on butterflies*, V. Terrestrial Radioisotopes in Environment: International Conference on Environmental Protection. Veszprém, Hungary, 17-20 May 2016, Social Organization for Radioecological Cleanliness 87 (2016)

DELAYED NEUTRON COUNTING TO DETERMINE NANOGRAM QUANTITIES OF ^{235}U

László Szentmiklósi, Zoltán Hlavathy, Dénes Párkányi, József Janik, Csaba Katona

Objective

To establish a delayed neutron counting facility (DNC) at the fast pneumatic rabbit system of the NAA laboratory of the Budapest Neutron Centre and assess its analytical performance for rapid and selective ^{235}U quantification.

Methods

Delayed neutron counting (DNC) is a rapid analysis technique to determine the fissile-material content of samples. Recently the application of the DNC technique is once again increasing around the world, driven by the needs of nuclear safeguards rather than uranium prospecting.

Results

We integrated a Canberra JCC-31 type neutron counter into the fast pneumatic rabbit system of the NAA laboratory. A bypass of the transfer system allowed the transfer of the irradiated sample directly into the neutron counter (Fig. 1 left). Special parts of the system were manufactured by 3D printing. The counting electronics (PTR-32 HV, with a breakout module to accept external triggers) was coupled with the control software and hardware of the facility. The shielding was optimized by Monte Carlo calculations using the MCNP5 code.

We determined the analytical performance indicators of this setup, including background, blanks, linearity, and lower limit of quantification. The setup was calibrated with a dilution series. It was decided that the sample shall be irradiated for 60 s, as longer irradiation does not substantially increase the useful signal. We have proven that the analytical signal, i.e. the net count rate of the neutron detector, shows the expected time behaviour (Fig. 1 right) and the method is linear in the range of 4 ng – 40 μg of natural uranium. Irradiations of strongly depleted uranium as well as thorium samples evidenced that the interference reactions caused by fast neutrons do not bias the ^{235}U quantification significantly. Uncertainties of these preliminary results are 5-10% at the low U range whereas 2-3% for the high part of the calibration range. At present 100 ng of natural uranium, corresponding to about 1 ng of ^{235}U can be reliably quantified. This is in the range of similar facilities worldwide, but still there is a room for improvement by fine tuning the experimental conditions.

The present methodology gave three orders of magnitude gain in the uranium detection limit over the previous technologies using external beams, giving a new, complementary procedure, extending MTA EK's portfolio for nuclear safeguards.

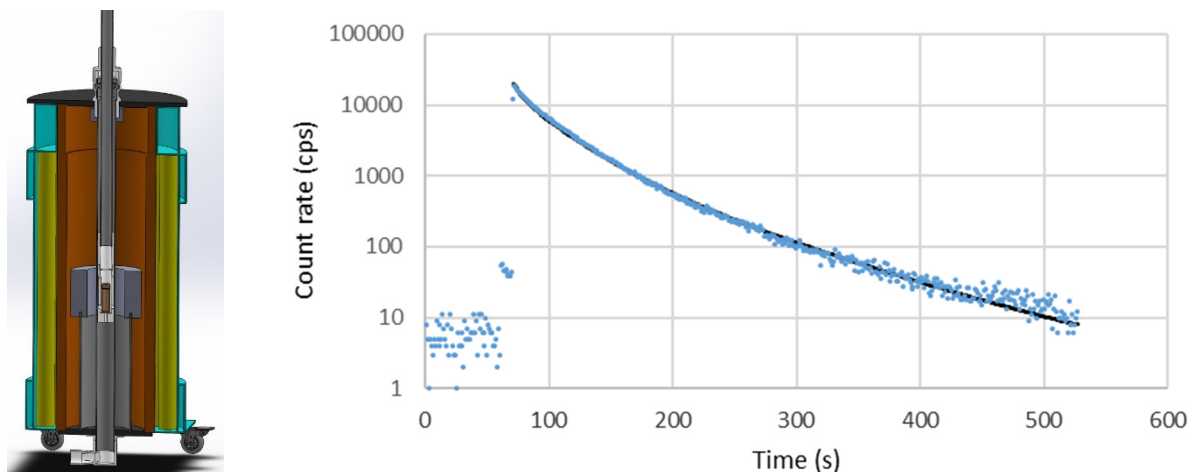


Figure 1: Left: integration of the delayed neutron counter into the fast rabbit system of the NAA laboratory. Right: delayed neutron emission of ^{235}U as a function of time, fitted with the eight-group model

Remaining work

To reduce the blank signal by using high-purity sample containers. To improve the detection limit by more reproducible background level and better estimation of its statistical variation.

Related publication

- [1] L. Szentmiklósi, Z. Hlavathy, D. Párkányi, J. Janik and Cs. Katona: *Fast pneumatic rabbit system combined with delayed neutron counting system to determine small quantities of ^{235}U* , OAH-ABA-22/16-M report EK-NAL-2016-254-001, in Hungarian (2016)



IV. ENERGY AND ENVIRONMENTAL STUDIES



THE EVALUATION OF THE METEOROLOGICAL DATABASE OF THE PAKS NPP

Sándor Deme, Dorottya Jakab, Tamás Pázmándi, Péter Szántó

Objectives

In order to extend a previous research, comparative analysis was performed for one-year meteorological data of the Paks Nuclear Power Plant (NPP) site obtained from different data sources. The examined meteorological data were measured by the meteorological tower and the SODAR (SONic Detection And Ranging) system, which are both located at the site. In addition to the measured data, predicted values of meteorological parameters were also available provided by the ALADIN Numerical Weather Prediction System, which was developed by an international collaboration in which the Hungarian Meteorological Service (OMSZ) was also involved.

The aim of this work was to compare the different meteorological datasets, primarily focusing on the meteorological parameters which are used in atmospheric dispersion modelling. The differences of the meteorological data in the results of the dispersion calculations were also investigated. Based on the findings of this research, it can be determined which system or model provides the most adequate and reliable meteorological data to use as input for dispersion modelling.

Methods

The evaluation was made for one-year of meteorological data measured in 2015 at the Paks NPP site. During the assessment, the wind speed, the wind direction, the precipitation, the wind direction fluctuation data and the stability parameter (Pasquill-category) – which was derived from the wind direction fluctuation data – were evaluated. The data from different sources were compared regarding several measurement heights (10, 20, 50, 120 m).

To assess the effect that the differences in the meteorological parameters have on the estimated doses, sensitivity analysis was performed using the SINAC (Simulator software for Interactive modelling of environmental consequences of Nuclear Accidents) program, which was developed by MTA EK.

Results

The correlation between the wind speed and the wind direction data, provided by the meteorological tower and the SODAR, is sufficient regarding the dispersion modelling. However, it was found that the resolution of the anemometer used for the measurement of the wind direction is inadequate for the standard's specifications; therefore, the use of an equipment with higher resolution is recommended.

On the basis of the evaluated data, it was revealed that there are significant differences between the wind direction fluctuation data measured by the meteorological tower and the SODAR system at the 20 m measuring height. Since this data both in the case of the tower and the SODAR is the primary source parameter for the determination of the Pasquill-category, the difference can lead to significant deviations in the dispersion model results. It was demonstrated that the wind direction fluctuation data of the SODAR is an underestimation compared to the data provided by the meteorological tower, which generally results in a one-category difference between the Pasquill-categories. The sensitivity analysis of the Pasquill-classification showed that the one-category difference can result in 40-50 % difference in the above-ground activity concentration values. In the case of the meteorological tower, the most common Pasquill-categories are the instable and neutral categories, while concerning the SODAR, the neutral and stable categories are dominant.

The data availability of the meteorological tower is sufficient; the few absences of the data were caused by equipment maintenance. In case of the SODAR measurements, the absence of the data was more frequent and typically over 10-to-60-minute long periods. It was found that the meteorological tower provides meteorological data with the same precision at every measuring height, unlike the SODAR system which provides data with worse signal-to-noise ratio as the measuring height increases. Since the precision of the data provided by the meteorological tower is adequate for the atmospheric dispersion calculations, it is recommended for use in dispersion modelling. If the data from the meteorological tower is not available, the SODAR can be used as a secondary data source.

The predicted wind speed data provided by the ALADIN model were underestimations in the lower wind speed-range and overestimations in the higher wind speed-range. It was also shown that the ALADIN model properly predicts the precipitation events, though the expected precipitation values provided by the model and the data measured on-site were significantly different.

Remaining work

The main objective of the project was to compare the available one-year meteorological datasets at the Paks NPP, which has been accomplished. Although the planned work has been completed, with further evaluation of datasets with longer timespans, the used data processing methods and the results can be verified.

Related publication

- [1] S. Deme, D. Jakab, T. Pázmándi and P. Szántó: *The evaluation of the meteorological database of the Paks NPP*, EK-SVL-2016-703-01-01-00, in Hungarian (2016)

SUPPRESSING COKE FORMATION DURING DRY REFORMING ON SODIUM OR INDIUM PROMOTED NICKEL CATALYSTS

Ferenc Somodi, Miklós Németh, Johanna Károlyi, György Sáfrán, Anita Horváth

Objective

The selective conversion of methane with carbon dioxide yields hydrogen and carbon monoxide as reaction products in equimolar ratio (dry reforming, DRM: $\text{CH}_4 + \text{CO}_2 \rightleftharpoons 2\text{CO} + 2\text{H}_2$). Development of carbon tolerant nickel catalyst for DRM was aimed by 0.7 wt% Na or 2 wt% In modification of the 3% Ni/ZrO₂ or 3% Ni/SiO₂ catalysts, respectively. Structural differences between the samples were studied and the catalytic transformations were followed with special attention to the unwanted surface coke forming processes.

Methods

The Na-promotion was studied on the bare ZrO₂ support (Zr-Na), on Ni impregnated onto this modified support (Ni/Zr-Na), on sample when NaHCO₃ was concomitantly added during wet impregnation of the support (Ni-Na/Zr), and finally without any Na (Ni/Zr). The In-promoted SiO₂ support (SiO₂-In), the bare Ni/SiO₂ and the In containing counterpart with 3:1= Ni:In ratio (Ni-In/SiO₂) was prepared by deposition precipitation with urea. Structural investigations were carried out by X-ray powder diffraction (XRD), X-ray Photoelectron Spectroscopy (XPS) and Transmission Electron Microscopy (TEM). Reducibility of calcined samples was studied by Temperature Programmed Reduction (TPR) experiments. Metal dispersion was measured by CO pulse chemisorption. Temperatures programmed desorption of chemisorbed CO and other species was followed by QMS. Diffuse Reflectance Fourier Transform Infrared Spectroscopy (DRIFTS) was applied to detect the surface-adsorbed species in presence of CO, CO₂ or dry reforming mixture. Temperature-programmed or isothermal dry reforming experiments were done i) in plug flow reactor in excess methane or ii) in a closed loop circulation system using labelled ¹³CO₂. Subsequent temperature programmed oxidation (TPO) measurements were carried out to compare the reactivity of deposited carbon.

Results

Concerning the Na-promoted system, CO pulse chemisorption measured less available Ni surface in Ni-Na/Zr than in Ni/Zr, and the subsequent high temperature CO₂ TPD peak proved a highly increased basicity of the former sample. During DRIFTS measurements in the presence of reforming reactant mixture or CO₂/He stream, monodentate and bridged carbonates were seen on Ni-Na/Zr, while bicarbonates and formates on Ni/Zr catalyst. The formate species produced in diluted CO stream at 300 °C on the reduced catalysts converted fast to carbonates at the metal-support interface in this order: Ni-Na/Zr > Ni/Zr > Zr-Na and non on Ni/Zr meaning that active oxygen or OH species are available even on reduced form of the promoted catalysts. DRM stability tests for 24 hours showed a stable performance for Ni-Na/Zr while Ni/Zr was deactivated with Ni/Zr-Na in between them. Our isotope labeled ¹³CO₂+¹²CH₄ dry reforming experiments showed that CH₄ dissociation is slower, and a highly reactive type of coke originating from methane deposits over Ni-Na/Zr having strong metal-support interaction. Pulse experiments with CO₂ or CO pulses into H₂ or He flow over the catalysts were conducted to approximate the methanation, water-gas shift and/or the CO₂→CO→C dissociation ability of the samples. According to these results, CO₂ and moreover, CO methanation is depressed on sodium containing samples. The absence of high amount of formate species during low temperature dry reforming and the decreased methanation activity of sodium promoted catalysts is explained by the efficient (redox) co-operation of Ni/Ni(OH)₂ surface surrounded by Na₂O/NaHCO₃/Na₂CO₃ ensembles that are embedded in ZrO₂ matrix providing active oxygen species.

Concerning the In-promoted system, the temperature-programmed reduction measurements of the catalysts showed that both nickel and indium was in metallic state after one-hour reduction at 700 °C, which suggested bimetallic interaction. CO pulse chemisorption experiments revealed that the particle size is similar on both Ni-In/SiO₂ and Ni/SiO₂, but CO-TPD measurements showed completely different desorption behaviour of CO, suggesting the presence of different active sites on the two catalysts. In XPS experiments surface enrichment of indium was observed after reduction treatment. The lack of coke formation on Ni-In/SiO₂ during dry reforming might be explained by the suggested decoration of coke-forming active sites of Ni particles by indium and/or providing an oxygen rich indium suboxide surface through the reaction with CO₂ in the close vicinity of catalytically active nickel sites during DRM.

Remaining work

The project will be continued according to the on-going EK 161 project and the new proposals to be submitted next year. The other corresponding EK 167 project ends in 2016.

Related publications

- [1] M. Németh, J. Károlyi, F. Somodi, D. Srankó, Gy. Safran, I. Sajó and A. Horváth: *CO₂ reforming studies in excess methane using Ni/ZrO₂ catalysts*, 13th Pannonian International Symposium on Catalysis, presentation (70. page, ISBN 978-963-9970-56-4) Siófok, sept. 19-23. (2016)

- [2] M. Németh, J. Károlyi, D. Srankó, F. Somodi, Gy. Sáfrán and A. Horváth: *Low temperature dry reforming of methane over Ni/ZrO₂ catalysts: the effects of sodium promotion*, 13th Pannonian International Symposium on Catalysis, poster (115. page, ISBN 978-963-9970-56-4), Siófok, sept. 19-23, (2016)
- [3] F. Somodi, J. Károlyi, M. Németh and A. Horváth: *Carbon dioxide reforming of methane over Ni-In/SiO₂ catalyst without formation of carbon deposits*, (83. page, ISBN 978-963-9970-56-4) presentation, Siófok, sept. 19-23, (2016)
- [4] J. Károlyi, A. Horváth, M. Németh and F. Somodi: *Effect of indium on silica supported nickel dry reforming catalysts*, 13th Pannonian International Symposium on Catalysis, poster (118. page, ISBN 978-963-9970-56-4), Siófok, sept. 19-23, (2016)
- [5] M. Németh, J. Károlyi, F. Somodi, D. Srankó, Gy. Safran, I. Sajó and A. Horváth: *Dry reforming studies in excess methane using Ni/ZrO₂ catalysts*, 16th International Congress on Catalysis, poster PA098, Peking, july 3-8, (2016)
- [6] M. Németh, J. Károlyi, D. Srankó, F. Somodi, Gy. Sáfrán, I. Sajó and A. Horváth: *Tracking of carbon species during dry reforming of methane on different Ni/ZrO₂ catalysts*, 11th Natural Gas Conversion Symposium, poster, Tromso, june 6-9, (2016)
- [7] F. Somodi, J. Károlyi, M. Németh and A. Horváth: *Carbon dioxide reforming of methane over Ni-In/SiO₂ catalyst without coke formation*, 3rd International Symposium on Catalysis for Clean Energy and Sustainable Chemistry (CCESC 2016), presentation, Madrid (Spain) 7th to 9th September, (2016)

CHARACTERIZATION OF BIMETALLIC CATALYSTS BY ^{197}Au MÖSSBAUER SPECTROSCOPY

Károly Lázár, Sándor Stichleutner, Andrea Beck, Nagy Gergely

Objective

Results of the project entitled “Visible light promoted aerobic benzyl alcohol oxidation on alumina supported Au-Cu catalysts” have been reported in EK progress report 2015. Completion of analysis of involved bimetallic particles by ^{197}Au Mössbauer spectroscopy was specified as remaining work for this mentioned study.

Methods

The principal applied method was ^{197}Au Mössbauer spectroscopy. Spectra were collected at 4.2 K at liquid He temperature. For better interpretation of data results of corresponding HRTEM and catalytic measurements are also cited.

Results

Au-Cu/Al₂O₃ catalysts: Results of structural and catalytic evaluation of alumina supported Au-Cu catalysts were presented in an international conference. Increase of lattice constant attributed to Au-Cu alloy formation was detected in corresponding HRTEM data. Mean particle diameter was also determined, 2 - 3 nm was found. Activity of catalysts prepared by co-reduction and consecutive reduction were compared. The co-reduced Au-Cu catalyst exhibited the best performance in the oxidation of benzyl alcohol [1]. This sample was characterized by ^{197}Au spectroscopy, too (Fig. 1). The spectrum can be decomposed to a dominant bulk Au-Cu alloy (singlet) and a minor doublet contribution attributed to Au atoms located on the surface of particles. The corresponding parameters are shown in Table 1. The interpretation of data is in good correspondence with results presented in [1].

Table 1: Mössbauer parameters of ^{197}Au spectra of Au&Cu/Al₂O₃ and Au₈₀Ag₂₀/SiO₂ catalysts

Sample	Comp.	δ^a	Δ^b	Rel. Int. ^c
Au&Cu /Al ₂ O ₃	Au-Cu alloy	0.26	-	63
	Au(surface)	0.67	2.22	37
Au ₈₀ Ag ₂₀ /TiO ₂	Au-Ag alloy	0.30	-	69
	Au(surface)	0.44	1.75	31

^a isomer shift, related to metallic Au, mm/s;

^b quadrupole splitting, mm/s; ^c relative intensity, %.

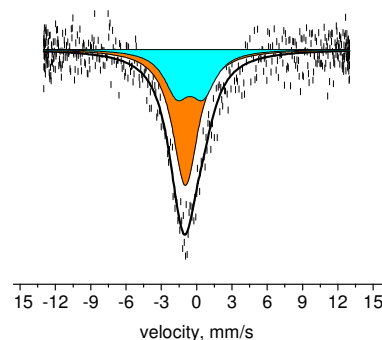


Figure 1: ^{197}Au Mössbauer spectrum of the Au&Cu/Al₂O₃ catalyst

Au-Ag/TiO₂ catalyst: For comparison to Au-Cu/Al₂O₃ catalysts an Ag-Au/TiO₂ catalyst was also characterized with ^{197}Au spectroscopy. Due to the titania support this catalyst may probably attain promising applications in photocatalytic processes. Further on, a similar, Au₈₀Ag₂₀/SiO₂ alloy catalyst exhibited the best activity in glucose oxidation in comparison with alloy catalysts with other Au : Ag ratios (T. Benkó et. al. Appl. Catal., A: General, 479 (2014) 103). The corresponding ^{197}Au Mössbauer spectrum of the Au₈₀Ag₂₀/TiO₂ catalyst can also be decomposed to a singlet and a doublet. (Related data are shown in Table 1.)

In summary it can be concluded that both the ^{197}Au Mössbauer spectra of Au-Cu/Al₂O₃ and Au-Ag/TiO₂ can be decomposed to a singlet and a doublet component. The isomer shifts in both cases exhibit certain positive shift in comparison to metallic gold, which can be explained by formation of bimetallic alloys. The doublet component with smaller intensity can probably be attributed to contribution originated from surface gold atoms. The mentioned results of ^{197}Au measurements have also been presented in an international workshop [2].

Related publications

- [1] G. Nagy, D.F. Srankó, G. Sáfrán, L. Borkó, Z. Schay, A. Deák, B. Maróti, F. Schmidt, F. Hofer and A. Beck: *Aerobic oxidation of benzyl alcohol and glucose on Au-Cu bimetallic catalysts: Relation between structure and catalytic activity*, 13th Pannonian International Symposium on Catalysis, (ISBN 978-963-9970-56-4) 45 (2016)
- [2] S. Stichleutner, K. Lázár, L. Szentmiklósi and T. Belgya: *^{197}Au Mössbauer measurements and the in-beam facility at the Budapest Neutron Centre*, 3rd Annual Meeting of Hungarian Mössbauer spectroscopists, 5th October, 2016, Budapest.

AU-CONTAINING BIMETALLIC CATALYSTS IN HIGHLY SELECTIVE AEROBIC OXIDATION REACTIONS

Andrea Beck, Gergely Nagy, Somodi Ferenc, László Borkó, Zoltán Schay, Antal Tungler

Objective

The reported work belongs to our research project started in 2012 (OTKA #101854) on study of gold-based bimetallic systems as promising catalysts for aerobic selective oxidation processes, which are high importance green transformations in fine chemistry and in application of biomass derived feedstocks. Earlier we demonstrated the synergetic effect of Au with Ag and Cu in bimetallic sol derived AuAg/SiO₂ and AuCu/Al₂O₃ catalysts in base free selective oxidation of benzyl alcohol model substrate. The work was continued with the study of sol derived alumina supported AuAg, AuRu and AuIr.

Methods

The bimetallic Au-M (M: Cu, Ag, Ru, Ir; Au/M atomic ratio: 1/1) and corresponding monometallic nanoparticles were produced by aqueous phase reduction providing metal sols (SOL method), Au-Ag colloids also by solvated metal atom deposition (SMAD method, at Institute of Molecular Science and Technologies (IMST), CNR) in acetone followed by adsorption on Al₂O₃ support. AuAg samples with Au/Ag = 4/1 as well were formed by both methods. The catalysts were characterized in as prepared state and after oxidation and reduction pretreatments by HR-TEM (performed by G. Sáfrán, MFA), high resolution EDS (by Franz Schmid, Institute for Electron Microscopy and Nanoanalysis, Graz University of Technology; Claudio Evangelisti, IMST-CNR), UV-vis spectroscopy, temperature programmed oxidation and reduction (TPO, TPR), CO adsorption measured by QMS analysis and followed by FT-IR spectroscopy, and tested in oxidation of benzyl alcohol and glycerol (in Laura Prati's research group at Department of Inorganic, Organometallic and Analytical Chemistry, University of Milan) in toluene solution by O₂ at 80°C with or without addition of equimolar K₂CO₃ and in aqueous solution by O₂ at 50°C with addition of NaOH, respectively.

Results

The addition of the second metal in Au/M=1/1 atomic ratio decreased the benzyl alcohol oxidation activity of Au/Al₂O₃ in different extent in order Ag>Ir>Ru in base free conditions, while in case of Cu as second metal the gold activity could be doubled. All the active catalysts showed strong deactivation in the reaction by the strong poisoning effect of benzoic acid side product. The second metals in the corresponding monometallic samples had negligible (Ru, Ir) or no activity (Ag, Cu). In presence of K₂CO₃ AuAg, monometallic Ag as also Cu was still inactive as in base free reaction, but the activity of the other samples highly increased, in case of AuRu and AuIr after an induction period of about 10 minutes. After this, reaction rate over AuRu/Al₂O₃ exceeded that one measured over Au/Al₂O₃ with the same gold content. In case of AuCu/Al₂O₃ in presence of K₂CO₃ beside activity increase and the elimination of benzoic acid inhibiting effect, the weakening of the promoting effect of Cu on Au was observed. AuAg/Al₂O₃ of Au/Ag=4/1 prepared using sol method reached about the same activity related to the same Au content as Au/Al₂O₃, but presented synergetic activity increase in the preliminary glycerol oxidation tests. The corresponding SMAD derived sample was much less active in both reactions. In benzyl alcohol oxidation the selectivity (over 90% to benzaldehyde) was not significantly affected by the second metal, in glycerol oxidation selectivity also changed on Ag addition.

To understand the reasons of the bimetallic effect observed in catalysis detailed structural characterization was required. TEM studies showed that the particle size of gold containing particles were in the range of 2-3 nm in AuAg and AuCu and monometallic Au and around 4 nm in AuRu and 5-6 nm in AuIr samples. The presence of bimetallic particles, intimate contact of the two metals in the bimetallic catalysts were indirectly indicated by shifted SPR band of gold, modified TPR properties of the second metal, and shifted IR bands of adsorbed CO after oxidative treatment suggesting larger electron deficiency on gold in bimetallic samples, while directly confirmed by HR-EDS. In the measured particles the Au/M ratio was close to the bulk ratio in the AuAg and AuRu samples, while in AuCu samples the Au/Cu in single particles was about 85/15 instead of 1/1 characteristic of bulk. The top surface composition of the bimetallic catalysts strongly affects the catalytic performance. The determination of that is a difficult task especially in these systems, however, the CO adsorption measurement on the different bimetallic catalysts after different pretreatments showed large differences in the number of Au sites adsorbing CO, which correlated quite well with the catalytic activities. In the bimetallic effect, beside the type of the second metal, the structure has a decisive role.

Remaining work

The support effect will be studied in AuCu and AuAg systems using further supports of different acid-base properties.

Related publications

- [1] G. Nagy, D.F. Srankó, G. Sáfrán, L. Borkó, Z. Schay, A. Deák, B. Maróti, F. Schmidt, F. Hofer and A. Beck: *Aerobic oxidation of benzyl alcohol and glucose on Au-Cu bimetallic catalysts: Relation between structure and catalytic activity*, 13th Pannonian International Symposium on Catalysis, (ISBN 978-963-9970-56-4) **45** (2016)
- [2] G. Nagy, G. Sáfrán, D. F. Srankó, L. Borkó, Z. Schay, B. Maróti, F. Schmidt, F. Hofer and A. Beck: *Aerobic oxidation of benzyl alcohol and glucose on alumina supported Au-containing bimetallic catalysts: Comparison of Ag, Cu, Ru and Ir as second metals*, 13th Pannonian International Symposium on Catalysis, (ISBN 978-963-9970-56-4) **122** (2016)

NEW SYSTEMS TO PROMOTE WATER OXIDATION

József S. Pap, Róbert Horváth, Enikő Farkas, Dávid F. Srankó, Zsolt G. Kerner

Objective

Water oxidation (or the oxygen evolving reaction, OER): $2\text{H}_2\text{O}(\text{l}) \rightarrow \text{O}_2(\text{g}) + 4\text{H}^+(\text{aq}) + 4\text{e}^-$ ($E^\circ = 1.23 \text{ V}$) remains a hot topic in catalysis research due to its importance in renewable water splitting to H_2 and O_2 . A major problem stems from the current application of expensive and less abundant elements, namely Ir and Ru. Our objective is to find catalysts that can participate in a complex (photo)electrocatalytic water splitting system and contain more abundant transition metals like Cu. Another aim is to gather information on the mechanism of the proposed key step in OER that is the activation of an oxido ligand and its role in the O-O bond formation step (water nucleophilic attack). This has been studied in high details for Ru complexes. The initial objectives for 2016 therefore were set as: (1) exploring Ru complexes and their catalytic properties in homogeneous solution, anchoring options on supports, design and synthesis of photosensitizers (PS) or photosensitive compounds. (2) Synthesis and characterization of Cu-complexes for catalysis and looking into their anchoring options on electrode surfaces with diimine ligands, or with branched peptides.

Methods

(1) Ru compounds were synthesized and characterized at UW-Madison including reactivity tests that were evaluated in collaboration (some methods have been explored by Pap earlier). Peptides were synthesized by an improved solid phase method in Poland. Electrocatalytic tests were run by cyclic voltammetry (CV) or controlled potential electrolysis (CPE), and dioxygen evolution was monitored by a fluorescent probe. Surface-deposited Cu compounds were investigated by X-ray photoelectron spectroscopy (XPS) and atomic force microscopy (AFM). The kinetics of deposition was performed by optical waveguide lightmode spectroscopy (OWLS), the *operando* tests on the deposits by EC-OWLS (OWLS combined with electrochemistry).

Results

(1) New diruthenium oxyanion complexes have been prepared, crystallographically characterized, and screened for their potential to photochemically generate a reactive Ru-Ru=O intermediate. The most promising candidate, $\text{Ru}_2(\text{chp})_4\text{ONO}_2$ (chp = 6-chloro-2-hydroxypyridinate), displays a set of signals in its mass spectrum, consistent with the formation of the $[\text{Ru}_2(\text{chp})_4\text{O}]^+$ ion. These signals shift by using ^{18}O -labeled nitrate. Photolysis of the complex in CH_2Cl_2 at room temperature in the presence of excess PPh_3 yields OPPh_3 in 173% yield; control experiments implicate $\text{Ru}_2(\text{chp})_4\text{O}$, NO_2^\bullet , and free NO_3^- as the active oxidants. Notably, $\text{Ru}_2(\text{chp})_4\text{Cl}$ is recovered after photolysis that is the direct precursor to $\text{Ru}_2(\text{chp})_4\text{ONO}_2$ therefore the results constitute the first example of a synthetic cycle for O-atom transfer that makes use of light. Synthesis and anchoring of Ru-photosensitizers on active carrier/catalysts was suspended for this year due to Srankó's leave for a postdoc position. He returns in the frame of an NKFIH PD grant: Development of organic-inorganic nanocomposites and their application in artificial photosynthesis.

(2) Cu-complexes that were documented earlier to promote the OER were layered with polyelectrolytes onto semiconducting indium-tin-oxide (ITO) in order to support their heterogenization in surface coatings. The electrocatalysts, i.e. Cu(II)-branched peptide complexes, could be heterogenized by the alternating deposition with poly(L-lysine) or poly(allylamine hydrochloride) in the presence of phosphate in a pH range of 7.5–10.5. The composite layer buildup was followed by OWLS to reveal the layer-by-layer formation of a Cu-ligand/polyelectrolyte/phosphate coating. The fabricated structures had a nanoporous topography (AFM). Electrocatalytic OER and accompanying changes of the layers indicated improved electrocatalysis vs. the neat ITO and dependence of this improvement on the presence or absence of a histidine ligand in the deposited Cu(II)-complexes equally, as observed in homogeneous systems. EC-OWLS revealed changes in the coatings *operando*: after some initial loss of mass, steady-state electrolysis was sustained by a compact and stable layer. According to XPS, Cu remains in an N-donor ligand environment after electrolysis. A number of Cu-catalysts (including Cu-peptides) utilize Cu(III) as part of a catalytic cycle. However, the Cu(III) state for several complexes has been less studied. The systematic evaluation of their Cu(III)/Cu(II) redox processes is scarce. Considering their potential catalytic applications understanding their redox behaviour is essential. In an extended comment a methodology and its background were discussed to highlight relations between the Cu(III)/Cu(II) formal potentials, the difference in the association constants (stability) of the oxidized and reduced forms and the ligand constitution for a number of mononuclear copper-peptide complexes. In addition to the papers, one invited conference lecture was given at 2MMAP in Cancun, Mexico.

Remaining work

We wish to extend the studies with branched peptides: exploring new single site catalysts, characterize 1st gen. pseudo-metallo dendrimers and anchoring new catalysts onto electrode surface and start the new projects (Srankó and Ollár).

Related publications

- [1] A. Corcos, J. S. Pap, T. Yang, and J.F. Berry: A Synthetic Oxygen Atom Transfer Photocycle from a Diruthenium Oxyanion Complex, *J. Am. Chem. Soc.* 138 (2016) 10032.
- [2] E. Farkas, D. Sranko, Zs. Kerner, B. Setner, Z. Szewczuk, W. Malinka, R. Horvath *, L. Szyrwiel *, and J.S. Pap *: Self-assembled, nanostructured coatings for water oxidation by alternating deposition of Cu-branched peptide electrocatalysts and polyelectrolytes, *Chem. Sci.* 7 (2016) 5249.
- [3] J.S. Pap * and Ł. Szyrwiel: On the Cu(III)/Cu(II) Redox Chemistry of Cu-Peptide Complexes to Assist Catalyst Design, *Comm. Inorg. Chem.* 36 (2016) AiP-19.

CATALYTIC PROPERTIES OF 2D MoS₂ CATALYSTS DURING ELECTROLYSIS OF WATER

*Tamás Ollár, Antal Koós, Gergely Dobrik, Zsolt Horváth, Zsolt Kerner, Ferenc Somodi József
Sándor Pap, Levente Tapasztó*

Objective

The main objective of our research was to identify the catalytically active sites of molybdenum disulphide single and few layers and reveal the correlations between the catalytic activity and the atomic scale structural defects. In the present project we proposed and carried out the growth of MoS₂ single and few-layer films on graphite (HOPG) substrate by the chemical vapour deposition (CVD) method. Another achievement that has emerged during the work was the ability to deposit metal nanoparticles (Pt, Ni) on the surface of the MoS₂ and their characterization by X-ray photoelectron spectroscopy (XPS), scanning tunneling microscopy (STM) and atomic force microscopy (AFM). We have performed electrochemical tests of such electrodes comprising MoS₂ layers and modified by Pt nanoclusters. Our final goal is to propose a more efficient electrode design method for the water splitting reaction and the hydrogen production process.

Methods

The experimental techniques employed in the project: chemical vapour deposition (CVD, 2D MoS₂ growth), scanning tunneling microscopy (STM, atomic scale defect structure of MoS₂), X-ray photoelectron spectroscopy (XPS, surface microanalysis), atomic force microscopy (AFM, number of MoS₂ layers, Pt clusters), Kelvin Probe (KP, work function, *e.g.*, the amount of energy needed to release electrons from a material's surface), cyclic voltammetry (CV, prompt analysis of electrocatalytic response under various conditions), Raman spectroscopy (MoS₂ surface coverage and layer number).

Results

We have successfully performed the resulfidation of fully oxidized MoS₂ single layer grown on SiO₂ substrate. After months under ambient condition Raman spectroscopy analysis revealed that the MoS₂ layer has completely oxidized. The successful resulfidation was achieved by a heat treatment at 300 °C in H₂S atmosphere. The regenerated MoS₂ films again displayed the characteristic Raman spectra, but the morphology of the film has substantially changed, instead of a continuous single layer, 5 nm high MoS₂ nanoparticles have been formed as revealed by AFM measurements.

The long-term oxidation (degradation) of the 2D MoS₂ crystals under ambient conditions is a common problem. By STM measurements we were able to follow this oxidation process at the atomic scale. The dominant atomic mechanism is the formation of more and more sulphur vacancies in MoS₂ layer. We have successfully reversed this oxidation process and vacancy formation by an annealing process at 200 °C in H₂S atmosphere. Atomic resolution STM measurements showed that S atom vacancies almost completely disappear using this procedure. Our results pointed out that the structure of partially oxidized MoS₂ single layer can be perfectly regenerated on the atomic level.

The electro-chemical water splitting reaction was studied by cyclic voltammetry (CV) in 0.5 M H₂SO₄ electrolyte solution. CV studies showed that thinner MoS₂ layers (single and few layers) are more active in hydrogen evolution than electrodes with thicker MoS₂ multilayers. After several cycles the activity of electrodes has increased. We attribute this to the creation of more defects, followed by the thinning MoS₂ layers. After applying high voltages, the electrochemical activity of the MoS₂ electrodes has also significantly increased. XPS results indicate that platinum nanoparticles have been deposited on the MoS₂ surface from the platinum counter electrode and this might be at the origin of the improved catalytic activity.

Outlook

Our results clearly indicate that it is possible to deposit metal nanoparticles onto MoS₂ films by electrochemical deposition, which is able to improve the catalytic activity of the electrodes. As a next step, we are planning to use this effect for the deposition of various types of metal (Ni, Cu, Fe, W) nanoparticles onto atomically thin MoS₂ films, in order to improve the catalytic activity of such electrode as much as possible.

TOWARDS SUPPORTED FePt FERROMAGNETIC NANOPARTICLES

Anita Horváth, Ferenc Somodi, Károly Lázár, András Deák, Szilárd Pothorszky, Miklós Serényi, János Szívós, György Sáfrán

Objective

As-prepared FePt nanoparticles have usually a face centred cubic (fcc) structure and are superparamagnetic at room temperature. Annealing around 500 °C may convert them into ferromagnetic face centred tetragonal (fct) nanocrystals that have regular arrays of Fe atoms inserted into the Pt rows forming a superstructure and thus, showing high magnetocrystalline anisotropy. These could be useful as an ultrahigh-density perpendicular recording medium. Our aim was the production of FePt nanoparticles with wet-chemical methods followed by thermal and laser treatment in order to get the face centred tetragonal so-called L1₀ phase. Particles from aqueous and organic sols were to be investigated as self-assembled on a carbon coated TEM grid or in oxide supported form (for future catalytic purpose), both in as prepared state and after the attempt to produce the L1₀ phase. Amorphous SiO_x shell was to be built around individual particles in order to prohibit oxidation, facilitate the transition to fct structure upon laser or heat treatment and separate the nanosize magnets.

Methods

FePt nanoparticles were prepared in water or organic phase using several stabilizer and reducing agents and different Pt and Fe precursor solutions. Elemental composition of the bimetallic particles was checked with EDS analysis. The SiO_x layer around the particles was formed by hydrolysis of tetraethylorthosilicate in methanol after adjusting the pH to 11. The particle size of colloidal solutions before and after the SiO_x shell formation was measured by dynamic light scattering. The size, morphology and the line spacing of the parent FePt alloy particles and those of supported and heat treated (reduced in 5% H₂/Ar gas mixture), or SiO_x-encapsulated and laser treated samples were studied by high resolution TEM. XRD measurement was carried out on the as prepared organic FePt sol.

Results

FePt nanoparticles prepared in dioctyl ether solvent (organic) were homogenous and around 2-3 nm with the required Fe:Pt =1:1 composition, but particle coalescence was observed with time. XRD could not detect any FePt phase probably due to the small particle size. Unfortunately, SiO_x shell could not be produced in this system. The Al₂O₃ supported and reduced form contained tiny bimetallic particles and larger ones apparently in strong interaction with the support (Figure 1 a), however, line spacing around 3.7 Å representative to L1₀ phase could be discerned only in aggregated metallic islands that were not in strong interaction with the support (Figure 1 b). Question arises whether the L1₀ phase transition is restricted by the metal-support interaction. Most aqueous sols faced the problem of different degree of Fe leaching, uneven FePt distribution in the individual particles, or particle coalescence. Finally, we successfully prepared stable aqueous sols with particles between 2-5 nm could be used for SiO_x encapsulating. The thin SiO_x shell around most FePt particles can be observed in Figure 1 c, and the according size increase was measured also by DLS technique. The SiO_x-modified samples were laser treated, and the bare particles were supported and pretreated on Al₂O₃ and ZrO₂ as well. However, the L1₀ phase was not revealed by HRTEM. Increase of pretreatment temperature above 500 °C will hopefully help with this.

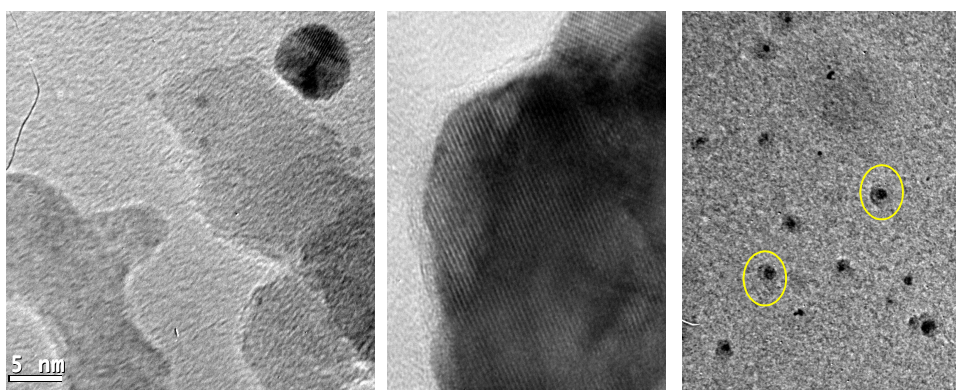


Figure 1: a) FePt-org/Al₂O₃ after reduction at 500 °C; b) large ~50 nm FePt aggregate on the same sample with L1₀ line spacing of 3.7 Å and c) 2-5 nm size FePt particles in SiO_x shell

Remaining work

After finding the optimal preparation conditions, the existence of L1₀ phase must be ascertained by XRD, TEM and magnetic measurements and the fcc-fct transition will be followed by Mössbauer spectroscopy. The SiO_x layer will be built up around the organic phase nanoparticles as well. Moreover, oxygen-free preparation conditions in a Schlenk line must be realized that will hopefully lead to highly reproducible sample preparation without Fe leaching by oxidation. The homogeneous distribution and stability of the FePt particles on Al₂O₃ and ZrO₂ supports offer the possibility of their catalytic application in dry reforming reaction.

RADIOACTIVE WASTE MANAGEMENT: NEW VITRIFICATION PROCESS AND INVESTIGATION OF RADIONUCLIDE UPTAKE

Margit Fábíán, Felicián Gergely, János Osán, Szabina Török

Objective

High-level radioactive waste (HLW) produced by spent fuel reprocessing of nuclear reactors is currently incorporated into an inert host material. Borosilicate glass is a preferred and accepted waste form. Essentially, the most important task in this area is to find a simple and well controllable process where we can immobilize the HLW's. Our first aim is to develop, optimize and compare the basic network structure of these glasses especially regarding the matrix glass with that of the uranium containing glassy network and to define the maximum concentration of UO_3 which can be stable in the matrix glass form.

In Hungary, Boda Claystone Formation (BCF) is considered as the potential host rock formation for HLW disposal. In case of water intrusion, the uptake mechanisms have to be investigated. Micro- and macrospectrometric analyses were necessary to determine the sorption mechanisms between key cations and mineral phases present in the host rock. Inactive Cs(I) and U(VI) ions were selected for the experiments. For this reason, a series of diffusion experiments was designed and performed in order to provide a link between macroscopic and microscopic measurements.

Methods

Simple and multi-component sodium borosilicate glasses were investigated. In this study we focused on the investigation of 70wt% $[\text{55SiO}_2 \cdot 10\text{B}_2\text{O}_3 \cdot 25\text{Na}_2\text{O} \cdot 5\text{BaO} \cdot 5\text{ZrO}_2] + x\text{wt}\% \text{UO}_3$, $x=10, 20, 30, 40$ samples. B_2O_3 was isotopically enriched with ^{11}B -isotope (99.6%). The glassy samples were prepared by melt-quenching technique, melted under atmospheric conditions, at temperatures between 1300-1450°C in Pt crucibles. Neutron diffraction measurements were performed in a broad momentum transfer range, combining the data measured by the 2-axis PSD (Diffractometer with Position Sensitive Detector) monochromatic neutron diffractometer ($\lambda_0=1.068 \text{ \AA}$) at the 10 MW Budapest research reactor and by the 7C2 diffractometer at the LLB-Saclay ($\lambda_0=0.726 \text{ \AA}$). The structure factors were evaluated from the raw experimental data. The experimental structure factors data have been simulated by the RMC (Reverse Monte Carlo) method using the software package RMC++.

Sorption experiments were prepared in order to compare the Cs content of the thin sections and that in the corresponding equilibrated modelled pore water solutions. Different solid-to-liquid (S/L) ratios, initial Cs concentrations and treatment during immersing were investigated. A special sample holder from PTFE (Polytetrafluoroethylene) was developed for the experiments allowing placement of magnetic stirrer below the thin section. Thin sections were reacted during 72-hour sorption experiments with Cs(I) or U(VI). The elemental composition of the solid phase was measured using laboratory X-ray fluorescence (XRF) while the Cs concentration was determined using total-reflection XRF (TXRF). The U(VI)-loaded thin sections were measured by combined microscopic XRF (μ -XRF), microscopic X-ray diffraction (μ -XRD) and microscopic X-ray absorption spectrometry (μ -XAS) employing SR (Synchrotron radiation).

Results

In the U doped matrix glasses we have a compact structure, where the network former atoms as Si and B atoms play an important role. Based on our RMC calculation basic network structure was established formed by mixed $^{[4]}\text{Si-O-}^{[3]}\text{B}$ and $^{[4]}\text{Si-O-}^{[4]}\text{B}$ linkages, which results shows good correlation with the basic structure of matrix glasses. Significant second neighbour correlations may be observed at characteristic r -values, finding that U atoms are in correlations with the network former Si and B atoms. These pronounced correlations show that U atom can incorporate on the matrix glass structure. These results also lead to the compact glassy structure possessing ability to include high stability uranium ions and also are a fingerprint for strong atomic correlations and indicate the existence of a pronounced intermediate-range ordering. It was established that the stable matrix can incorporate a maximum of 40 w% UO_3 (simulated HLW).

The use of the same S/L ratio as in the wet chemistry experiments ($5 \cdot 10^{-3} \text{ kg/l}$) and a low volume of the liquid phase (3 ml) highly concentrated in Cs resulted in similar but lower solid phase Cs concentration as expected from macroscopic sorption isotherms. Higher Cs load was obtained on thin sections treated in 50 ml pore water solution with downscaled Cs content, if the solution was properly mixed during immersing of test samples. High-resolution SR micro-XRF/XRD mapping results of U(VI)-loaded thin sections clearly showed that the fracture infilling region of the BCF samples contained zoned dolomite rhombohedra with outer Mn-rich areas. These rhombohedra were covered with ankerite rims that were coincident with U enrichment. U uptake induced by ankerite would require formation of FeOOH via Fe oxidation and U reduction. Partial reduction of U could be proved from the μ -XAS results, elucidated from U distribution maps collected at five different excitation energies near the U-L_3 absorption edge (17166 eV). This phenomenon caused an enhanced uranium uptake in addition to the the argillaceous matrix mainly composed of illite. The investigations provided essential information in clarifying the uranium uptake process of different mineral phases in argillaceous rocks of BCF on the microscale [2].

Related publications

- [1] F. Gergely, J. Osán, M. Fábíán, Á. Szabó, N. Vér and S. Török: *Optimization of sorption experiments involving argillaceous rock thin sections for microspectrometric investigations*, *Spectrochimica Acta Part B*, **116**, 75-84 (2016)
- [2] M. Fabian and Cs. Araczk: *Basic network structure of $\text{SiO}_2\text{-B}_2\text{O}_3\text{-Na}_2\text{O}$ glasses from diffraction and reverse Monte Carlo simulation*, *Physica Scripta*, **91**, 054004 (2016)

VITRIFICATION – DEVELOPMENT OF GLASS MATRICES FOR HIGH-LEVEL RADIOACTIVE WASTES

Margit Fábíán, Felicián Gergely, János Osán

Objective

The final and safe storage of radioactive waste materials is nowadays an existing and urgently to be solved problem. Understanding of the incorporation of actinides in borosilicate matrix used for nuclear waste storage is of a great importance for radioactive waste immobilization. This study carried out on matrix glasses doped with UO_3 .

Methods

During the project more than 20 glass samples were successfully prepared using a high-temperature furnace. The raw materials used were all of p.a. grade, SiO_2 , B_2O_3 (^{11}B -isotope (99.6%)) are the basic glass forming oxides while Na_2O is glass modifier; while BaO , ZrO_2 serve both as network modifier, glass and hydrolytic stabilizers and UO_3 . The atomic structure of the glasses was studied by neutron diffraction measurements (ND), combining the data measured by the PSD monochromatic neutron diffractometer ($\lambda_0=1.068 \text{ \AA}$; $Q=0.45\text{-}9.8 \text{ \AA}^{-1}$) at the 10 MW Budapest research reactor and by the 7C2 diffractometer at the LLB-Saclay ($\lambda_0=0.726 \text{ \AA}$; $Q=0.52\text{-}16 \text{ \AA}^{-1}$). The powder specimens of about 3-5 g/each were filled in cylindrical V-sample holder of 8 and 6 mm diameter for the two experiments, respectively. The structure factors were evaluated from the raw experimental data, using the programme packages available at the two facilities. Diffraction experiments performed up to high- Q values are important to obtain fine r -space resolution of the atomic distribution function analyses. The experimental structure factors, $S(Q)$ data have been simulated by the RMC method using the software package RMC++.

Results

Based on the experience of our previous studies new glassy samples were synthesized. The composition of the investigated glassy specimens are $(100-x)\text{wt}\% [55\text{SiO}_2\text{-}10\text{B}_2\text{O}_3\text{-}25\text{Na}_2\text{O}\text{-}5\text{BaO}\text{-}5\text{ZrO}_2] + x\text{wt}\% \text{UO}_3$, $x=10,20,30,40$. Neutron diffraction measurements indicate that the new compositions are stable glassy samples, no crystalline phase was detected.

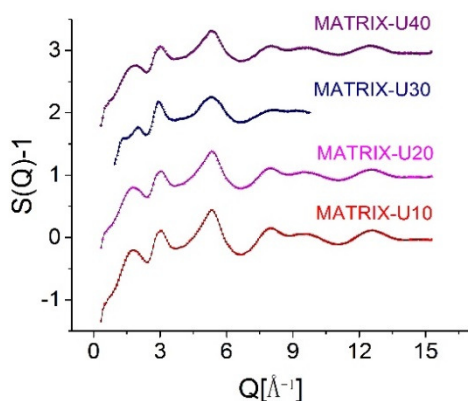


Figure 1: ND structure factor of glassy samples, experimental data (marks) and RMC simulation solid line.

Several RMC runs have been completed by modifying the cut-off distances in the way, that the results of each run have been carefully checked to obtain reliable data for each partial pair correlation functions and coordination number distributions. We have obtained very good agreement between the experimental and the calculated $S(Q)$ data (Figure 1). Here we focus our interest on the investigations of basic network structure in function of uranium concentration. The atom pairs responsible for building up the glassy network show characteristic first neighbour distributions.

In the studied matrix glasses we have a compact structure, where the network former atoms as Si and B atoms play an important role.

The RMC modelling provides information on the second coordination sphere. The analysis of the silicon-metal and boron-metal pair correlation functions show pronounced peaks.

The RMC modelling provides information on the second coordination sphere. The analysis of the silicon-metal and boron-metal pair correlation functions show pronounced peaks. The relatively shortest second neighbour distances are obtained for the Si-U and B-U pair correlation functions, suggests that uranium ions take part as partly as network former in the structure, indicated that U atoms can incorporate on the matrix glass structure even when is present with high-concentration. From these results we may conclude that also for the doped glasses we have a stable basic network structure and U accommodates in both silicate and borate site. This may be the reason of the observed good glassy stability and incorporation ability of the ions.

Remaining work

The evaluation of the chemical-physical glass properties and the leachability tests are in progress.

Related publications

- [1] M. Fabian, and Cs. Araczk: *Basic network structure of $\text{SiO}_2\text{-B}_2\text{O}_3\text{-Na}_2\text{O}$ glasses from diffraction and reverse Monte Carlo simulation*, Physica Scripta, **91**, 054004 (2016)
- [2] Fábíán M.: *Amorf anyagok összetételének optimalizálása radioaktív hulladékok kondicionálására*, Fizikai Szemle LXVI, **7-8.**, 221-228 (2016)
- [3] M. Fabian, E. Svab and K. Kiril: *Formation of Mixed Bond-Angle Linkages in Zinc Boromolybdate Glasses*, J. Am. Ceramic Soc. 1-8 (2016)
- [4] M. Fabian, E. Svab, and K. Krezhov: *Network structure of molybdate glasses by neutron and X-ray diffraction and reverse Monte Carlo modelling*, J. Phys.-Conf. Series **746**(1), 012068 (2016)

ATOMIC STRUCTURE OF HIGH-ENTROPY ALLOYS

Margit Fábíán, Eszter Dian, Dénes Párkányi

Objective

High Entropy Alloys, HEAs, are loosely defined as solid solution alloys that contain more than five principal elements in equal or near equal atomic percentage. The concept of high entropy introduces a new path of developing advanced materials with unique properties, which cannot be achieved by the conventional micro-alloying approach based on only one dominant element. The relative complexity seems to be a blessing and a curse of HEAs. On the one hand, it leads to very interesting and useful properties, including high-strength at room and elevated temperatures, low temperature toughness, high wear-resistant and irradiation resistance, making HEAs attractive to various structural applications, and finally, the general corrosion resistance, much better than that of the conventional 304-stainless steel.

Methods

Neutron diffraction is the first choice for getting detailed structural information on the HEA samples. However, due to the high number of contributing elements, it is difficult to derive adequate structural data from a single diffraction experiment. In many cases, HEAs possess single phase bcc or fcc structures. Neutron diffraction experiments were performed on the PSD diffractometer ($\lambda_0=1.068 \text{ \AA}$) at the 10 MW Budapest research reactor in the momentum transfer range $Q=0.5\text{-}10 \text{ \AA}^{-1}$. Data were corrected for detector efficiency, background scattering and absorption effects. However, the information content in these studies is often rather poor because of the limited Q -range of the experiment. The morphology, grain size distribution and composition study was performed by transmission electron microscopy (TEM). Dark field images are formed by a selected Bragg reflection of the sample. In this way the grains/phases, giving the selected reflection will become visible in the image.

Results

Mechanical alloying was carried out by induction melting of metals. Our main efforts currently are concentrated on measuring detailed structural parameters and learn about the microstructure evolution. There exist only a few compositions of HEA's that has high strength, stable at high temperature, resistant to radiation damage, therefore are optimal for the purposes of reactor vessel material, fuel cladding etc. Based on these considerations we intend to study the following samples: Al20-Mo20-Nb20-V20-Ti20, Al20-Mn20-Cr20-Fe20-Ni20, Al8-Mo5-Nb5-Cr22-Fe5-Ni55, Zr20-Hf20-Nb20-V20-Ti20 and Ni29.5-Fe39.8-Cr20-Mo6-W4.7. These HEA alloys have been studied using neutron diffraction and TEM investigation, some of the results are shown in Figure 1. and 2.

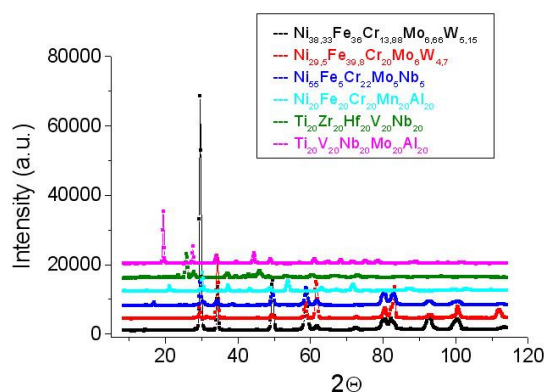


Figure 1. Neutron diffraction patterns for HEA series.



Figure 2. TEM image showing the dislocation structures on samples: Ni29.5Fe39.8Cr20Mo6W4.7.

Neutron diffraction pattern at room temperature showing the mixed FCC reflections and BCC reflections with some superstructure reflections. TEM microscopy images visualize the microstructure and the possible nano-grains. Figure 2 show an interesting dislocation appearances on Ni29.5Fe39.8Cr20Mo6W4.7 sample.

Intense research efforts are underway to develop and study high-entropy alloys with exceptional nuclear engineering properties. The present work addresses the fundamental need to understand the structural properties of HEA alloys.

Remaining work

The evaluation of the chemical-physical and mechanical properties and the irradiation tests are in progress.

Related publications

Manuscript in preparation.

PREPARATION, STRUCTURAL STUDIES AND OPTIMIZATION OF OXIDE GLASSES FOR HLW STORAGE APPLICATIONS

Margit Fábrián

Objective

The aim of the project is to synthesize novel glass matrices for long term storage of radioactive waste materials, and to determine the atomic structure of these new glass compositions. The Mo environment has been investigated in inactive nuclear glasses using diffraction methods. This report summarizes the activity connected to Mo-based system study of the 3rd year of an OTKA three years long project.

Methods

The glassy samples were prepared by melt-quenching technique, from reagent grade powders ($^{11}\text{B}_2\text{O}_3$, MoO_3 , Nd_2O_3 , ZnO , MgO) melted in a platinum crucible. B_2O_3 enriched with ^{11}B isotope (99.6% enrichment) has been used in order to avoid the high neutron absorption cross section of the ^{10}B isotope. The glasses were obtained by pouring the melts onto an iron plate and by pressing with another iron plate (cooling rate: 10^2 K/s).

Neutron diffraction (ND) measurements have been performed in a relatively broad momentum transfer range, $Q=0.4\text{--}35\text{Å}^{-1}$, combining the data measured by the PSD (Diffractometer with Position Sensitive Detector, $\lambda_0=1.068\text{Å}$) at the 10 MW Budapest Research Reactor, by the 'HIPD' instrument at the LANSCE (Los Alamos Neutron Science Center) pulsed neutron source and by the '7C2' diffractometer at the LLB (Neutron diffractometer for liquids and disordered materials) at the Saclay ($\lambda_0=0.726\text{Å}$). The high-energy X-ray diffraction (XRD) measurements were carried out at the BW5 (high energy x-ray diffractometer) experimental station at HASYLAB (Hamburger Synchrotronstrahlungslabor) DESY (Deutsches Elektronen Synchrotron). The structure factors were evaluated from the raw experimental data, using the programme packages available at the facilities. Simultaneous reverse Monte Carlo (RMC) simulation of the diffraction data sets was applied to generate reliable 3D atomic configurations and to calculate the atomic parameters.

Results

A better understanding of the behaviour of Mo-based glasses will allow the development of new waste forms. During the work we studied simple and multi-component Mo-glasses, as the: $90\text{MoO}_3\text{--}10\text{Nd}_2\text{O}_3$, $80\text{MoO}_3\text{--}15\text{Nd}_2\text{O}_3\text{--}5\text{MgO}$, $75\text{MoO}_3\text{--}12.5\text{Nd}_2\text{O}_3\text{--}12.5\text{MgO}$; $50\text{MoO}_3\text{--}25\text{Nd}_2\text{O}_3\text{--}25\text{B}_2\text{O}_3$, $(100\text{--}x)\text{MoO}_3\text{--}30\text{Nd}_2\text{O}_3\text{--}xB_2\text{O}_3$ $x=30,50\text{mol}\%$ and $x\text{MoO}_3\text{--}50\text{ZnO}\text{--}(50\text{--}x)\text{B}_2\text{O}_3$, $x=10,20,30\text{mol}\%$. The fit of the RMC calculations was good, the final $S(Q)$ s matched very well the experimental ones, shown in Fig. 1.

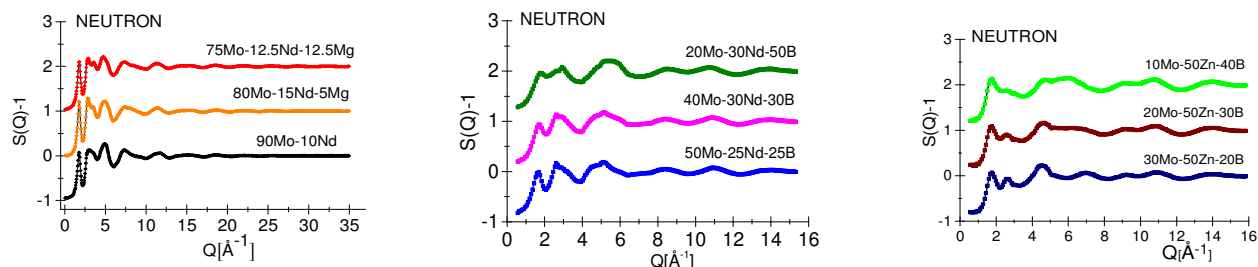


Figure 1: Experimental data (colour) and RMC simulation (solid line): Neutron and X-ray diffraction for Mo-Nd-Mg-O, MO-Nd-B-O and Mo-Zn-B-O series.

From the RMC modelling the partial atomic correlation functions, the coordination number distributions and bond angle distributions have been revealed. Formations of MoO_4 units were established with $1.75/1.80\text{Å}$ Mo-O distances. In the binary glass MoO_4 (55%) and MoO_6 (25%) structural units were revealed. In ternary systems mainly MoO_4 units are present, and with decreasing MoO_3 concentration, the ratio of MoO_6 units roughly decreases. For the B-containing ternary glasses B-O first neighbour distance was obtained at 1.40Å , the B-O network is formed by BO_3 and BO_4 groups. ZnO proved to be a network former, not a modifier as it is often reported in the literature for similar systems. From the analyses of the obtained structural parameters we have concluded that the glassy network is formed by trigonal BO_3 and tetrahedral BO_4 , MoO_4 , ZnO_4 groups. Concentration dependence was found for the BO_4/BO_3 fraction, it increases with increasing B_2O_3 content. We have calculated the three-particle bond-angle distributions using the final atomic configuration of the RMC algorithm. For the Mo-O-B and Mo-O-Zn the peak positions are at $149\pm 3^\circ$ and $104\pm 5^\circ$, respectively, which are very close values to the ideal tetrahedral configuration. B-O-Zn distribution also shows a close link between the boron and zinc units. We have concluded that the network is formed by BO_3 and BO_4 organized into superstructure units, and linked to MoO_4 or ZnO_4 , forming in this manner mixed bond-linkages.

Related publications

- [1] M. Fábrián, E. Sváb and K. Kiril: *Formation of Mixed Bond-Angle Linkages in Zinc Boromolybdate Glasses*, J. Am. Ceramic Soc. 1-8 (2016)
- [2] M. Fábrián, E. Sváb and K. Krezhov: *Network structure of molybdate glasses by neutron and X-ray diffraction and reverse Monte Carlo modelling*, J. Phys.-Conf. Series **746**(1) 012068 (2016)
- [3] M. Fábrián, E. Sváb, M. Milanova and K. Krezhov: *Network structure of Mo-oxide glasses*, J. Phys.-Conf. Series Volume 794, Number 1 (2016)

POSSIBILITY OF NUCLEAR COGENERATION DEVELOPMENT IN THE REGION OF PAKS

Endre Böröcsök, János Osán, Attila Talamon, Szabina Török

Objective

Almost half of GHG emission of energy sectors in the world is related to heat demand. The development of nuclear cogeneration offers a convenient possibility for emission reduction; however, examination of economic constrains is essential. This study is focused on heat demand of households in the vicinity of Paks NPP and compares domestic heating alternatives using economic and environmental cost-benefit analysis.

Methods

Nuclear energy based district heating is a mature technology for low carbon households heating in Hungary. Paks NPP supplies the heat demand of 2600 households located at 4.5 km distance, however, the district heating/electricity ratio is far below the global average. The first objective of this study is to find the conditions when the nuclear energy based district heating with new transmission pipeline could substitute natural gas based district heating on economic grounds. In this part of calculations fuel, nuclear heat and capital costs played the key role and effects of different GHG emission price were examined in sensitivity analysis. The second objective is the comparison of nuclear heat cost provided through district heating with heat costs of conventional systems. In economic assessment of nuclear cogeneration, the fuel, operation and maintenance (O&M) costs of existing natural gas based district heating as "status quo" was compared to nuclear heat cost and investment cost of transmission pipeline installation with corresponding O&M costs. Whereas the forecasted costs (fuel and carbon price, neglected retrofit of gas boilers...) promote the revenues of the investment markedly, it means our calculations can be considered like "worst case study". The results were extended to estimate whether extending the existing district heating network to large-scale multi flat buildings is appropriate. For comparison three building typological groups were established: large-scale, medium-scale multi flat buildings and single family houses with existing heating alternatives. In three cases the heat load densities are different that influence on capital cost of district heating network is significant. For comparability, unified heat demand of households (10.6 kW) was considered. Annual cost of domestic heating in standardized case was compared and the technical operation time of alternatives were considered (discount rate was 4%) disregarding the carbon emission price and external cost of environmental impacts.

Results

The detailed analysis suggests that, substitution of natural gas combustion based district heating with nuclear cogeneration can be beneficial considering the lower fuel, O&M and carbon emission costs. Two towns in the vicinity have sufficient heat demand to consume nuclear heat in economic way; Paks and Szekszárd. On the basis of partial sensitivity analysis, the transit pipeline development to the town Dunaújváros results positive net present value only at around 25 €/t CO₂ price being considerably higher than the actual price (in 2015: 4.5-4.9 €/t). In present situation only one economically feasible solution is a heat transit pipeline to Szekszárd. An important additional objective was whether the extension of district heating network could be an economically attractive way for the domestic sector. Consequently, heating alternatives based on standardized heat demand for three building typological groups. Nuclear heat was found to be the most competitive alternative in medium and large-scale multi flat buildings (Fig. 1), assumed that district heating network achieves a high penetration. The stand-alone heating could be favourable in single family houses due to the higher specific capital cost [1].

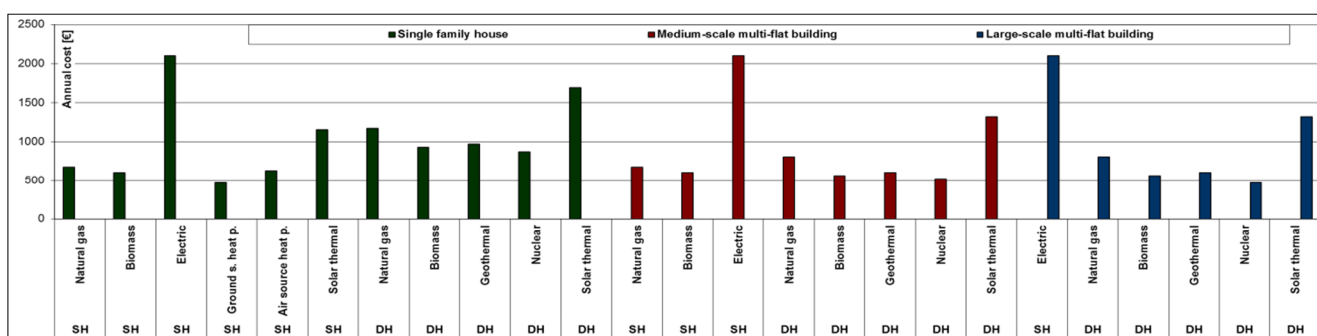


Figure 1. Annual cost of domestic heating in standardized case (140 m²; 10.6 kW). SH: Stand-alone heater; DH: District heating

Remaining work

Comparison of heat alternatives was carried out with standardized heat demand and the final results established the examination possibility of optimal heat supply in future works.

Related publication

- [1] E. Böröcsök, J. Osán and Sz. Török: *Possibility of nuclear cogeneration development in the region of Paks*, Case study for OECD NEA 2016

MICROSCALE X-RAY SPECTROMETRY INVESTIGATION OF RADIONUCLIDE UPTAKE ON ARGILLACEOUS ROCKS

Felicián Gergely, Margit Fábián, János Osán, Szabina Török

Objective

In Hungary, Boda Claystone Formation (BCF) is considered as the potential host rock formation for high-level radioactive waste (HLW) disposal. Several of the safety approaches for the geological disposal of HLW rely on the strong uptake of radio-contaminants by clay minerals. Micro- and macrospectrometric analyses were necessary to determine the sorption mechanisms between key cations and mineral phases present in the host rock. The studied cations were selected in order to chemically represent radionuclides dissolved from HLW. Inactive Cs(I) and natural U(VI) ions were selected for the experiments. Macroscopic wet chemistry determination of sorption isotherms is based on powdered rock samples; however microscopic investigations usually involve petrographic thin sections. Sorbate concentrations in the solid phase measured for thin sections are different from the ones calculated from isotherms based on macroscopic experiments. For this reason, a series of diffusion experiments was designed and performed in order to provide a link between macroscopic and microscopic measurements.

Microspectrometry experiments involving synchrotron radiation (SR) were performed on U(VI)-loaded thin sections in order to obtain information on the uranium uptake mechanism and the crystalline phases involved.

Methods

Sorption experiments were prepared in order to compare the Cs content of the thin sections and that in the corresponding equilibrated modelled pore water solutions. Different solid-to-liquid (S/L) ratios, initial Cs concentrations and treatment during immersing were investigated. A special sample holder from PTFE was developed for the experiments allowing placement of magnetic stirrer below the thin section. Two points were chosen from the isotherm, each of them four loaded thin sections were prepared. The conditions were the following:

- Solution was stirred, the S/L ratio was shifted towards the liquid phase and the initial Cs concentration in the solution was reduced. The special sample holder was used.
- Method 1 but not stirred.
- Original method with high initial concentration and the same S/L ratio like macroscopic investigation was used without special holder.
- Method 2 without using the special holder.

Thin sections were reacted during 72-hour sorption experiments with Cs(I) or U(VI). The elemental composition of the solid phase was measured using laboratory X-ray fluorescence (XRF) while the Cs concentration was determined using total-reflection XRF (TXRF).

The U(VI)-loaded thin sections were measured by combined microscopic XRF (μ -XRF), microscopic X-ray diffraction (μ -XRD) and microscopic X-ray absorption spectrometry (μ -XAS) employing SR. Undulator radiation focused to 2 μ m by Kirkpatrick-Baez mirrors was used, which was monochromatized by a Si(111) double-crystal monochromator. Simultaneous collection of energy-dispersive X-ray spectra and 2D diffraction patterns was performed allowing extracting of elemental and crystalline phase maps on selected areas.

Results

Results of the test sorption experiments are summarized below. The use of the same S/L ratio as in the wet chemistry experiments ($5 \cdot 10^{-3}$ kg/l) and a low volume of the liquid phase (3 ml) highly concentrated in Cs resulted in similar but lower solid phase Cs concentration as expected from macroscopic sorption isotherms. Higher Cs load was obtained on thin sections treated in 50 ml pore water solution with downscaled Cs content, if the solution was properly mixed during immersing of test samples. This method was found to be preferred for preparation of optimally loaded thin sections. Without mixing an order of magnitude lower Cs load was obtained [1].

High-resolution SR micro-XRF/XRD mapping results of U(VI)-loaded thin sections clearly showed that the fracture infilling region of the BCF samples contained zoned dolomite rhombohedra with outer Mn-rich areas. These rhombohedra were covered with ankerite rims that were coincident with U enrichment. U uptake induced by ankerite would require formation of FeOOH via Fe oxidation and U reduction. Partial reduction of U could be proved from the μ -XAS results, elucidated from U distribution maps collected at five different excitation energies near the U-L₃ absorption edge (17166 eV). This phenomenon caused an enhanced uranium uptake in addition to the the argillaceous matrix mainly composed of illite. The investigations provided essential information in clarifying the uranium uptake process of different mineral phases in argillaceous rocks of BCF on the microscale [2].

Related publications

- [1] Gergely F, Osán J, Szabó BK, Török S: *Analytical performance of a versatile laboratory microscopic X-ray fluorescence system for metal uptake studies on argillaceous rocks*, Spectrochimica Acta Part B, **116**, 75-84 (2016)

HIGH-ENERGY IONIZING RADIATION INDUCED DECOMPOSITION OF PHARMACEUTICAL COMPOUNDS

Erzsébet Takács, László Szabó, Tünde Tóth, László Wojnárovits

Objective

$\cdot\text{OH}$ and $\text{Cl}_2^{\cdot-}/\text{Br}_2^{\cdot-}$ are one-electron oxidants that are generated during ionizing radiation treatment of aqueous solutions. The objective of this work was to use these radicals for the elimination of the residual antibacterial activity of wastewater matrices that has a stimulating effect on the evolution of antibiotic resistance.

Methods

Amoxicillin, ampicillin, cloxacillin, 6-aminopenicillanic acid, 4-hydroxy-D-phenylglycine and the salts (NaBr and NaCl) were purchased from Sigma-Aldrich.

Electron pulse radiolysis measurements were performed with a Tesla Linac LPR-4 accelerator using kinetic spectrophotometric detection.

Results

The $\cdot\text{OH}$ induced oxidation of penicillins reveals a reaction mechanism typical for one-electron oxidation of organic sulfides. The contribution of the side chain aromatic constituent is of minor importance. Penicillins exhibit appreciable reactivity towards $\text{Cl}_2^{\cdot-}$, which targets predominantly the sulfur atom, again. In this case, much higher concentration of the sulfur radical cation was achieved, due to the inhibiting effect of a stabilized OH-adduct at the sulfur. $\text{Br}_2^{\cdot-}$ also comes into play in destructing penicillins with a mechanism similar to that of $\text{Cl}_2^{\cdot-}$.

Oxidation of the sulfur atom adjacent to the key antimicrobial β -lactam structure and the potential of $\text{Cl}_2^{\cdot-}/\text{Br}_2^{\cdot-}$ for one-electron oxidation of penicillins are promising for implementation of advanced oxidation techniques on broader fields to eliminate the antibacterial activity of several wastewater matrices. The reported reaction pathways are anticipated to provide information for understanding the influence of process parameters on the efficiency of antibacterial inactivation.

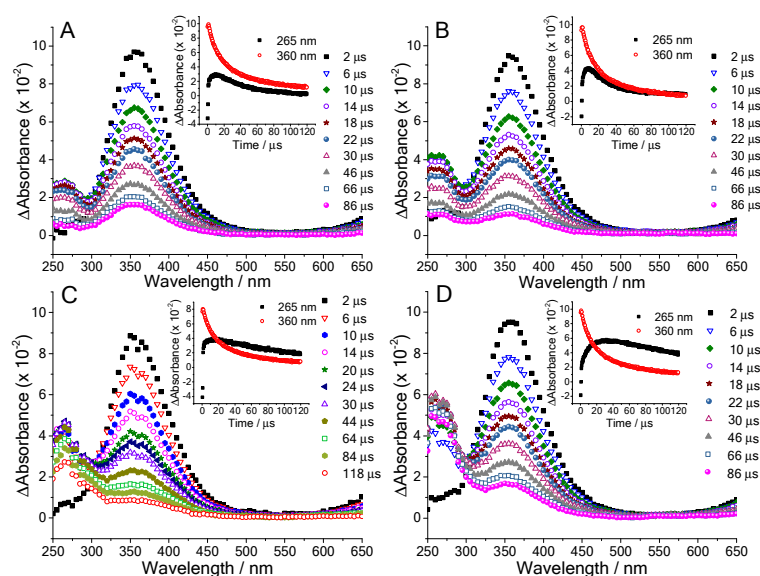


Figure 1: Transient spectra recorded in N_2O -saturated solution containing A) 0.1 M KBr, B) 0.1 M KBr and 1 mM 6-aminopenicillanic acid, C) 0.1 M KBr and 1 mM amoxicillin, D) 0.1 M KBr and 1 mM ampicillin at pH 5. Insets show the kinetic trace recorded at 265 and 360 nm in a solution as specified for the figure.

Remaining work

The project was finalized.

Related publication

- [1] L. Szabó, T. Tóth, E. Takács and L. Wojnárovits: *One-electron oxidation of molecules with aromatic and thioether functions: $\text{Cl}_2^{\cdot-}/\text{Br}_2^{\cdot-}$ and $\cdot\text{OH}$ induced oxidation of penicillins studied by pulse radiolysis*, Journal of Photochemistry and Photobiology A: Chemistry **326**, 50-59 (2016)

REMOVAL OF ANTIBIOTICS AND PESTICIDES FROM WASTEWATER USING HIGH-ENERGY IONIZING RADIATION

László Szabó, Gyuri Sági, Krisztina Kovács, Renáta Homlok, Tünde Tóth, Erzsébet Takács, László Wojnárovits

Objective

This research aimed at establishing relations between toxicity, antimicrobial activity, biodegradability and absorbed dose on the examples of β -lactam and sulfonamide type antibiotics and phenylurea type pesticides.

Methods

Samples were irradiated by a Co-60 gamma source. FTIR spectra were obtained with Unicam Mattheson Research Series 1 equipment. Chemical analytical works (UV-Vis and FTIR spectroscopy, HPLCMS/MS and GC/MS, Chemical Oxygen Demand (COD) and Biological Oxygen Demand (BOD) measurements) and biological assays with several test organisms were conducted. Biodegradability has been determined by calculation of BOD COD⁻¹ ratio that is a good indicator of the proportion of biologically degradable matter present.

Results

Ionizing radiation treatment is a promising technology for removal of antibiotics from wastewater. However, the studies have demonstrated the remaining antibacterial activity of the products at low doses in the degradation of amoxicillin, ampicillin and cloxacillin β -lactam antibiotics. A special analytical technique was elaborated, based on FTIR spectroscopy, to follow up the degradation of the β -lactam pharmacophore (Fig. 1). Multisite attack occurs on the penicillin skeleton, and only some of them leads to destruction of β -lactam ring and by that to elimination of the antimicrobial activity. A fraction of reactions takes place on the aromatic ring producing OH-substituted products. An increase in acute toxicity was observed at low doses. Irradiation with higher doses resulted in products, e.g. polyhydroxylated phenolic compounds, being also deleterious for bacteria. Therefore, the dose in the advanced oxidation process should be judiciously optimized.

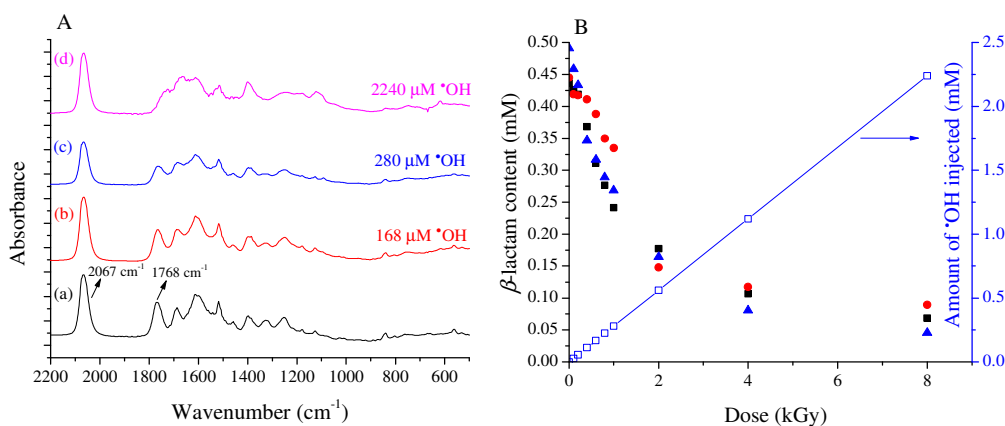


Figure 1: (A) FTIR spectra of amoxicillin, without treatment (a) and after a dose of 0.6 kGy (b), 1 kGy (c) and 8 kGy (d).

(B) quantitative FTIR analysis of the β -lactam content in the case of amoxicillin (■), cloxacillin (●) and ampicillin (▲) as a function of absorbed dose.

Impact of sulfonamide type antibiotics on individual living organisms and communities have been examined by a novel approach that involves equal load based sample introduction and removal of interfering effects not attributed to parent molecules or oxidized derivatives. Oxidative decomposition of persistent sulfonamide type antibiotics through processes occurring under natural conditions (\cdot OH-induced degradation) resulted in transformation to substances biologically degradable by river water and activated sludge communities. Ready biodegradability has been achieved in case of all test solutions, although higher level of oxidation is needed to reach the same biodegradability in river water, as in activated sludge. Generally, the toxicity was reduced in oxidized solutions, but increased negative effects have been also detected in some cases.

The decomposition of monuron pesticide was investigated in dilute aqueous solutions using pulse radiolysis and γ -radiolysis in order to identify the intermediates and final products. The main reaction takes place between monuron and the hydroxyl radicals yielding hydroxycyclohexadienyl type radicals with a second order rate constant of $(7.4 \pm 0.2) \times 10^9 \text{ mol}^{-1} \text{ dm}^3 \text{ s}^{-1}$. In \cdot OH reactions the aminyl and phenoxyl radicals may also form. Dechlorination was observed in both hydroxyl radical and hydrated electron reactions. In \cdot OH induced reactions it is suggested to occur through OH substitution or phenoxyl radical formation. The rate of oxidation is very high in the presence of dissolved oxygen. The results are also supported by quantum chemical calculations.

Remaining work

The change in antimicrobial activity is a question of utmost importance. Therefore, it should be followed with other methods, like agar diffusion test.

Related publications

- [1] Z. Kozmér, E. Takács, L. Wojnárovits, T. Alapi, K. Hernádi and A. Dombi: *The influence of radical transfer and scavenger materials in various concentrations on the gamma radiolysis of phenol*, Radiation Physics and Chemistry **124**, 52 (2016)
- [2] Gy. Sági, K. Kovács, A. Bezsenyi, T. Csay, E. Takács and L. Wojnárovits: *Enhancing the biological degradability of sulfamethoxazole by ionizing radiation treatment in aqueous solution*, Radiation Physics and Chemistry **124**, 179 (2016)
- [3] L. Szabó, T. Tóth, G. Rácz, E. Takács and L. Wojnárovits: *$\cdot\text{OH}$ and e_{aq}^- are yet good candidates for demolishing the β -lactam system of a penicillin eliminating the antimicrobial activity*, Radiation Physics and Chemistry **124**, 84 (2016)
- [4] L. Szabó, T. Tóth, E. Takács and L. Wojnárovits: *One-electron oxidation of molecules with aromatic and thioether functions: $\text{Cl}_2^{\cdot-}/\text{Br}_2^{\cdot-}$ and $\cdot\text{OH}$ induced oxidation of penicillins studied by pulse radiolysis*, Journal of Photochemistry and Photobiology A: Chemistry **326**, 50 (2016).
- [5] L. Wojnárovits and E. Takács: *Radiation induced degradation of organic pollutants in waters and wastewaters*, Topics in Current Chemistry, **374**:(4) 50 (2016) (DOI: 10.1007/s41061-016-0050-2)
- [6] L. Wojnárovits, E. Takács and L. Szabó: *Gamma-ray and electron beam-based AOPs*. In: *Advanced Oxidation Processes for Water Treatment Fundamentals and Applications*. Stefan M., (Editor). Chapter 6, 56 pages 241-295. IWA Publishing (2018)
- [7] L. Wojnárovits and E. Takács: *Wastewater treatment with ionizing radiation*, Journal of Radioanalytical and Nuclear Chemistry **311**:(2) 973-981 (2017)
- [8] E. Takács, Gy. Sági, T. Csay and L. Wojnárovits: *Water, wastewater and sewage sludge treatment using radiation technology*, In *IAEA TECDOD-1786 Radiation Technology for Cleaner Products and Processes*, Proceedings of the Technical Meeting on Deployment of Clean (Green) Radiation Technology for Environmental Remediation. IAEA Vienna, 16-20 June 2014. p. 62. (2016)
- [9] A. Tegze, E. Illés, E. Takács: *Ciprofloxacin és norfloxacin nagyenergiájú ionizáló sugárzással indukált bontása híg vizes oldatban*, In: Szentmiklósi L (szerk.) *Őszi Radiokémiai Napok 2016*. 104 p. Balatonszárszó, Magyarország, 2016.10.10-2016.10.12. Budapest: MKE, 2016. p. 39 (ISBN:978-963-9970-69-4)
- [10] L. Szabo, T. Toth, G. Racz, T. Engerhardt, Cs. Mohacsi-Farkas, E. Takacs, L. Wojnarovits: *$\cdot\text{OH}$ induced oxidation of penicillins in relation to advanced oxidation techniques*, lecture RANC2016 10–15 April, 2016, Budapest, Hungary

HYDROXYL RADICAL INDUCED TRANSFORMATION OF PHENYLUREA HERBICIDES: A THEORETICAL STUDY

Viktória Mile, Ildikó Harsányi, Krisztina Kovács, Tamás Földes, Erzsébet Takács, László Wojnárovits

Objective

On the example of phenylurea herbicides, the objective of the present work was to suggest the possible attack sites of OH radical to aromatic molecules.

Methods

The computational analysis was carried out using Density Functional Theory (DFT) methods. Becke's three parameter hybrid functional has been applied with the Lee-Yang-Parr correlation extension, generally known as B3LYP. The standard 6-311++G(d,p) basis set was applied for geometry optimizations. Frequency calculations were also performed for establishing the stationary points (i.e. ground state: frequencies are all positive, transition state: there is one imaginary frequency). The electronic energy was refined by single-point energy calculations at the B3LYP/6-311++G(3df,3pd) level. The Gibbs free energies are reported for $T = 298.15$ K and corrected for $c = 1$ mol dm⁻³. The calculations were performed with the Gaussian program package. The Solvation Model Based on Density model (SMD) was applied in order to model the aqueous media. The geometries were also reoptimized under the effect of the solvation model. Based on Gibbs free energies of the reactions and activation free energies we make suggestions for the most probable sites of •OH attack, and also we clarify the details of the dechlorination reaction.

Results

The attack of •OH to aniline, phenol, fenuron, monuron, diuron has been studied by using B3LYP/6-311++G(d,p) DFT simulation technique, applying corrections of the single point energy at the level of B3LYP/6-311++G(3df,3dp). Both gas and aqueous phase (Solvation Model Based on Density) calculations were conducted. Equilibrium geometries and energies of all stationary points had been obtained. Applying the water model at the addition of •OH to *ortho*-2 position no transition states could be found due to the secondary interaction in the transition states. The H-bond contributions are higher in *ortho*-1 product than in *ortho*-2. When chlorine atoms are not relevant in the reaction, a simple •OH addition takes place to the ring by forming a hydroxycyclohexadienyl type radical. According to the energy data the hydroxyl radical addition is probable to any ring positions but the *ortho*- and *para*-reactions are energetically more favorable in good agreement with the experimental results obtained in radiolysis. As the results of calculations also show, this selectivity is connected to the effect of electron releasing -OH, -NH₂ and -NH-CO-N(CH₃)₂ groups in the molecule. The •OH/Cl substitution in monuron and diuron occurs without cyclohexadienyl type intermediate in cases where chlorine is released. The solvation energy of Cl may also contribute to the high probability of this reaction.

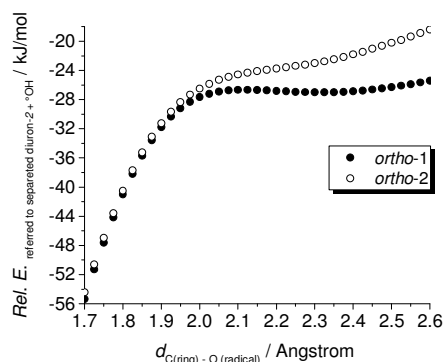


Figure 1: Constrained partial optimization calculations of diuron-2 + •OH reaction in kJ/mol.

Remaining work

The simulation of the intermediate spectra and the comparison of the simulated spectra with those obtained in pulse radiolysis measurements would be important.

Related publications

- [1] K. Kovács, S. He, V. Mile, T. Földes, I. Pápai, E. Takács and L. Wojnárovits: *Ionizing radiation induced degradation of monuron in dilute aqueous solution*, Radiation Physics and Chemistry **124**, 191 (2016)
- [2] V. Mile, I. Harsányi, K. Kovács, T. Földes, E. Takács and L. Wojnárovits: *Hydroxyl radical induced transformation of phenylurea herbicides: a theoretical study*, Radiation Physics and Chemistry **132**, 16-21 (2017)

SEPARATION OF PLUTONIUM AND LANTHANIDES ON DGA RESIN BY EXTRACTION CHROMATOGRAPHY FROM HUMAN URINE – DEVELOPMENT OF A RAPID METHOD

Márton Zagyvai, Nóra Vajda, László Szentmiklósi

Methods

Americium, plutonium and uranium species were separated from human urine by extraction chromatography on a DGA column. A previously elaborated procedure [1] was abbreviated by omitting digestion and preconcentration from the operational sequence. It was observed and then experimentally proven that some of Am is fixed strongly to the column in the presence of carbamide – a major organic constituent of urine – and this non-removable part will decrease the chemical recovery of Am. We are further developing this method for samples taken at a nuclear reactor as well as for those from the environment e.g. for soil and sediment samples. In order to reveal the details of this phenomenon sorption of lanthanides showing characteristics similar to Am (Nd, Eu and Tb) was investigated in the presence of carbamide. These lanthanides (Nd-147, Eu-155, Tb-160) were quantified by gamma spectrometry. The effect of carbamide to the separation of Pu was also studied by keeping its oxidation number at 3 by applying Fe(II) in the solution as it is the only oxidation number of Am and the lanthanides as well. The concentration of Pu was determined by LSC.

Results

It was found that lanthanides (Table 1.) and Pu(III) behaved similarly to Am in the presence of carbamide, that is they could not be eluted completely from the DGA column. The recovery of Pu reduced from 96% to 84,7% because of carbamide present.

Table 1 Elution of Nd, Eu and Tb from DGA resin starting from pure water and carbamide solution, respectively.

Nuclide	Recoveries (%)	
	From Water	From Carbamide Solution
Nd-147	102,7	71,6
Eu-155	110,5	67,2
Tb-160	86	70,1

Remaining work

- Rapid digestion methods (fusion, microwave digestion) will be developed for different matrices of soil and sediment samples.
- Separation of actinides will be examined for soil and sediment samples by extraction chromatography based on DGA resin. High selectivity of DGA will probably unnecessitate the preconcentration step.
- Feasibility of different α -source preparation procedures (electroplating, micro-coprecipitation) will be examined for processing suitable actinides to multiple or single-element sources.
- Different spectrum processing software programs (Hypermet, Genie2000) will be applied for evaluation.

Related publication

- [1] J. Groska, N. Vajda, Zs. Molnár, E. Bokori, P. Szeredy and M. Zagyvai: *Determination of actinides in radioactive waste after separation on a single DGA resin column*, Journal of Radioanalytical and Nuclear Chemistry **309**:(3) 1145-1158 (2016)

MATHEMATICAL MODELLING OF LOW DOSE HYPERSENSITIVITY

Balázs G. Madas, Emese Drozsdik, Lívia Hanusovszky, Anikó Fülöp

Objective

Low-dose hyper-radiosensitivity (HRS) and increased radioresistance (IRR) have been observed in many different cell lines. However, the underlying mechanisms of these phenomena are quite unclear. We showed earlier that the local minimum in surviving fractions can be the result of a global optimization process that minimize mutation rate at the tissue level [1]. However, the model had a problematic assumption that every cell communicates with every other cell independently on the distance. The objective of the present study was to elaborate a spatial model where cells minimize mutations based on their local neighbourhood and test whether it shows hypersensitivity in cell survival.

Methods

In the new numerical model, cells are placed on a rectangular lattice. Radiation induces pro-mutagenic DNA damages. The number of such damages follows Poisson distribution over the cells with a mean proportional to absorbed dose. Cells detect the average number of pro-mutagenic lesions in their neighbourhood. Cells stop dividing if they have more damages than the average damage number in their neighbourhood plus a given threshold equal to the average number of mutations occurring during cell division. In this way, cells can decrease the global mutation load by their individual decisions without communication with non-neighbouring cells.

Results

Simulations show that minimizing mutation rate results in local minimum in surviving fractions as it is observed in experiments [2]. The model can provide as good fits as the descriptive Induced Repair model if we suppose that survival is out of biological control (determined by physics) at high doses (Fig. 1). Considering the induction rate of spontaneous pro-mutagenic DNA damages, the model can account for multiple minima in surviving curves and for normalized surviving fractions exceeding 100% [3]. It is concluded that the principle of minimizing mutation rate can provide a mechanistic explanation for HRS/IRR response without introducing CFA-specific parameters. Experimental confirmation of the theory would have significant implications for radiation protection meaning that the health risks of low dose exposures are lower than the linear no-threshold model suggests. The principle is probably more general. The mechanism may work even without radiation exposure.

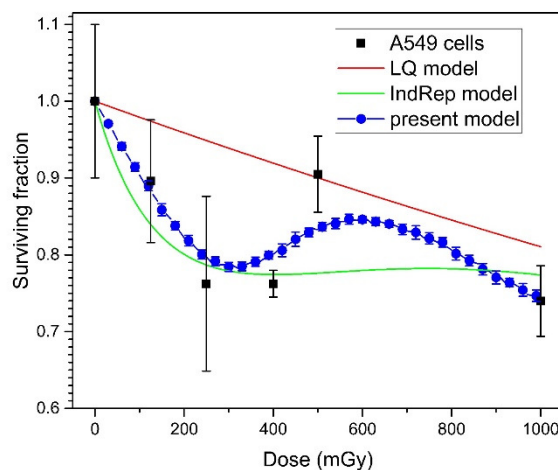


Figure 1: Cell survival (S) as the function of absorbed dose (D) at doses below 1 Gy. Black squares denote experimental data, the red line denotes the linear-quadratic function ($S = \exp(-\alpha \times D - \beta \times D^2)$) fitted to high-dose data, green line shows the descriptive Induced-Repair model fitted to experimental data, and the blue line and blue squares show the results of our simulations.

Related publications

- [1] B. G. Madas, L. Hanusovszky and E. Drozsdik: *Kis dózis, nagy érzékenység: a sugárvédelmi szabályozás alapfeltevése és a sejtek hiperszenzitivitása*, Magyar Tudomány **177**, 62-67 (2016)
- [2] L. Hanusovszky: *Kis dózisonál megfigyelt hiperszenzitivitás matematikai modellezése*, MSc thesis, Eötvös University (2016)
- [3] B. G. Madas, L. Hanusovszky and E. Drozsdik: *Low-dose hyper-radiosensitivity and increased radioresistance can be the result of processes that minimize mutation rate at the tissue level*, 62nd Annual Meeting of the Radiation Research Society, Waikoloa Village, United States of America (2016)

SURVEYING METHODS FOR DEVELOPMENT OF RENEWABLE ENERGY POTENTIAL

Bálint Hartmann, Attila Talamon

Objective

The objective of the KEOP 7.9.0/12-2013-0017 „Energy map (E-map)” project is to create a national scale “energy map”, which provides a foundation for the programming period of 2014-2020 in source-planning and implementation works by containing the summary of the regional energy data from all available statistical databases, as well as providing input data for planning by sectors using geospatial methods. The current renewable energy related primary databases are not suited to be used for a territorial data report, and the available applications do not contain the necessary information for responsible decision making. The present project aims to create a methodology, complying with the main European Union and national regulations and strategical documents, which is suitable to survey the theoretical, technological and economic potential of different renewable energy sources on a micro-regional level.

Methods

The reliability of initial estimation data of renewable energy sources is similar, as they are based on easily measured physical parameters (radiation energy, wind speed, water flow, and geothermal gradient). Thus the theoretical potential calculated from the aforementioned data is suited to quantify the physically available amount of energy. The base set defined by the theoretical potential can be used in developing several subsets.

One of these subsets is the ecologically sustainable potential (potential of different types of renewable energy and their ecological aspects), which is a definition closely connected to the goals of the project. It specifies the known energy amount which the already existing, as well as future projects can depend on. Another commonly used subset of the theoretical potential is the economic potential, which in accordance with its name quantifies the amount of renewable energy that can be utilized cost-efficiently. The intersection of the economic and ecological sets is called, in short, the sustainability potential, which is sustainable from both economic and environmental points of view. In addition to the above terms the convertible potential should be mentioned, which shows the proportion of energy demand that can be served by the available sources and known technologies.

Results

The output information was used to create an interactive map, which can support the future projects and responsible decision making related to sustainable energy planning.

Remaining work

The project was finished in 2016.

Related publication

- [1] A. Talamon A., V. Sugár and B. Hartmann: *Fine adjustment of heating system design parameters considering the Urban Heat Island Effect in case of Hungary*, 2016 International Conference on Engineering and Natural Science – Summer Session Conference (2016.07.12-14.)



V. NUCLEAR ANALYSIS



Kerámia



GAMMA-RAY STRENGTH FUNCTIONS

Tamás Belgya, László Szentmiklósi

Objective

Extreme statistical model is developed and applied to explain radiative neutron capture (n,γ) spectra measured at our Prompt-gamma Activation Analysis (PGAA) experimental facility. Our first attempt is the unfolded ^{114}Cd spectrum obtained from $^{113}\text{Cd}(n,\gamma)$ reactions. Our goal is to model the ^{114}Cd decay scheme using the extreme statistical model continuously developed by the first author.

Methods

Unfolding procedure had been developed using GEANT4 Monte Carlo package of CERN to obtain detector independent spectra from our HPGe detector spectra. These unfolded spectra and the decay scheme of the neutron captured nucleus can be simulated by the extreme statistical model that is under development.

Results

Modelling of ^{114}Cd radiative neutron capture spectrum was improved by introducing and developing gamma decay-scheme up to 3.25 MeV using our experimental data and a paper reporting experiments at Institut Laue-Langevin (ILL). Since the gamma-ray resolution of the ILL detector system was much better up to 2 MeV, the two data sets were combined. Above 2 MeV our own data were better, thus above this energy they were used. The construction of the decay-scheme is based on known levels and Ritz-combination rule. Details of the present status of modelling was orally presented at the Nuclear Data 2016 conference and the corresponding paper was accepted for publication in EPJ web conference series.

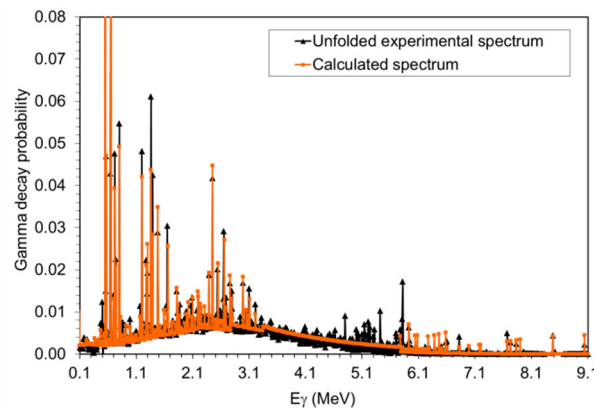


Figure 1: Simulation of $^{113}\text{Cd}(n,\gamma)^{114}\text{Cd}$ full range γ -spectrum

Two important conclusions should be mentioned:

- a/ In order to describe the correct position of the continuum bump, low-energy enhancement had to be included.
- b/ The statistical model feeds discrete levels in such a way that it could be described by 3rd-order polynomial fitting. This can help to decide spin and parity of levels.

To check the validity of the developed decay-scheme, $^{113}\text{Cd}(n,\gamma\gamma)$ coincidence experiments were suggested to our Prague collaborators (Ivo Tomandl and Milan Krlicka). Ivo Tomandl had performed two-step cascade or coincidence experiments using a ^{113}Cd target and radiative capture reactions on their well-established setup at the Czech Research Reactor.

To understand the nature of low-energy enhancement in ^{113}Cd , shell model calculations are under way in collaboration with Ronald Schwengner, Helmholtz Zentrum Dresden Rossendorf (HZDR). The first calculations were done using ^{78}Ni core. The main components of the wave functions of the states emitting transitions with large $B(M1)$ values are of $\pi[(pf)g_{9/2}^{-2}] \nu [g_{7/2}^6 d_{5/2}^6 d_{3/2}^3 s_{1/2}^1]$ configuration space for positive parity levels and $\pi[(pf)^{-1}g_{9/2}^{-1}] \nu [g_{7/2}^6 d_{5/2}^6 d_{3/2}^3 s_{1/2}^1]$ for negative parity levels.

The calculations yielded about 32000 transitions, however further improvements are needed because the cumulative number of levels was by a factor of two low at 3.25 MeV.

Remaining work

To improve decay scheme by analysing the ($n,\gamma\gamma$) spectra and extending shell model calculations to describe the levels up to 3.25 MeV.

Related publication

- [1] T. Belgya, L. Szentmiklósi, R. Massarczyk, et al.: *High-resolution study of the $^{113}\text{Cd}(n,\gamma)$ spectrum by statistical decay model with discrete levels and transitions*, EPJ conf. series (accepted)

BACKGROUND RADIATION STUDY FOR MULTI-GRID NEUTRON DETECTOR

Eszter Dian, Péter Zagyvai, Szabina Török

Objective

The Multi-Grid detector is a large area neutron detector for chopper spectrometry, with boron-carbide converter and Ar/CO₂ counting gas, invented by researchers of ILL (Institut Laue-Langevin) and now jointly developed by ILL and ESS (European Spallation Source). Since the signal of the inelastic instruments is a few orders-of-magnitude lower than the one of the elastic instruments, the high signal-to-background ratio (SBR) is a key issue for the detectors at these instruments. The aim of the current study is modelling the background components, induced in the Multi-Grid detector.

Methods

In this study the scattered neutron background and the neutron induced prompt and decay gamma radiation are observed via calculation and Monte Carlo simulation. The neutron induced gamma radiation was studied generally in a typical Ar/CO₂-filled detector with analytical calculation and MCNP6.1 simulation, taking into account the counting gas and the detectors' aluminium housing as sources of radiation. The scattered neutron background was studied in realistic models of the Multi-Grid detector. The model was built in Geant4 within the ESS Coding Framework.

Results

On the basis of the study on neutron induced activation it was found that only a low level activity is expected from the counting gas during operation and after 1 day of storage only a negligible level of activity will be present in the waste Ar/CO₂ stream. It was also shown that for the typical neutron wavelength range of the cold neutron instruments the SBR from gamma background varied between 10⁹-10¹⁰ for general boron-carbide-based detectors (Fig. 1), and still would be 10⁵ for beam monitors [1].

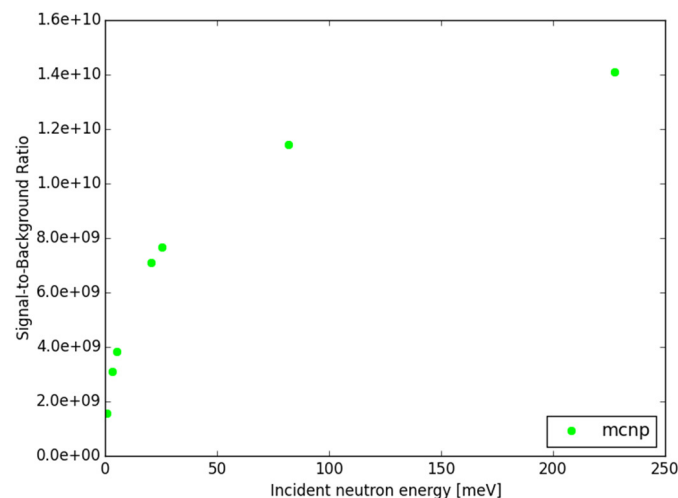


Figure 1: Signal-to-background ratio from neutron-induced prompt and decay gamma background in general boron-carbide-based detectors

For the scattered neutron background study the validation of the model was started via comparison of the simulated data (Time-of-Flight, detection coordinates and derived energy transfer) to the already published values measured at different neutron energies and experimental setups [2].

Remaining work

The scattered neutron background study is still in progress. After validating the model, it will be applied to study the components of the scattered neutron background and then the model will be used for optimizing the shielding of the detector to maximize the signal-to-background ratio.

Related publications

- [1] E. Dian, K. Kanaki, R. J. Hall-Wilton, P. Zagyvai and Sz. Czifrus: *Neutron activation and prompt gamma intensity in Ar/CO₂-filled neutron detectors at the European Spallation Source*, Applied Radiation and Isotopes **128**: 275-286 (2017)
- [2] E. Dian, K. Kanaki, R. J. Hall-Wilton, A. Khaplanov and T. Kittelmann: *Shielding Optimization Study for ¹⁰B-Based Large Area Neutron Detectors with Detailed Geant4 Model*, IEEE NSS-MIC 29. 10 - 5. 11. 2016, Strasbourg (2016)

COMPOSITION MEASUREMENTS FOR ACTIVATION STUDY OF SHIELDING MATERIALS TO BE APPLIED AT THE EUROPEAN SPALLATION SOURCE

Eszter Dian, Dávid Hajdú, János Osán, Dénes Párkányi, Péter Zagyoai

Objective

When the European Spallation Source (ESS) reaches its design configuration, protons of 2 GeV will impact a tungsten target resulting in spallation neutrons. The task of shielding – instruments and personnel from neutrons escaping the target-moderator-reflector system as well as from gamma photons – will be undertaken by a combination of mainly steel and concrete. To improve the neutron absorption effect of concrete below 10 MeV where iron has resonances in the cross section, a new PE-B₄C-concrete (polyethylene, boron-carbide) has been developed. It is essential to be prepared for the eventual activation of the shielding material, like concrete and metal components, considering both short-term effects on personnel and long-term effects on the decommissioning.

Methods

Prior to the irradiation experiments, elemental-analysis was achieved with X-ray fluorescence (XRF) spectroscopy on metal and concrete samples. Three metal samples, 5×5×5 cm³ cubes of aluminium, copper and steel were measured with a handheld XRF device (Niton X3Lt GOLDD+, Thermo Scientific). Two concrete samples, an average reference concrete and the PE-B₄C-concrete, which contains 0.76% B₄C and 10.2% polyethylene were also studied with a polarizing XRF device (Epsilon5, PANalytical).

Results

For both sets of samples, the measurements revealed minor discrepancy between the measured and the nominal composition for major components (e.g. Table 1 for metal samples), and gave a set of trace elements for the concrete samples [1]. The reference values are calculated from given nominal concentrations and provide no information about any trace elements. XRF is capable to quantify trace elements but does not detect light elements below Na. For the concrete, major components are not detectable with XRF, however due to the high neutron capture cross section of some trace elements XRF analysis is essential.

Table 1: Measured and nominal composition of metal samples

wt. %	Copper					Steel					Aluminium				
	Handheld XRF			Reference Cu-HCP		Handheld XRF			Reference Steel CK45		Handheld XRF			Reference 6082-T6	
	Average	St Dev	LOD	Min	Max	Average	St Dev	LOD	Min	Max	Average	St Dev	LOD	Min	Max
C									0.46	0.460					
Mg	< LOD		0.003			< LOD		0.003			0.952	0.511	0.650	0.600	1.200
Al	< LOD		0.756			0.537	0.162	0.582			97.032	0.570	0.518	95.200	98.300
Si	< LOD		0.106			0.203	0.017	0.049	<	0.400	1.024	0.072	0.087	0.700	1.300
P	< LOD		0.037	0.002	0.007	< LOD		0.036			< LOD		0.003		
Ti	< LOD		0.006			< LOD		0.008			< LOD		0.007	<	0.100
V	< LOD		0.008			< LOD		0.009			0.010	0.004	0.008		
Cr	< LOD		0.014			0.186	0.007	0.008	<	0.400	0.438	0.290	0.014	<	0.250
Mn	< LOD		0.017			0.609	0.014	0.032	0.650	0.650	0.591	0.100	0.030	0.4	1.000
Fe	< LOD		0.009			98.767	0.186	0.320	<	0.400	0.220	0.036	0.016	<	0.500
Co	< LOD		0.010			0.119	0.060	0.128			< LOD		0.010		
Cu	99.938	0.036	0.388	>=	99.950	0.027	0.019	0.012			< LOD		0.005	<	0.100
Zn	0.069	0.042	0.041	<	0.030	< LOD		0.011			< LOD		0.003	<	0.200
Mo	< LOD		0.003			0.003	0.000	0.002	<	0.100	< LOD		0.003		
Ag	< LOD		0.025	<	0.015	< LOD		0.017			< LOD		0.005		
Sn	< LOD		0.016			0.010	0.005	0.008			< LOD		0.003		
Bi	< LOD		0.007	<	0.001	< LOD		0.003			< LOD		0.003		

Remaining work

Samples of the materials are prepared for insertion in the Budapest Research Reactor where they will be subject to irradiation in both thermal and fast neutron fluence for a duration ranging from a few minutes to hours. The irradiation experiments will be planned on the basis of the measured compositions. After irradiation, activities and decay gamma spectra of the samples will be measured and compared to the corresponding measurements on standard concrete as a function of cooling time. Detailed set of data will be collected about the activation properties of the mentioned shielding materials both in terms of personnel safety and radioactive waste management.

Related publication

- [1] E. Dian, E. Klinkby, C.P. Cooper-Jensen, D. Párkányi, D. Hajdú, J. Osán, G. Patrsikov, U. Filges and P. Bentley: *Activation measurements of the concrete and PE-B₄C-concrete for neutron shielding at the European Spallation Source.*

CHEMICAL APPLICATIONS OF NUCLEAR ANALYTICAL METHODS

László Szentmiklósi, Boglárka Maróti, Zoltán Kis

Objective

It was aimed to apply the prompt-gamma activation analysis and the instrumental neutron activation analysis to determine elemental compositions of samples. Research was performed in the fields of catalysis, material science, e-waste.

Methods

PGAA with cold neutrons has been applied, occasionally in combination with NAA to measure major, minor and trace components of the samples

Results

- Catalytic HBr oxidation is an integral step in the bromine-mediated functionalization of alkanes to valuable chemicals. We established relationships between the mechanism of HBr oxidation over rutile-type oxides (RuO₂, IrO₂, TiO₂) and their apparent catalytic performance. Comparison with the well-studied HCl oxidation revealed distinct differences surface chemistry between HBr and HCl oxidation that impact the stability and activity of the catalysts. The gas-phase oxidation of hydrogen halides was studied in a quartz fixed-bed micro-reactor (8 mm internal diameter) at ambient pressure and in the temperature range of 413-713 K. The reactor was loaded with 0.5 g of RuO₂ or 0.23 g of TiO₂ catalyst (particle size = 0.4-0.6 mm) and was placed inside a furnace in the path of the neutron beam. A total volumetric flow of 250 cm³ STP min⁻¹ consisting of 10 vol.% HBr or HCl (Air Liquide, anhydrous) and 0-90 vol.% O₂ (Linde, purity 4.5) balanced in N₂ (Linde, purity 5.0) was continuously fed. Furthermore, 0-4 vol.% Br₂ (Acros, 99.8%) were added to the gas feed by passing a split of the N₂ flow through a saturator filled with liquid Br₂ at STP conditions. The halogen formation was quantified by iodometric titration using a Mettler Toledo G20 Compact Titrator. Br, Cl, Ru, and Ti were determined from the characteristic peak areas. The gas-phase signals of HBr, Br₂, HCl, and Cl₂ were subtracted, thus, all reported values correspond only to the solid catalyst. The surface coverage was calculated as the amount of halogen per surface sites taking into account the surface area of the catalysts and the density of sites. The quantitative determination of the halogen uptake under operando conditions using Prompt-Gamma Activation Analysis demonstrates that RuO₂ suffers from extensive subsurface bromination upon contact with hydrogen bromide, particularly at low temperature and low O₂:HBr ratios, which negatively affects the stability of the catalyst. TiO₂ exhibits intrinsically low halogen coverage (30-50%) at all the conditions investigated due to its unique defect-driven mechanism that renders it active and stable for Br₂ production. On the contrary, in HCl oxidation, TiO₂ is inactive and the chlorination of the highly active RuO₂ is limited to the surface. Differences in the extent of surface halogenation of the materials, were also confirmed by High-Resolution Transmission Electron Microscopy and explained by the DFT calculations. These insights into the molecular-level processes taking place under working conditions pave the way to the design of the next generation catalysts for bromine production [1].
- In framework of a MSc. thesis work by Mariann Papp [2], representative pieces of electronic waste were studied by nuclear analytical and imaging techniques. The combination of PGAA, PGAI, NAA, neutron and X-ray imaging could reveal the distribution of elements classified as toxic or with limited availability. Using PGAI the spatial distribution of the elements within a memory card as eWaste was directly studied. With neutron and X-ray imaging the heterogeneities of the samples were visualized. We found that the analysed electronic waste samples do contain many of the critical elements, such as platina or rare earth elements.
- A review paper about the PGAA user program has been published [3]. Statistical breakdown of completed proposals confirmed the widespread applicability of the technique and a dominant position of our team in the PGAA field.

Remaining work

We will continue the applications of PGAA related to thematic research projects and also ad-hoc proposals coming from international TNA projects (IPERION CH, C-ERIC).

Related publications

- [1] Moser M, Paunovic V, Guo Z, Szentmiklosi L, Hevia MG, Higham M, Lopez N, Teschner D and Perez-Ramirez J: *Interplay between surface chemistry and performance of rutile-type catalysts for halogen production*, Chemical Science, **7**, 2996 (2016)
- [2] Papp Mariann: *Elektronikai hulladékok vizsgálata nukleáris analitikai és képalkotó módszerekkel*, ELTE TTK Vegyész MSc diplomadolgozat. Témavezető: Szentmiklósi László, Konzulens: Salma Imre
- [3] L. Szentmiklósi, Z. Kasztovszky, T. Belgya, Z. Révay, Z. Kis, B. Maróti, K. Gméling and V. Szilágyi: *Fifteen years of success: user access programs at the Budapest prompt-gamma activation analysis laboratory*, Journal of Radioanalytical and Nuclear Chemistry **309**, 71 (2016)
- [4] BNC at the Automotive exhibition - <http://autopro.hu/szolgáltatok/Neutronvizsgalat-uttoro-technologia-a-jarmugyartas-szolgالاتaban/20763/>

APPLICATIONS OF PROMPT GAMMA ACTIVATION ANALYSIS AND OTHER ANALYTICAL METHODS IN HERITAGE SCIENCE (ARCHAEOLOGY) - HIGHLIGHTS

Zsolt Kasztovszky, László Szentmiklósi, Boglárka Maróti, Ildikó Harsányi, Zoltán Kis

Objective

It was aimed to apply the prompt-gamma activation analysis and the instrumental neutron activation analysis to determine elemental compositions of samples. Mostly, provenance studies were performed in the field of heritage science. Within the project, the activities related to an OTKA and the EU-funded IPERION CH projects were supported, too.

Methods

PGAA with cold neutrons has been applied in combination with NAA and portable XRF to measure major, minor and trace components of the samples, to benefit from the complementarities of these methods.

Results

- Partly related to a project supported by the Hungarian Scientific Research Fund (OTKA), compositions of polished stone axes made of metamorphic rocks have been analysed. A minor set nephrite, serpentinite, greenschist and hornfels archaeological and geological samples from Hungarian museums and from fieldwork have been measured. Most of the archaeological objects belong to the historical Mihálydy- and Ebenhöch collections. The aim of the study is to identify the origin of the raw materials (i.e. provenance of the objects). Besides PGAA, SEM-EDS have been applied on the intact objects. The results of the two methods agree well. When it was possible, optical microscopy on thin sections have been also done.

As regards the hornfels raw material, we have identified its characteristic high Ca and relatively high Al-content, as well as low amount of alkaline. Based on the PGAA and SEM-EDS measurements of hornfels, we have identified similar rock types in the SW of Rusca Mts., close to the village Novákfalva (Glimboca), and also in the South of Apuseni Mts., near the village Obersia (Obârșea) in Romania. On both territories hornfels were formed on the contact zone of banatite subvolcanic rocks and high Ca-content clayish Cretaceous Gosau-facies sediments. As a result of our work, we could discover and localize the provenance of a special rock type, the hornfels, which was a widely used raw material for polished stone tools in the studied area [1].

- Prompt Gamma Activation Analysis has successfully been applied to provenance research on Carpathian obsidians. The efficiency of PGAA and portable XRF in discriminations of various origin obsidians was compared on 81 geological samples representative for the major European-Mediterranean sources. Several multivariate analyses have been made based on the individual PGAA and XRF data, as well as on the combination of both data types. Instrumental Neutron Activation Analysis was also applied on a group of 17 samples. The advantages and disadvantages of each method are discussed to determine the best possible way of investigations to fingerprint and characterize long-distance trade items with minimal damage to the samples. We have demonstrated that although XRF and INAA measure more trace elements in obsidian than PGAA, PGAA is unique in the ability to determine boron, chlorine and hydrogen, as well also measuring well most of the main components. As it was demonstrated, PGAA gives reliable composition data representative for a few cm³ bulk sample, whereas XRF provides information only on the near-surface composition, and the result is somewhat influenced by sample geometry. Composition data provided by INAA is also representative of the bulk, as is PGAA, but unfortunately INAA is destructive in most instances. We have shown that grouping on the basis of B, Cl and Ti content measured by PGAA is more definite and more detailed than on the basis of Rb, Sr and Zr measured by portable XRF.

When exact and absolute compositional data are requested, for instance in order to build a database for characterisation in archaeometry or geochemistry, we recommend PGAA or, when sampling is allowed, INAA. PGAA is especially useful for items far from their place of origin where the physical integrity of the sample is crucial. A portable XRF is useful when fast grouping into known categories is requested for a large set of objects and absolute concentration data are not of highest priority. [2]

- Aim of the SOFIA experiments within the H2020 IPERION CH project was to study a processional cross, coming from the abbey of Chiaravalle (close to Milan, Italy) and dated to the 13th century. The cross is of rather complex construction of rare beauty, being decorated by 985 gems and fine gold filigree. During a recent restoration, some very small pieces of gold filigree were made available for scientific analyses. The techniques of choice will be XRF, PIXE and PGAA, in order to get compositional information both from the surface and from the bulk of three fragments from the cross that became available for analysis thanks to the restoration of the cross. Users from the Università degli Studi di Milano-Bicocca, Milan, Italy aimed to verify the use of amalgam technique (mix of Au and Hg) over a silver sample. From the presence of unusual minor/trace elements, indications on both the provenance of the metals used and the soldering technique could be inferred.

PGAA, XRF and PIXE analysis were carried out on all the three filigrees. The major advantage was that all the techniques were non-invasive and not-destructive and the samples were returned to the owners. Based on the PGAA results on the bulk elemental composition, as well as on indications of chemical elements on some local spots by PIXE, the following preliminary results were obtained:

The presence of Hg confirms the use of amalgam technique. The amounts of Ag, Au and Cu can characterize the raw material that was used for production of the cross.



Figure 1: Photo of the 13th c. Italian processional cross from the abbey of Chiaravalle



Figure 2: Photo of the three filigrees that were analysed by PGAA, milli-beam PIXE and XRF

Related publications

- [1] Gy. Szakmány, S. Józsa, Zs. Bendő, Zs. Kasztovszky and F. Horváth F: *Magyarországon előkerült hornfels (mész-szilikát szaruszirt) anyagú csiszolt kőeszközök nyersanyaglelőhelyének felkutatása* (in Hungarian), *Archeometriai Műhely* **XIII. 1**, 43 (2016)
- [2] Zs. Kasztovszky, B. Maróti, I. Harsányi, D. Párkányi and V. Szilágyi: *A comparative study of PGAA and portable XRF used for non-destructive provenancing archaeological obsidian*, *Quaternary International*, X: p. AiP. (2018)
- [3] E. Palamara, N. Zacharias, M. Xanthopoulou, Zs. Kasztovszky, I. Kovács, D. Palles, and E. I. Kamitsos: *Technology issues of Byzantine glazed pottery from Corinth, Greece*, *Microchemical Journal* **129**, 137 (2016)
- [4] A. Moropoulou, N. Zacharias, E. T. Delegou, B. Maróti and Zs. Kasztovszky: *Analytical and technological examination of glass tesserae from Hagia Sophia*, *Microchemical Journal* **125**, 170 (2016)
- [5] M. I. Prudêncio, M. I. Dias, C. I. Burbidge, Zs. Kasztovszky, R. Marques, J. G. Marques, G. J. O. Cardoso, M. J. Trindade, B. Maróti, F. Ruiz, L. Esteves, M. A. Matos and A. Pais: *PGAA, INAA and luminescence to trace the "history" of "The Panoramic View of Lisbon": Lisbon before the earthquake of 1755 in painted tiles (Portugal)*, *Journal of Radioanalytical and Nuclear Chemistry* **307**, 541 (2016)
- [6] G. Ilon and Zs. Kasztovszky: *Untersuchung spätbronzezeitlicher Glasperlen aus West-Ungarn* (in German), *Archeometriai Műhely* **XIII. 1**, 55 (2016)
- [7] Zs. Kasztovszky, Gy. Káli, Z. Kis, I. Kovács, A. Len, B. Maróti, K. Pánczél-Bajnok, L. Rosta and Z. Szókefalvi-Nagy: *Applications of neutron-based and ion beam methods in Cultural Heritage research at the Budapest Neutron Centre*, *Techné - La Science Au Service De L'histoire De L'art Et Des Civilisations* **43**, 70 (2016)
- [8] M.I. Dias, Zs. Kasztovszky, M.I. Prudêncio, A.C. Valera, B. Maróti, I. Harsányi, I. Kovács and Z. Szókefalvi-Nagy: *X-ray and neutron-based non-invasive analysis of prehistoric stone artefacts: a contribution to understand mobility and interaction networks*, *Archaeological and Anthropological Sciences* **9**, 1-15 (2017)
- [9] M. I. Dias, M. I. Prudencio, Zs. Kasztovszky, B. Maróti, I. Harsányi and P. Flor: *Nuclear techniques applied to provenance and technological studies of Renaissance majolica roundels from Portuguese museums attributed to della Robbia Italian workshop*, *J Radioanal Nucl Chem*, **312**, 205-219 (2017)
- [10] V. Hnatowicz, Zs. Kasztovszky, J. Kucera, A. Macková and L. Rosta: *Neutron beam analytical methods*, In: A. Macková et al. (ed.) *Nuclear Physics for Cultural Heritage - A topical Review by the Nuclear Physics Division of the European Physical Society*, published by the Nuclear Physics Division of the European Physical Society, 23 (2016)
- [11] V. Crupi, Zs. Kasztovszky, F. Khalilli, M. F. La Russa, A. Macchia, D. Majolino, B. Rossi, N. Rovella, S. A. Ruffolo and V. Venuti: *Evaluation of complementary methodologies applied to a preliminary archaeometric study of glazed pottery from Agsu (Azerbaijan)*, *International Journal of Conservation Science* **7, 2**, 901 (2016)
- [12] Zs. Kasztovszky, V. Szilágyi, K. T. Biró, J. Zöldföldi, M. I. Dias, A. Valera, E. Abraham, M. Bessou, F. LoCelso and V. Benfante: Chapter 6: *Ceramics, Marbles and Stones in the Light of Neutrons: Characterization by Various Neutron Methods*, In: N. Kardjilov and G. Festa (eds.) *Neutron Methods for Archaeology and Cultural Heritage*, Springer International Publishing Switzerland, 89 (2017)

and 9 posters and 16 oral presentations

Appearance in the Media:

- M1 Minden Tudás TV show: <http://www.mediaklikk.hu/video/minden-tudas-2016-10-14-i-adas-5/>

DEVELOPMENT OF NUCLEAR ANALYTICAL TECHNIQUES, NUCLEAR DATA MEASUREMENTS, AND RELATED DISSEMINATION ACTIVITIES

László Szentmiklósi, Tamás Belgya, Zoltán Kis, Dénes Párkányi, Boglárka Maróti, Ildikó Harsányi

Objective

To develop our analytical capabilities and know-how in Prompt-Gamma Activation Analysis, Neutron Activation Analysis, XRF, to accurately determine related nuclear data, and to provide training and education for guest researchers and students

Methods

(n,γ) measurements, PGAA, NAA, evaluation of nuclear data, computer programming, Monte Carlo modelling, teaching.

Results

Significant progress was achieved in nuclear instrumentation, methodology, and nuclear physics applications. Partial γ -ray production cross sections and the total radiative thermal-neutron capture cross section for the $^{185}\text{Re}(n,\gamma)^{186}\text{Re}$ reaction were measured at the Prompt Gamma Activation Analysis facility with an enriched ^{185}Re target. The ^{186}Re cross sections were standardized using well-known $^{35}\text{Cl}(n,\gamma)^{36}\text{Cl}$ cross sections from irradiation of a stoichiometric natural ReCl_3 target. The resulting cross sections for transitions feeding the ^{186}Re ground state from low-lying levels below a cut-off energy of $E_c = 746$ keV were combined with a modelled probability of ground-state feeding from levels above E_c to arrive at a total cross section of $\sigma_0 = 111(6)$ b for radiative thermal-neutron capture on ^{185}Re . A comparison of modelled discrete level populations with measured transition intensities led to proposed revisions for seven tentative spin-parity assignments in the adopted level scheme for ^{186}Re . Additionally 102 primary γ -rays were measured, including 50 previously unknown. A neutron-separation energy of $S_n = 6179.59(5)$ keV was determined from a global least-squares fit of the measured γ -ray energies to the known ^{186}Re decay scheme. The total capture cross section and separation energy results are comparable to earlier measurements of these values [1].

The distribution of the electromagnetic dipole strength below the neutron separation energy and its influence on the photon distribution after neutron capture were investigated in two experiments for the compound nucleus ^{114}Cd . By measuring the photo-absorption cross section at the bremsstrahlung facility γELBE at Helmholtz-Zentrum Dresden-Rossendorf it was possible to deduce the distribution of dipole strength below the neutron separation energy. The de-excitation spectrum after cold-neutron capture in ^{113}Cd was measured at the Budapest Neutron Centre. In a combined analysis, the experimentally deduced spectra after photon scattering on ^{114}Cd and the neutron capture in ^{113}Cd were analysed in terms of electric and magnetic strength functions and nuclear level density with the help of the statistical code γ DEX.

The initiative aiming at new calibration data for high-energy detector calibration in NAA was started. We produced ^{72}Ga by rector-irradiation, to make able to transfer the accurate calibration for PGAA station to the NAA counting stations. For this purpose, highly-accurate energy- and intensity-values were obtained. Mirror experiment is being made at FRM II, Garching. A poster is presented at RANC conference about the partial results [3].

We published a technical paper about the upgrade of the neutron activation analysis laboratory, clearly showing the high potential in the combined use of PGAA and NAA [4]. The results of an IAEA-coordinated round robin exercise was finalized and published about the ^{99}Mo production via neutron capture pathway. The most significant challenge here was to accurately account for the thermal and epithermal neutron self-shielding. Our lab was one of the best in this context [5].

We were involved in the organization of the First International Conference on Radioanalytical and Nuclear Chemistry, RANC 2016. We hosted three IAEA-delegates and two RadEff-colleagues for long-term visits. We continued our educational efforts, reaching about hundred BSc, MSc and PhD students of the relevant universities. We contributed to the annual Central European Training School on Neutron Scattering with PGAA and imaging training.

Related publications

- [1] D.A. Matters, A.G. Lerch, A.M. Hurst, L. Szentmiklósi, J.J. Carroll, B. Detwiler, Z. Révay, J.W. McClory, S.R. McHale, R.B. Firestone, B.W. Sleaford, M. Krτίčka and T. Belgya: *Investigation of Re 186 via radiative thermal-neutron capture on Re 185*, Physical Review C, **93** 054319 (2016)
- [2] R. Massarczyk, G. Schramm, T. Belgya, R. Schwengner, R. Beyer, D. Bemmerer, Z. Elekes, E. Grosse, R. Hannaske, A.R. Junghans, Z. Kis, T. Kögler, C. Lorenz, K. Schmidt, L. Szentmiklósi, A. Wagner and J.L. Weil: *Role of electric and magnetic dipole strength functions in the Cd 114 (γ,γ') and Cd 113 (n,γ) reactions*, Physical Review C **93**, 014301 (2016)
- [3] L. Szentmiklósi, Zs. Révay, B. Maróti, D. Párkányi and I. Harsányi: *High-energy calibration data for neutron activation analysis*, poster at the RANC 2016 conference, 10-15 April 2016., Budapest
- [4] L. Szentmiklósi, D. Párkányi and I. Sziklai-László: *Upgrade of the Budapest neutron activation analysis laboratory*, J. of Radioanal. Nuclear Chem. **309**, 91 (2016)
- [5] M. Blaauw, D. Ridikas, S. Baytelesov, P.S.B. Salas, Y. Chakrova, C. Eun-Ha, R. Dahalan, A.H. Fortunato, R. Jacimovic, A. Kling, L. Muñoz, N.M.A. Mohamed, D. Párkányi, T. Singh and Van Dong Duong: *Estimation of ^{99}Mo production rates from natural molybdenum in research reactors*, J. Radioanal. Nuclear Chem., **311**, 409-418 (2017)

PROVENANCE STUDY OF LITHIC RAW MATERIALS OF STONE TOOLS FOUND IN THE CARPATHIAN BASIN – CLOSING YEAR OF THE OTKA K100385 PROJECT

Zsolt Kasztovszky, György Szakmány, Zsolt Bendő, Katalin T. Biró, András Markó, Bálint Péterdi, Ildikó Harsányi

Objective

Prompt Gamma Activation Analysis (PGAA) has successfully been applied to investigate various lithic assemblages, chipped and polished stone tools made of obsidian, flint, radiolarite, and greenschist-metasite varieties. The absolute non-destructive feature of PGAA is highly capitalised on the study of intact museum pieces. The present report is about the fifth year of an OTKA* project. The main objective of the project is the archaeometry study of stone tools and raw materials in the Carpathian Basin and its wider environment – with the help of field work and mostly non-destructive analytical methods. The project time frame was originally 4 years with 1 year extension. Our results can contribute to the reconstruction of prehistoric exchange of goods (stone tools and raw materials) in the Carpathian Basin, regarding raw materials, such as obsidian, radiolarite, flint, „greenstone” (i.e. HP metamorphite, serpentinite, nephrite). The originally four-year project has started in April 2012, and will finish – after one year extension – in 2017.

Methods

Two main non-destructive analytical methods were chosen: the prompt-gamma activation analysis (PGAA), which is applied in archaeometry at the Budapest Research Reactor since 1998 and the „Original Surface” SEM-EDX (OS-SEM-EDX), which was developed during this project at the Department of Petrography and Geochemistry of the Eötvös University. PGAA is applicable to quantify all the major components and some trace elements in the lithic material. It is unique in determination of the elements H and B. Besides PGAA, OS-SEM-EDX has become a significant method to study the elemental and mineralogical composition of polished stone tools. Occasionally, we perform complementary measurements using portable XRF, INAA and EPMA.

Results

In 2016, mostly provenance studies of prehistoric polished stone tools have been done. The tools belong to the Mihálydy and Ebenhöch historical collections, the parts of them are exhibited in various Hungarian museums. The objects were made of hornfels, nephrite, serpentinite, blueschist, greenschist and other metamorphic rocks. Their compositions have been determined using PGAA and „original surface” SEM-EDX. The results of the two methods agreed well. On fieldtrips, comparative geological materials (jadeit and eclogite) from the supposed sources have been collected. Based on the analytical results, it was possible to identify the raw materials of various archaeological objects that took part in the long-distance prehistoric trade. Furthermore, other archaeological objects have been assigned to certain raw material sources that have been identified in fieldwork.

Two methodological studies have been performed on obsidians that were common raw material types in the Prehistory. PGAA and portable XRF were compared on a set of European and Mediterranean obsidians of the Hungarian National Museum. The compositional data determined by PGAA, portable XRF and NAA have been compared, as well as the applicability of the results of each method for provenance studies. According to our results, based on PGAA data (especially on B, Cl and Ti concentrations), the major obsidian types and subtypes can be as effectively separated as using XRF data (mostly Rb, Sr and Zr). In another study, the geochemical specifications of a very rare obsidian variety, the mahogany obsidian have been studied by Mössbauer spectroscopy, PGAA and electron microscopy.

Remaining work

In case of successful application, this work is planned to be completed in a new OTKA project from 2017.

Related publications

- [1] Gy. Szakmány, S. Józsa, Zs. Bendő, Zs., Kasztovszky and F. Horváth: *Magyarországon elokerült hornfels (mész-szilikát szaruszirt) anyagú csiszolt koeszközök nyersanyaglelohelyének felkutatása*, *Archeometriai Műhely*, **XIII/1**, 43 (2016)
- [2] Zs. Kasztovszky, K. Lázár, V. Kovács Kis, A. Len, J. Füzi, A. Markó and K.T. Biró: *Novel investigations on the mineralogy of Carpathian mahogany obsidian*, *Quaternary International* (submitted in 2017)
- [3] Zs. Kasztovszky, B. Maróti, I. Harsányi, D. Párkányi and V. Szilágyi: *A comparative study of PGAA and portable XRF used for non-destructive provenancing archaeological obsidian*, *Quaternary International*, **468**: Part A, 179-189 (2018)
- [4] B. Péterdi, K. T. Biró, Z. Tóth, É. Bertalan, Zs. Horváth, Á. Freiler, Zs. Beke and F. Budai: *Domoszló: örlő- és malomkő nyersanyag-kitermelőhely és műhely a Mátrában: Első régészeti elterjedés-vizsgálatok*, *Archeometriai Műhely* **13**:(4). 219-236. (2016)

SEPARATION OF LANTHANIDES AND AMERICIUM IN LIQUID NUCLEAR WASTE

Dénes Párkányi, László Szentmiklósi

Objective

In the nuclear fuel cycle, several lanthanide and trivalent actinide isotopes are produced by fission or transmutation of the uranium fuel. These nuclides are usually present in low quantities and they are often pure alpha/beta emitters. Based on these two features they are classified as difficult-to-measure nuclides (DMNs). In order to analyse these DMNs successfully, a separation procedure using extraction chromatography with DGA resin (diglycolamine derivative) was developed, preparatory to the radiochemical detection.

Methods

For the separation a glass column, filled with DGA resin was used. A peristaltic pump was used to pass the solvents through the resin bed with a flow rate of 0.1-0.25 cm³. The column can be heated with water flow (typically 40°C) from an external thermostat to keep constant and well-regulated temperature. During the elution, 0.5-2.0 cm³ fractions were collected. To optimize and verify the separation of the elements, short-lived gamma-emitter lanthanide isotopes (ie. La-140, Ce-141, Nd-147, Pm-151, Sm-153, Eu-152, Tb-160) – prepared by neutron capture in the reactor core – as well as Am-241 tracer were used. The „optimized” separation method was found to be applicable for the lanthanide and minor-actinide separation in our experiment with real liquid nuclear waste samples. The 0.7-0.8 recovery factor deduced from Tb-160 for the complete sample preparation was also quite acceptable. The relevant fractions could be investigated with LSC (see the spectra in Figure 3). The separation quality was confirmed here with lanthanide tracer in another aliquot, using identical separation procedures and the same DGA column.

Results

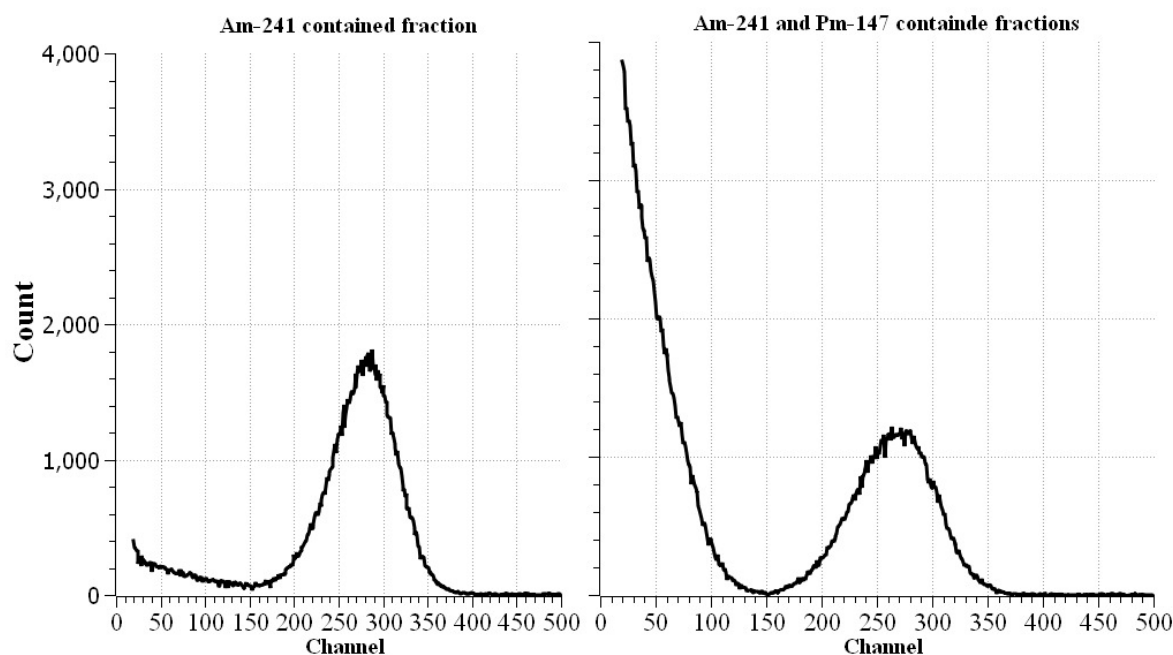


Figure 1: LSC spectra of the Am-241 and Pm-147 containing fractions of nuclear waste sample

Promising results were obtained for the applicability of the column separation of lanthanides and americium from nuclear waste, following a pre-concentration - group-precipitation step. Pm-147 and Am-241 (Figure 1.) became detectable in the separated fractions with liquid scintillation counting (LSC). Sophisticated gamma-spectrometry (low-level background, optimized signal-to-noise ratio, properly counting time) were successfully applied to determine Ce-144, Eu-154, Eu-155.

Remaining work

For investigation of the remaining DMNs and validate the quantities, additional radiochemical detection techniques, such as alpha-spectrometry and ICP-MS will be involved, subsequently to the proven preparation and separation steps.

Related publications

- [1] D. Párkányi, L. Szentmiklósi and N. Vajda: *Separation of lanthanides and americium in liquid nuclear waste by extraction chromatography with DGA resin*, in: L. Szentmiklósi (szerk.) Őszi Radiokémiai Napok 2016.10.10-10.12. Budapest: MKE, 2016. pp. 52-57. (ISBN: 978-963-9970-69-4) Balatonszárszó, Magyarország

NON-DESTRUCTIVE ANALYSIS OF METALLIC SAMPLES USING PGAA AND COMPLEMENTARY METHODS

Boglarika Maróti, László Szentmiklósi, Tamás Belgya

Objective

To synergetic use of PGAA, pXRF and neutron imaging in order to answer complex questions concerning composition, provenance, conservation, manufacturing of contemporary and historical metal samples in a non-invasive way and by minimizing the activation risk

Methods

Analytical methods based on X-ray fluorescence (portable XRF spectrometer) and neutron-based techniques (conventional PGAA, attenuated PGAA, high-resolution PGAA, in-beam NAA and INAA) were used in order to measure the specimens in a non-destructive way. Besides ancient, mainly copper alloys, contemporary alloys and material science samples were also investigated. For full comparability, a series of copper-alloy certified reference materials were analysed using all methods listed above.

Results

High-resolution PGAA method was already applied successfully in the compositional analysis of metallic samples, especially in the cases of samples with strong prompt gamma lines below 500 keV, such as Co-Re alloys, Ru and Ir content of Ti mesh monolith catalysts. PGAA with a gamma attenuator is a useful technique in the detection of components with high-energy gamma lines. As the installed Pb attenuator layer absorbs most of the gammas from the sample below 300 keV (e.g. Cu has its most intense gamma line at 278 keV), the relative counts in the high energy region can be tripled in the same period of time. In case of in-beam activation analysis the irradiation was performed in the guided cold neutron beam of the FRM II PGAA station. The subsequent off-line measurements took place in a low-level counting chamber. As the XRF method is a surface analytical technique, both the polished and the rear side of the copper-alloy discs were measured. The results below show the averages of 5 measurements on each side. Fig. 1. shows the result of the tin-lead-bronze alloy, representing the precision of the applied methods. In-beam activation analysis was the most precise and accurate method to determine the alloying and minor components. However, Fe and Pb could not be determined in any sample, and one has to consider the longer storage time in order to meet the clearance level. XRF proved to be the most productive technique, although its low penetration depth resulted in large concentration differences between the two sides of the discs (e.g. Pb), or large variance in results (e.g. Mn, Fe).

Table 1: Comparison of the measurement parameters of the three main applied non-destructive method. The analyzed volumes and the necessary measurement times are also listed.

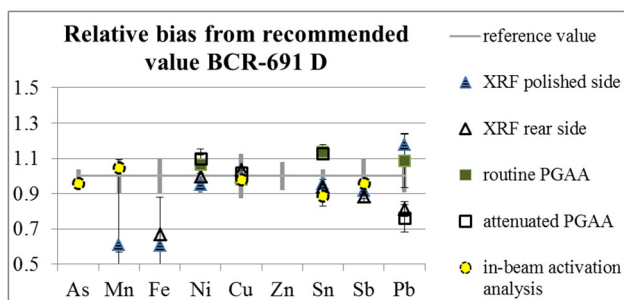


Figure 1: Relative bias of the results determined by different methods from the certified and the recommended reference values

	pXRF	PGAA	In-beam activation analysis
Information depth	few tens of μm	few mm	few mm
Spot/beam size	7 mm ²	24-44 mm ²	150 mm ²
Irradiated mass	-	0.5-1 g	1-3 g
Time required for the whole analytical procedure	30 seconds per each measurements	1-3 hours of measurement + 1.5 hour evaluation	5 minutes of irradiation, 4 hours of measurement in total + 1 hour evaluation

Remaining work

To summarize all the results. Discussion and draw the conclusions. To prepare the PhD thesis.

Related publications

- [1] B. Maróti, L. Szentmiklósi and T. Belgya: *Comparison of low-energy and coaxial HPGe detectors for prompt gamma activation analysis of metallic samples*, Journal of Radioanalytical and Nuclear Chemistry **310**, 743 (2016)
- [2] E. Szabados, D. F. Srankó, F. Somodi, B. Maróti, S. Kemény and A. Tungler: *Wet oxidation of dimethylformamide via designed experiments approach studied with Ru and Ir containing Ti mesh monolith catalysts*, Journal of Industrial and Engineering Chemistry **34**, 405 (2016)
- [3] B. Maróti: *On-site handheld XRF measurements on 17 pieces of Bronze Age gold hair rings and 2 pieces of gold arm rings in the Hungarian National Museum*, Kutatási jelentés, MTA EK-NAL-2016-139-1-1-M0, NAL2016/126, in Hungarian (2016)
- [4] B. Maróti, L. Szentmiklósi, Zs. Révay and T. Belgya: *Comparative measurements on certified reference copper alloys using different PGAA settings* in: Szentmiklósi L (szerk.) *Őszi Radiokémiai Napok*. 2016.10.10-10.12. Budapest: MKE, 2016. pp. 58-63. (ISBN: 978-963-9970-69-4) /Vértés Attila award/ Balatonszárszó, Hungary

SELECTED APPLICATIONS OF MÖSSBAUER SPECTROSCOPY

Károly Lázár, Sándor Stichleutner

Objective

Potentials of application of Mössbauer spectroscopy are demonstrated. First, ^{57}Fe transmission spectroscopy was used to identify Fe(IV) oxidation state in a non-heme oxoiron complex able to catalyse highly selective asymmetric oxidation. Further on, transformations of $\beta\text{-FeOOH}$ to various crystalline forms of iron-phosphates were followed. ^{57}Fe conversion electron spectroscopy (CEMS) was used to detect presence of superparamagnetic iron in electrodeposited layers formed in heavy iron irradiation. Combination of ^{57}Fe and ^{119}Sn CEMS spectroscopy was applied to study electrodeposited Fe-Sn binary alloys. ^{119}Sn CEMS was used to study Sb doped SnO_2 . Finally, ^{197}Au spectroscopy was used to identify various species of gold present in 1.3 – 4 nm size thiol stabilized nanoparticles.

Results

^{57}Fe transmission spectroscopy: The chiral pentadentate low-spin ($S = 1$) oxoiron(IV) complex $[\text{Fe}^{\text{IV}}(\text{O})(\text{asN4Py})]^{2+}$ was synthesized and spectroscopically characterized. Its formation kinetics, reactivity, and enantioselectivity in an oxygen-atom-transfer reaction was investigated [1]. The corresponding Mössbauer spectrum of the complex is shown in Fig. 1. In another study phase controlled synthesis of iron phosphate dihydrates either to monoclinic or orthorhombic structure was developed starting from $\beta\text{-FeOOH}$ nanorods. Stages of transformation of different phases were followed by Mössbauer spectroscopy, too [2].

^{57}Fe and ^{119}Sn conversion electron spectroscopies (CEMS) were applied to reveal the effect of addition of peptone to the aqueous gluconate based electrolyte used to prepare electrodeposited Sn-Fe layers. Addition of peptone resulted in changes in the composition and improved the crystallinity of the deposited Fe-Sn alloy [3]. **^{57}Fe CEMS** was utilized to study the effects of irradiation of α -iron layers with 247 MeV Kr ions. Irradiation with 10^{13} ion cm^{-2} fluence converted ca. 50 % of crystalline iron into amorphous and superparamagnetic phases [4]. **^{119}Sn CEMS** was used to study transparent conductive layers prepared by DC sputtering of Sb to SnO_2 . Doping of Sb to SnO_2 results in electron transfer from Sb to Sn(IV) resulting in an increase of the isomeric shift [5].

^{197}Au spectroscopy was used to identify various gold species present in buthlyldithiol stabilized 1.3 – 4 nm diameter gold particles. Four types of Au could be distinguished, namely, metallic gold in the bulk, metallic gold on the surface of particles, surface gold atoms linked to sulfur atoms and gold located in S-Au-S bridges formed on the top of particles [6]. Corresponding Mössbauer spectrum is shown in Fig. 2.

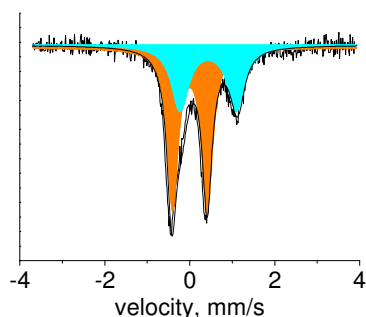


Figure 1: 77 K Mössbauer spectrum of a mixture of low-spin $[\text{Fe}^{\text{IV}}(\text{O})(\text{asN4Py})]^{2+}$ (orange), and high-spin $[\text{Fe}^{\text{II}}(\text{asN4Py})(\text{CH}_3\text{CN})]^{2+}$ (light blue) [1]

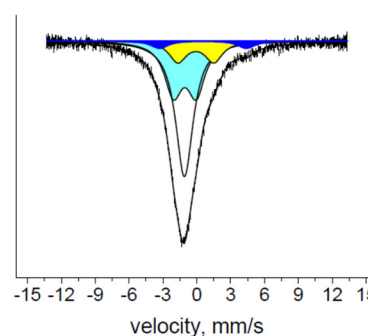


Figure 2: 4.2 K Mössbauer spectrum of thiol stabilized Au nanoparticles with decomposition of contributions of various gold species (see text) [6]

Related publications

- [1] D. Lakk-Bogáth, R. Csonka, G. Speier, M. Réglér, A.J. Simaan, J-V. Naubron, M. Giorgi, K. Lázár and J. Kaizer: Formation, characterization and reactivity of a nonheme oxoiron(IV) complex derived from the chiral pentadentate ligand asN4Py, *Inorganic Chemistry*, **55**, 10090 (2016)
- [2] R. Lin, A.P. Amrute, F. Krumreich, K. Lázár, R. Hauert, M. Yulikov and J. Pérez-Ramirez: Phase-controlled synthesis of iron phosphates via phosphorylation of $\beta\text{-FeOOH}$ nanorods, *CrystEngComm*, **18**, 3174 (2016)
- [3] G.B. Lak, L. Sziráki, E. Kuzmann, S. Stichleutner, C.U. Chisholm, M. El-Sharif, G. Varga, K. Havancsák and Z. Homonnay: The effect of the peptone on the structure of electrodeposited Sn-Fe binary alloys, *Hyperfine Interact.*, **237**, 20 (2016)
- [4] E. Kuzmann, S. Stichleutner, Z. Homonnay, K. Havancsák, C.U. Chisholm, M. El-Sharif, V.A. Skuratov, A. Nakanishi and K. Nomura: Generation of superparamagnetism in metallic α -iron by swift heavy ion irradiation, *Radiation Physics and Chemistry*, **127**, 165 (2016)
- [5] K. Nomura, E. Kuzmann, V.K. Garg, A.C. de Oliveira, S. Stichleutner and Z. Homonnay: ^{119}Sn CEMS study of Sb doped SnO_2 film, *Hyperfine Interact.*, **237**:5 (2016)
- [6] E. Kuzmann, E. Csapó, S. Stichleutner, V.K. Garg, A.C. de Oliveira, S.W. da Silva, L.H. Sing, S.S. Pati, E.M. Guimaraes, A. Lengyel, I. Dékány and K. Lázár: Fine structure of gold nanoparticles stabilized by buthlyldithiol: Species identified by Mössbauer spectroscopy, *Colloids and Surfaces A. Physicochem. Eng. Aspects*, **504**, 260 (2016)

RADIOGRAPHY AND TOMOGRAPHY AT BRR

Zoltán Kis, László Horváth, László Szentmiklósi

Objective and Methods

The objective is to develop and apply imaging instrumentation and methodology at the Budapest Research Reactor (BRR). The RAD facility is to study larger objects with bimodal (neutron, X-ray) imaging, even in real-time. The NIPS-NORMA facility is to make neutron imaging of smaller objects in combination of position-sensitive element analysis by prompt-gamma activation imaging (PGAI). In 2016 the RAD station has been upgraded with a *removable sapphire filter*, an option to decrease effectively the fast neutron component. The NORMA station has been upgraded with a *motorized pinhole collimator with three different hole sizes and a graphite scatterer*, which are capable of increasing the L/D ratio of the beam considerably while makes it more homogeneous. The *neutron tomography (NT) of the IAEA test objects* have been accomplished at both stations. For the *ANCARA supercritical loop* a further series of thermohydraulic measurements and neutron imaging was carried out to better cover the pressure and temperature range and the related changes in the radiographic projections. Pilot *fast neutron imaging* experiments were carried out at BRR in collaboration with PSI, Switzerland.

Results

The 3D imaging for objects up to ~200 mm with a thermal beam has been implemented at RAD. The neutron flux (Φ , $\text{cm}^{-2}\text{s}^{-1}$) at the screen and the dose rate (D , $\text{mSv}\cdot\text{h}^{-1}$) at the camera of the *RAD station when applying the sapphire filter* are as follows: $\Phi_{\text{th}} = 2.92 \times 10^7$, $\Phi_{\text{epi}} = 8.19 \times 10^3$ and $\Phi_{\text{fast}} = 8.36 \times 10^5$; $D = 2.77$. The filter yielded a significant decrease (new/original) of the dose rate (0.13) and for the fast (0.0304) and epithermal flux (0.009) but kept well the thermal flux (0.63), i.e. the camera could better be protected while maintaining its imaging capabilities in the thermal range. The L/D ratio of the *NORMA station with the interchangeable pinhole system* was significantly improved from 233 to 1832 when applying the smallest pinhole of 10 mm^2 . It means that the distance from the screen where the spatial resolution is mostly affected only by the inherent resolution of the scintillation screen could be extended from 20 mm to about 100 mm (Fig. 1a). The *NT measurements of the IAEA test objects* were accomplished with success (Fig. 1b). As a result of this international round robin these test objects were recommended for the neutron imaging community to be the standard tools for measuring the spatial resolution in 3D NT. The coupled evaluation of the radiographic images and the thermophysical properties of the *pseudocritical water* have shown that the main driving force behind the decrease of the neutron attenuation is the decreasing water density as the bulk-fluid temperature increases (Fig. 1c). These data help the validation of the ongoing CFD simulations. In the course of the *fast neutron tomography* experiments a spatial resolution of about 1.3 mm has been achieved. Typically, 10-minute long exposures were needed to obtain reasonable quality radiographic images. For tomographic imaging, several hours of acquisition were typically needed to obtain reasonable image quality on non-symmetric and larger (e.g. $10 \times 10 \times 10 \text{ cm}^3$) objects (Fig. 1d). Bimodal imaging and PGAI were applied in a pilot experiment for *electronic waste (eWaste)* characterization.

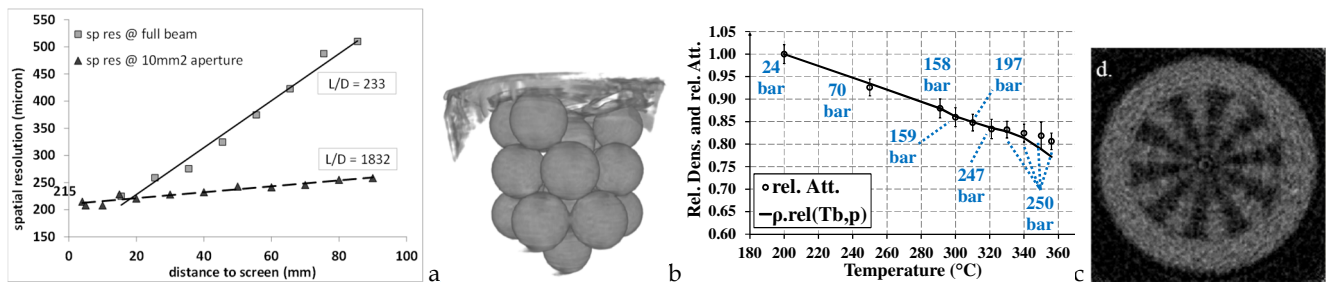


Figure 1: (a) The spatial resolution values of NORMA station with full beam and smallest pinhole (b) NT image of the IAEA sphere samples at the RAD station (c) The relative density (ρ_{rel}) and relative attenuation (rel. Att.) of the water at different temperatures and pressures (d) Fast neutron tomogram of a plastic Siemens star inside a 1 cm thick steel annulus.

Remaining work

To further study the *vibration effects* from the reactor hall on the high resolution imaging system.

Related publications

- [1] A. Kaestner, Z. Kis, M.J. Radebe, D. Mannes, J. Hovind, C. Grünzweig, N. Kardjilov and E. Lehmann: *Samples to determine the resolution of neutron radiography and tomography*, Physics Procedia **88**: 258-265 (2017)
- [2] A. Kiss, M. Balaskó, L. Horváth, Z. Kis, Z. and A. Aszódi: *Experimental investigation of the thermal hydraulics of supercritical water under natural circulation in a closed loop*, Annals of Nuclear Energy **100**, **2**, 178-203 (2017)
- [3] Z. Kis, L. Szentmiklósi, R. Schulze and E. Abraham: *Prompt Gamma Activation Imaging (PGAI)* In: N. Kardjilov and G. Festa (eds.): *Neutron Methods for Archaeology and Cultural Heritage*, 303-320, Springer International Publishing (2016)
- [4] R. Zboray, R. Adams and Z. Kis: *Fast neutron radiography and tomography at a 10 MW research reactor beamline*, Applied Radiation and Isotopes, **119**, 43-50 (2017)

In addition to journal publications, six oral presentations were presented at conferences and meetings.

SYNTHESIS OF CARBOXYMETHYLCELLULOSE/ACRYLIC ACID HYDROGELS WITH SUPERABSORBENT PROPERTIES BY RADIATION-INITIATED CROSSLINKING

Tamás Fekete, Judit Borsa, Erzsébet Takács, László Wojnárovits

Objective

The aim of this work is to form gels at milder synthesis conditions and to achieve better gel properties compared to the pure CMC gels through introduction of low concentrations of acrylic acid.

Methods

Aqueous solutions of CMC and AAc were prepared from 5 to 40 w/w% solute concentrations. The CMC:AAc ratio varied from 100:0 to 20:80. The solutions were irradiated with ^{60}Co γ -source at a dose rate of 9 kGy h⁻¹ with an absorbed dose of 1 to 80 kGy. The gel fraction (GF) was calculated from the dry gel weight before (w_0 ; calculated from the solution concentration) and after (w_1) the washing process: $\text{GF}(\%) = (w_1/w_0) \times 100$. The degree of swelling (Q) was calculated from the weight of the swollen (w_s) and the dry gel (w_d): $Q(g_{\text{water}}/g_{\text{gel}}) = (w_s - w_d)/w_d$.

Results

Superabsorbent hydrogels were prepared by gamma irradiation from aqueous solutions of carboxymethylcellulose (CMC) and acrylic acid (AAc) with varying CMC:AAc ratio. The gelation of carboxymethylcellulose/acrylic acid solutions required much milder synthesis conditions than pure CMC solutions. Absorbed dose required for adequate gelation decreased with the increase in AAc ratio. Moreover, significantly higher gel fraction was achieved at the expense of lower water uptake (Fig. 1). Unlike CMC solutions, CMC/AAc systems showed good gelation even below 10 w/w% solute concentration. Moreover, irradiation of 5-7.5 w/w% CMC/AAc solutions with small doses resulted in gels with excellent swelling properties and gel fraction. The replacement of CMC was very effective up to 10%. Very high AAc content (more than 50-60%) resulted in lower gel fraction unless higher absorbed doses were used. In summary, by substituting a small part of CMC with AAc under mild synthesis conditions both gel properties could be significantly improved simultaneously compared to pure carboxymethylcellulose gels.

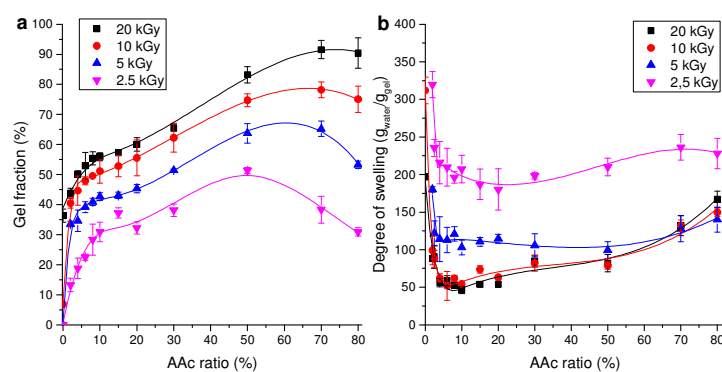


Figure 1: Effect of acrylic acid ratio on gel fraction (a) and degree of swelling (b) for CMC/AAc gels at different doses (20 w/w% solution)

Remaining work

The effect of alkali treatment on the swelling properties of the superabsorbent hydrogels will be investigated both at room temperature and at elevated temperatures. The modification of other (non-polyelectrolyte) cellulose derivative-based hydrogels with acrylic acid will also be examined.

Related publications

- [1] T. Fekete, J. Borsa, E. Takács and L. Wojnárovits: *Synthesis of cellulose-based superabsorbent hydrogels by high-energy irradiation in the presence of crosslinking agent*, Radiation Physics and Chemistry **118**, 114 (2016)
- [2] T. Fekete, J. Borsa, E. Takács and L. Wojnárovits: *Synthesis of carboxymethylcellulose/acrylic acid hydrogels with superabsorbent properties by radiation-initiated crosslinking*, Radiation Physics and Chemistry **124**, 135 (2016)
- [3] J. Borsa, K. László, L. Boguslavsky, E. Takács, I. Rácz, T. Tóth and D. Szabó: *Effect of mild alkali/ultrasound treatment on flax and hemp fibres: the different responses of the two substrates*, Cellulose **23**, 2117 (2016)
- [4] T. Fekete, J. Borsa, E. Takács and L. Wojnárovits: *Synthesis of cellulose derivative/acrylic acid hydrogels by radiation-initiated crosslinking*, lecture IRaP, September 25-30, 2016, Presqu'île de Giens, France

ADVANCED MODERATORS FOR INTENSE COLD NEUTRON BEAMS IN MATERIALS RESEARCH

József Janik, László Rosta

Objective

The Neutron Spectroscopy Department (NSD) of the Wigner Research Centre for Physics (Wigner FK), together with the Energy Research Centre (both members of the Budapest Neutron Centre - BNC consortium) in collaboration with spin-off companies has gained experience of cold moderator development and usage. The European Spallation Source (ESS) has developed a novel concept of so-called low dimensional moderators (LDM). Monte Carlo simulations have shown that this concept can improve the performance of the facility (measured in moderator brightness) by a factor of three in comparison to conventional, volume moderator designs. Even though this concept promises a significant performance, an engineering design has to be developed and operational experience has to be gained for this new type of moderator. Thus BNC has engaged itself in the BrightnESS Project (EU H2020) for a brighter neutron source in the cold spectral range - applied to the case of a reactor neutron source. According to the project plan, new liquid hydrogen (LH) cell configurations are to be studied for optimised geometry and also minimising neutron leakage from the unperturbed flux field in case of reactor neutron sources. Also a method, proposed by BNC/NSD, for moderator phase space mapping has been developed and this energy sensitive pinhole imaging (ESPI) technique is to be applied for wavelength dependent divergence mapping of the moderator and the beam path. During the current project, collaboration with the ESS project partners are being established.

Methods

1. Engineering design of the Budapest Research Reactor (BRR) low dimensional moderator: as a first step an initial document has been elaborated to fix the current configuration and status of the BRR Cold Neutron Source (CNS) facility. As a part of the LDM design various calculations and experiments with the operating CNS have been carried out. A series of measurements with the old moderator cell has been started. Detailed Monte Carlo simulations have also been prepared to optimize the neutronics performance of a new moderator chamber for the reactor case to be implemented at BRR.
2. Ortho-para hydrogen experiments: as a part of the moderator optimization the BRR CNS operation mode has been modified in order to allow precooling of the moderator chamber in advance of the reactor start. This enabled us to make a 14 days precooling of the moderator chamber to achieve the full conversion of H₂ into the para state, which is a prerequisite of the compact moderator concept. The time of flight small angle neutron scattering instrument (FSANS) instrument looking on the moderator through the NG3/2 neutron guide was then used to monitor the neutron intensity after the start of the reactor.
3. The Monte Carlo simulations: the engineering design of the LDM for the BNC reactor is helped by MC simulations. Monte-Carlo Mapped Power (MCMP) calculations were performed for the case of the current configuration of the BRR LH-CNS. These simulations are being considered for comparison with the performed intensity measurements on the BRR small angle neutron scattering (SANS) beamline.
4. The BRR test beam-line: as a part of the implementation of the BrightnESS project we have shown that a neutron source phase space mapping method is to be developed and used. This "camera obscura" technique has been demonstrated at BRR. A preliminary setup is used in the first phase of this project for intensity mapping of the existing liquid hydrogen moderator. In order to realize this technique at the BRR and at ESS a thorough conceptual design has been started for a properly adapted test beam-line. The following components have been specified for the engineering design to be started: beam extraction system from the neutron source, shutter, flight tube, vacuum pumps, diaphragm and attenuator system with remote control, chopper (highly absorbing double disc construction), monitor and detector for time-of-flight multiframe construction, biological shielding components, electronic control and integration, on-site assembling plan.

Results

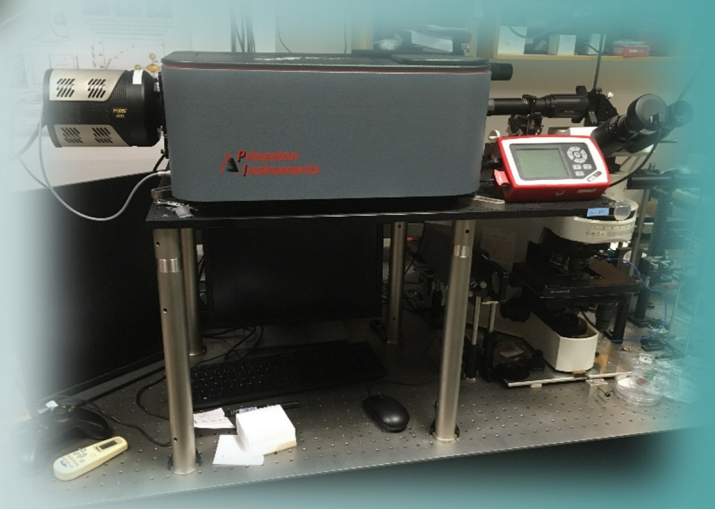
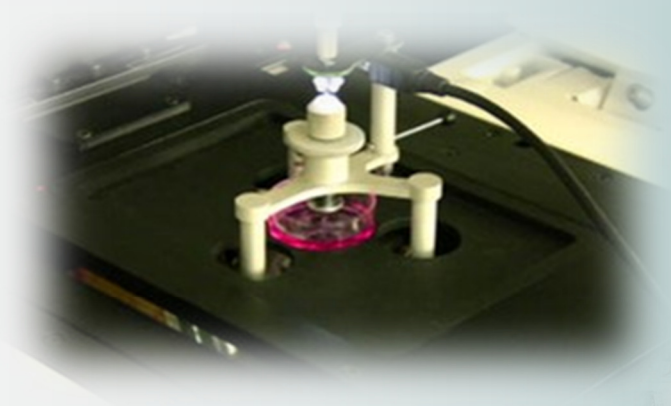
The project for the development of a compact moderator has well progressed. The following major milestones have been reached: - The ortho-para conversion measurements are very promising for a simplified scheme of a new CNS system at BRR. - Assuming a pre-cooling of the hydrogen the optimal para-hydrogen state can be preserved during a usual reactor operation cycle. - For a substantial modernization of the BRR cold source a compact moderator with para-hydrogen can be used without a complicated converter system and preserving the heat exchanger-free, direct condensation configuration.

Remaining work

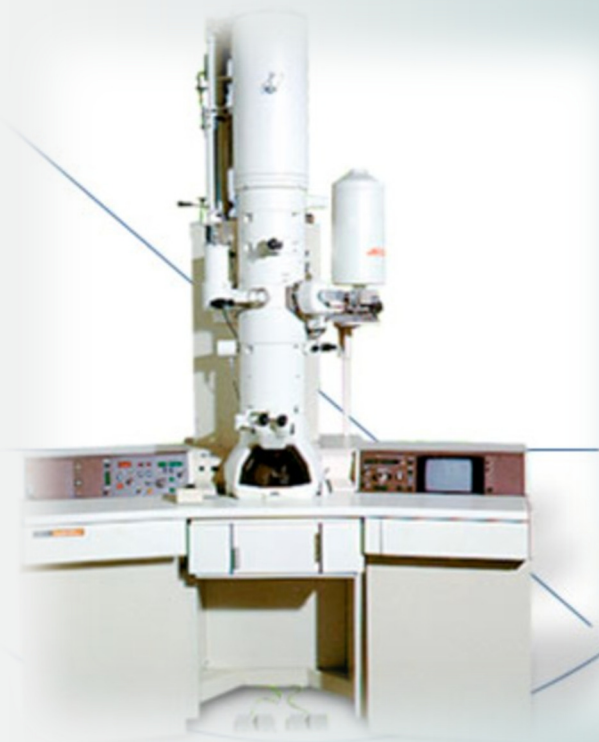
MC simulations support the design of a LDM. - For realistic fabrication-ready documents further engineering work is needed to optimize the neutron performance, calculate nuclear heat loads on the moderator chamber and thermo-hydraulic properties of the LDM cells.

Related publications

- [1] J. Janik and L. Rosta: *Budapest Cold Neutron Source*, Bhabha Atomic Research Centre (2016 Mumbai)
- [2] J. Janik and L. Rosta: *Cold Neutron Source at the Budapest Research Reactor*, (2016 Vienna)
Journal of Physics: Conference Series (JPCS) (2017)



VI. RESEARCH AND DEVELOPMENT IN INSTITUTE OF TECHNICAL PHYSICS AND MATERIAL SCIENCES



nano 
**Nanocsodák
Mozgásban**

TAMING DEFECTION – HOW WE ALL MIGHT BE BETTER OFF WITH CERTAIN LEVEL OF TOLERANCE

(OTKA K-120785)

A. Szolnoki, M. Perc

Leaving the joint enterprise when defection is unveiled is always a viable option to avoid being exploited. While loner strategy helps the population not to be trapped into the tragedy of the commons state, the resulting three-strategy solution is rather disappointing. Namely, the average payoff is unable to exceed the income of a loner's strategy significantly, hence participating in a public goods game does not necessarily provide an attracting option for competing players. This failure suggests that perhaps it is not the best option for cooperators to leave the group when defectors emerge because by switching to loner state they lose all benefits of mutual cooperation immediately. In this way the original dilemma can be transformed into a new form where cooperator players should decide how many defectors they tolerate in their group before leaving the group for a modest, but guaranteed payoff.

To explore this new dilemma, we introduce a spatial model of public goods game in which beside the unconditional defector (D), cooperator (C), and loner (L) strategies there are players with a certain degree of tolerance for the defectors among them. These players could choose to cooperate or abstain, depending on the actions of other players. By forming 5-member groups on a square lattice we allow the diversity of tolerance threshold. In particular, M_1, \dots, M_5 strategies behave as a cooperator as long as the number of defectors remains below a threshold value in the group but it switches to loner state otherwise. By following this approach, we can check the viability of this mixed strategy and clarify if there is an optimal level of tolerance which provides the highest income for the whole population.

Such a complex system is generally characterized by the presence of strong fluctuations, unpredictable and non-linear dynamics, multiple scales of space and time, and frequently some form of emergent structure. To handle this complexity during the Monte Carlo simulation we should apply stability analysis of sub-system solutions and also finite-size analysis. An example of a stability analysis is illustrated in Fig. 1 where two subsystem solutions, namely the three-strategy DCL and the four-strategy DCM_1M_2 phase are compared. The series of snapshots in the upper row shows the separation of the population in two parts, each of which is initially randomly distributed with the strategies that will form one of the two competing subsystem solutions (Fig. 1(a)). In Fig. 1(b), the subsystem solutions are formed in both halves of the space and their proper competition starts after removing the border between them (thus allowing strategy transfer across the border). Fig. 1(c) shows an intermediate state during the competition in which the DCL phase will ultimately turn out to be the winner. Fig. 1(d), on the other hand, shows an intermediate state during the competition in which the DCM_1M_2 phase will ultimately turn out to be the winner. Here only the synergy factor r is changed slightly while all other parameters are unchanged. The two graphs in the bottom row depict the corresponding time evolution of the strategy densities. After a relaxation of 20 000 Monte Carlo steps (marked by an arrow), the two subsystem solutions start competing for space. On the left ($r=2.80$) the DCL solution wins, while on the right ($r=2.81$) the DCM_1M_2 solution wins. The linear system size used for this example was $L = 2400$, but the snapshots in the upper row contain just a 200×200 cut-off of the whole population for clarity. Here, in agreement with the colours of legends, defectors are marked by red, pure cooperators by blue, M_1 strategy by yellow, M_2 by ochre, and loners by green.

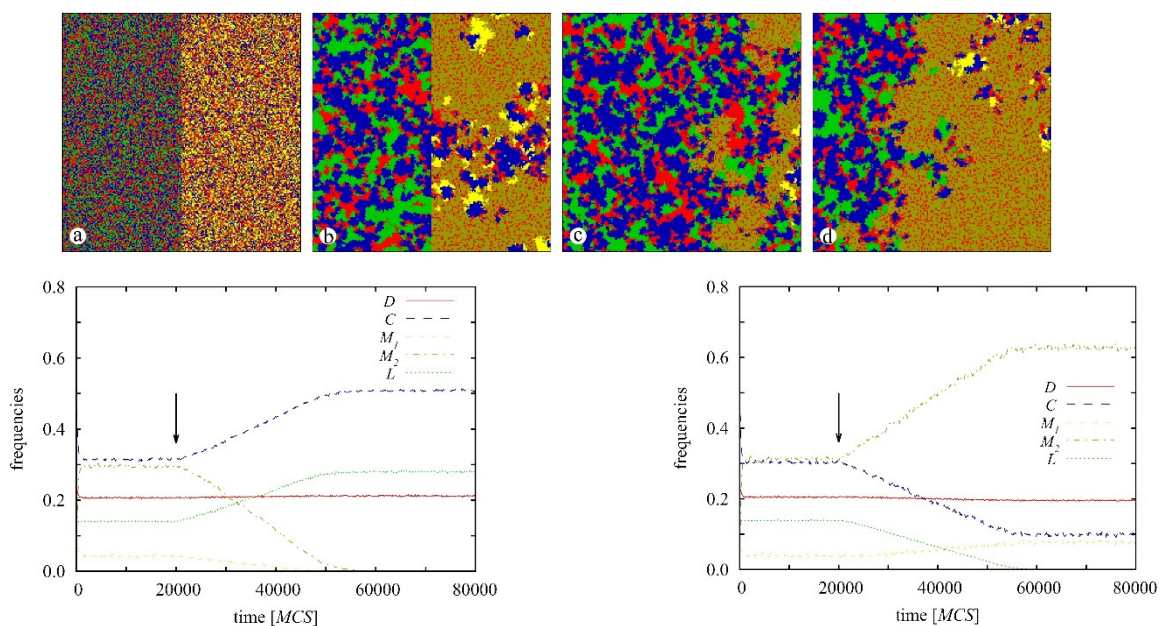


Figure 1: Stability analysis of two subsystem solutions at both sides of the discontinuous phase transition point

It is also worth stressing that simulations at small system can easily cause finite-size effects which may lead to misleading outcomes of the strategy competition. To illustrate it in Fig. 2 we start the evolution from a random initial state where all the eight strategies are present (Fig. 2 (a)). After relaxation only D (red) and M_2 (ochre) strategies survive, which also form a two-strategy solution (Fig. 2(b)). In Fig. 2(c), we then manually re-introduced small compact patches of three other strategies, namely strategy C (blue), strategy L (green), and strategy M_1 (yellow). Afterwards, loners die out (again) very soon within the DM_2 phase, as shown in Fig. 2(d). Later, C players also die out, but tolerant strategies M_1 and M_2 form a successful alliance, as shown in Fig. 2(e). Indeed, their formation turns out to be stronger than the previously declared victorious DM_2 phase, and the population terminates in a defector-free state, as shown in Fig. 2(f). Importantly, the defector-free state can evolve naturally from a random initial state if the system size is large enough.

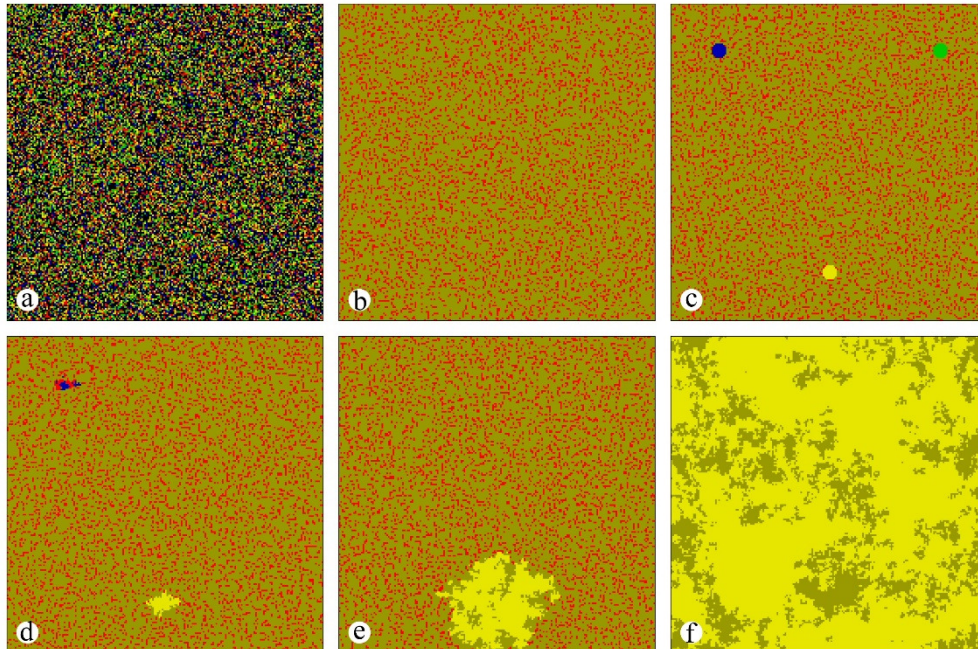


Figure 2: Finite-size effect can easily cover the viable stable solution. The latter, plotted in (f), can only emerge spontaneously if the evolution is launched for sufficiently high system size.

Our results are summarized in a phase diagram plotted in Fig. 3. It suggests that the diversity of tolerance proved optimal. When tolerant players had different thresholds for withstanding defection, they could turn the whole group towards cooperation in cases where defection would have otherwise dominated. As we noted, certain stable solutions only emerged when the number of players was large enough, lying largely undetected for smaller games. But once they emerged, they remained stable, even in small populations. These pattern formations may explain why tolerant behaviour remains stable during an evolutionary process especially when external conditions are demanding and they can only provide a modest benefit for cooperator strategy.

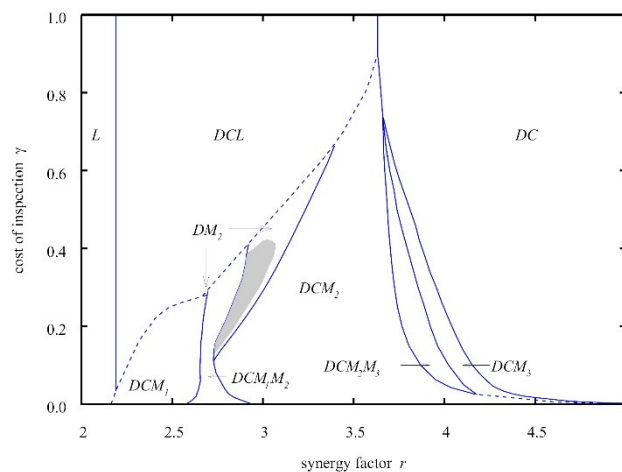


Figure 3: Full phase diagram of our model on the $r - \gamma$ (inspection cost – synergy factor) parameter plane. Dashed lines denote discontinuous, while solid lines mark continuous phase transitions. In structured population, in stark contrast to the well-mixed system, there also exist regions where the coexistence of different tolerance levels is the stable solution. The grey-shaded region in the two-strategy DM_2 phase denotes those parameter values where the population evolves into a full-cooperator, defector-free M_1M_2 phase, but only if the system size is large enough.

FLAGELLIN BASED BIOMIMETIC COATINGS: FROM CELL-REPELLENT SURFACES TO HIGHLY ADHESIVE COATINGS

(Lendület LP2012-26/2012, ERC_HU NKFIH, OTKA NN117849)

B. Kovács, D. Patkó, I. Székács, N. Orgován, S. Kurunczi, A. Sulyok, N. Q. Khánh, B. Tóth, F. Vonderviszt, R. Horváth

Biomimetic coatings with cell-adhesion-regulating functionalities are intensively researched today. For example, cell-based biosensing for drug development, biomedical implants, and tissue engineering require that the surface adhesion of living cells is well controlled. Recently, we have shown that the bacterial flagellar protein, flagellin, adsorbs through its terminal segments to hydrophobic surfaces, forming an oriented monolayer and exposing its variable D3 domain to the solution [Analytical Chemistry 85 (11), 5382-5389, 2013]. Here, we hypothesized that this nanostructured layer is highly cell-repellent since it mimics the surface of the flagellar filaments. Moreover, we proposed flagellin as a carrier molecule to display the cell-adhesive RGD (Arg-Gly-Asp) peptide sequence and induce cell adhesion on the coated surface. The proposed concept is visualized in Fig. 1.

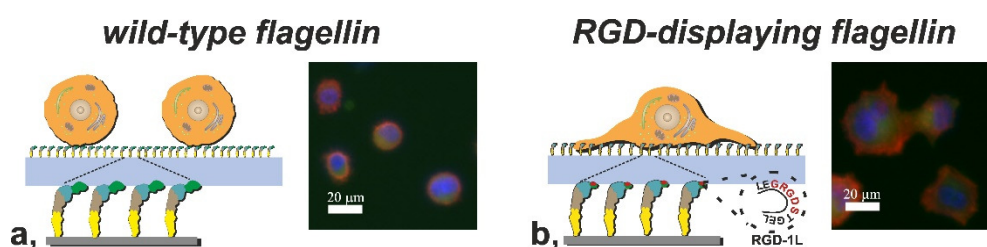


Figure 1: Schematic representation and fluorescent microscopic images of cells on anti-adhesive and adhesive surface coatings. a, Wild type flagellin hinder cell adhesion on the sensor surface. b, RGD displaying flagellin induce cell adhesion and spreading.

The details of this work can be summarized as follows:

During the mammalian HeLa cell adhesion experiments, we recorded the cell adhesion data with OWLS (Optical Waveguide Lightmode Spectroscopy) and applied a PLL-g-PEG polymer monolayer as reference anti-adhesive surface coating. The ΔN_{TM} (effective refractive index change) signals recorded on surfaces coated with either wild-type flagellin or PLL-g-PEG both remained at the level of the baseline during the whole time span of the cell-based assay (Fig. 2a). Since ΔN_{TM} is proportional to the degree of the cell adhesion [Journal of Receptors and Signal Transduction 29 (3-4), 211-223, 2009], we concluded that both surfaces were highly cell-repellent. The changes in the full width of the TM_0 resonant peak at half maxima (changes of W , i.e. ΔW) were also monitored [Applied Physics B: Lasers and Optics 91 (2), 319-327, 2008].

Cellular activity provoked negligible shifts in W , further proving that there was no significant cell adhesion on either wild-type flagellin or PLL-g-PEG layers (Fig. 2b). Cell adhesion and spreading would make ΔW increase due to the micron-scale optical inhomogeneities caused by the adhering cells at the sensor surface. Our conclusions are well supported by the phase contrast images of cells captured on the coated sensor surfaces after the OWLS measurements (Fig. 3).

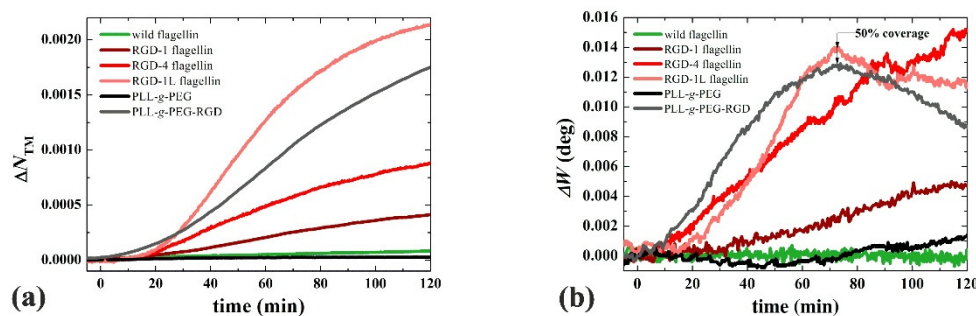


Figure 2: OWLS signals recorded after living cells were seeded on the surfaces of the OWLS chips coated with the indicated layers. (a) The measured ΔN_{TM} values correlating with the strength of cellular adhesion. (b) Temporal evolution of the width of the OWLS resonance peak (W).

We created flagellin-based fusion proteins in which the D3 domain of FliC is replaced by an oligopeptide segment containing one or more of the integrin binding RGD motif. Although the simple RGD motif is sufficient to mediate binding to integrin receptors, the flanking amino acid residues may further enhance binding affinity. Thus, we chose the more efficient GRGDS pentapeptide as the basic unit for insertion.

We tested the genetically modified flagellin variants as surface coatings, too. On the sensor surfaces coated with RGD-displaying flagellin variants, cells provoked a continuous increase (up to a maximum value) in N_{TM} . Cells seeded on the PLL-g-PEG-RGD-coated adhesive reference surface produced similar signals. The observed saturating sigmoid-shaped curves are clear characteristics of active cell spreading. The larger the signal the stronger is the cellular adhesion; cells induced the largest ΔN_{TM} signal thus showed the strongest adherence on the RGD-1L surface. The second, the third and the fourth highest cell adhesion were obtained with the PLL-g-PEG-RGD, RGD-4 and RGD-1 coatings, respectively (see Fig. 2a).

In conclusion, cells on the three different RGD-displaying flagellin layers adhered to different degrees, which could be explained by the fact that the RGD motif was integrated with different linker pairs, and most probably provided different accessibility and flexibility for the cells.

The temporal evolution of the width of the OWLS resonance peak (W) during cell adhesion was also recorded (Fig. 2b). In the case of the RGD-1 and RGD-4 flagellin-coated surfaces W increased monotonically and continuously until the end of the experiment. This suggests that the surface coverage did not reach 50% during the time of the experiment. In contrast, in case of the PLL-g-PEG-RGD and RGD-1L surfaces ΔW first increased, then reached a very clear maximum, and then decreased again. Previous experiments and numerical simulations suggest that such kinetic behaviour indicates that the cell coverage already increased above 50%. The half surface coverage is reached at the maximum value of the resonant peak width [Applied Physics B: Lasers and Optics 91 (2), 319-327, 2008]. This finding also suggests that the most intense cell adhesion and spreading took place on the PLL-g-PEG-RGD and RGD-1L coatings. The phase contrast images recorded well confirm the above findings (see Fig. 3).

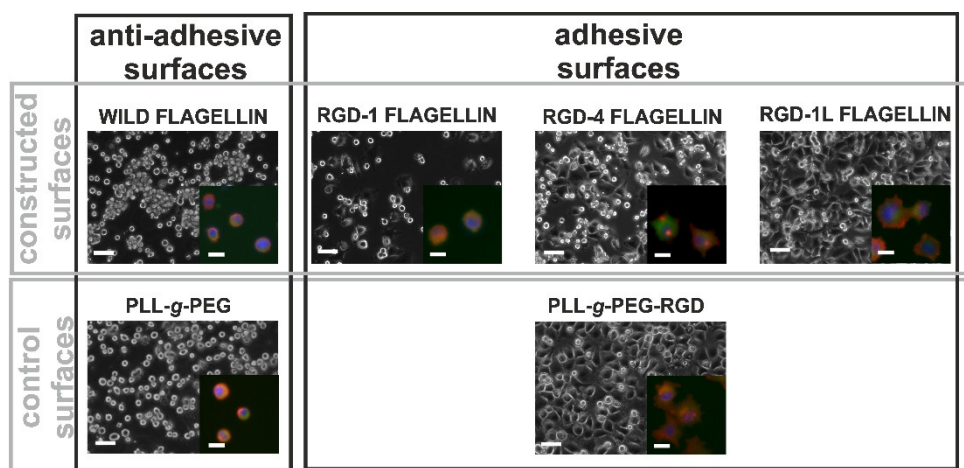


Figure 3: Microscope images of the cells seeded on the investigated surfaces. The phase contrast images (scale bar 50 μm) show cells on the biosensor surfaces right after the OWLS experiments. The insets (scale bar 20 μm) show fluorescently labelled cells cultured on glass coverslips in parallel experiments (red: F-actin, blue: nuclei, green: vinculin).

In conclusions, the application of flagellin-based fusion proteins for fabricating tunable surfaces opens up new avenues. Wild-type flagellin and its functionalized variants can be applied together in various mixing ratios. Thus, oriented affinity layers with negligible non-specific cell adhesion can be created with well controlled average distance between the binding sites.

Other peptide sequences can be easily introduced into flagellin in a similar manner. Therefore, surfaces with multiple functionalities can be fabricated in a straightforward manner. Flagellin variants exhibiting specific recognition functionalities offer the possibility to create a large variety of coatings on hydrophobic surfaces. Since flagellin does not adsorb at all on hydrophilic surfaces solution [Analytical Chemistry 85 (11), 5382-5389, 2013], patterned functional surfaces could be easily created in a straightforward and cost-effective manner by patterning the hydrophobicity of the surfaces and exposing them to the solutions of functionalized flagellin.

MOIRÉ SUPERLATTICES IN STRAINED GRAPHENE-GOLD HYBRID NANOSTRUCTURES

(EU FP7 Marie Curie CIG No.334377, János Bolyai Research Scholarship, OTKA K101599, NKFIH TÉT_12_SK-1-2013-0018)

A. Pálinkás, P. Süle, M. Szendrő, Gy. Molnár, C. Hwang (KRISS, Korea), L.P. Biró, Z. Osváth

Tailoring the atomic and electronic structure of graphene has been a subject of intense research, due to its possible applications in nanoelectronics. The local density of states (LDOS) can be modified, among other methods, by periodic potentials which create secondary Dirac points (SDP). Such periodic potentials can be induced in graphene by moiré patterns (Fig. 1) using crystalline substrates. The lattice mismatch and relative rotation between graphene and the crystalline substrate determine the period of the moiré pattern, and consequently the energy at which the SDPs appear.

Graphene grown by chemical vapour deposition was transferred on top of flat gold nanoislands and characterized by scanning tunneling microscopy (STM) and tunneling spectroscopy (STS). Here we show that the strength of graphene-gold interaction can be tuned by annealing the graphene-covered gold nanoislands at moderate temperatures and that graphene plays a key role in the formation of crystalline gold surfaces. Multiple annealing processes were applied: firstly, to increase the adhesion of graphene to the gold nanoislands, then to transform the supporting polycrystalline gold surfaces into (111) crystal planes. After annealing at 650 °C in Ar atmosphere, gold nanoislands covered by graphene have displayed Au(111) crystalline surfaces, while surface of non-covered nanoislands remained disordered.

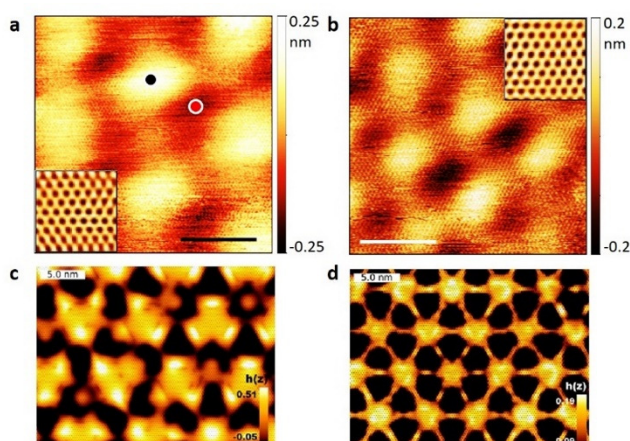


Figure 1 (a): STM image of graphene on top of gold (111) showing a moiré of 7.7 nm. STS measurements taken on topographically high and low positions, marked with black and red dot, respectively, are shown in (b). STM image of graphene on top of gold (111) showing a moiré of 5.1 nm. (c)-(d): DFT-adaptive CMD simulated images of the experimentally observed moiré patterns.

Considering the equilibrium interatomic distances of bulk Au (0.288 nm) and graphene (0.246 nm), a maximum moiré period of only 1.8 nm can be formed in graphene/Au(111), due to the significant misfit between the two lattice constants. This implies that large moiré periodicities (5.1 nm, 7.7 nm, see Fig. 1) can only be explained by considerable lattice distortions both in the graphene and in the support layers.

Various moiré patterns found experimentally were successfully reproduced by classical molecular dynamics (CMD) simulations. A new DFT-adaptive interface interaction potential has been developed which proved able to describe adequately the weak van der Waals forces at the graphene/Au(111) interface. CMD simulations reveal that in the case of anomalously large moirés the standard lattice constants do not apply, the crystal lattices are considerably distorted. The misfit is reduced from 12.8 % to 4.2 % and the moiré periodicity increases from 1.8 nm up to 7.8 nm.

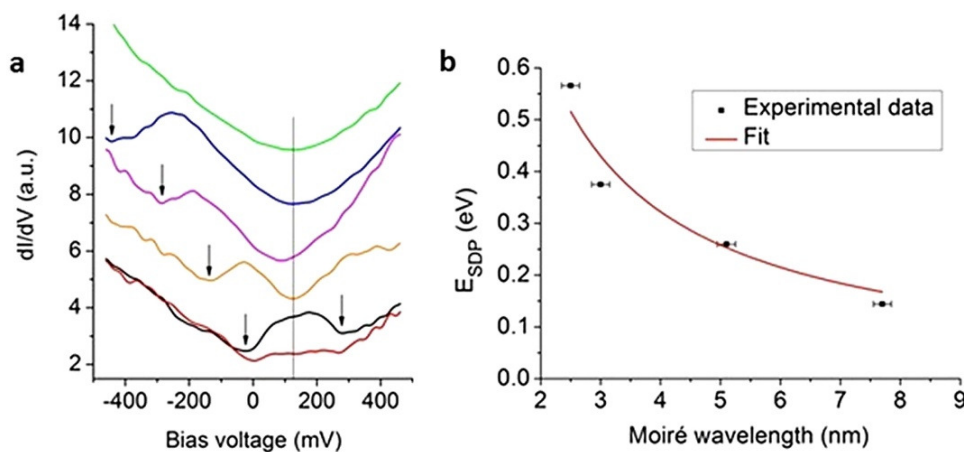


Figure 2: Local density of states of graphene on Au (111) showing secondary Dirac points. (a): Experimental dI/dV curves for five different moiré wavelengths: 1.9 nm (green), 2.5 nm (blue), 3.0 nm (magenta), 5.1 nm (orange), and 7.7 nm. For this latter, spectra measured on both topographically high (black) and low (red) positions are shown. The secondary dips in the spectra are marked by arrows. (b): Energy of the secondary dips measured from the Dirac point, as a function of the moiré wavelength. The black symbols are experimentally measured values, while the red line is the theoretical fit to the data.

moiré wavelength. The black symbols are experimentally measured values, while the red line is the theoretical fit to the data.

Tunnelling spectra were acquired on the moiré patterned graphene/Au(111) areas. The corresponding dI/dV curves display secondary dips in the LDOS. The energy of these secondary Dirac points depends on the moiré wavelength, as shown in Fig. 2(a,b). The experimentally measured values are in good agreement with the expected theoretical dependence $E_{SDP} = 2\pi\hbar v_F / (\sqrt{3} \cdot \lambda_M)$, where λ_M is the moiré wavelength.

MAGNETIC PHASE-TRANSITION GRAPHENE TRANSISTOR WITH TUNABLE SPIN POLARIZATION

(ERC StG NanoFab2D, Lendület LP2014-14)

P. Vancsó, I. Hagymási (Wigner FK), L. Tapasztó

Graphene has emerged as a material with strong potential for both electronic and spintronic applications, however the absence of a band gap in 2D graphene sheets turned the scientific attention towards graphene nanoribbons (GNRs). It has been shown that the semiconducting nature of zigzag nanoribbons (ZGNRs) is related to interaction effects and their oppositely spin polarized edge states. In this work, we propose a novel ZGNR device concept, enabling the control of both charge and spin signals, integrated within the simplest three-terminal device configuration (Fig 1). Our device is based on the strong interplay of the band structure and edge spin configuration in ZGNRs. While in the half-filled system antiferromagnetic (AF) state with oppositely spin-polarized edges is stable, in a doped ZGNR ferromagnetic (FM) state with parallel spin orientation on both edges can become energetically favourable. Therefore, by varying the carrier density of the ribbon a magnetic phase transition between AF and FM state can be achieved which is also an abrupt semiconductor (AF)-metal (FM) transition. This proposed switching mechanism is different as compared with the conventional FET devices, because the applied gate voltage can here dynamically open and close an interaction gap, with only a minor shift of the Fermi level.

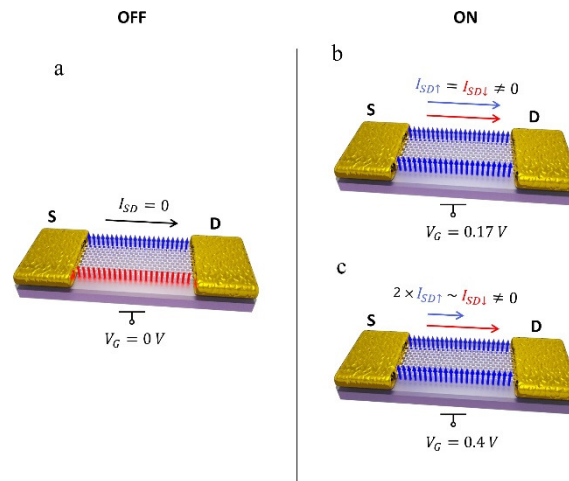


Figure 1: Schematic representation of the three states of the proposed ZGNR FET. (a): an insulating OFF state with antiparallel spin orientation on opposite ribbon edges in the absence of a gate bias, (b): the conducting ON state characterized by parallel spin orientation on ribbon edges but no net spin polarization of the current induced by an applied gate voltage, and (c): spin polarized ON state achieved by further increasing the gate potential.

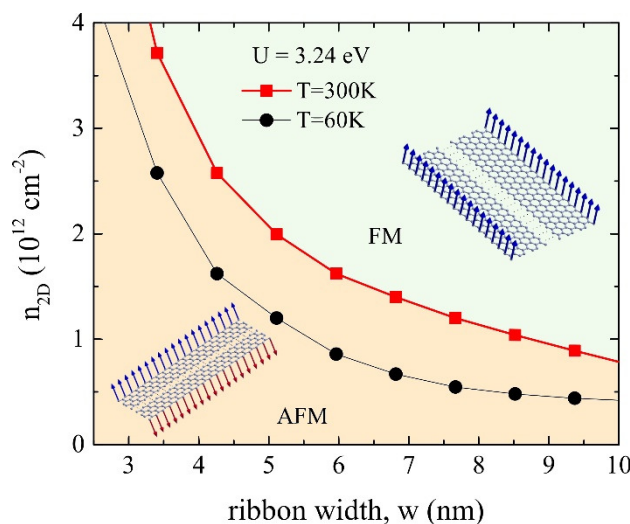


Figure 2: Phase diagram of ZGNRs as a function of charge carrier concentration (n_{2D}) and ribbon width (w) at two different temperatures ($T=60K$ and $T=300K$). The AF ground state is the only stable without external doping; however, the FM configuration can become favourable above a critical doping value and ribbon width.

Our experimentally validated Hubbard model revealed that for realistic ribbon widths the magnetic phase transition occurs in the low doping regime ($n_{2D} \sim 10^{12} \text{ cm}^{-2}$) which can be easily accessed experimentally by simple electrostatic gating (Fig 2). We found that gate voltage where the ZGNR transistors can switch is in the range of 0.1-1, depending on the width of the ZGNR and the properties of the gate insulator layer (SiO_2 , HfO). To explore the transport characteristics of the proposed novel

device we have performed Landauer transport calculations by using the spin dependent Hamiltonian matrix from our Hubbard calculations (Fig 3). We have found that such devices can operate at high speed ($S = 71 \text{ mv/dec.}$), while the spin polarization of the current can be tuned between 0 and 50% even at room temperature. The main advantage of our proposed device concept is that we are able to control both charge and spin currents by using a simple gate electrode, which could open new routes for novel data processing techniques.

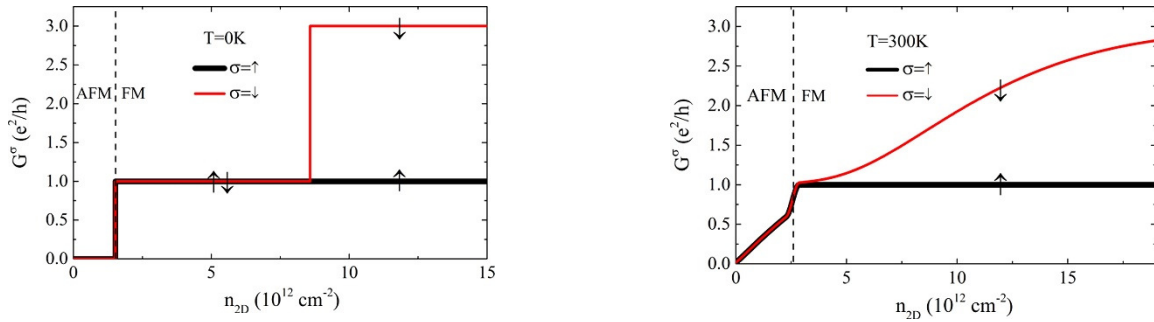


Figure 3: Spin dependent conductance (G) as a function of charge carrier density (n_{2D}) for a 4.2 nm wide ZGNR at (a): $T=0\text{K}$ and (b): $T=300\text{K}$. The AF-FM transition (dashed line) dynamically closes the bandgap of the ribbon switching the transistor into a conducting state. Further increasing the carrier concentration opens additional spin down channels leading to the spin polarization of the current.

OXIDATION OF TRANSITION METAL DICHALCOGENIDE MONOLAYERS

(Lendület LP2014-14, ERC StG NanoFab2D, Graphene Flagship)

J. Pető, P Vancsó, G. Z. Magda, L. Tapasztó

The chemical modification of 2D crystals holds the potential of engineering their physical and chemical properties. While graphene oxide is a widely investigated material, much less is known about the oxidation of various transition metal dichalcogenide (TMDC) single layers. This process is of particular importance, as, in contrast to graphene, oxidation of 2D TMDC crystals can spontaneously occur under ambient conditions. Nevertheless, the underlying atomic mechanisms of oxidation process, as well as the atomic-scale structural modifications induced by the oxidation remained so far largely unexplored. Here, we were able to image directly the ambient oxidation process of 2D MoS₂ crystals by Scanning Tunneling Microscopy (STM).

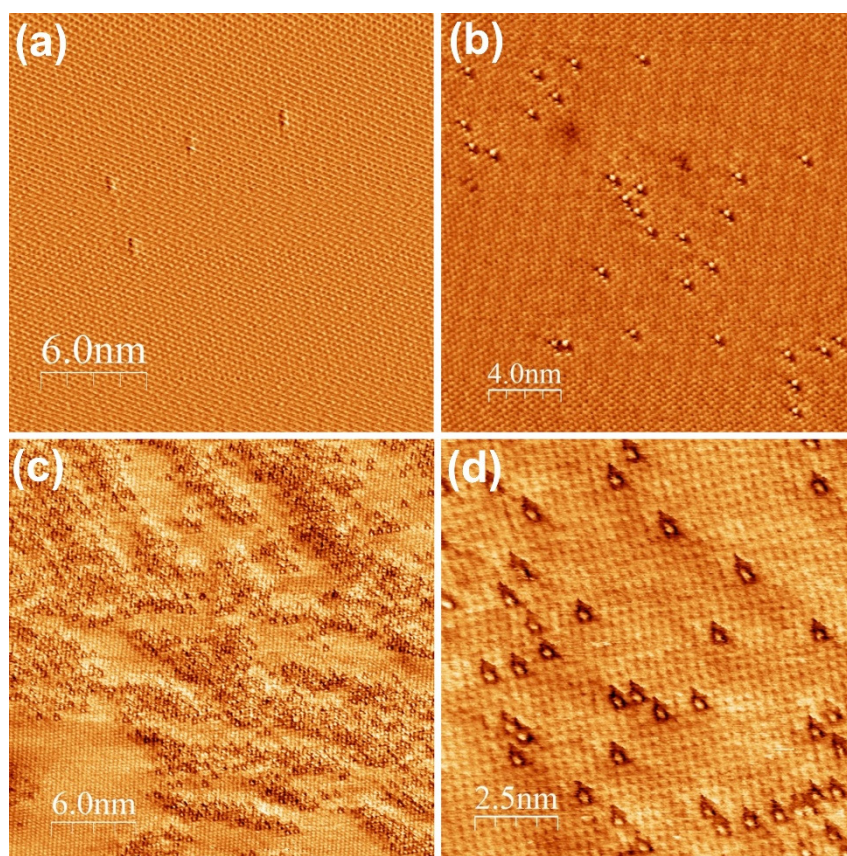


Figure 1: Atomic resolution STM images of the oxidation process of MoS₂ single layers exposed to ambient conditions. (a): as-prepared, (b): for 1 month and (c): for 1 year. (d): Higher resolution image revealing the substitution of S atoms by oxygen atoms.

In contrast to graphene, where the oxidation induces a massive amount of structural disorder, we found that the oxidation of 2D MoS₂ proceeds through individual atomic substitutions all over the 2D MoS₂ surface, while fully preserving the crystal lattice. Furthermore, such oxidized MoS₂ single layers can be easily reduced to a perfect MoS₂ lattice by a simple annealing step in H₂S. Such atomically ordered and reversible defect formation mechanism can be exploited in the defect engineering of various physical and chemical properties of 2D MoS₂.

By contrast, a strikingly different oxidation behaviour has been identified in MoSe₂ single layers, where, under ambient conditions, the surface remains structurally intact even after a year exposure to ambient, while the oxidation proceeds only at the edges.

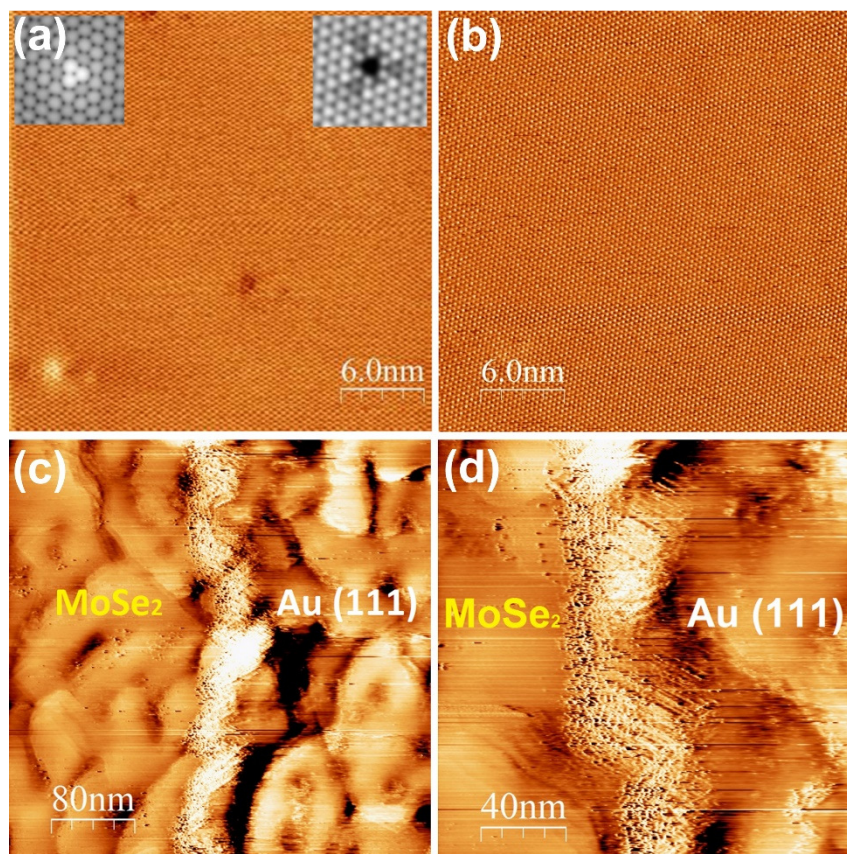


Figure 2: Atomic resolution STM images of MoSe₂ single layers exposed to ambient conditions for 1 year show no sign of oxidation on the surface (a-b). By contrast, STM images of MoSe₂ edges clearly reveal edge oxidation effects (c-d).

Monitoring the oxidation processes of TMDC single layers at the atomic scale, on one hand enables us to identify materials with increased chemical stability under ambient conditions, on the other hand, it opens the way towards understanding and exploiting the role of defects in various properties of 2D crystals, such as electrical transport, photoluminescence or catalysis.

DETERMINATION OF THE STM TIP-GRAPHENE REPULSIVE FORCES BY COMPARATIVE STM AND AFM MEASUREMENTS ON SUSPENDED GRAPHENE

(EU FP7 Marie Curie CIG No.334377, János Bolyai Research Scholarship, OTKA K101599, NKFIH TÉT_12_SK-1-2013-0018)

A. Pálinkás, Gy. Molnár, C. Hwang (KRISS, Korea), L. P. Biró, Z. Osváth

Graphene grown by chemical vapour deposition was transferred on top of flat gold nanoislands and characterized by scanning tunneling microscopy (STM) and atomic force microscopy (AFM). Graphene bubbles were formed with lateral dimensions determined by the size and shape of nanoislands. These graphene bubbles could be squeezed during STM imaging using bias voltages of less than 250 mV and tunneling currents of 1 nA (see Fig. 1). Nanoindentation measurements performed by AFM show that the squeezing of graphene bubbles occurs at repulsive forces of 20 - 35 nN. Comparing the AFM and STM results, this study reveals that mechanical forces of the order of 10^{-8} N occur between the STM tip and graphene under ambient imaging conditions and typical tunneling parameters.

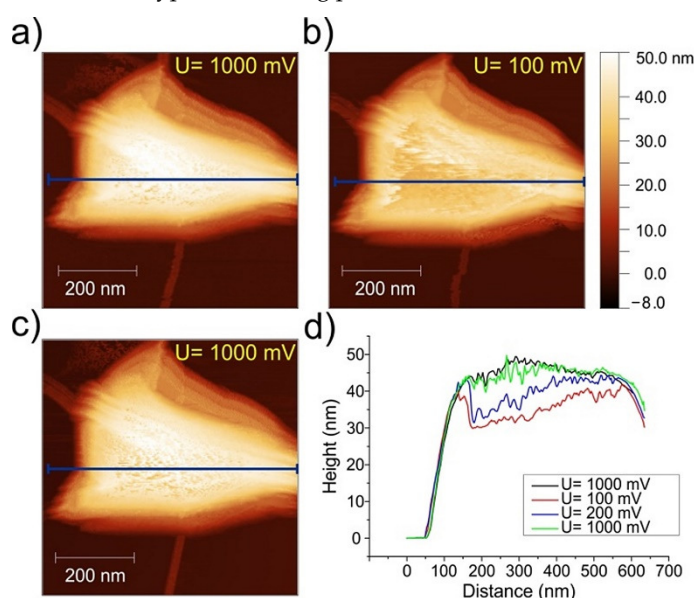


Figure 1: Series of STM images of a graphene nanobubble measured at bias voltages of (a): $U = 1000$ mV, (b): $U = 100$ mV, and (c): $U = 1000$ mV. Tunneling current: $I = 1$ nA. (d): Height profiles taken at different bias voltages along the same line section shown with horizontal line in (a-c).

The graphene bubble shown in Fig. 1, formed on the top of a gold nanoisland, is imaged first at $U = 1000$ mV (Fig. 1(a)). The height profile measured along the line section in Fig. 1(a) is shown in Fig. 1(d) (black line). Decreasing the bias voltage to $U = 100$ mV we observed that the graphene was pushed against the top of the gold nanoisland (Fig. 1(b)), as shown also by the corresponding height profile in Fig. 1(d) (red line). Somewhat higher graphene z-values were obtained for the same height profile as the bias voltage was increased to $U = 200$ mV (Fig. 1(d), blue line). Furthermore, when the bias voltage was increased again to $U = 1000$ mV, the graphene bubble recovers to the initial shape (Fig. 1(d), green line). The current was kept constant throughout the measurements ($I = 1$ nA). The results show that by decreasing the bias voltage the repulsive force regime starts to dominate the tip-graphene interaction, and the graphene bubble can be squeezed.

In order to evaluate the mechanical forces acting between STM tip and graphene, AFM measurements were performed in PeakForce® mode on similar graphene nanobubbles. The AFM image of a flat gold nanoisland with graphene bubble on top is shown in Fig. 2(a). This AFM image was obtained by scanning with a very low ($F = 1.5$ nN) force.

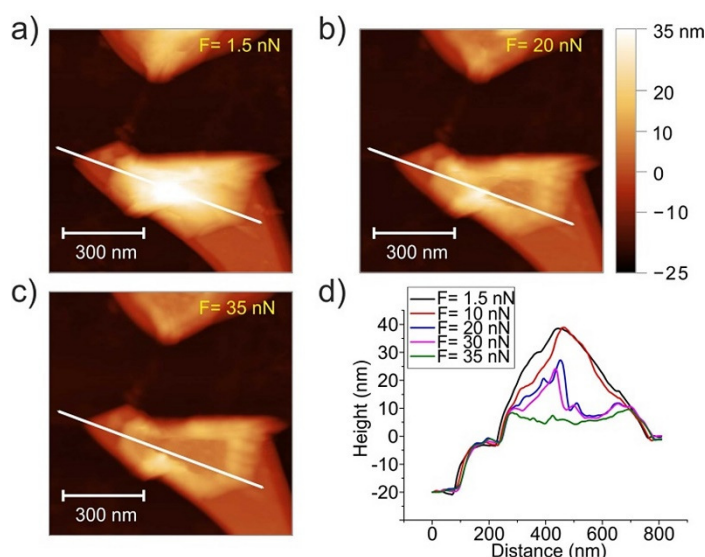


Figure 2: PeakForce AFM images of a graphene nanobubble measured with compressive forces of (a): $F = 1.5$ nN, (b): $F = 20$ nN, and (c): $F = 35$ nN. (d): Height profiles taken at different forces along the same line section shown in (a-c) (white line).

The height profile measured along the line section in Fig. 2(a) (white line) shows that the height of the graphene bubble is about two times the height of the gold nanoisland (Fig. 2(d), black solid line). AFM images were registered on the same area using forces up to 40 nN. A complete image was recorded for every force setpoint (F). It was observed that by increasing the scanning force the graphene bubble starts to collapse. This is shown in Fig. 2(b) and Fig. 2(c), which are topographic images measured with forces of 20 nN and 35 nN, respectively. Obviously, the shape of the graphene bubble is altered. Selected height profiles are shown in Fig. 2(d), which were taken along the same line section shown in Fig 2(a) (white line), extracted from the AFM images measured with the corresponding tip-sample force values. The bubble is considered 'squeezed' at $F = 35$ nN (Fig. 2(d), green line).

ELECTROMAGNETIC AND THERMAL PROPERTIES OF THREE-DIMENSIONAL PRINTED MULTILAYERED NANO-CARBON/POLY(LACTIC) ACID STRUCTURES

(OTKA K101599, Graphene Flagship)

A. Paddubskaya (Minsk), N. Valynets (Minsk), P. Kuzhir (Minsk), K. Batrakov (Minsk), S. Maksimenko (Minsk), R. Kotsilkova (Sofia), H. Velichkova (Sofia), I. Petrova (Sofia), I. Biró (3D Wishes), K. Kertész, G. I. Márk, Z. E. Horváth, L. P. Biró

Microwave is the ultimate range for open space communication. However, the drastic growth of the satellite data transmission in the past decade makes spectral bands allocated to different communication channels overcrowded. Along with the ever-increasing density of emitters in the environment, this jam makes the electromagnetic (EM) compatibility an important issue. In other words, any new equipment must have adequate immunity in order to function consistently and reliably, be resilient to major disturbances, and coexist with other equipment. The electromagnetic interference (EMI) shielding effectiveness (SE) is determined by material absorptivity, surface reflectivity, and multiple internal reflections. For a continuous metal sheet, the latter mechanism is negligible, not to mention the weight of metals, which may be prohibitive for space applications.

The EMI SE of a composite material mainly depends on the filler's intrinsic conductivity, dielectric constant, and aspect ratio. Nano-carbon fillers, such as graphene nanoplatelets and carbon nanotubes, are indeed interesting materials from the point of view of electromagnetic shielding. Though graphene/polymer heterostructures have several advantages in comparison with conventional metal shielding layers, such as its light weight, resistance to corrosion, and flexible absorption mechanism of shielding, their fabrication process is quite difficult because of the graphene transfer stage.

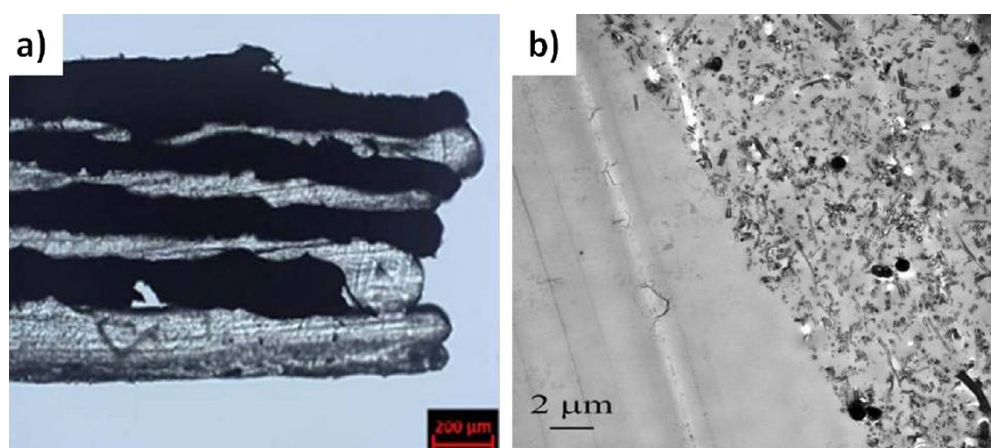


Figure 1 (a): Optical image of the cross section of 3D printed multilayered sample with 4 nano-carbon layers (black stabs), and (b): X-TEM image of the PLA/nano-carbon doped interface

In this study, our goal was to design a new type of light material having tunable electromagnetic absorption properties, by 3D printing of photonic type band gap structures by layer by layer deposition of nano-carbon doped polymer layers and pure (dielectric) polymer layers, Fig. 1. The source material for the nano-carbon layer is a commercial nanocomposite filament, named 3D Black Magic (3DBM), consisting of a nano-carbon filler incorporated in a polylactic acid (PLA) polymer, while the pure polymer layer is printed from a pure PLA filament.

The results demonstrate, Fig. 2, the potential of the 3D printing technique for producing multilayered structures by layer by layer deposition. The sandwich structure composed of continuous nano-carbon doped polymer layers and pristine polymer layers, the mixed nano-carbon filler consisting of graphene, short carbon nanotubes, and graphene sheet-like structures obviously determines both the microwave and the thermal properties of the complex material.

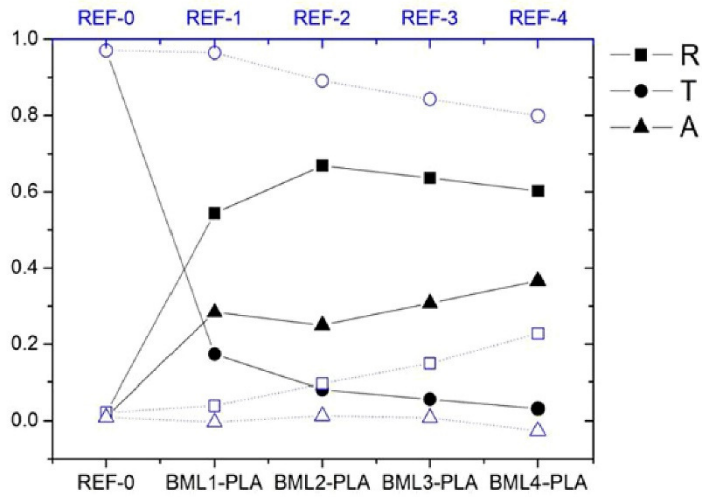


Figure 2: Reflectance, absorbance, and transmittance reconstructed from the experimental data of reference samples (open symbols) and samples contacting 1–4 nano-carbon layers (solid symbols) at 30 GHz

The electromagnetic measurements promise a great potential of such a type of materials for electromagnetic compatibility applications in microwave frequency range. Sandwich structures containing only two nano-carbon layers already become untransparent to microwaves, giving EMI SE at the level of 8–15 dB, and the contribution of absorption of the plane stratified sandwich structure is quite significant (30%–40%). In case of upgrading the structure with proper anti-reflection geometry – inspired from our work on biological photonic nanoarchitectures – we may obtain the same zero transmission originated from the full absorption of EM radiation.

PRETREATED BUTTERFLY WINGS FOR TUNING OF SELECTIVE VAPOR SENSING

(OTKA K 111741, OTKA K 115724)

G. Piszter, K. Kertész, Zs. Bálint, L. P. Biró

Photonic nanoarchitectures occurring in the scales of the blue butterflies are responsible for their vivid blue wing coloration. These nanoarchitectures contain quasi-ordered nanocomposites which are constituted from a chitin matrix with embedded air holes. Therefore, they can act as chemically selective sensors due to their colour change when mixing volatile vapours in the surrounding atmosphere, which condensate into the nanostructure through capillary condensation. The condensed vapours can alter the refractive index contrast in the nanoarchitecture which results in the colour change of the wings.

Using a home-built vapour mixing setup the spectral changes caused by the different air + vapour mixtures were efficiently characterized. It was found recently that the spectral shift is vapour specific and proportional with the vapour concentration.

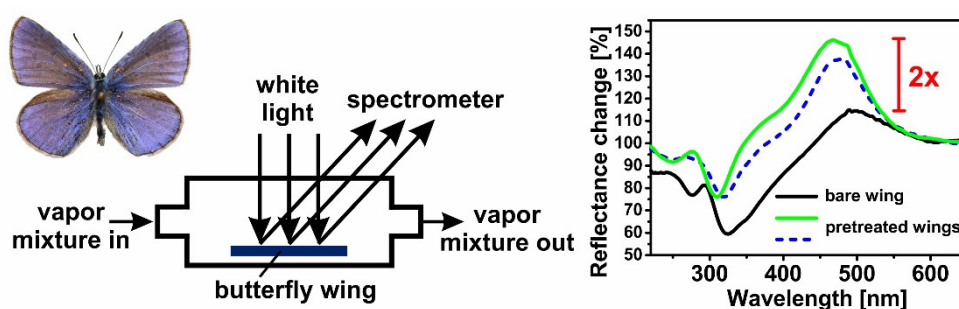


Figure 1: The wings of *Polyommatus icarus* males are suitable for optical vapour sensing. The image shows a blue male specimen, the schematics of the vapour sensing cell, and the typical optical response of the bare and pretreated butterfly wings during vapour exposition. In the latter case the optical reference (100%) was the pristine butterfly wing in artificial air atmosphere. The two coloured curves show the optical response of two ethanol pretreated wings.

Both the chemical selectivity and the sensitivity could be improved if arrays of sensitized butterfly wings would be used. Therefore, *P. icarus* butterfly wings were pretreated in liquid ethanol for 14 days to modify the surface of the photonic nanoarchitecture. After the complete drying, the standard vapour sensing measurements, using seven volatiles, were carried out to investigate differences in chemical selectivity and sensitivity of the modified wings.

Optical response of ethanol pretreated samples can be seen in Fig. 1. During the vapour exposition the optical response (colour change) of the wing can be measured using the initial colour (wing in artificial air) as a reference. One can see in Fig. 1 that the maximal intensity of the optical response curves is more than doubled when butterfly wings were pretreated in liquid ethanol for two weeks as compared to bare wings. This enhanced vapour sensing is reproducible, too: two wings of the same specimen were pretreated under the same conditions and after the measurements the significant spectral enhancement of both wings was observed.

The chemical selectivity of the bare and ethanol pretreated samples was analysed using principal component analysis (PCA). In Fig. 2 the PCA results of the bare (A) and ethanol pretreated (B) samples can be seen. Both samples show similar chemical selective behaviour as every vapour has individual trajectory in the graphs. The PCA score plot of the untreated and ethanol pretreated wings are compared in the low concentration range (C), too, where spread of the vapour sensing trajectories was significantly larger in case of the ethanol pretreated sample, showing the higher chemical selectivity in that concentration range.

These results show the way how to tune the chemically selective optical response of the photonic nanoarchitectures by modification of their surface.

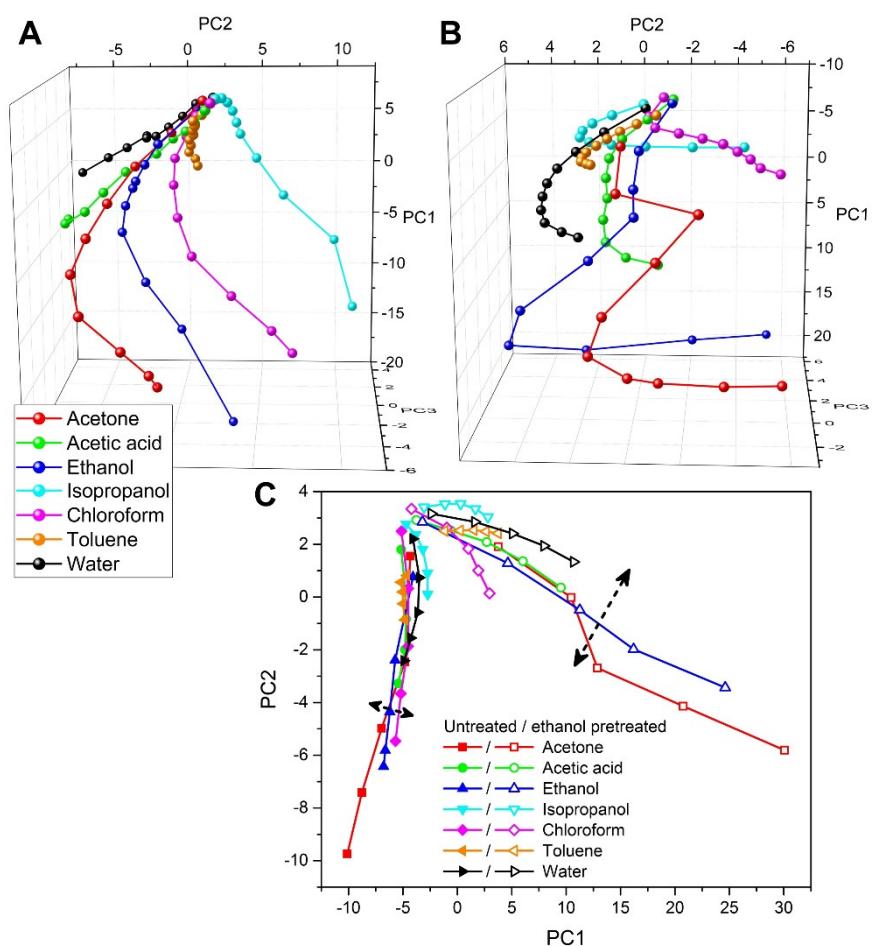


Figure 2: PCA score plots of (A): the untreated and (B): the 14 day ethanol pretreated *Polyommatus icarus* wings when used as a sensor material. The vapour concentration increases from the top to the bottom (to saturated vapours) in both graphs. (C): The low-concentration (<50%) behaviour was investigated in more detail using PCA, too.

SIMULATION OF MAGNETIC FLUX DISTRIBUTION DURING MEASUREMENT OF LOCAL THINNING OF FERROMAGNETIC PLATES

(OTKA K 111662)

G. Vértesy, Cs. S. Daróczy, A. Gasparics

For pipes used in industry, e.g. in chemical and power plants, wall thinning is one of the most serious defects. The detection and the evaluation of the thickness reduction of pipes are very important issues for the prediction of lifetime of the pipes in order to avoid severe accidents. There is a special concern on the local wall thinning at locations under an enforcement shield that covers outside of the pipe, where a branch pipe is connected to the main one. Because the enforcement shield and the pipe wall form two layers of metal, it is difficult to inspect inside of the pipe under the enforcement shield by currently used commercial methods. A recently developed nondestructive method called Magnetic Adaptive Testing (MAT), which is based on systematic measurement of minor magnetic hysteresis loops, was applied for detection of local wall thinning in ferromagnetic plates. It was shown that even a relatively small, local modification of the sample thickness could be detected with adequate signal/noise ratio from the other side of the specimen. The measurements gave sufficient results also, if the investigated plate was covered by other plate(s) [NDT&E International, 47 (2012) pp.51-55.], [E-Journal of Advanced Maintenance, Vol. 4, No. 2. (2012) pp.96-104].

The efficiency of MAT measurement can be improved by the proper choice of the measurement conditions. In cooperation with the co-workers of Budapest University of Technology and Economics (Department of Broadband Infocommunications and Electromagnetic Theory), the magnetic flux distribution was simulated. A system of three ferromagnetic plates was used for simulation, the bottom plates having an artificial slot in the bottom (One quarter of the system is illustrated in Fig. 1, if the magnetizing yoke is over the centre of the slot). Magnetization of the plates was performed by an attached magnetized yoke on the top of plates. The change of the magnetic flux was calculated in the cross section (blue area) of the magnetizing yoke, as indicated in Fig. 1.

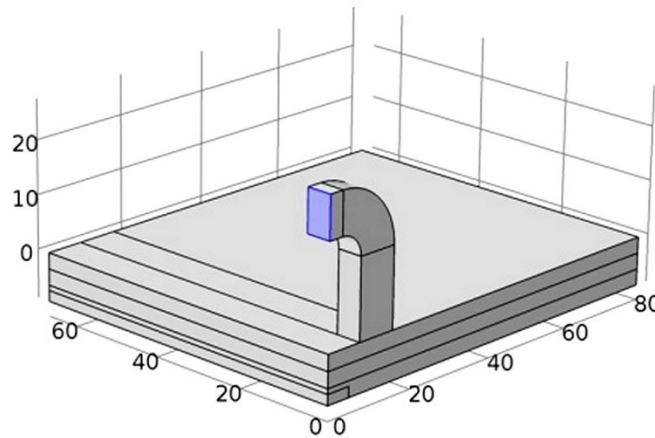


Figure 1: The magnetizing yoke over the system of three iron plates (with 180x170x3 mm dimensions), the bottom has the artificial slot (with 170x10x2 mm dimensions).

The magnetic flux was calculated according to the $\Psi = \int_A B * da$ expression, where "A" is the surface, indicated by blue colour in Fig. 1. The influence of air gap was also taken into account, between the yoke and the surface, and also between the plates.

As an illustration, it is shown in Fig. 2, how the magnetic flux changes due to the presence of a 2 mm deep, 10 mm wide slot in the bottom layer if the distance between the yoke legs (size of the yoke) and air gap is modified.

Similar calculations were carried out also for 5 and 15 mm wide slots. Fig. 3 shows the result of a calculation, where the influence of the slots on the magnetic flux is directly calculated. (In this case 50 μm air gap was supposed.) The influence of the size of the magnetizing yoke on the flux change is clearly seen. It is worth of mentioning as well, that the position of the maximal flux change depends on the size of magnetizing yoke, too. It turned out also (not shown here), that if air gap is increased, the position of the maximal flux change is significantly shifted towards larger size magnetizing yoke.

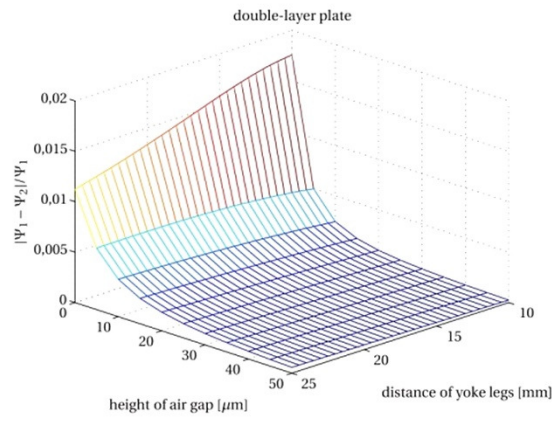


Figure 2: The modification of the magnetic flux due to the slot in the case of double layer configuration at the cross section of the magnetizing coil, positioned over the slot as a function of air gaps and as a function of the distance between yoke legs.

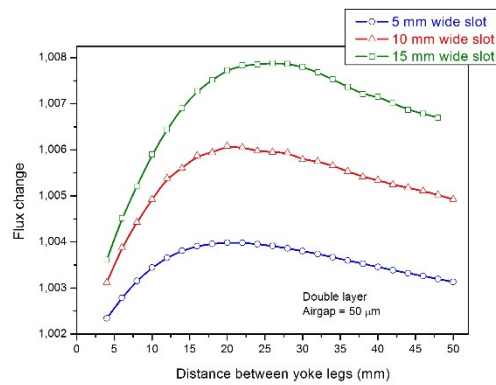


Figure 3: The modification of the magnetic flux due to the slot in the case of double layer configuration at the cross section of the magnetizing coil, positioned over the slot as a function of air gaps and as a function of the distance between yoke legs.

The above presented results help to optimize the parameters of the actual experimental arrangement for solving a given task.

SPECTROELLIPSOMETRIC DETECTION OF SILICON SUBSTRATE DAMAGE CAUSED BY RADIOFREQUENCY SPUTTERING OF NIOBIUM OXIDE

(OTKA K115852, M-ERA.NET “Watersafe”)

T. Lohner, M. Serényi, E. Szilágyi, Zs. Zolnai, Zs. Czigány, N. Q. Khánh, P. Petrik, M. Fried

Substrate surface damage induced by deposition of metal atoms by radiofrequency (rf) sputtering or ion beam sputtering onto single-crystalline silicon (c-Si) surface has been characterized earlier by electrical measurements. The question arises whether it is possible to characterize surface damage using spectroscopic ellipsometry (SE). In our experiments niobium oxide layers were deposited by rf sputtering on c-Si substrates in gas mixture of oxygen and argon. Multiple angle of incidence spectroscopic ellipsometry measurements were performed, multilayer optical models (niobium oxide layer, native silicon oxide layer and ion implantation-amorphized silicon (i-a-Si) layer) on a c-Si substrate were created in order to evaluate the spectra. The evaluations (fitting the layer thicknesses) yielded thicknesses of several nm for the i-a-Si layer. Better agreement could be achieved between the measured and the generated spectra by inserting a mixed layer with components of c-Si and i-a-Si applying the effective medium approximation (EMA, fitting the layer thicknesses and compositions) between the silicon oxide layer and the c-Si substrate.

In cooperation with Wigner Research Centre for Physics high depth resolution Rutherford backscattering (RBS) measurements were performed to investigate the interface disorder between the deposited niobium oxide layer and the c-Si substrate. High resolution cross-sectional transmission electron microscopy (HRTEM) investigation was applied to visualize the details of the damaged subsurface region of the substrate (see Fig. 1).

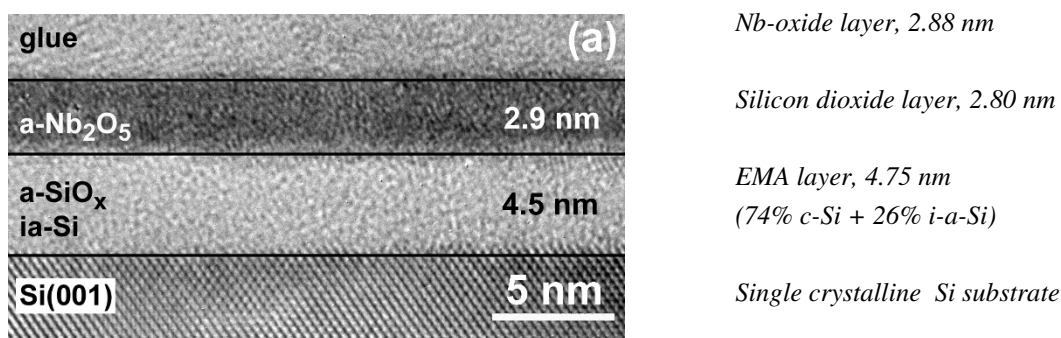


Figure 1 (a): Cross sectional HRTEM image of a Nb-oxide sample rf deposited for 100 s (2.0 kV wall potential). The thicknesses of the amorphous layers are indicated in the image. On the right: The three-layer optical model constructed on basis of the results of the RBS and HRTEM measurement for the evaluation of the measured spectroellipsometric data. The values are from the SE evaluations.

Sputtering at higher wall potential results in higher thickness of the mixed layer with i-a-Si and c-Si components in the damaged subsurface region. During the rf sputtering the energetic oxygen and argon ions and neutral atoms may penetrate into the c-Si substrate to a depth of several nm causing displacement of host silicon atoms and consequently producing damaged regions.

MAKYOH TOPOGRAPHY

F. Riesz

Within the project KMR_12-1-2012-0226, in collaboration with Mirrotron Ltd and the Wigner Research Centre for Physics, the surface flatness of large-area (57 mm × 175 mm) polished Ni(P)-coated Al blocks were characterized for next-generation neutron guide applications. Using highly overlapping sub-aperture measurements with sample translation, it was concluded that the overall flatness of the samples is smaller than the measurement error, that is, it is below 0.5 μm (discounting some edge effects). The error margin was also confirmed by elementary calculations. In addition, a featureless and smooth surface morphology was confirmed. Fig. 1 shows the purpose-built sample positioning/translation stage.

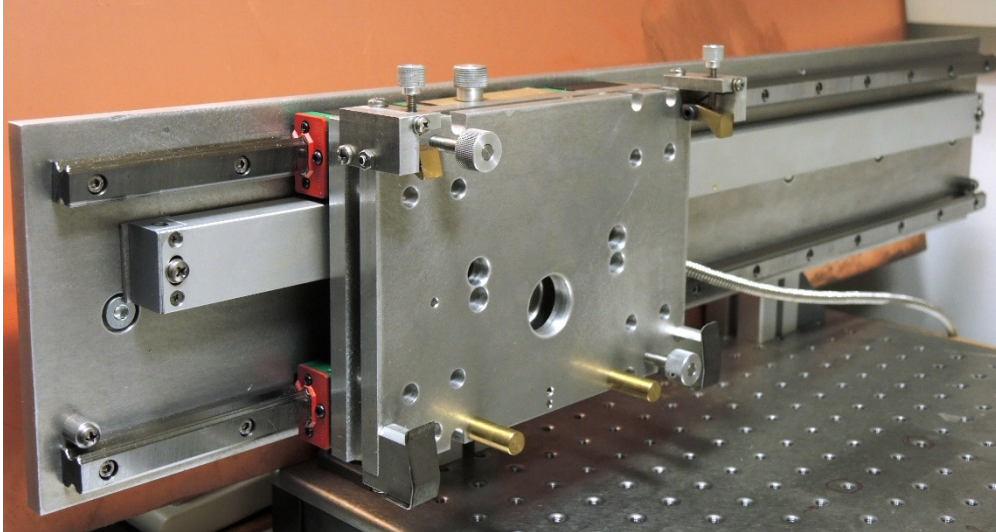


Figure 1: Sample positioning stage for flatness characterisation of large-areas samples

The surface shape and morphology of hot-wall VPE SiC/Si heterostructures grown at IMEM-CNR, Parma, have been characterized with Makyoh topography in order to study the effects of the addition of methyl trichloro silane. Low amount of sample bow was obtained in an optimized growth process.

GRATING COUPLED OPTICAL WAVEGUIDE INTERFEROMETRY COMBINED WITH IN SITU SPECTROSCOPIC ELLIPSOMETRY

(OTKA K115852, H2020-SMEINST-2-2014-683541, M-ERA.NET "Watersafe", FP7 ENIAC "E450EDL", "SEA4KET")

E. Agócs, P. Kozma, J. Nádor, A. Hámori, M. Janosov, B. Kalas, S. Kurunczi, B. Fodor, E. Ehrentreich-Förster, M. Fried, R. Horváth, P. Petrik

Two surface-sensitive label-free optical methods, grating coupled interferometry (GCI) and spectroscopic ellipsometry (SE) were integrated into a single instrument. The new tool combines the high sensitivity of GCI with the spectroscopic capabilities of SE. This approach allows quantification with complex optical models supported by SE and accurate measurements with the evanescent field of GCI. A flow cell was developed to perform combined and simultaneous investigations on the same sensor area in liquid (or gas) environments. The capabilities of the instrument were demonstrated in simple refractometry and protein adsorption experiments.

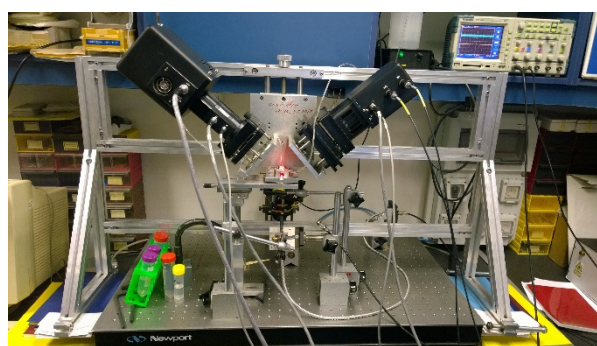
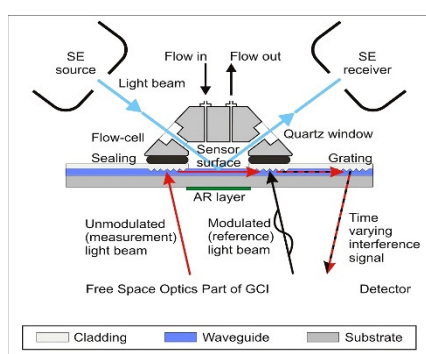


Figure 1: Schematic representation of the configuration and the working principle of the combined GCI-SE setup

In the first experiment, Milli-Q water and glycerol solutions were applied in order to demonstrate the simultaneous measurement capabilities and to check the limit of refractive index detection of the two system components. The uncertainty of the refractive index determination was 9×10^{-7} and 4.8×10^{-5} for GCI and SE, respectively (Fig. 2 left).

In the second experiment, fibrinogen surface adsorption was monitored by means of the combined sensor tool in order to demonstrate its capabilities in biological experiments, as well. The phase shift measured by GCI informed us about the changing of the sensing area with high sensitivity. Exploiting the capabilities of SE for a more complex evaluation, the surface mass density of the fibrinogen layer was determined by analysing the ellipsometric spectra, and it was found to be approximately 0.4 ng/mm^2 at the end of the adsorption process (Fig. 2 right).

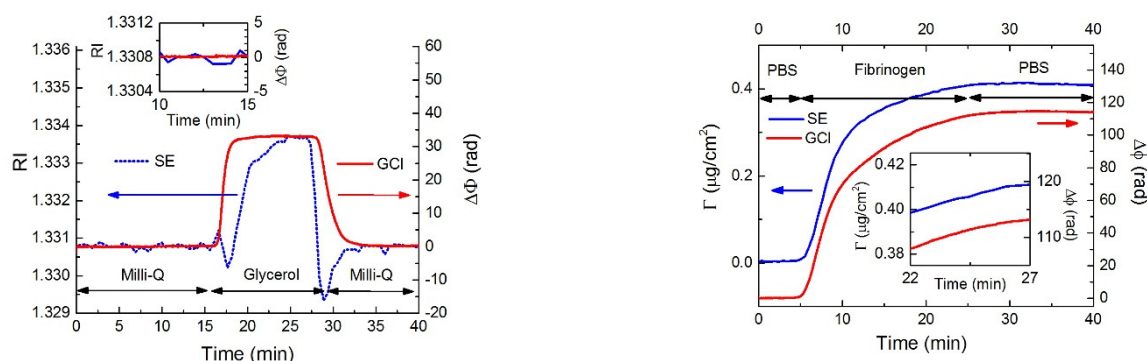


Figure 2: Simultaneous GCI and SE refractometric measurements for the estimation of LOD values of the combined configuration (left) and for the investigation of the fibrinogen surface adsorption (right)

PERFORMANCE ANALYSIS OF PLASMON-ENHANCED ELLIPSOMETRY FOR PROTEIN ADSORPTION MEASUREMENTS

(OTKA K115852 and M-ERA.NET "WaterSafe", TÉT_12_DE-1-2013-0002)

B. Kalas, J. Nádor, E. Agócs, A. Saftics, S. Kurunczi, R. Horváth, M. Fried, P. Petrik

We studied gold nanolayers with six different thicknesses (5, 10, 20, 30, 40 and 50 nm), and the adsorption of protein nanolayers on these gold surfaces by *in situ* ellipsometry. The gold nanolayers were evaporated onto BK7 glass substrates with a 2-nm CrO₂ interface layer to enhance the adhesion of the gold to the glass.

We acquired the optical properties of the structures by a Woollam M-2000DI rotating compensator ellipsometer. During the *in situ* investigation we used a laboratory-built semi-cylindrical Kretschmann-Raether flow cell. By measuring the interface through the substrate we were able to exploit the surface plasmon resonance (SPR) phenomenon in order to increase the sensitivity (40 pg/mm²) of the measurement.

This instrument has numerous advantages compared to our former constructions (using standard flow cell arrangement). For example, the signal to noise ratio is better and the probability of the appearance of a bubble in the flow cell is much lower. This makes the measurement faster and more stable. We used fibrinogen as a model protein to study the adsorption to the various gold surfaces.

In contrast to traditional SPR-devices the ellipsometer provides phase information of the reflected light, so we acquired more information that enabled us to increase the sensitivity by two orders of magnitude compared to the case of having only amplitude information. The other advantage was that we could choose the SPR-angle very precisely (within 0.1 degree) and we used a broad wavelength range from 400 nm to 1690 nm. Using a spectroscopic ellipsometer gave us the opportunity to build a complex optical model and use it to determine optical properties and thicknesses of multi-layer structures simultaneously and quantitatively (Fig. 1). (The results are accepted for publication in the journal of Applied Surface Science.)

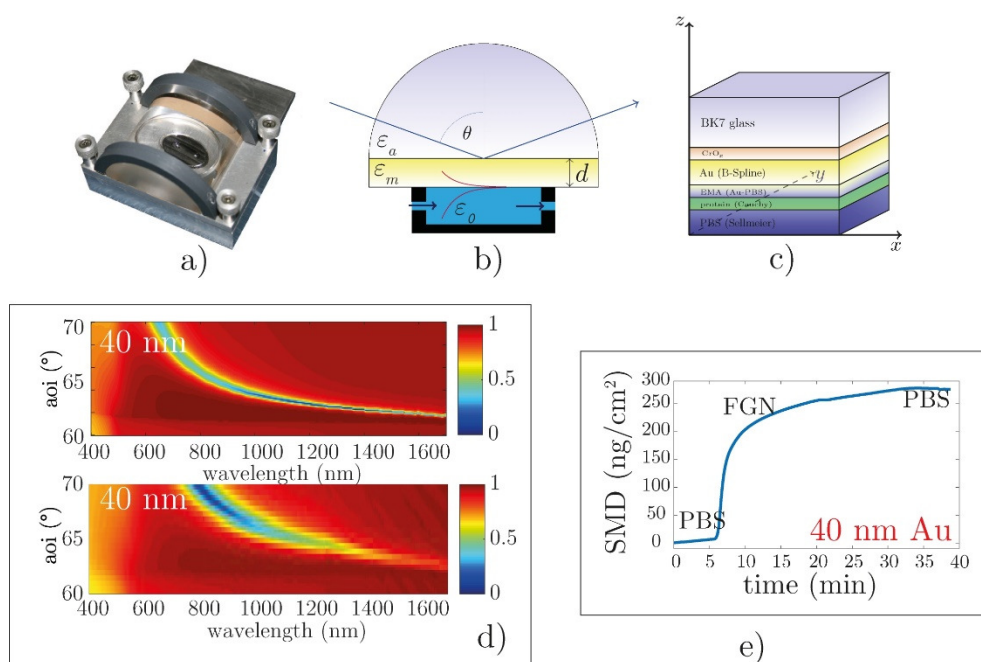


Figure 1: a): Photo of the SPR flow cell designed in the Photonics Laboratory, b): schematic figure of the flow cell, c): structure modelled to investigate the adsorption process, d): the modelled (top) and the measured (bottom) $\tan(\psi)$ maps and e): surface mass density of the adsorbed protein as a function of time.

OPTICAL CHARACTERIZATION OF COLUMNAR POROUS Si THIN FILMS AND Si NANOWIRES EXHIBITING LARGE STRUCTURAL ANISOTROPIES

(OTKA K115852, H2020-SMEINST-2-2014-683541, FP7 E450EDL, SEA4KET, TÉT_14_FR-1-2015-0041, CampusFrance Balaton PHC)

B. Fodor; T. Defforge; E. Agócs; M. Fried; G. Gautier; P. Petrik

In a continuing cooperation with the GREMAN laboratory of the University of Tours, we characterized columnar mesoporous Si thin films (PSi) and dense nanowire (SiNW) carpets by spectroscopic ellipsometry in the visible-near-infrared wavelength range. Porous Si layers were formed by electrochemical etching while structural anisotropy was controlled by the applied current. Layers of highly oriented SiNWs, with length up to 4.1 μm were synthesized by metal-assisted chemical etching. Ellipsometric spectra were fitted with different multi-layered models, based on effective medium approximation (EMA). Isotropic, in-depth graded, anisotropic and hybrid EMA models were investigated with the help of the root mean square errors obtained from the fits. In the case of PSi, characterization revealed that, at low current densities ($< 100 \text{ mA/cm}^2$), in-depth inhomogeneity shows a more important feature in the ellipsometric spectra than anisotropy. On the other hand, at high current densities ($> 100 \text{ mA/cm}^2$) this behavior turns around, and anisotropy becomes the dominant feature of the spectra. SiNW evaluations revealed that the layers are also highly anisotropic, but derived prolate spheroid aspect ratios showed that the best ordered orientation is obtained in samples formed of $\approx 1 \mu\text{m}$ nanowires. For the thicker layers, the long nanowires start to collapse into bundled states, decreasing the anisotropy.

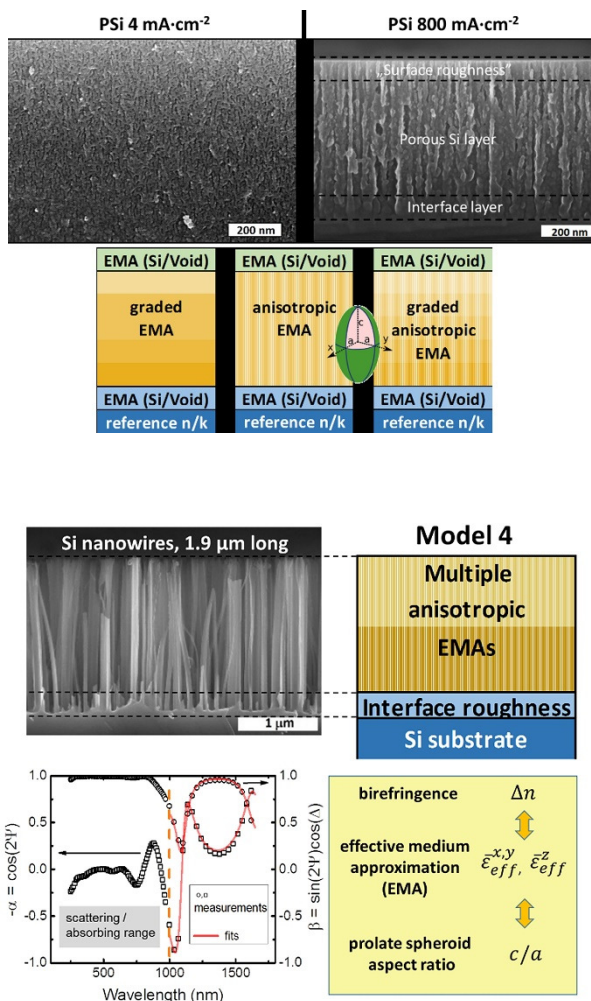


Figure 1: Cross-sectional SEM images (top left) of a porous Si sample prepared by small current density showing a dendritic structure and of a sample prepared by large current density revealing a highly columnar structure (top right) and the three EMA-based model-structures (bottom) tested for all the PSi layers. The optical response of the dendritic structures shows an isotropic while the columnar structures show an anisotropic behaviour.

Figure 2: Cross-sectional SEM image of one of the SiNWs (top left). EMA based model-structure (top right). Corresponding α and β measured and fitted ellipso-metric values at an AOI of 65° (bottom left). With the help of the anisotropic EMA models (Model 2, 3 and 4), we can fit the birefringence and the dichroism of the anisotropic structures and also derive an average ellipticity for either the pores of the PSi or for the NWs.

OPTICAL PROPERTIES OF ZR AND ZRO₂

(OTKA K115852, MTA EK Grant, M-ERA.NET “Watersafe”)

P. Petrik; A. Sulyok; T. Novotny, E. Perez-Feró, B. Kalas, E. Agócs, T. Lohner, M. Menyhárd, Z. Hózer

In cooperation with the Fuel and Reactor Materials Laboratory and the Thin Films Physics Laboratory we characterized Zr tubes for nuclear fuel cladding, with special emphasis on the optical properties. We have shown that ellipsometry with focusing can routinely be used to measure thin layers and surface properties on Zr tubes with a diameter as small as 9.1 mm (see Fig. 1). Multi-sample and depth profiling models have been used to determine reference dielectric function spectra for both the Zr substrate and its oxide. Temporal behaviour of the oxide thickness has been measured for oxidation temperatures of 600 °C and 800 °C. A vertical inhomogeneity of the oxide properties has been found by the optical measurements as well as by depth-profiling X-ray photoelectron spectroscopy investigations that revealed the formation of sub-oxides at the interface region of Zr and its surface oxide.

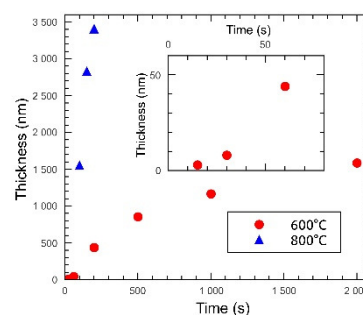
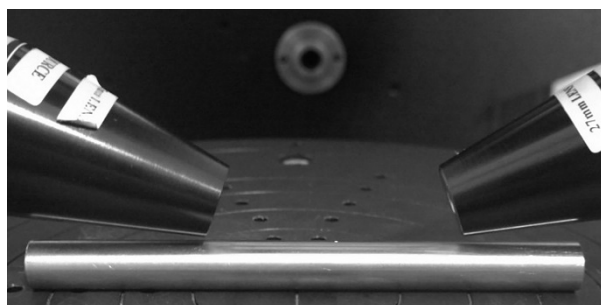


Figure 1: a): Ellipsometric measurement with focusing on a 9.1-mm diameter Zr tube for nuclear cladding. b): Thickness of oxides created at temperatures of 600 °C and 800 °C. The inset shows the behaviour at small oxidation times.

DEVELOPMENT OF OPTICAL METROLOGY TOOL FOR IN-LINE QUALIFICATION OF THIN FILMS ON LARGE AREA

(EU FP7 SEA4KET, ENIAC E450EDL)

Cs. Major, Gy. Juhász, P. Petrik, M. Fried

We are involved in 2 EU-projects („SEA4KET” and the ENIAC-2012-2 “E450DL”) to develop “Imaging Optical Inspection Device with a Pinhole Camera”. We developed 30, 45-60 and 60-90 cm wide prototypes for mapping the optical properties of thin films of big area samples.



Figure 1: We successfully installed our optical mapping device in the clean-room of IISB (Erlangen, Germany). A 300 mm diameter wafer can be seen on the robotic arm (left side).

NiSi thin film covered and Plasma Immersion Ion Implanted 300 mm diameter Si-wafers was measured on the robotic arm in clean room environment. We determined the thickness maps on these big wafers.

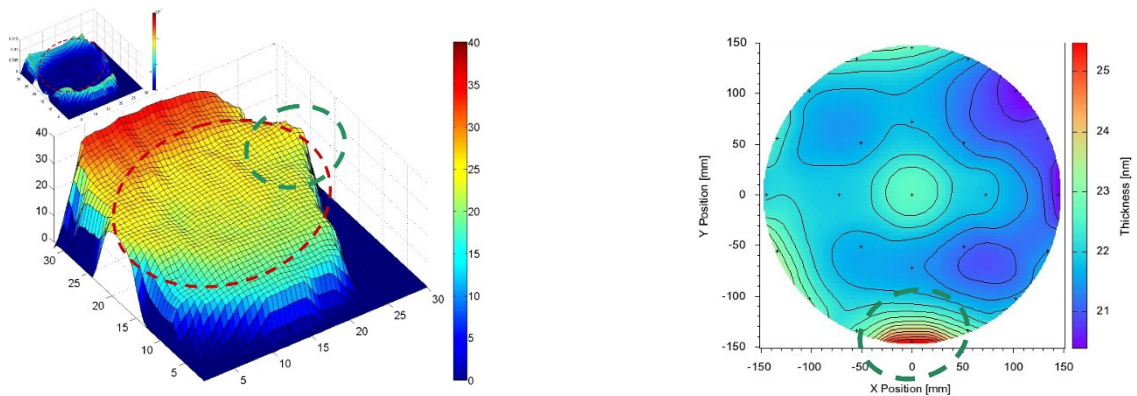


Figure 2: Thickness-map of a NiSi covered 300 mm diam. Si-wafer (complete annealing at 350 °C) and control measurement by a SEMILAB-SOPRA SE (right). The big dashed curve shows the edge of the sample (from the inserted MSE-map, upper-left), the small dashed curves show the maximum place.

AGGREGATION KINETICS AND CLUSTER STRUCTURE OF AMINO-PEG COVERED GOLD NANOPARTICLES

(OTKA K112114, PD105173 and FP7 No.310250)

D. Zámbo, Sz. Pothorszky, D. F. Brougham, A. Deák

In this study, controlled clustering kinetics is demonstrated for PEG (polyethylene glycol) grafted gold nanoparticles, in response to applied environmental stimuli; the temperature and ionic strength of the medium (Fig. 1). It is also found that the rate of assembly determines the structure of the prepared nanoparticle clusters (NPCs). After the system is brought out of equilibrium, time-dependent extinction and dynamic light scattering data are used to follow the evolution of nanoparticle cluster formation in real time. The results show that the rate of assembly increases with increasing ionic strength or temperature of the medium. As a result, the nanoparticle cluster size scales with ionic strength and temperature, over a cluster size range from a few particle sizes up to the micron-scale. It is found that, even at the lowest ionic strength, the electric double layer repulsion is eliminated; hence the observed differences in kinetics and in cluster structure arise from modulation of the repulsive steric interactions between nanoparticles.

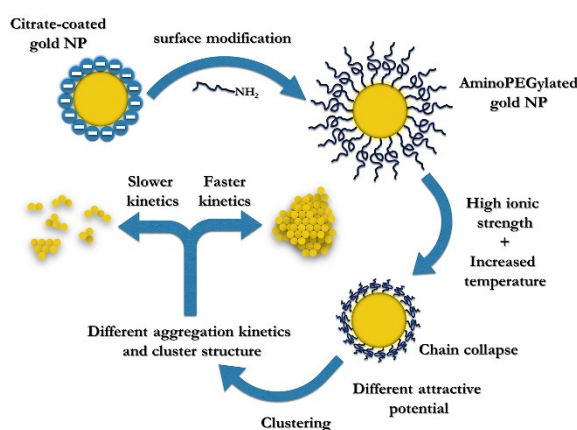


Figure 1: Schematic representation of self-assembly of aminoPEGylated gold nanoparticles into different nanoparticle structures

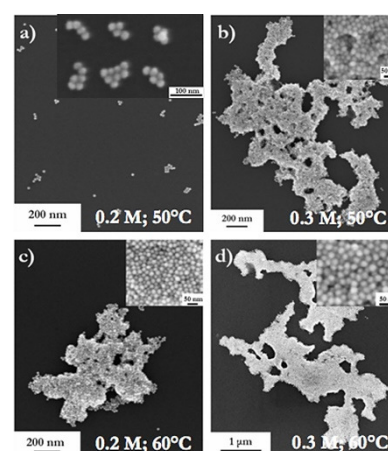


Figure 2: Structure of the gold NPCs evolved under different experimental conditions

For different sets of parameters, entirely different NPC structures evolved over time (Fig. 2), which can be attributed to the modulation of the steric repulsion arising from the PEG grafts. When the driving force for the clustering is smaller, only NPCs composed of a few particles are formed which can be effectively disassembled by providing external energy e.g. by ultrasonication. As the driving force increases, faster assembly occurs resulting in compact 3D assemblies. The approach should be extendable to suspensions of other nanoparticle types, where the nanoparticle stability is determined by surface-grafted responsive macromolecules.

SELF-ASSEMBLY OF LIKE-CHARGED NANOPARTICLES INTO VORONOI DIAGRAMS

(OTKA K104666, PD105173 and TÉT_12_JP-1-2014-0005)

D. Zámbo, K. Suzuno, Sz. Pothorszky, D. Bárdfalvy, G. Holló, H. Nakanishi, D. Wang, A. Deák, I. Lagzi

The self-assembly of nanoscopic building blocks into higher order macroscopic patterns is one possible approach for the bottom-up fabrication of complex functional systems. Macroscopic pattern formation, in general, is determined by the reaction and diffusion of ions and molecules. In some cases, macroscopic patterns emerge from diffusion, and interactions exist between nanoscopic/microscopic building blocks. In systems where the distribution of the interaction-determining species is influenced by the presence of a diffusion barrier, the evolving macroscopic patterns are determined by the spatiotemporal evolution of the building blocks. A macroscopic pattern can be generated by the spatiotemporally controlled aggregation of like-charged carboxyl-terminated gold nanoparticles in a hydrogel (Fig. 1), where clustering is induced by the screening effect of the Na^+ ions that diffuse in a hydrogel. Diffusion fronts of the Na^+ ions and the induced nanoparticle aggregation generate Voronoi diagrams, where the Voronoi cells consist of aggregated nanoparticles and their edges are aggregation-free and nanoparticle-free zones (Fig. 2). We also developed a simple aggregation-diffusion model to describe the evolution of the observed Voronoi patterns.

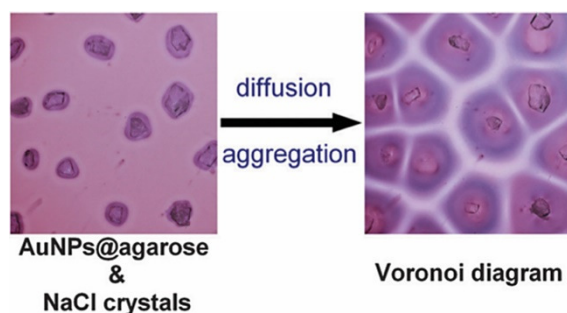


Figure 1: Representation of aggregation process triggered by the diffusion of sodium ions in a hydrogel

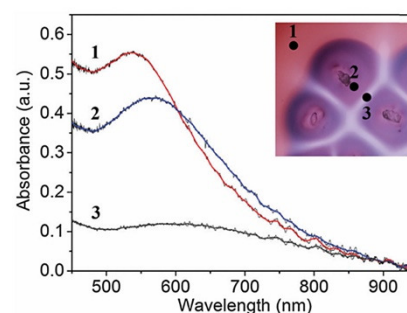


Figure 2: UV-vis spectra of different regions in the hydrogel. (1): Dispersed NPs; (2): aggregated NPs; (3): aggregation-free zones

The aggregation process of NPs was triggered by the electrostatic screening of negatively charged carboxyl protecting groups by Na^+ ions. The coupling diffusion of NPs and sodium ions and the aggregation of NPs generate Voronoi diagrams, where the Voronoi cells consist of aggregated NPs and their edges are aggregation-free and NP-free zones due to diffusion and fast aggregation processes. Our research provides an idea how to control spatiotemporally the self-assembly of nanoscopic building blocks by a diffusion front. Control of nanoscale systems by propagating reaction fronts could open up new avenues for research on nanostructured materials.

ASSEMBLING PATCHY NANORODS WITH SPHERES: LIMITATIONS IMPOSED BY COLLOIDAL INTERACTIONS

(OTKA K112114, PD105173, and FP7 No.310250)

Sz. Pothorszky, D. Zámbo, A. Deák.

In the absence of external fields, the directed assembly of nanoparticles can be realized based on colloidal or other bio-specific interactions. Rod shaped nanoparticles can benefit simultaneously from shape and surface chemistry anisotropy (patchiness), making them excellent candidates for directed assembly.

Cetyltrimethylammonium bromide (CTAB) stabilized gold nanorods offer the possibility for regio-selective surface modification since they feature a less compact ligand shell at the tip region. By careful controlling the concentration of thiol-containing molecules during a ligand exchange, selective tip-functionalisation of the rods can be achieved. The aim of the present work was to perform directed assembly of patchy nanorods and nanospheres with precision control over the resulting structure. The driving force for spatially defined assembly is provided by carefully engineered surface chemistry of the assembling species. Two binding sites are created at the tips of gold nanorods where spherical particles can bind based on electric double layer interaction. The selectivity of the process is enhanced by covering the sides of the nanorods with large molecule polymer, providing an effective steric blocking in these regions of the nanorods (Fig. 1).

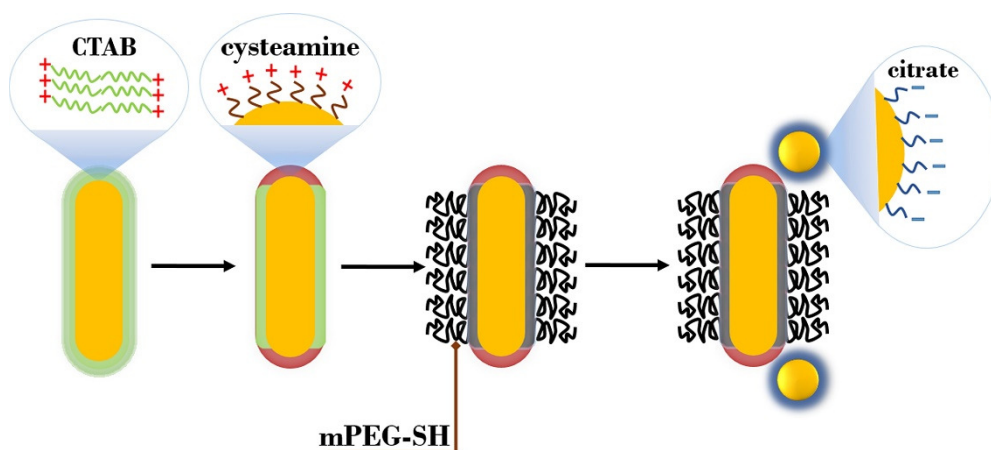


Figure 1: Schematic display of the surface modification steps and the assembled structure

First, Au NRs with tip-selective surface modification were prepared using cysteamine-hydrochloride, starting from CTAB capped NRs. The second step of the procedure was the replacement of CTAB at the side region with mPEG-SH. For the self-assembly experiments the central building block was this patchy nanorod and citrate stabilized spherical gold particles. As observed in the SEM images, the rods preferentially accumulate two spheres in their tip regions at the opposite ends of the rod (Fig. 2a). The ensemble extinction spectra measured in solution upon assembly (Fig. 2b) for the same system show a clear redshift and broadening of the longitudinal band position indicating plasmon coupling between the spherical particles and the nanorods' tip region, in agreement with structure observed in SEM.

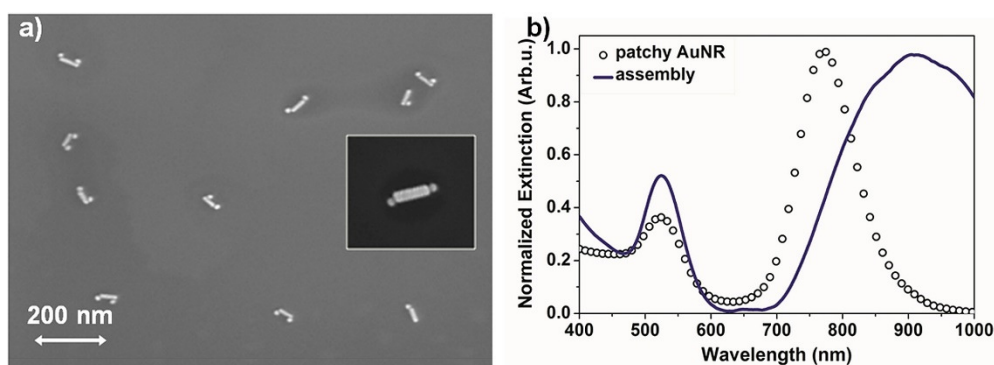


Figure 2: The SEM image of the patchy nanorods (54x15 nm) assembled with 19 nm nanospheres (a), and the corresponding extinction spectrum (b)

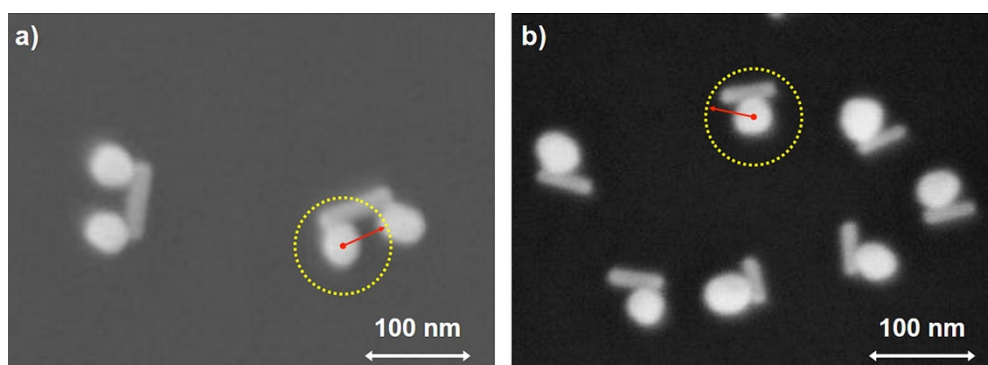


Figure 3: Assembled structures using 40 nm gold nanospheres with gold nanorods having the same aspect ratio (3.8) but different dimensions: 80x21 nm (a), and 60x16 nm (b). The red arrows and the dotted circle indicate the separation distance where the value of the net particle-particle repulsion is 5 kT.

As the relative size of the spherical particles increases, however, the two particles are shifted around the perimeter of the nanorod, finally only a single sphere gets assembled at the side of the rods (Fig. 3). The apparent cross-over of the regioselectivity can be interpreted in terms of colloidal interactions, i.e. the second spherical particle is excluded due to nanosphere-nanosphere electric double layer repulsion, while the large van der Waals attraction results in a side positioning of the single adsorbed spherical particle. The results underline the importance of absolute values of the different interaction strengths and length scales in the programmed assembly of patchy nanoscale building blocks.

A different patchy particle type can be obtained by using interfacial templating. Instead of relying on the patchy surface coverage, structural and composition inhomogeneity can be achieved by this approach. Our recent work connected to this field reports the preparation and optical properties of gold/silica “mushroom” nanoparticles, where a gold particle is only partially covered by the silica cap. The interfacial preparation method relies on partially embedding the gold particles in a polystyrene layer that masks the immersed part of the gold particle during silica shell growth from an aqueous solution. By adjusting sacrificial polystyrene film thickness and silica growth time, precise control over the coverage and cap thickness can be achieved (Figs. 4a,b).

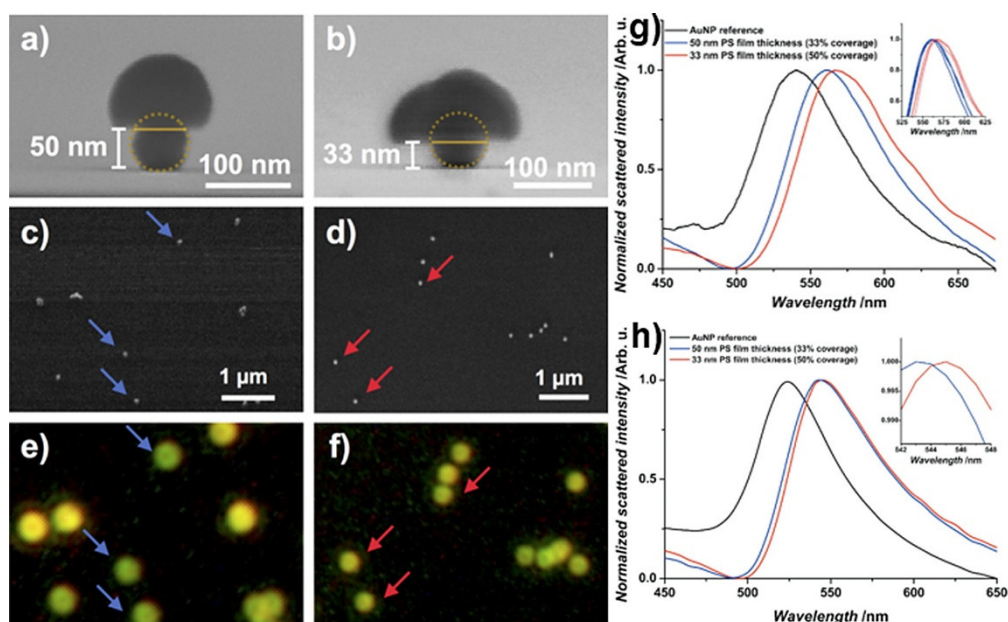


Figure 4: (a,b): Side-view, and (c,d): top-view SEM images of the measured particles. (e,f): Dark field scattering optical images of the same areas. Arrows mark the individual particles used to obtain single particle scattering spectra. g): Averaged and normalized single particle scattering spectra. The inset shows the magnified region around the resonance peak for each individual spectra. h): Simulated single particle spectra obtained for the reference particles (no coating), and the particles having 50% and 33% core-particle coverage by the silica cap after normalization.

Correlative electron microscopy and single particle scattering spectroscopy measurements under-line the high precision and reproducibility of the method (Figs. 4c,d,e,f). The good agreement between the measured and simulated single particle spectra supported by near-field calculations indicates that the observed changes in the dipolar plasmon resonance are influenced by the extent of coverage of the gold core by the silica cap (Figs. 4g,h). The straightforward methods readily available for gold and silica surface modification using range of different (bio)molecules make these well-defined nanoscale objects excellent candidates to study fundamental processes of programmed self-assembly or application as theranostic agents.

IDENTIFICATION OF DEWETTING STAGES AND PREPARATION OF SINGLE CHAIN NANOPARTICLE RINGS BY COLLOIDAL LITHOGRAPHY

(OTKA K112114, PD105173, and FP7 No.310250)

N. Nagy, D. Zámbo, Sz. Pothorszky, E. Gergely-Fülöp, A. Deák

Stages of drying after the wetting of template monolayer with aqueous gold nanoparticle solution were identified based on SEM images. Dewetting stages and characteristic particle deposits are summarized in Figure 1. During initial stage of drying, menisci are formed between neighbouring template particles generating liquid bridges parallel to the substrate. This results remaining particles trapped at the lateral contact point of the particles (green square). Liquid level exceeds the equatorial plane of the particles which induces a faster evaporation in the triangular openings due to the 'chimney' effect.

This manifests in gold NP deposits at the triple points on the substrate (red square). During further evaporation, liquid film starts to evolve between neighbouring PS particles and the silicon substrate, but these particles cannot be investigated from top-view. After the suspended film breaks up, liquid bridges evolve between neighbouring particles whose thinnest point can be found at the midpoint between two PS particles. This causes random deposition of nanoparticles along the triple line, but trapped ones at the midpoints (purple square).

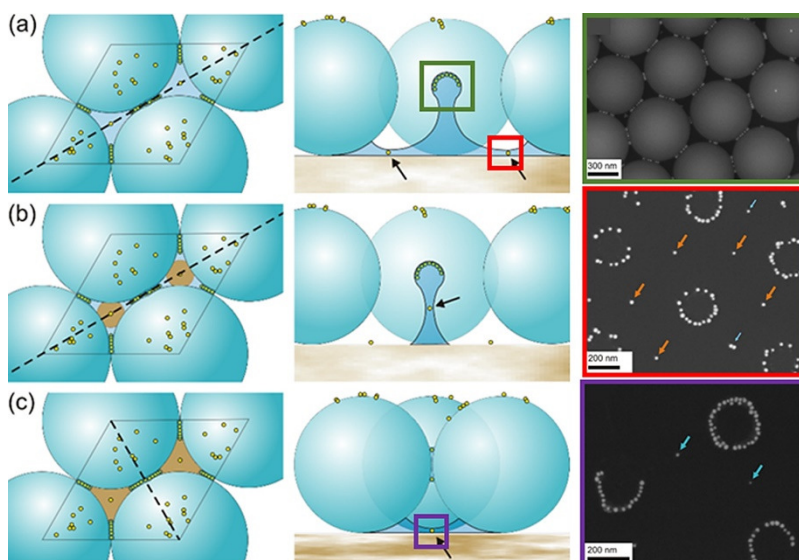


Figure 1: Stages of the dewetting process below the equatorial plane of the template particles. Left panel shows the top view of the unit cell, where dashed lines indicate the plane of cross sections showed in the middle panel. (a): Nanoparticle trapped at the triple point, where the liquid film is the thinnest; (b): assumed particle trapping at the thinnest point of the liquid bridge between two neighbouring template particles; (c): nanoparticles trapped at the midpoint of the liquid bridge. SEM images of coloured regions are represented in the right panel.

In the final stage of the drying, the volume of these circular films decreases and the nanoparticles will be pressed into the wedge between PS and the substrate. Finally, the nanoparticles accumulate in a circular shape underneath the template particle forming single chain nanorings. Nanorings formed from 45 nm and 65 nm Au NP and different PS template particle sizes are demonstrated in Figs. 2(a-d). Diameter of produced nanorings shows dependency on the template particle diameter: using smaller PS beads smaller nanorings can be created. The internal diameter of gold nanorings can be estimated theoretically as well. Calculations and real internal diameters have excellent agreement demonstrated in Fig. 2(e).

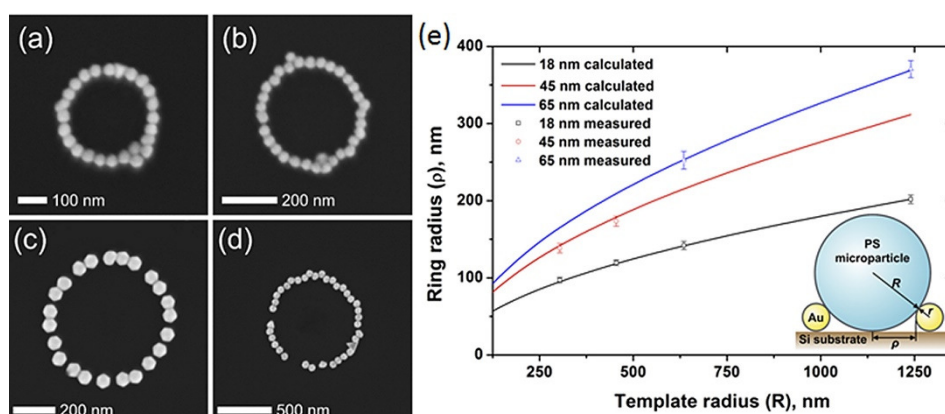


Figure 2: Single chain gold nanoparticle rings of (a,b): 45 nm, and (c,d): 65 nm nanoparticles under (a): 608 nm, (b): 909 nm, (c): 1.27 μm and (d): 2.48 μm PS particles. (e): Calculated (solid line) and measured (scatter plots) internal ring radii in a function of template radius. Inset shows the calculation parameters according to hard sphere contact model.

Effect of local defects and defect sides in template monolayer on the resulting structure was also investigated. Vacancies in the monolayer induce NP accumulation in the middle of the vacancy according to the “chimney” effect (Fig. 3(a)). Line defects indicate particle deposition between four PS particles (Fig. 3(b)). Domain boundaries cause broad disordered regions, where the surface coverage of the microparticles is smaller and the hexagonal order is missing. Here random depositions, thick rings and connected wires can be observed (Fig. 3(c)).

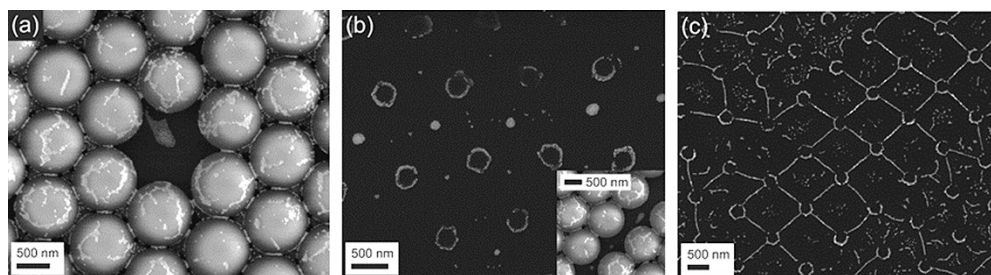


Figure 3: Effect of vacancies (a), defect sites (b), and domain boundaries (c) on the structure after the drying process

FORCE FEEDBACK CONTROL SYSTEM FOR ROBIN HEART SURGICAL ROBOT

Cs. Dücső, Z. Baji, I. Bársony, G. Battistig, L. Dózsa, P. Földesy, P. Fürjes, Z. Hajnal, Gy. Molnár, A.E. Pap, V. Rakovics, J. Radó, I. Réti, Zs. Zolnai, F. Biró, M. Takács

Minimally invasive surgery (MIS) offers several advantages for the patient and also for the society. The smaller trauma and faster recovery are obviously essential for the patient, whereas the reduced hospitalization and recovery time helps the society to spend the medical costs more effectively. INCITE project is intended to reveal and describe the advantages of the integration and application of various sensing capabilities in Minimal Invasive Surgery (catheter or surgery robot) systems. The future aim is to improve the functional characteristics, safety and standards of medical devices (catheters, robotic tools) applicable to minimal invasive cardiac intervention and surgery.

The lack of force feedback is one of the main barriers in the progress and widespread application of robotic surgery. The main tasks of the surgical robot control (Fig. 1) are the mapping and analysis the movements of the surgeon operator (position/velocity and possibly other physical parameters), as well as facilitating arm movement by providing control signals to the actuators. Additionally, it is desirable to feed-back the force/touch information to the person handling the tools. These signals can help the operator to make immediate correcting actions during the operation: cutting, separation, handling and moving tissues, to execute vascular clamping, to tie a knot, to recognize the type of tissue (pathology, calcification), to manipulate between different elements of internal organs without the risk of harming neighbouring tissue, and also to sense collision of arms/or tools by automatic recognition.

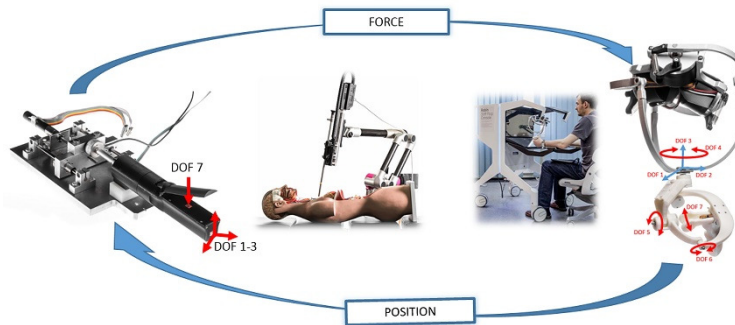


Figure 1: Schematic representation of the master-slave systems with force-feedback and manipulation

Fabrication and integration of the 3D MEMS force sensors

3D force sensors were developed to further integration in laparoscopic heads of surgery robots. The Si sensors operate with piezoresistive transduction principle by measuring the stress induced signals of the symmetrically arranged four piezoresistors in a deforming membrane (Fig. 2). As the chip size has to be reduced to a few mm², the conventional anisotropic alkaline etching technique was replaced by deep reactive ion etching (DRIE) for membrane formation. Moreover, DRIE enables to form any geometry of the membrane and offers the formation of monolith force transfer rod protruding over the chip surface (Fig. 2). This rod increases shear sensitivity of the structure, thereby plays a crucial role in tactile sensing. The technology applies SOI (silicon on insulator) wafers of appropriate device layer thickness. This results in highly uniform membranes and good reproducibility of the process.

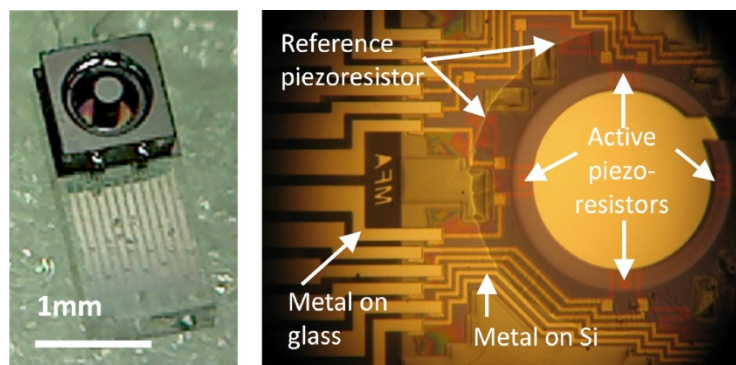


Figure 2: Optical views of glass bonded chip from the top (left) and the same chip from the glass side (right)

According to the medical and functional requirements the sensors must be covered by biocompatible and sterilisable elastic polymers. As the elastomer drastically affect the performance of the device, the proposed sensor structures were modelled by coupled finite element simulation to determine the appropriate geometric parameters to meet the functional requirements. Sensors were covered with spherically shaped PDMS (polydimethylsiloxane) polymer and the effect of the elastic coating was

studied in terms of sensitivity and response time. The standard test included the measurements of the four out-of-balance voltages over the applied force range. As experienced the geometry and elasticity of the elastic coverage may result in sensitivity loss up to 50-90%.

Preliminary functional tests of the force sensors

Model tools were equipped with two 3D force sensors of MFA: one mounted on a tip of grasper for generation of a tactile signal, whereas the other directly placed inside the tool for measuring the gripping forces (Fig. 3). Appropriate control systems and test beds have been developed at FRK.



Figure 3: Model of INCITE tools with tactile sensor on the tip and the 3D force sensor for gripping inside the grasper

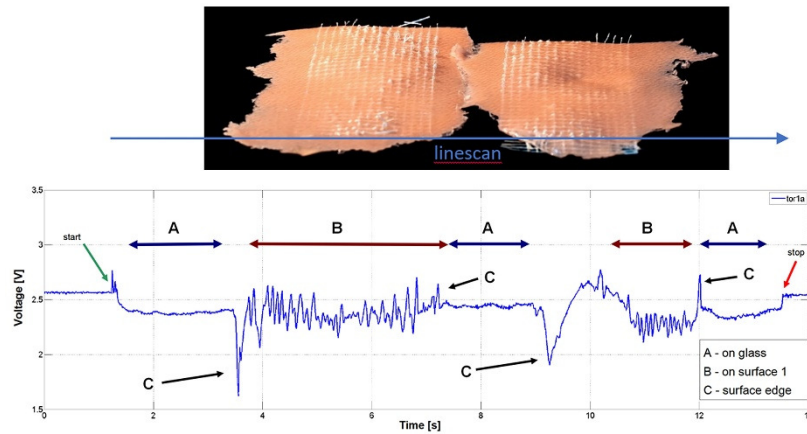


Figure 4: Preliminary measurements for surface characterization by tip integrated tactile sensor

Preliminary tests were accomplished to reveal the possible information the force/tactile sensors integrated in the laparoscope head can provide. Our work is also focused on the preliminary definition of the biomechanical effects present during surgical operations. Tactile measurements were also accomplished on artificial and real animal tissues to evaluate the applicability of the sensors for biomechanical screening during MIS surgery (Fig. 4).

DEVELOPMENT OF GAS DENSING MICROSTRUCTURES

Cs. Dücső, Z. Baji, I. Bársony, G. Battistig, L. Dózsa, P. Földesy, P. Fürjes, Z. Hajnal, Gy. Molnár, A.E. Pap, V. Rakovics, J. Radó, I. Réti, Zs. Zolnai, F. Biró, M. Takács

The existing micro-hotplate structure was further developed to investigate the limits of possible applications. A double-spiral Pt filament was integrated in a cantilever type hotplate built up from a reduced stress SiO₂/Si₃N₄/SiO₂ multilayer elaborated earlier. The hotplate exhibits 15% less power dissipation of the full membrane type reference as revealed from resistance and micro-melting point measurements (Fig. 1). Nevertheless, the average temperature provides limited information about the temperatures distribution across the hot-plate, thereby may lead to false consequences when the sensing principle is governed by chemical reactions. To clarify this a detailed investigation was started to identify degradation mechanism and optimize the layout according to the requirements of the targeted applications.

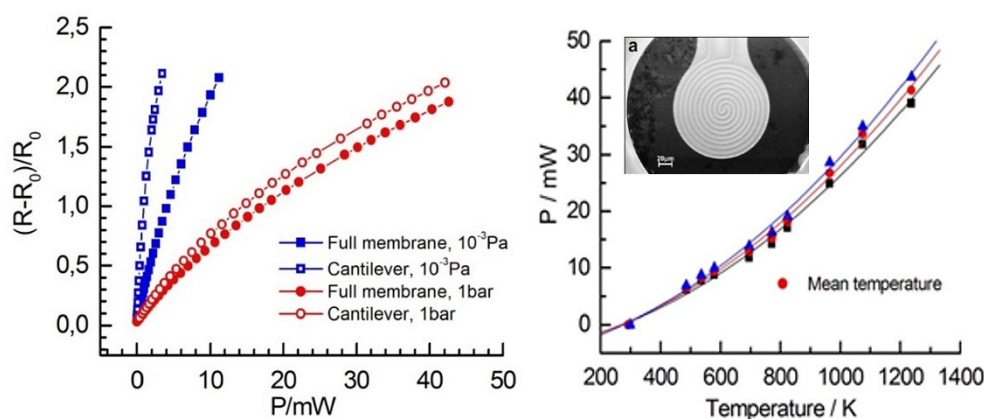


Figure 1: Power dissipation of the double spiral Pt heater hotplate (insert on the right) as measured by resistance (left) and micro melting point technique (right)

Deposition of catalyst in nanoporous sensing layers

Pt and Au nanoparticles were deposited in the porous sensing layer formed on the top of the microhotplates. The WO₃ nanorod based conductivity sensors were sensitized by Pt and Au nanoparticles (28 nm, 20 nm) and the effect of catalyst was investigated in detail. Drop deposited Au nanoparticles enhanced the sensitivity by a factor of 20 and showed the best performance by selective detection of H₂S over NH₃ in the ppb range (Fig. 2).

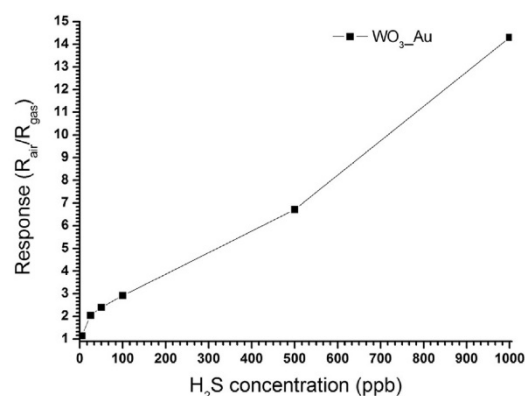
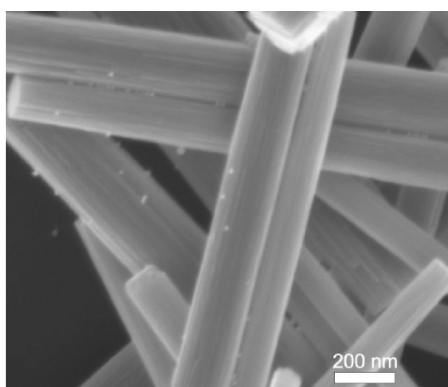


Figure 2: WO₃ nanorods sensitized with 20 nm Au nanoparticles (left). Sensor responses for H₂S exposure in the ppb range (right).

For the catalytic-calorimetric devices high operation temperature and large surface catalyst is needed to generate sufficiently large heat to be measured by the change of filament resistance. In order to meet this requirements ALD deposition technology of Pt was elaborated to cover uniformly the electrochemically formed porous Al₂O₃ layer on the top of the micro-hotplate (Fig. 3). The ongoing characterization of the device aims at the detection of hydrocarbons (LPG and methane) below the lower explosion limit (LEL) for commercial safety application.

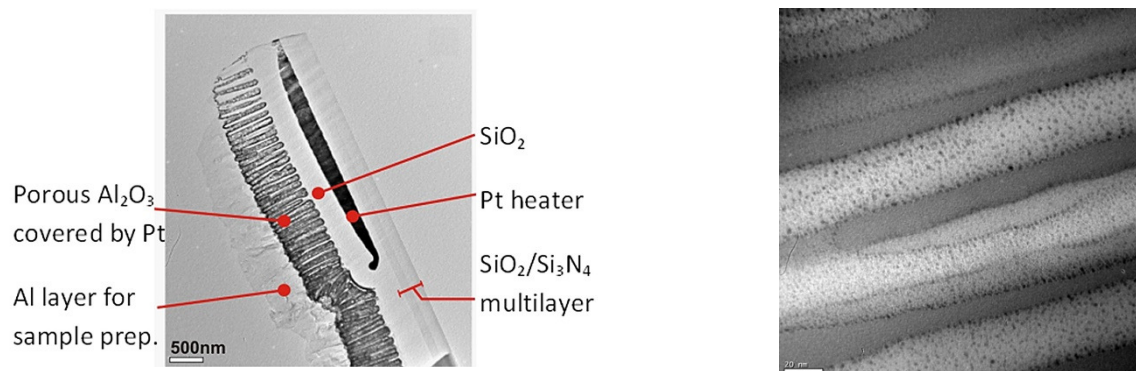


Figure 3: Cross sections of the micro-hotplate with ALD coated porous Al₂O₃ on top (left). Magnified view (right) shows the uniformly distributed Pt nanoparticles in the full depth of pores. TEM images.

EFFECTIVE FLOW CONTROL IN AUTONOMOUS POLYMER MICROFLUIDIC SYSTEMS BASED ON SURFACE MODIFICATION AND BIOINSPIRED MICROPATTERNING

P. Fürjes, Zs. Baji, O. Bálint-Hakkel, P. Földesy, Z. Hajnal, E. Holczer, E.L. Tóth, J. Radó, A.B. Tóth, B.V. Farkas, A. Füredy

Precise and fast PoC monitoring of disease related blood protein marker levels could be crucial in effective therapies. Due to the development of microtechnology and especially Lab-on-a-Chip (LoC) and microfluidic devices these cost-effective complex but miniaturized analytical systems became available and applicable for implementing the overall sample analysis from preparation to molecular diagnostics. The microfluidic system has to transport the sample and the washing buffer to the active area of the chip while mixing and incubate the sample with reagents. As the incubation and read-out needs a specified time, precise sample handling and flow control are crucial. The use of biological sample also requires bioinert surface properties with minimized non-specific adsorption and coagulation in the channels. The medium term target of our work is to develop a polymer based microfluidic cartridge for autonomously controlled sample transport and preparation to be incorporable into bioanalytical device.

Surface modification of self-driven microfluidic systems

Polymer based microfluidic sample transport system with multiple functions was developed for further application in bioanalytical devices detecting blood protein biomarkers or cells. Significant flow controlling subparts of the overall microfluidic system were designed, fabricated and characterized considering different surface modifications and microscale geometries. In order to fulfil the requirements, the polydimethylsiloxane (PDMS) based material was modified by embedding PDMS-b-PEO molecules into the PDMS matrix. PDMS-b-PEO molecules change the inherent hydrophobicity of the polymer ensuring adequate capillary pressure for self-driven transport simultaneously affecting the level of the non-specific protein adsorption. The non-specific adsorption of the major blood proteins on the surfaces were recorded by fluorescent microscopy (Fig. 1). It was proven that precise sample handling and flow rate control with minimized non-specific adsorption on the surface can be achieved by combination of these surface modification techniques and bio-inspired microstructures.

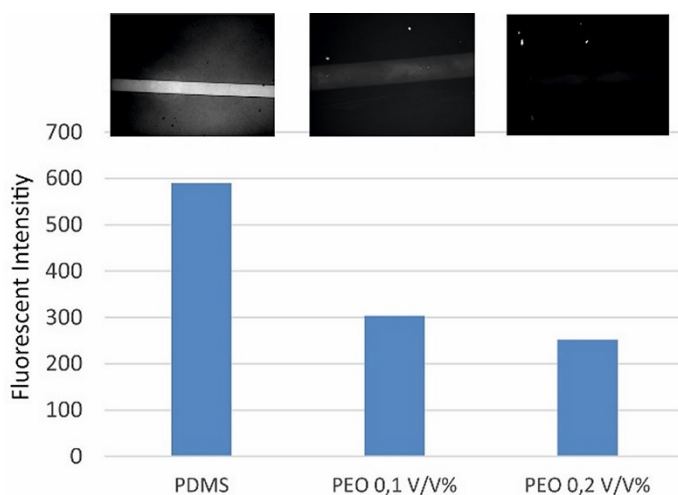


Figure 1: Non-specific fluorescent labelled HSA molecule adsorption on the microfluidic channel-surface in case of different PDMS-b-PEO concentrations

Bioinspired microcapillary systems

We tested different geometries including biomimetic structures to form both special capillary and flow stopping or rectifying structures to set (to enhance or decrease) local flow rates in the autonomous microfluidic system. The influence of the micropatterning of the transport channels was also analysed. Enhanced capillary pump systems were designed, fabricated and evaluated to prove the advantage of secondary microstructures inspired by natural water transport systems (Fig. 2).

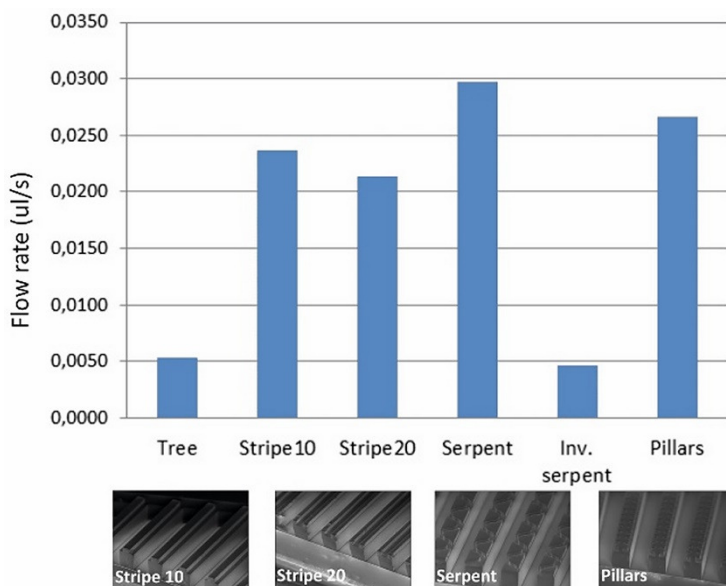


Figure 2: Micro-patterned capillary channels in surface modified PDMS: secondary structures significantly modify the flow rates

Asymmetric capillary structures were implemented to enable unidirectional or at least direction dependent sample transport by mimicking the micro ornamentation of the natural surfaces (Fig. 3).

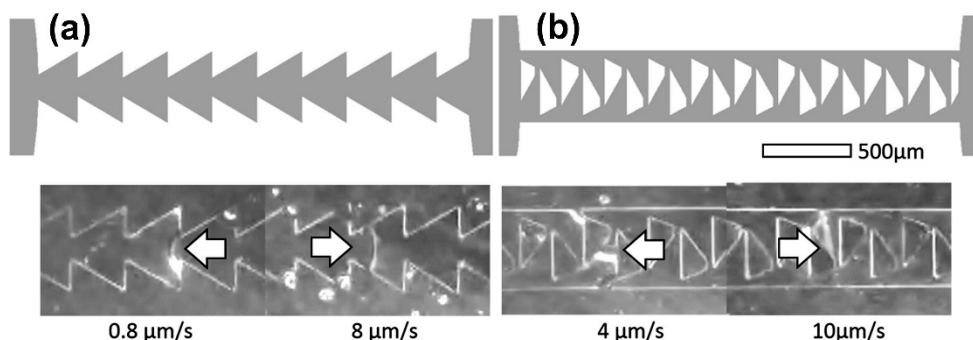


Figure 3: Direction dependent flow rates in asymmetrically patterned microfluidic structures. (a): flow stop, (b): Texas horned lizard's skin

Biosensing applications

In cooperation with the MTA-ELTE Immunology Research Group we have identified and optimized the physical conditions suitable to promote strong interactions. Permanent binding, between RBCs and functionalized microfluidic channel surface results in altered flow properties of the test blood sample. This deviation is characterized by an overall retardation of blood flow and a concomitant, as well, as a more pronounced retardation of the RBC components of blood (Fig. 4). Using the model system of blood type group AB0 we also demonstrated that this phenomenon can be applied to reliably identify the blood group without the need of any preanalytical steps.

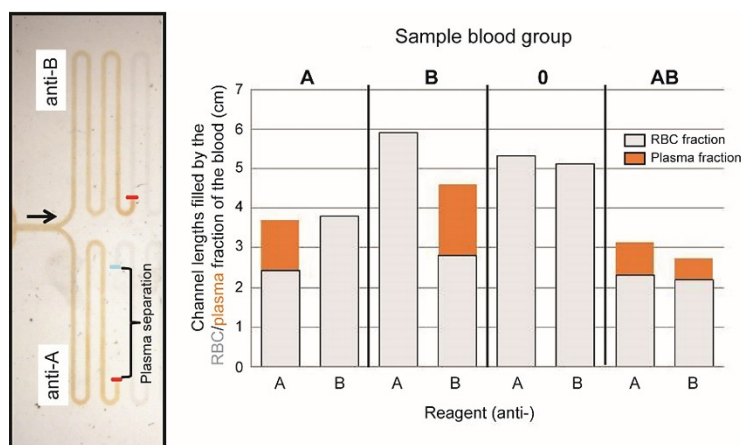


Figure 4: Development of plasma front in samples of (a) 0, (b) A, (c) B, and (d) AB blood types

Autonomous sample transport microfluidic systems were designed and fabricated to be integrated in Point-of-Care Lab-on-a-Chip based diagnostic cartridges in cooperation with 77 Elektronika Ltd.

PARTICLE MANIPULATION IN MICROFLUIDIC SYSTEMS

P. Fürjes, Zs. Baji, O. Bálint-Hakkel, P. Földesy, Z. Hajnal, E. Holczer, E.L. Tóth, J. Radó, A.B. Tóth, B.V. Farkas, A. Füredy

The rapid development of microscale diagnostic (Lab-on-a-Chip) devices has underlined the importance of microfluidics enabling fast and effective preparation and analysis of liquid samples. This leads to the development of novel microfluidic structures based on the physical laws of this size domain.

Hydrodynamic particle separation in microfluidic systems

The aim of our work was to develop a passive microfluidic separation system applicable for pre-sorting pollutant particles (pollens, bacteria, grains) in environmental samples having different geometric or physical parameters. To achieve effective size dependent sorting of the particles dispersed in the liquid sample a combination of different inertial separation methods was applied, utilizing the pinched flow fractionation, the Dean and the lateral migration based separation subsequently.

Microfluidic systems were designed and fabricated for particle separation and sorting by their hydrodynamic parameters such as cell size or density to be applied for sample preparation in optical scattering based pollution monitoring device. The hydrodynamic behaviour of the microfluidic structure was modelled and predicted by Finite Element Method (FEM) using COMSOL Multiphysics code to calculate the flow field and the geometry dependent particle trajectories. The separation of black (10 μm particle diameter) and white (16 μm diameter) lines were visible and also demonstrated by their spatial distribution in Fig. 1.

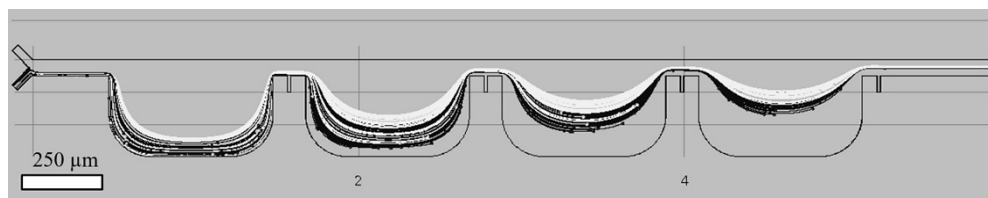


Figure 1: Modelled particle trajectories developing in the lateral migration based passive separation system (particle diameters: 16 μm - white lines and 10 μm - black lines)

The microfluidic system was manufactured by soft lithography and verified by fluorescent microscopy applying two differently labelled particles with 10 and 16 μm diameters. The results of the experiment were in good agreement with the prior FEM estimations and proved successful size dependent sorting of particles (Fig. 2).

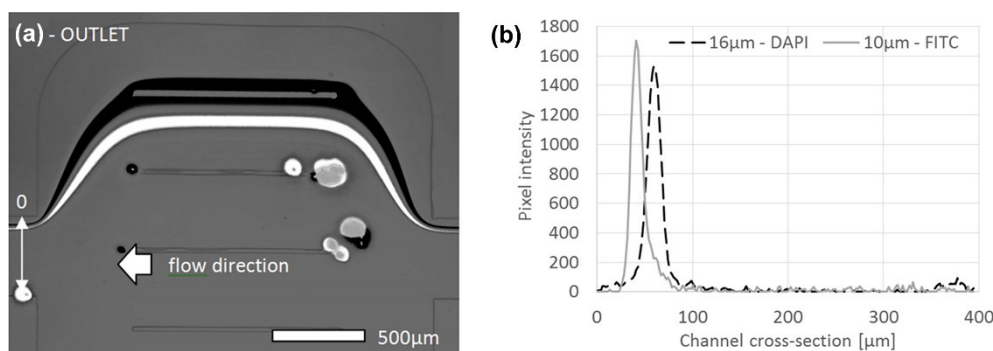


Figure 2: Recorded trajectories (a), and intensity analysis (b), of different fluorescent labelled beads at the outlet (diameters: 16 μm - white lines - DAPI and 10 μm - black lines - FITC). The two bead sizes are separated by their respective peak positions.

Particle trapping in microfluidic magnetic separation (MMS) system

Particle separation is challenging since the particles often have physical parameters (density, dielectric constant, etc.) similar to that of the solvent. Active separation techniques could offer several effective solutions, although they require an external field and power. Microfluidic Magnetic Separation (MMS) devices utilize the effective magnetophoresis based magnetic bead manipulation applying microfabricated paramagnetic patterns to locally amplify the magnetic field. Microfluidic magnetic particle trapping system was modelled, designed and manufactured to characterize and improve the separation efficiency during sample preparation and analysis.

Coupled multiphysics model of the evolving magnetic field, fluid dynamics and particle trajectories was implemented in COMSOL Multiphysics. The movement and entrapment of magnetic beads in the MMS system were analysed and the spatial distribution of the trapped magnetic particles was compared to experimental results (Fig. 3).

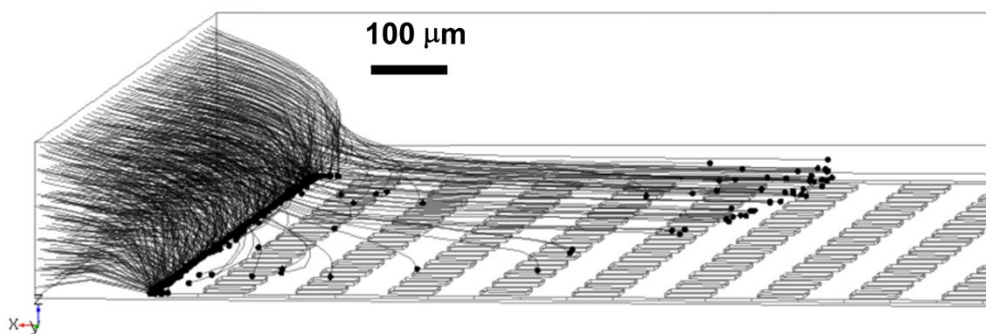


Figure 3: Particle trajectories over the grid type paramagnetic pattern in the MMS structure

For functional validation the microfluidic system was manufactured in polydimethyl-siloxane (PDMS) by soft lithography technique, and special Fe-Ni pattern was deposited onto a glass wafer to amplify the magnetic field locally inside the chip. Experimental results showed the capturing effect of the paramagnetic grid (Fig. 4(a)). Untrapped particles followed the gridlines parallel to the flow direction (Fig. 4(b)) and maintained these trajectories after leaving the pattern as well.

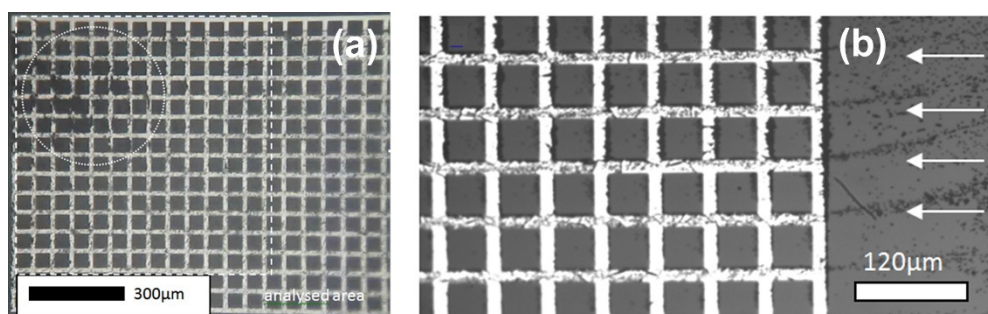


Figure 4: Movement of the magnetic beads over the paramagnetic pattern: trapped magnetic beads on the paramagnetic (Fe-Ni) pattern of the MMS chip (a), untrapped particles follow the grid lines parallel to the flow direction (b)

PRECISELY TAILORED SOLID STATE NANOPORES FOR MOLECULE RECOGNITION

P. Fürjes, Zs. Baji, O. Bálint-Hakkel, P. Földesy, Z. Hajnal, E. Holczer, E.L. Tóth, J. Radó, A.B. Tóth, B.V. Farkas, A. Füredy

Nanoporous membranes are the fundamental components of the transport modulation based label free electrochemical biosensors envisioned to be applicable for high sensitive molecule detection. The sensitivity and the specificity of these sensors are significantly affected by the evolved pore geometry which has to be fitted to the target molecule size and conformation. Commercialization of the nanopore based biosensors or Lab-on-a-Chip devices seems to depend on the development precise and high throughput nanofabrication techniques enabling reliable and reproducible shaping nanopore geometries in solid state membranes.

Controlled nanopore fabrication by focused ion beam (FIB) milling

This work is intended to demonstrate a significant improvement regarding reliability and reproducibility of the Focused Ion Beam (FIB) milling for nanofabrication solid state nanopore arrays to achieve precise and predictable nanopore geometries fit to the targeted molecule conformation to be recognized. Solid state nanopores were fabricated by the combination of MEMS and NEMS technology. First a dielectric membrane was released by alkaline or DRIE etching from the backside, and then the nanopores were drilled by program controlled Focused Ion Beam (FIB) milling using accelerated Ga^+ ions applying different milling currents and doses to obtain various pore geometries. The geometries of the nanopores were analysed in detail by high resolution SEM and TEM imaging (Fig. 1(a-b)).

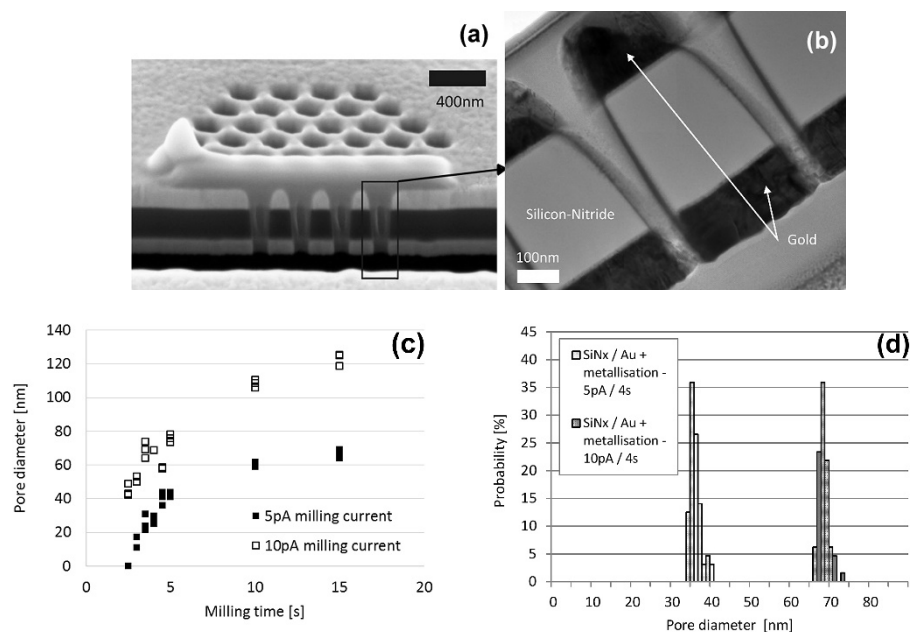


Figure 1: Cross-sectional SEM (a), and TEM view (b) of the nanopore array revealed by FIB milling of Au/SiN_x/Au membrane and the measured time dependent pore diameters in case of Au/SiN_x layer structure and different ion currents (5 pA and 10 pA) (c). Statistical pore diameter distribution was significantly improved by additional front side metallisation (d).

The statistical geometric parameters of the fabricated nanopores as a function of the fabrication parameters were recorded and studied (Fig. 1(c)). To improve the reproducibility of geometrical parameters of the nanopores an additional metallization step was applied. During the fabrication process it had to passivate the sensor structure while applying the Focused Ion Beam milling for the complex material composition of the sensor structure. The work proved that the conformity of the pore geometry and the reliability of the fabrication process could be significantly improved by the advanced nanofabrication process (Fig. 1(d)).

SILICON MICROELECTRODES FOR INFRARED NEURAL STIMULATION

Z. Fekete, A. Pongrácz, Á.Cs. Horváth, A. Zátonyi, Zs. Bérces, D. Szegedi, B. Csernyus, Sz. Barna, D. Pinke

Infrared neural stimulation (INS) was discovered in 2005, when action potentials were successfully elicited using infrared light. Histology performed after revealed that there is a radiant exposure range, where action potentials are elicited without damage.



Figure 1 (a): Concept of a silicon microelectrode that provides infrared stimulation and records the electrical activity of neurons simultaneously. (b): Implantable MEMS device for simultaneous optical stimulation and electrical recording of neural activity. Scale bar: 10 mm Components of the system: (1): Silicon microelectrode chip, (2): PCB, (3): Electrical connector, (4): Optical fiber, (5): Optical connector.

In our work, a Michigan-type silicon microprobe for infrared neural stimulation was designed and investigated in terms of technology induced surface roughness and optical transmission. The fabrication of such optrode was realized by deep reactive ion etching and subsequent wet chemical polishing (Fig. 1).

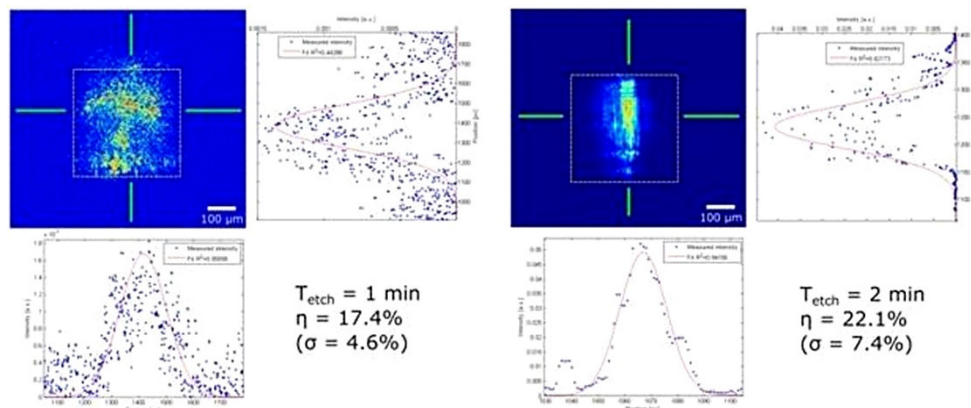


Figure 2: Beam profile of P1 (left) and P2 (right). Dashed yellow lines represent the contour of the probe shaft, while green lines indicate the X and Y cross-section of represented data on optical power (reprinted from Kiss et al., 2016, Sens. & Act. B).

The overall efficiency was further boosted by integrated couplers and focusing microlenses etched into the silicon substrate. By the proposed fabrication approach, 22.1% in system efficiency was achieved at a wavelength of 1310 nm. We observed that system efficiency does not increase significantly by increasing the time of sidewall polishing, however, the beam shaping effect of the coupling lens is more significant, when the tip roughness is reduced to 8.7 nm RMS value. The spatial distribution of the delivered light can also be controlled through integrated micromirrors at the probe tip, which facilitates lateral out-coupling with a Gaussian beam profile (Fig. 2).

SIMULTANEOUS IN VIVO RECORDING OF LOCAL BRAIN TEMPERATURE AND ELECTROPHYSIOLOGICAL SIGNALS WITH A NOVEL NEURAL PROBE

Z. Fekete, A. Pongrácz, Á.Cs. Horváth, A. Zátanyi, Zs. Bérces, D. Szegedi, B. Csernyus, Sz. Barna, D. Pinke

Temperature is an important factor for neural function both in normal and pathological states, nevertheless, simultaneous monitoring of local brain temperature and neuronal activity has not yet been undertaken. In our work, we propose an implantable, calibrated multimodal biosensor that facilitates the complex investigation of thermal changes in both cortical and deep brain regions, while recording multiunit activity of neuronal populations in mice. The fabricated neural probe contains four electrical recording sites and a platinum temperature sensor filament integrated on the same probe shaft within a distance of 30 μm from the closest recording site. The feasibility of the simultaneous functionality is presented in *in vivo* studies. The probe was tested in the thalamus of anesthetized mice while manipulating the core temperature of the animals. We obtained multiunit and local field recordings along with measurement of local brain temperature with accuracy of 0.14 $^{\circ}\text{C}$. Brain temperature generally followed core body temperature, but also showed superimposed fluctuations corresponding to epochs of increased local neural activity. With the application of higher currents, we increased the local temperature by several degrees without observable tissue damage between 34–39 $^{\circ}\text{C}$.

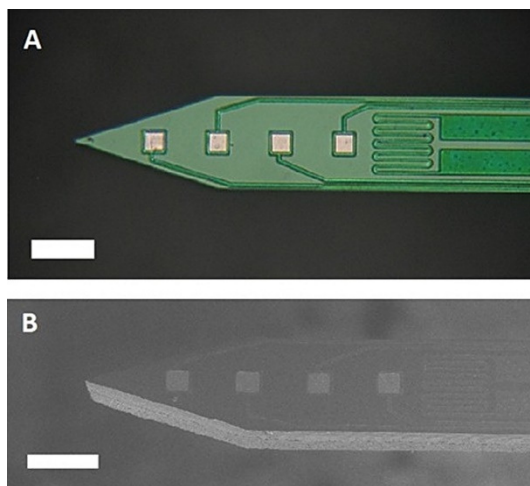


Figure 1: A): Optical microscopy views of a 4-channel microelectrode with integrated platinum temperature sensor filament. B): Perspective scanning electron micrograph of an as-fabricated probe shaft. Scale bar represents 100 μm on each figure. (Reprinted from Fekete et al. 2017, *J Neural Eng.*)

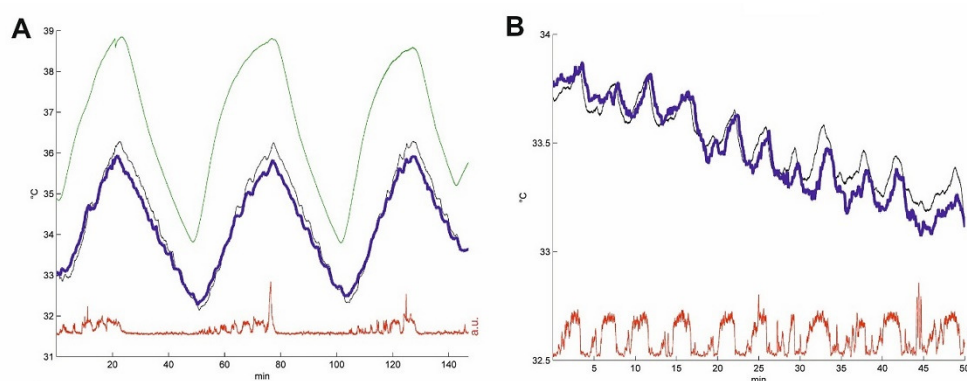


Figure 2: Validation of the thermoelectrode by temperature measurement *in vivo* (A): Parallel changes of core body temperature, brain temperature, and neural activity. Effect of a series of heating cycles between 34–39 $^{\circ}\text{C}$ performed by a heating plate directly placed under urethane anaesthetized mouse. (B): Brain temperature and multiunit activity in an anaesthetized mouse without active heating. Microfluctuations in brain temperature are associated with elevated multiunit activity. Green line: rectal temperature sensor, black line: contralateral reference NTC thermistor, blue line: temperature sensor of our thermoelectrode. Red curves show the smoothed multiunit activity (arbitrary units) recorded simultaneously by the thermoelectrode (reprinted from Fekete et al. 2017, *J Neural Eng.*)

A MULTIMODAL, SU-8 - PLATINUM - POLYIMIDE MICROELECTRODE ARRAY FOR CHRONIC IN VIVO NEUROPHYSIOLOGY

Z. Fekete, A. Pongrácz, Á.Cs. Horváth, A. Zátanyi, Zs. Bérces, D. Szegedi, B. Csernyus, Sz. Barna, D. Pinke

Utilization of polymers as insulator and bulk materials of microelectrode arrays (MEAs) makes the realization of flexible, biocompatible sensors possible, which are suitable for various neurophysiological experiments such as in vivo detection of local field potential changes on the surface of the neocortex or unit activities within the brain tissue. In this paper the microfabrication of a novel, all-flexible, polymer-based MEA is presented. The device consists of a three dimensional sensor configuration with an implantable depth electrode array and brain surface electrodes, allowing the recording of electrocorticographic (ECoG) signals with laminar ones, simultaneously. In vivo recordings were performed in anesthetized rat brain to test the functionality of the device under both acute and chronic conditions. The ECoG electrodes recorded slow-wave thalamocortical oscillations, while the implanted component provided high quality depth recordings. The implants remained viable for detecting action potentials of individual neurons for at least 15 weeks.

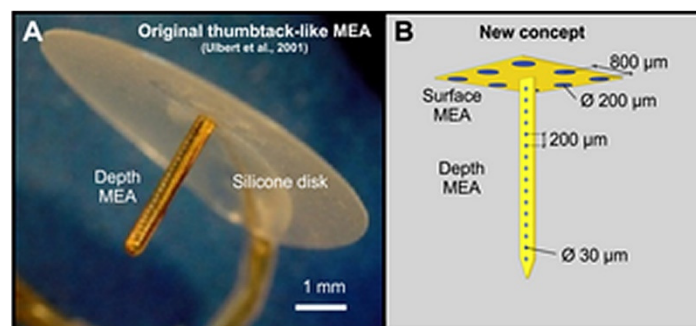


Figure 1: Design concept. (A): The thumbtack electrode, containing a 3 mm long shaft with an array of insulated fine wires and a silicone disk (www.plexon.com). (B): Design concept of the multimodal polymer-based MEMS electrode array (reprinted from Márton et al., 2016, PLOS One).

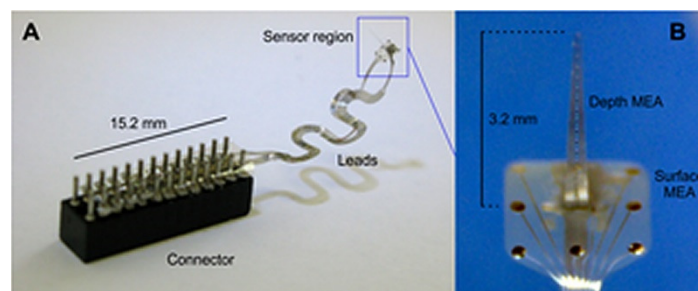


Figure 2: Photographs of the assembled device. (A): Macroscopic view. (B): A microscopic image of the sensor region, containing the microelectrodes (reprinted from Márton et al., 2016, PLOS One).

NEUROBIOCHEMICAL CHANGES IN THE VICINITY OF A NANOSTRUCTURED NEURAL IMPLANT

Z. Fekete, A. Pongrácz, Á.Cs. Horváth, A. Zátanyi, Zs. Bérces, D. Szegedi, B. Csernyus, Sz. Barna, D. Pinke

Neural interface technologies including recording and stimulation electrodes are currently in the early phase of clinical trials aiming to help patients with spinal cord injuries, degenerative disorders, strokes interrupting descending motor pathways, or limb amputations. Their lifetime is of key importance, however, it is limited by the foreign body response of the tissue causing the loss of neurons and a reactive astrogliosis around the implant surface.

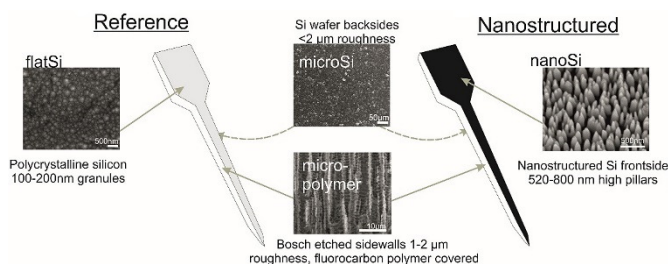


Figure 1: The two types of fabricated devices are: the one with nanostructured shank (right side) and a reference with polycrystalline Si front-side (left side). The two sidewalls of both devices are microstructured with a fluorocarbon polymer layer on the Si wafer as a result of the Bosch etching step (micro-polymer). The backsides of the devices are the non-polished Si wafer (microSi). Front-side of the reference device is a polycrystalline Si layer with 100-150 nm grain size (flatSi), and the front-side of the nanostructured device has 520-800 nm high pillars in a 18-70 pillars/ μm^2 density (nanoSi) (reprinted from [8]).

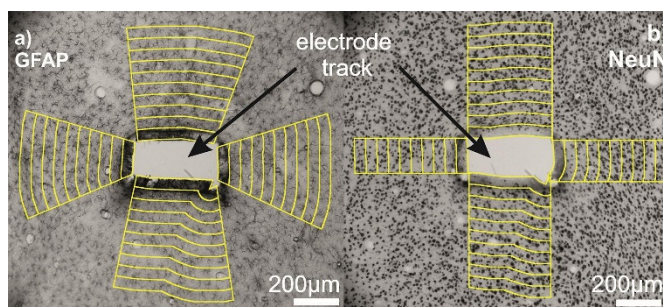


Figure 2: Light micrographs of the electrode tracks were segmented by a custom made ImageJ macro. From the manually defined track outlines 50 μm wide regions were segmented up to 500 μm along the selected shape of the track. Yellow-edge stripes represent the 50 μm wide manually selected ROIs. Different sides of the electrode track were also selected manually. In the case of GFAP staining (a), average pixel intensities were calculated in each ROI. On the NeuN stained images (b), cell numbers were determined manually in each ROI.

Improving the biocompatibility of implant surfaces, especially promoting neuronal attachment and regeneration is therefore essential. In our work, bioactive properties of implanted black polySi nanostructured surfaces (520-800 nm long nanopillars with a diameter of 150-200 nm) were investigated and compared to microstructured Si surfaces in eight-week long *in vivo* experiments (Fig. 1). Glial encapsulation and local neuronal cell loss were characterized using GFAP and NeuN immunostaining respectively, followed by systematic image analysis (Fig. 2). Regarding the severity of gliosis, no significant difference was observed in the vicinity of the different implant surfaces, however, the number of survived neurons close to the nanostructured surface was higher than that of the microstructured ones. Our results imply that the functionality of implanted microelectrodes covered by Si nanopillars may lead to improved long-term life.

PIEZOELECTRIC BASED NANOWIRE SENSORS

J. Volk, Zs. Baji, A. Békési, G. Battistig, Cs. Dücső, P. Földesy, N. Q. Khánh, I. Lukács, Gy. Molnár, A. L. Tóth, Zs. Zolnai, Z. Szabó, I. Bársony

The aim of the project is to demonstrate a novel tactile sensor for ultrahigh resolution fingerprint detection using vertical piezoelectric nanowires (NW). Three different configurations have been selected by the project partners: NWs contacted at the side (Option 1), at the bottom with multiple electrodes (Option 2), whereas in Option 3 NWs are sandwiched between top and bottom contacts. ZnO nanowires were grown for all types of chips by MFA (Fig. 1). Research partners at Tyndall, Ireland, succeeded in the fabrication of side-contacts using electron beam induced deposition (EBID) and recorded a significant signal upon nanowire bending. We optimized the fabrication of Option 2 type chip having 8×8 active NWs (Fig. 2(a)). Acrylate based polymer encapsulation was used for strengthening (Fig. 2(b)).

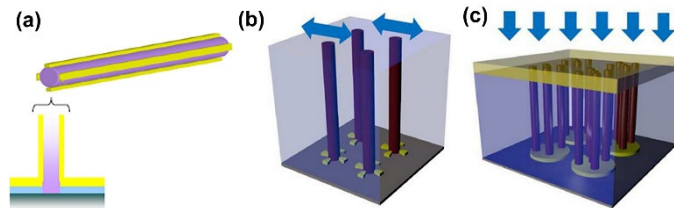


Figure 1: Targeted contacting schemes: sideways (a), multiple bottom (b), top-bottom (c)

In 2016 we focused on the characterization of these sensors. The static bending tests were carried out by the simultaneous detection of lateral force signal of an AFM and the source-drain current (Fig. 3).

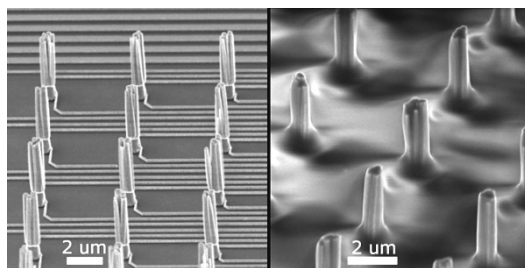


Figure 2: SEM images of ZnO NWs before and after polymer encapsulation

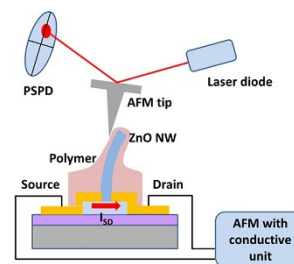


Figure 3: Schematics of the AFM based NW bending setup

Lateral force signal was calibrated by a vertically mounted compliant AFM cantilever. At first the selected NW was localized in dynamic AFM mode, which was followed by a carefully driven vertical approaching. After reaching a direct contact the AFM tip was pressed against the NW.

Current-voltage curve of the circuit changed significantly upon the influence of the NW bending, as shown in Fig. 4. Time domain cyclic tests carried out at a fix bias voltage have also revealed a strong correlation between the source-drain current and the lateral bending load, which offers itself for novel high resolution tactile imaging sensors having large gauge factor.

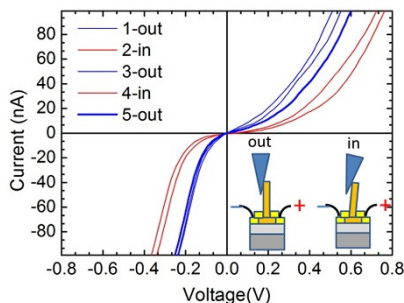


Figure 4: Current-voltage curves taken at subsequent loading cycles

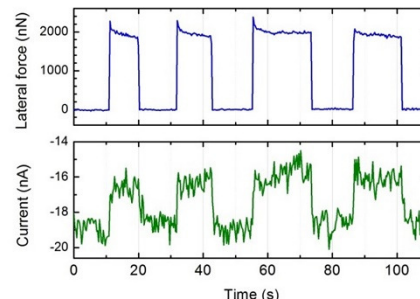


Figure 5: Time domain measurement of the lateral bending force and source-drain current at a bias voltage of 0.2V

In 2017 we plan to extend the AFM tests to reveal the influence of the contact material, the geometry, and the free carrier concentration, besides macroscopic “pressing tests” to study the tactile imaging capabilities of the sensors.

NEW APPROACHES IN THE DEVELOPMENT OF HYPOALLERGENIC IMPLANT MATERIAL IN ORTHOPAEDICS: STEPS TO PERSONALIZED MEDICINE

K. Balázs, N. Oláh, Zs. Fogarassy, V. Varga, T. Sopczák, T. Zagyva, L. Illés, D. Delfonse, C. Lohman, J. Lorenzen, M. Ignatiev, Cs. Balázs

Joint replacement is one of the most successful areas in current orthopaedics. Although many improvements have been made, tissue reactions to biomaterials, infection and lacking osseointegration are still the main reasons for the failure of implants and for revision surgery. Various materials - considered as "ideal" to wear resistance (e.g. CoCr-alloys) or "bioinert" (Ti-alloys) - are found to induce adverse tissue reactions or to support biofilms. Patients with a known metal allergy are at a higher risk of developing sensitivity against biomaterials. HypOrth Program helps understanding local adverse reactions around artificial joint replacements and to improve integration of potential hypoallergenic implants with improved biocompatibility.

HypOrth has already developed bioactive implant surfaces including bioceramics. Those surfaces and implant materials are being tested in material tests as well as cell culture experiments. From these results, prototypes are being designed. A very unique surface coating will be realized by using eggshells and seashells as a source for calcium/ hydroxyapatite coating to enhance osseointegration and mimic biocompatibility. This technology has been proven to be efficient and effective in simulator tests.

It can be assumed that the initiative HypOrth has direct impact on the health of European citizens but also on the technology transfer by stimulating metal forming industries. Already today, the prototype surfaces are expected to show superior properties as compared with existing technologies.

MECHANICAL CHARACTERIZATION AND CORROSION OF PROTECTIVE TiC/AMORPHOUS C NANOCOMPOSITE COATING AS SURFACE THIN FILM

N. Oláh, Zs. Fogarassy, A. Sulyok, J. Szívós, T. Csanádi, M. Furkó, Z. May, K. Balázs

Ceramic titanium carbide / amorphous carbon (TiC/a:C) protective nanocomposite thin film may be a potential candidate for such a surface protection coating to the different implant materials which serve as barrier layer. Our developments are focused on the biological application of these thin films [www.hyporth.eu].

The main goal of our current research work is to investigate the relationship between mechanical and corrosion properties of the different films. For this purpose, coatings with different structures were developed by co-depositing Ti and C on SiO₂/Si, TiAl6V4 and Titanium wafers (blasted and unblasted) using DC magnetron sputtering system in argon (0.25 Pa) at room temperature. Roughening the surface by sandblasting was applied for better adhesion between the TiC/a:C protective coating and the substrate. The DC magnetron sputtering of TiC/a:C surface thin films on sandblasted (s.b.)/polished Ti and TiAl6V4 substrates showed improved corrosion properties as compared with known implant materials. The comparison of structural changes before and after corrosion tests as well as any release of metal ions was investigated. The mechanical and tribological properties of TiC/a:C nanocomposite coatings on s.b./polished Ti and TiAl6V4 substrates were also examined and compared with those of bare substrates. Hardness (H) of ~26 GPa and elasticity (E) of ~220 GPa with μ of ~0.268 was observed in case of the film prepared at ~38 at% Ti content which consisted of 4-10 nm width TiC columns separated by 2-3 nm thin a:C layers. The H^3/E^2 ratio was ~0.4 GPa that predicts high resistance to plastic deformation of the C-Ti nanocomposites besides great wear-resistant properties (H/E of ~0.12) [81]. It was also shown, that the hardness and the tribological property of the bare implant materials was improved by four orders of magnitude with application of TiC/a:C nanocomposite coating with a moderate elastic modulus value (Fig. 1.). In the case of this (~38 at% Ti content) TiC/a:C coated s.b. TiAl6V4 alloy, after 10 days of immersion time its j_{corr} value started to decrease with increasing its R_p value, while the SEM micrograph does not show any special changes of the surface morphologies of the samples after the corrosion tests. It is proved that roughening the surface by sandblasting can enhance the corrosion resistance. However, the presence of V was detectable in each case, the Al and Ti ions have been detained by the TiC/a:C thin film coated s.b. TiAl6V4. The main conclusion of our research is that a ceramic TiC/a:C thin film with ~20 at% a:C and ~38 at% Ti contents would be a suitable choice for a protective nanocomposite coating.

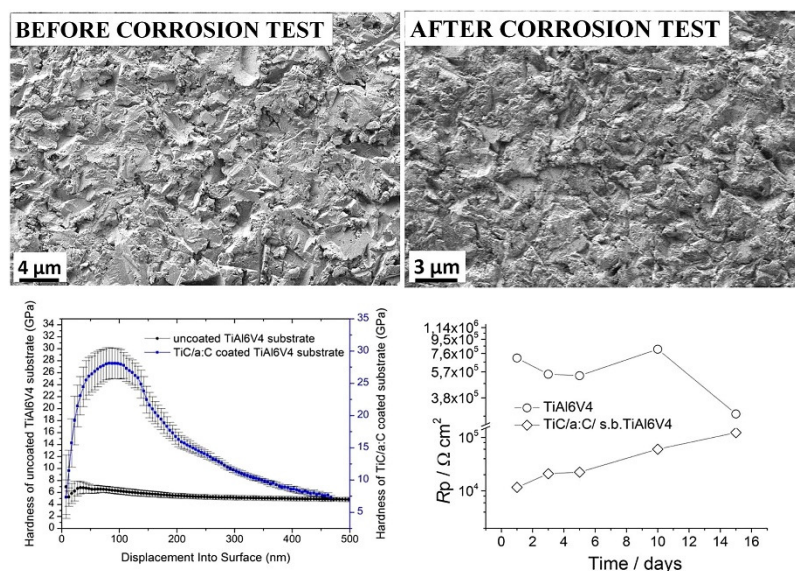


Figure 1: SEM images about the TiC/a:C/s.b. TiAl6V4 before and after corrosion tests, comparison of the H values of the uncoated with μ of $\sim 0.60 \pm 0.04$ and TiC/a:C coated with μ of $\sim 0.20 \pm 0.07$ TiAl6V4 substrate and R_p values of TiC/a:C coated and uncoated s.b. implant materials derived from potentiodynamic curves depending on the immersion time.

DEVELOPMENT AND CHARACTERIZATION OF MULTI-ELEMENT DOPED HYDROXYAPATITE COATINGS ON METALLIC IMPLANT MATERIALS

M. Furkó, Cs. Balázs

The research scope is to develop coatings onto implant materials which possess simultaneous antimicrobial and biocompatible properties. The coatings were prepared by pulse current deposition method. The coatings were also doped with silver (Ag) zinc (Zn) magnesium (Mg) and strontium (Sr) elements either with co-deposition or with surface post-treatment with solutions containing the corresponding element. The basic electrolyte solution contained $\text{Ca}(\text{NO}_3)_2$, $\text{NH}_4\text{H}_2\text{PO}_4$ and H_2O_2 at pH 4.3 at 70 °C. Since the as-deposited calcium phosphate coating is mainly in Monelite phase, after deposition, the samples were immersed into 1 M NaOH solution at 70 °C to achieve phase transformation into Hydroxyapatite phase. The biodegradable properties of the layers were evaluated by electrochemical tests in simulated body fluid (SBF) at temperature of 37 °C. Electrochemical Impedance Spectroscopy (EIS) measurements were performed also to test the samples' corrosion stability. All the electrochemical tests were carried out using a classical three-electrode cell with platinum as counter electrode, using saturated calomel electrode SCE as reference electrode and the samples themselves as working electrode. The surface morphologies and grain size of samples were also observed by SEM measurements (Figs. 1 and 2). These materials, which are reached already at low graphene contents, offer the possibility to reduce efforts in manufacture and to create new functionalities that may be utilized for technical applications.

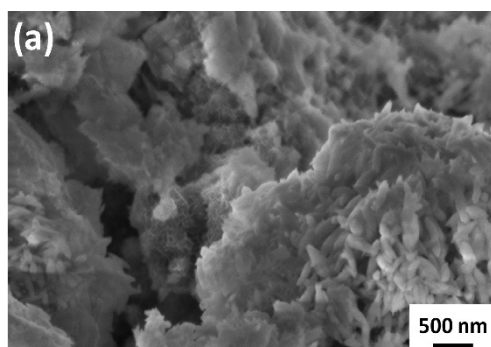


Figure 1: SEM images of multi-element doped HAp

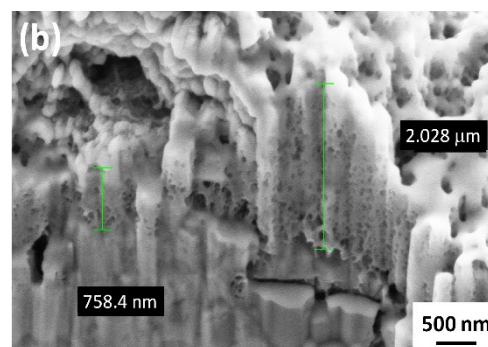


Figure 2: Cross sectional analysis of coating by SEM/FIB measurement

GRAPHENE-CERAMIC COMPOSITES FOR TRIBOLOGICAL APPLICATION IN AQUEOUS ENVIRONMENTS

Cs. Balázsi, Zs. Fogarassy, V. Varga, M. Knoch, J. Dusza, A. Kailer, K. Balázsi

There is a strongly growing demand for high wear resistant and reliable ceramic materials that may be widely used in industrial applications and in energy production. Special attention is paid to components to be used under severe conditions and lubricated by the surrounding media which is mainly aqueous. Reliability and efficiency of these components need to be improved by using high performance ceramics with superior tribological (low friction, high wear, and corrosion resistance) and mechanical (fracture toughness, strength) properties.

The main aim of this work was development of novel, highly efficient tribological systems on the basis of ceramic/graphene nanocomposites, to prove their superior quality, and to demonstrate their suitability for technical applications, e.g., for slide bearings and face seals in aqueous media. The ceramic nanocomposites show that it is possible to prepare ceramic materials with improved mechanical and tribological properties by incorporating graphene into the Si_3N_4 structure using different sintering methods. Multilayered graphene (MLG) was prepared by attritor milling at 10 hours intensive milling of graphite powder with few micrometer size. The rather large quantity, cheap and rather quick preparation process are main strengths of our MLG technique. The Si_3N_4 / MLG nanocomposites were prepared by attritor milling and sintered by hot pressing (HP, Fig. 1), or hot isostatic pressing (HIP, Fig. 2) and with spark plasma sintering (SPS, Fig. 3). The Si_3N_4 ceramics were produced with 1wt%, 3wt%, 5wt% and 10wt% content of MLG. The tribological behaviour of composites in different environment was investigated and showed the decreasing character of wear with increased MLG content. This new approach is very promising, since ceramic microstructure can be designed with high toughness and provide improved wear resistance at low friction.

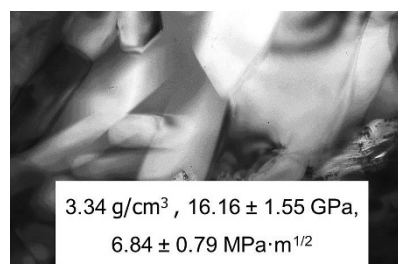


Figure 1: Si_3N_4 /MLG prepared by hot press (HP)

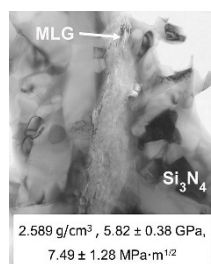


Figure 2: Si_3N_4 /MLG prepared by hot isostatic press (HIP)

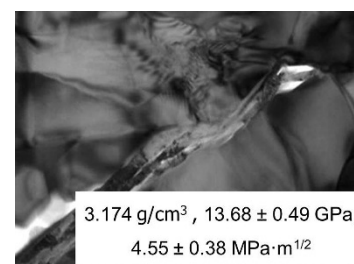


Figure 3: Si_3N_4 /MLG prepared by spark plasma sintering (SPS)

In all composites, densities between 97 and 100 % were obtained (as compared to fully densified reference Si_3N_4). The alpha- Si_3N_4 to beta- Si_3N_4 phase transformation was completed during hot pressing. The structural investigations and phase analysis measurements confirmed the presence of MLGs in all composites after the sintering process. The presence of very fine nanostructured zirconia on the silicon nitride grains is the effect of high efficient milling process. Vicker hardness (HV) values decreased with increasing of MLG content from 18.86 GPa to 9.69 GPa. The small increase to 18.86 GPa of HV at 1wt% MLG content in comparison to 17.01 GPa reference Si_3N_4 might be attributed to smaller grain sizes. The results show that improved tribological properties, more stable frictional behaviour and a significant increase of the wear resistance at MLG contents beyond 5 wt% can be achieved in case of composites sintered by HP.

IMPROVING THE TRIBOLOGICAL PERFORMANCE OF CERAMIC COMPOSITES BY A CONTINUOUS FEW-LAYER GRAPHENE TRIBO-FILM

O. Tapasztó, J. Balko, V. Puchy, J. Dusza, P. Kun, L. Tapasztó

Graphene nanoplatelets (GNPs) are regarded as a particularly promising nanoscale filler material for various composites. Improvement in the tribological properties of ceramic composites could be achieved. Here, we propose to employ a novel mechano-chemical method, based on the ball milling of graphite with melamine addition to increase the exfoliation efficiency, but without chemically modifying the resulting few-layer graphene sheets. We have prepared Si_3N_4 composites reinforced by these ultra-thin few-layer graphene nanoplatelets (FL-GNPs) using the Spark Plasma Sintering method. We found that the composites prepared with only 5wt% of FL-GNPs are characterized by more than 20 times increased wear resistance, while their friction coefficient is reduced to nearly its half, as compared to monolithic Si_3N_4 (Fig. 1).

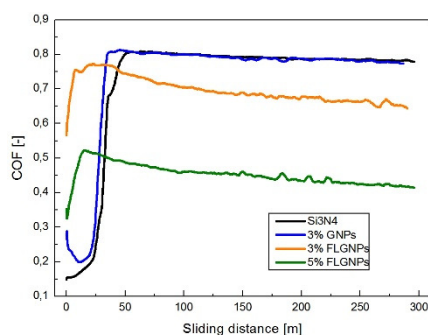


Figure 1: Composites with 5wt% of FL-GNP addition display a highly-reduced friction coefficient

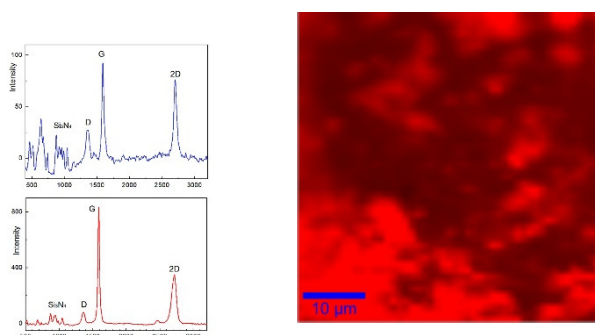


Figure 2: Raman spectroscopy map of the graphene G peak (a) indicating a continuous few-layer graphene coverage of the wear track (b)

By confocal Raman spectroscopic mapping of the wear tracks we have shown that this outstanding improvement in the tribological properties can be attributed to the formation of a continuous protecting and lubricating tribo-film consisting of FL-GNPs of high structural quality (Fig. 2). There are key technological advantages in developing highly wear-resistant and low-friction ceramic composite materials. Components produced from such materials enable a substantial reduction of losses during operation, as well as a significant increase of their durability.

DEVELOPING AN IMPROVED PRODUCTION TECHNOLOGY FOR THE CERAMIC BLOCK OF THE PORTL DOSIMETER SYSTEM

K. Balázsi, Zs. Fogarassy, S. Gurbán, V. Varga, Cs. Balázsi, I. Apáthy, A. Csőke, T. Pázmándi, P. Szántó, B. Zábori, A. Hirn

The portable thermoluminescent dosimeter (TLD) system PorTL consists of several dosimeter cells of compact and robust design and a light-weight battery-powered TLD reader. The TL block inside the PorTL cells consists of a ceramic plate with a miniature heater fixed on one side and a thermocouple and the $\text{Al}_2\text{O}_3\text{:C}$ TL tablet on the other side. An improved production technology of the ceramic block has been developed based on attritor milling and hot isostatic pressing (HIP) using a novel Si_3N_4 ceramic nanocomposite material. The main objective was to decrease the manufacturing lead time of the PorTL cells and to extend the lifetime of the TL block (Fig 1).

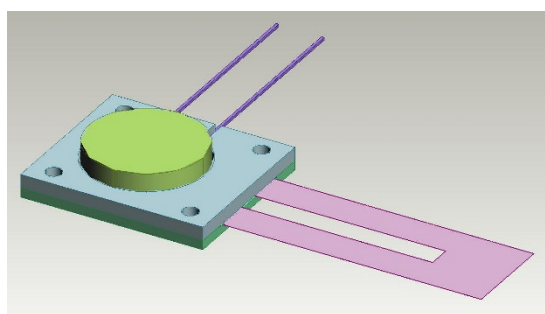


Figure 1: The novel design of the PorTL block; the ceramic plates are prepared with HIP technology.

Five of the ceramic materials tested had significant radioactive background radiation probably due to their potassium (^{40}K) content; only the Si_3N_4 ceramic nanocomposite material was found to be suitable for using as basic material of the TL block.

Since the sensitivity of $\text{Al}_2\text{O}_3\text{:C}$ TL tablet dropped significantly after heating it at $1700\text{ }^\circ\text{C}$, the technology to produce the TL block was split into two: 1) production of ceramic components and 2) integration of the heater, the thermocouple, and the TL tablet into the block.

The advantages of this approach are:

- the use of Si_3N_4 material and the corresponding technology (HIP), with which the MTA EK MFA has already extensive experience;
- the manufacturing of the tools needed for the production of the ceramic block is relatively simple;
- much less work hours required than in the case of the original technology;
- shorter manufacturing lead times.

GRAPHITIC FILMS OF GROUP III NITRIDES AND GROUP II OXIDES: PLATFORM FOR FUNDAMENTAL STUDIES AND APPLICATIONS

I. Cora, L. Tóth, B. Pécz, R. Yakimova, A. Kakanakova, F. Gianazzo

In this cooperative project, range of structural and material properties of innovative van der Waals heterostructures of group III nitrides (AlN, GaN, and InN) with graphene and ultrathin graphitic films of group III nitrides was explored. MOCVD of AlN (Fig. 1) and GaN was performed in Linköping onto epitaxial graphene on 4H-SiC substrates within the temperature range of 1100-1410 °C, and with sequential introduction of precursors. Graphene templates were predominantly one monolayer, whereby a buffer layer exists at the interface with the SiC substrate.

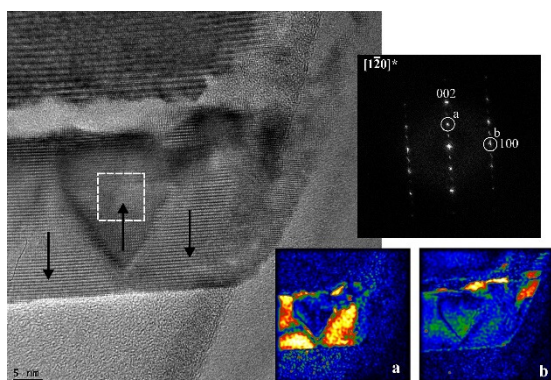


Figure 1: HRTEM and FFT images show that AlN grows onto the substrate epitaxially and voids between them are common. Geometric phase maps calculated by the two reflections show that the layer is inhomogeneous and it grows in 3D.

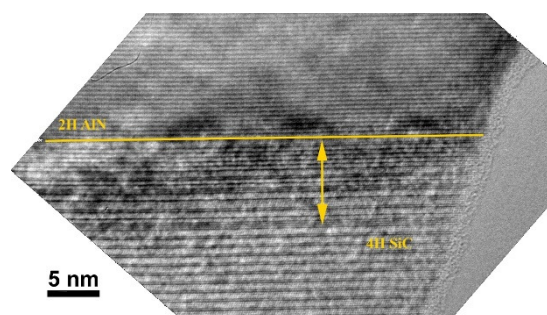


Figure 2: HRTEM image of the AlN-SiC interface grown at 1410 °C. The 4H SiC show stacking disorder at the top and the AlN grows onto it epitaxially, while graphene diminishes from the interface.

In our lab, structural characterization of the samples by TEM and AFM was performed. Raman characterization of the layers was done by the colleagues in Catania. With the TEM study of the work we could demonstrate how the growth parameters influence/affect the quality of the nitride layer and the stability of the graphene.

At 1410 °C the top surface of the SiC substrate shows stacking disorder, and the AlN grows epitaxially onto it, while the graphene layer diminishes (Fig. 2). Voids between the SiC and the AlN are common if the substrate is pre-treated by H₂/NH₃. At 1240 °C the AlN grows onto SiC with epitaxial orientation (Fig. 3). The AlN crystals grow in islands and at their coalescence threading dislocations are common. Graphene diminishes again. At 1100 °C graphene is still stable, but the layer is polycrystalline (Fig. 4).

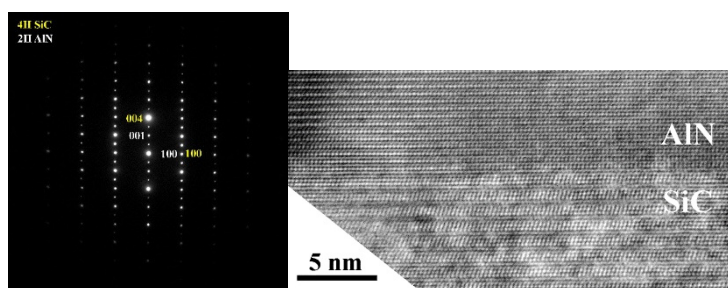


Figure 3: HRTEM and SAED patterns show that AlN epitaxially grows onto the 4H SiC at 1240 °C, but graphene still lacks from the interface.

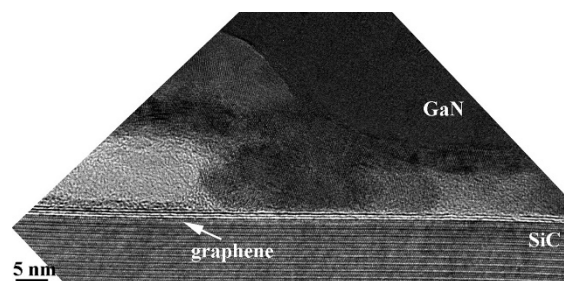


Figure 4: HRTEM image of the sample grown at 1100 °C. Graphene remained at the interface, but the GaN layer is polycrystalline.

TEM STUDY OF THE AS-DEPOSITED AND ANNEALED Ga_2O_3 FILMS GROWN BY VAPOR PHASE EPITAXY

I. Cora, B. Pécz, F. Mezzadri, F. Boschi, M. Bosi, R. Fornari, M. Čaplovičová, I. Dódony

Ga_2O_3 is a wide bandgap semiconducting oxide (~ 4.7 eV), promising for UV optoelectronics and power electronics. Ga_2O_3 layers were grown onto (001) surface of $\alpha\text{-Al}_2\text{O}_3$ by vapour phase epitaxy at 650°C and were annealed at 1000°C for 2 and 6 hours. The as-deposited layers and the two annealed samples were studied by high resolution transmission electron microscopy and X-ray diffraction.

Previous XRD studies on the as-deposited film showed that these films are single crystal epitaxial layers and exhibit hexagonal $P6_3mc$ space group symmetry, characterized by partial occupation of the Ga sites, which corresponds to the ϵ phase, -with disordered Ga atoms in the structure. In the present work detailed TEM studies allowed to investigate the real structure of this phase at the nanoscale (Fig. 1). The structure is ordered in 5-10 nm large (110)-twinned domains, and each domain has an orthorhombic structure with $Pna2_1$ space group symmetry, called $\kappa\text{-Ga}_2\text{O}_3$. This phase is a new polymorph among the Ga-oxides. Parallel XRD analysis carried out on thicker samples ($9\text{-}10\ \mu\text{m}$) confirmed the same results, and permitted to provide the refined structural parameters.

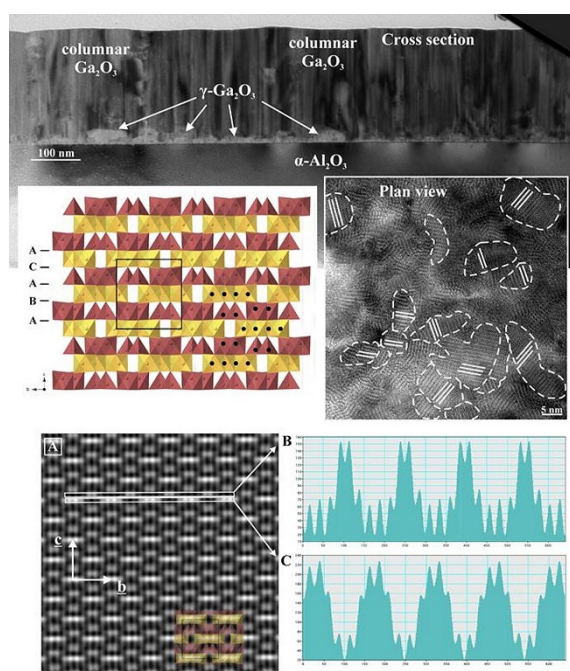


Figure 1: TEM images of the cross section and the plan view TEM specimens of the as-deposited layers with the corresponding crystal structure of $\kappa\text{-Ga}_2\text{O}_3$. The structure is textured consisting of 5-10 nm large (110)-twinned orthorhombic domains. STEM image (at the bottom) with the corresponding line scans shows the Ga atoms in [102] projections. Spurious peaks are due to overlapping of the twin domains.

The crystal structure of these Ga_2O_3 layers consists of an ABAC oxygen close-packed stacking, where Ga atoms in between occupy octahedral and tetrahedral sites forming two types of polyhedral layers parallel to (001). The edge-sharing octahedra and the corner-sharing tetrahedra form zig-zag ribbons along the [102] direction. Anti-phase boundaries are common inside the domains. The polar character of the structure is confirmed, in agreement with the characteristics of the $Pna2_1$ space group and explaining the ferroelectric nature measured earlier.

At $600\text{-}700^\circ\text{C}$ degree the sample starts to transform to $\beta\text{-Ga}_2\text{O}_3$. The duration of the thermal treatment at 1000°C strongly influenced the crystallinity of the samples: while for a 2 hour annealing the sample was found to be polycrystalline and strongly textured, the sample annealed for 10 hours was almost single crystalline. The sample that was annealed for 2 hours, consists of pure $\beta\text{-Ga}_2\text{O}_3$. The layer is polycrystalline and strongly textured: [-201] direction of each $\beta\text{-Ga}_2\text{O}_3$ crystal is perpendicular to the (001) of $\alpha\text{-Al}_2\text{O}_3$.

The 10 hours-long annealed sample is pure $\beta\text{-Ga}_2\text{O}_3$ and almost single crystalline: $\beta\text{-Ga}_2\text{O}_3$ grow onto the $\alpha\text{-Al}_2\text{O}_3$ with epitaxy: $(310)/[-13-1] \beta\text{-Ga}_2\text{O}_3 \parallel (001)/[1-10] \alpha\text{-Al}_2\text{O}_3$. The upper part of the layer grows with epitaxy but with a different orientation: $(310)/[-130] \beta\text{-Ga}_2\text{O}_3 \parallel (001)/[1-10] \alpha\text{-Al}_2\text{O}_3$.

HIGHLY SAFE GAN METAL-OXIDE-SEMICONDUCTOR TRANSISTOR SWITCH (SAFEMOST)

L. Tóth, I. Cora, B. Pécz, M. Tapajna, J. Kuzmik, B. Adamowicz, T. Hashizume

The present project started in 2016 is part of a multinational Slovakian-Japanese-Polish-Hungarian research project which was granted in the frame of the JST-V4 call of proposals. The research within the consortium is financed by the four national funding organizations as well as the International Visegrád Fund (IVF). The main goal of this project is to develop a GaN based metal-oxide-semiconductor (MOS) structure with a sufficiently low density of surface donor states at the gate-oxide/heterostructure interface thus allowing the realization of normally-off switching devices and decreasing conversion losses in electronics. Our Slovakian colleagues at IEE SAS manufactured several samples consisting of very thin gate dielectric layers prepared by various deposition techniques onto standard GaN/AlGaN/GaN heterostructures serving as substrates. All these layers were made of Al₂O₃ but the way of deposition varied from low temperature atomic layer deposition (ALD) using several precursors to a high temperature metalorganic chemical vapour deposition (MOCVD) process. The samples were studied by a complex way by the participants of the consortium. Electrical characterization and X-ray studies were performed in Bratislava, photo-capacitance investigation, Auger electron spectroscopy and photoluminescence in Gliwice, Poland, while XPS studies and modelling of the processes in Sapporo, Japan.

Our task in this cooperation was the structural characterization of the heterostructures, particularly of the dielectric film deposited on the top surface by means of transmission electron microscopy. In the first series of experiments Al₂O₃ layers deposited by ALD with different conditions were studied. These dielectric films were proved to possess somewhat higher density of surface donor states and so were regarded as less suitable for the required parameters than e.g. MOCVD deposited dielectrics. We have observed, however, that all these ALD layers show a crystalline microstructure – even those deposited as low as at 100 °C (Fig. 1). Also the study of MOCVD deposited dielectric layers has been started and will be continued next year.

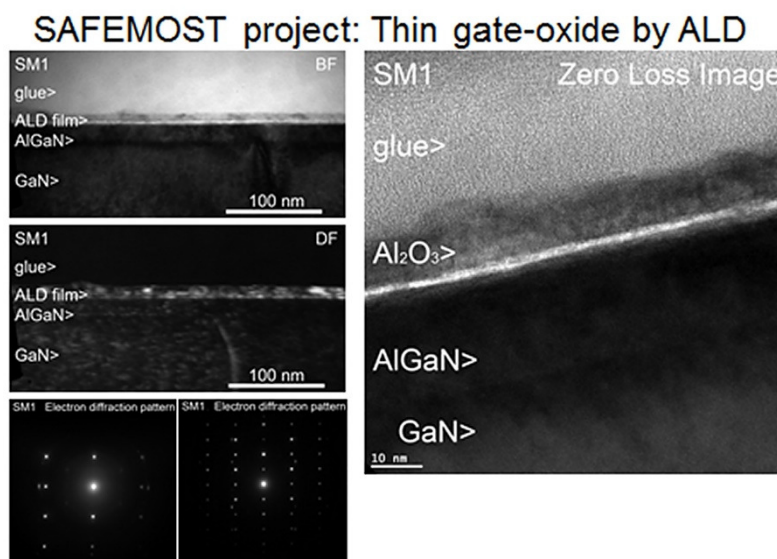


Figure 1: Bright field and dark field micrographs (left) and high resolution image (right) of a 10 nm thick gate dielectric layer grown by atomic layer deposition (ALD) at 100 °C. The Al₂O₃ film was found crystalline as shown on the electron diffraction patterns below.

INCLUSIONS IN SI WHISKERS OBTAINED IN METAL (Ni) INDUCED LATERAL CRYSTALLIZATION OF AMORPHOUS SI THIN FILMS

Gy. Z. Radnóczy, E. Dodony, G. Battistig, B. Pécz, I. Stoimenos, N. Frangis, N. Vouroutzis, D. Knez, F. Hofer

The crystalline silicon obtained in metal induced crystallization was further characterized based on the results from recent years. Si whiskers were investigated in detail to gather data on the tetrahedral NiSi₂ inclusions found in the whiskers earlier. Based on geometrical considerations and literature data a theoretical prediction was made on the atomic configuration of the Si/NiSi₂ interface that needed to be confirmed experimentally. High resolution STEM-HAADF images were taken on a spherical aberration corrected TEM to locate the Ni containing atomic columns inside the inclusions and determine their relative position to the Si lattice (Fig. 1(a)).

Based on the images taken on the lattice exactly aligned to the [110] zone and image simulation results (Fig. 1(b)) we identified the type Ia interface (Fig. 1(c)) in agreement with our prediction. The results also lead to the conclusion that the inclusions cannot form as precipitates during cool down as the amount of Ni inside the inclusions exceeds the solubility limit by several orders of magnitude. It is likely that inclusions form during whisker growth at the leading edge of the whisker by trapping NiSi₂ from the NiSi₂ cluster leading the whisker growth.

The research leading to these results has received funding from the European Union Seventh Framework Programme under Grant Agreement 312483- ESTEEM2 (Integrated Infrastructure Initiative-I3).

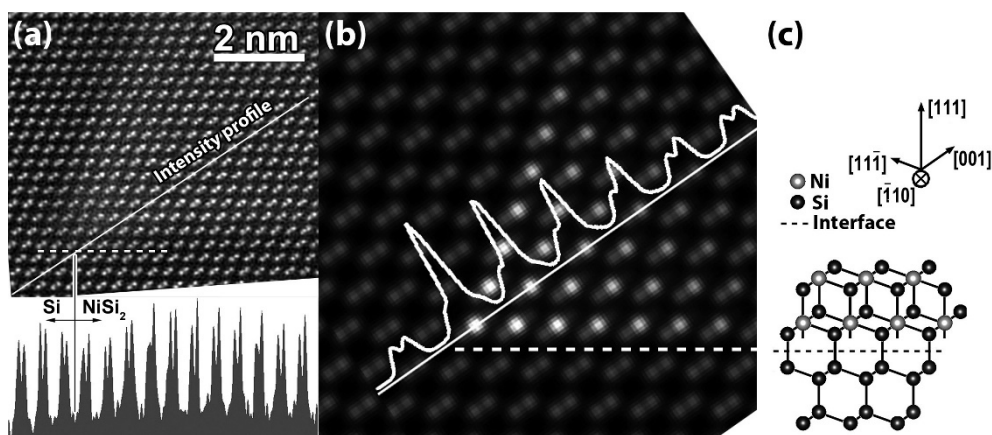


Figure 1: (a): noise filtered STEM-HAADF image of a NiSi₂ inclusion. The sample is viewed along the [110] direction. (b): Simulated image of the same structure giving the same type of asymmetric dumbbells (c): model of the identified atomic configuration at the interface.

COMPARATIVE STUDY OF DIRECT CURRENT MAGNETRON SPUTTERING (DCMS) AND HIGH POWER IMPULSE MAGNETRON SPUTTERING (HiPIMS) PROCESSES FOR CN_x THIN FILM GROWTH WITH DIFFERENT INERT GASES

S. Schmidt, Zs. Czigány, J. Wissting, G. Greczynski, E. Janzén, J. Jensen, I. G. Ivanov, L. Hultman

Reactive DCMS and HiPIMS discharges of C in N_2/Ne , N_2/Ar , and N_2/Kr were investigated by positive ion mass spectrometry in cooperation with Linköping University (LiU). The cation energies depend on the type of inert gas and the amount of N_2 in the sputter gas mixture. The sputter mode gains major significance with regards to the ionization of species originating from the target relative to the ionization of the sputter gases. HiPIMS processes yield approximately ten times higher flux ratio of ions originating from the target compared to those originating from the process gas (Fig. 1). For the case when graphite is sputtered in N_2/Ne mixtures containing up to $\sim 20\%$ N_2 , the influence of the sputter mode on cation energies and degree of ionization was insignificant.

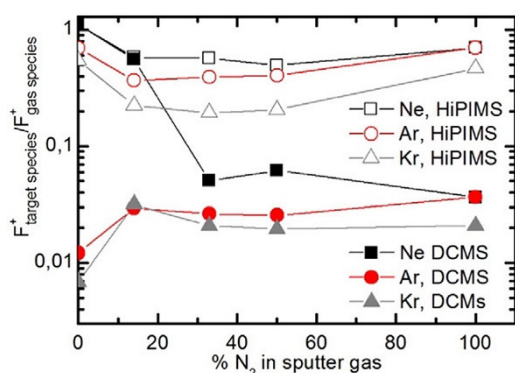


Figure 1: Sum of the total ion flux of species originating from the target in relation to the sum of process gas ion species over the amount of N_2 in the inert gas for DCMS and HiPIMS discharges

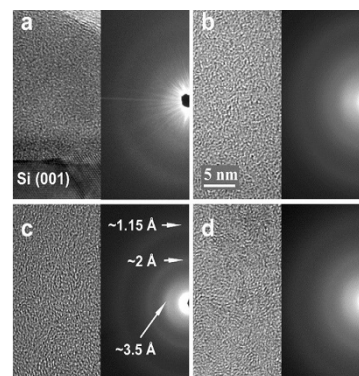


Figure 2: Cross-sectional HRTEM images with corresponding SAED patterns of CN_x thin films deposited in $Kr/14\%$ N_2 by a): DCMS at $T_s=110$ °C, b): HiPIMS at $T_s=110$ °C, c): DCMS at $T_s=430$ °C, and d): HiPIMS, $T_s=430$ °C

The structure of the films deposited in 14% N_2 /noble gas mixtures was investigated by transmission electron microscopy (TEM). It is shown that reactive DCMS and HiPIMS discharges using 14% N_2 /noble gas mixtures at a substrate temperature of 430 °C produce graphitic or fullerene-like CN_x thin films, with one exception: the reactive HiPIMS discharge in N_2/Ne yields an amorphous structure. At a low substrate temperature of 110 °C the synthesized films are amorphous, only the CN_x film deposited by HiPIMS in reactive N_2/Kr atmosphere shows a weak graphitic short range ordered microstructure (Fig. 2).

A characteristic process in reactive sputtering of CN_x films is chemical sputtering which is described as the dynamic adsorption and desorption of plasma species at the substrate, where dangling C or CN bonds get passivated and structure-defining C_xN_y ($x,y \leq 2$) species adsorb, thus contributing to the film growth, additionally volatile C_xN_y ($x,y \leq 2$) clusters lift off. Therefore, high deposition rates and particle energies may counteract the formation of a fullerene-like structure. The structural evolution of CN_x thin films sputtered in HiPIMS mode was more pronounced, even though higher ion energies were measured for corresponding HiPIMS processes. The result suggests the occurrence of a pulse-assisted chemical sputter process not only at the substrate, but also at the target resulting increased number of sputtered C_xN_y ($x,y \leq 2$) species.

The film properties show a correlation to the substrate temperature, the applied inert gas and sputter mode. The mechanical performance of the films is mainly governed by their morphology and composition, but not by their microstructural short range order. Amorphous and fullerene-like $CN_{0.14}$ films (Fig. 2) exhibiting a hardness of ~ 15 GPa and an elastic recovery of $\sim 90\%$ were deposited at 110 °C in reactive Kr atmosphere by DCMS and HiPIMS.

FePt NANOPARTICLES; COLLOID CHEMISTRY TOWARDS CATALYSTS AND MAGNETIC RECORDING MEDIA

A. Horváth, F. Somodi, A. Deák, G. Sáfrán

In frame of an "Home-financed Project" of the Centre of Energy Research, a co-operative work of MFA and Institute for Energy Security and Environmental Safety, was carried out with the aim of preparation of FePt nanoparticles with fct (L_{10}) structure and its testing (1) if they can be applied as catalyst for dry reforming of methane and (2) can we put FePt nanoparticles on a surface as separate and self-organized layer? The FePt particles after synthesis are, usually, paramagnetic and show fcc structure. Suitable annealing, however, may transfer the fcc phase to fct in which Fe and Pt are organized into discrete atomic rows (superlattice) and the alloy exhibits high magnetic anisotropy. The FePt nanoparticles have been synthesized in both aqueous (aq) and organic (org) media using reducing agents and precursors. On one hand, the FePt particles were deposited onto oxide substrates, on other hand they were encapsulated in silica shell and put on carbon coated TEM microgrid.

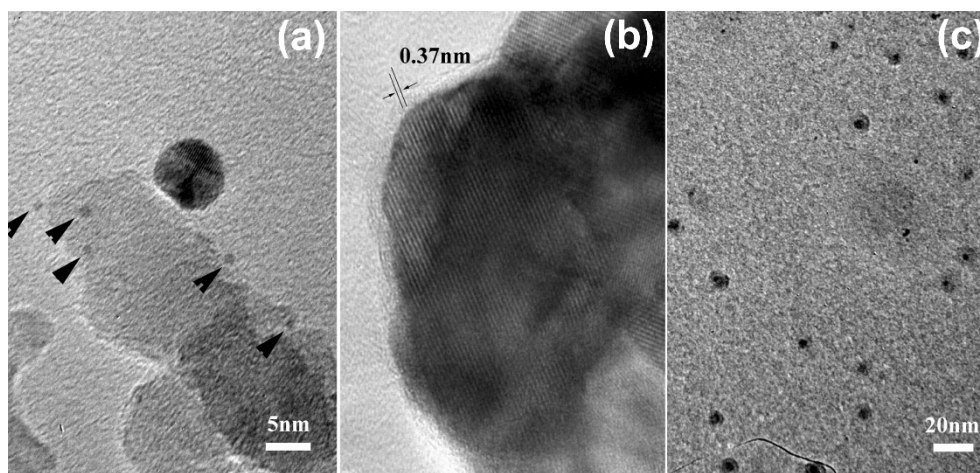


Figure 1: (a): TEM micrographs of FePt_{org}/Al₂O₃ TEM after 500 °C reduction; (b): FePt aggregate with 0.37 nm period characteristic to the (100) lattice of L₁₀, (c): 2-5 nm size FePt particles in SiO_x shell (FePt_{aq} sample)

The former samples were annealed in inert gas (5% H₂/Ar) atmosphere at 500 °C, while the latter were heat treated by means of UV excimer laser pulses. The function of the silica coating was the protection against oxidation and the separation of elemental magnets from each other. The ratio of the two constituting component was measured by EDS. The microstructure was characterized by TEM and HRTEM in the as deposited and in the heat treated state. The size of the FePt_{org} particles after 500 °C reduction treatment was non-uniform (Fig. 1(a)), while FePt_{aq} particles showed homogeneous size distribution. Based on their stability on Al₂O₃ and ZrO₂ substrates FePt_{aq} samples are promising candidates as catalysts in dry reforming of methane. In nano-size particles it was not the case but in large FePt agglomerates the L₁₀ ferromagnetic phase could be produced and observed (Fig. 1(b)) suggesting that the fcc phase was stabilized by small size and interaction with the substrate. It was possible to form the silica shell around FePt_{aq} nanoparticles prepared in aqueous media (Fig. 1(c)), however, the identification of developed phases due to laser treatment and the self-organization of silica-coated particles needs further studies.

VERSATILE NANOPATTERNING TECHNIQUE USING RF PLASMA ETCHING THROUGH LANGMUIR-BLODGETT FILMS

J. Szívós, M. Serényi, Sz. Pothorszky, G. Vértesy, G. Sáfrán

The nanoscale modification of materials has attracted wide research interest recently. In a Ph.D. work a cheap and fast technique was proposed in 2014 [J. Szívós et al., *Vacuum* 109, 200 (2014)] to produce ordered nanopatterns directly for nanolithography and for nanoimprinting. This technique applies a monolayer of self-assembled silica nanospheres (Langmuir-Blodgett (LB) film) as a template and the sample surface is treated by a single UV laser ($\lambda=248$ nm) pulse through the LB film that results in nanocraters.

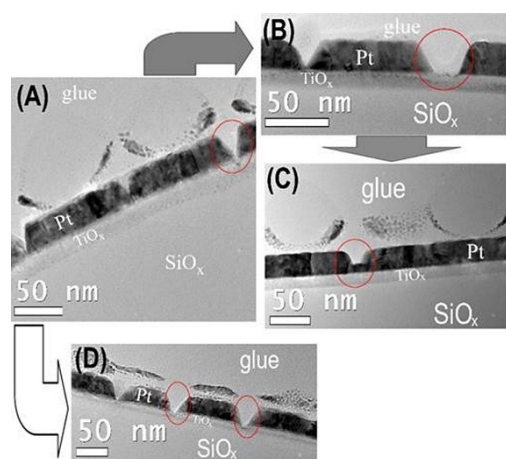


Figure 1: Typical cross sectional (X-) TEM images of Pt samples RF plasma etched for 100 s, (a): $U_{DC}=1200$ V and $P_{Ar}=2.5 \cdot 10^{-2}$ mbar - 'basic settings'; (b): $U_{DC}=1000$ V and $P_{Ar}=2.5 \cdot 10^{-2}$ mbar; (c): $U_{DC}=800$ V and $P_{Ar}=2.5 \cdot 10^{-2}$ mbar; (d): $U_{DC}=1200$ V and $P_{Ar}=2 \cdot 10^{-2}$ mbar

We could pattern Al-oxide but UV laser patterning was hardly effective for metal surfaces: the (quasi-)free electrons thermalize the lattice, thus the energy is absorbed nearly uniformly [M. S. Brown, C. B. Arnold: Springer Series in Materials Science Volume 135, 91-120 (2010)]. The next aim was to find a suitable solution for nanoscale patterning metallic, as well magnetic layers for increasing the capacity of FePt or CoPt magnetic layers by realizing Bit Patterned Media (BPM). In 2016 a technique to nanopattern diverse materials was introduced based on RF plasma etching through the LB film [J. Szívós et al., *Surf. Coat. Technol.* 313, 115-120 (2017)]. The LB film-covered sample is placed at the „target” position of the RF sputtering source and is subjected to ~ 1 kV Ar plasma. The nanospheres of the LB film protect the surface and sputtering takes place between them. This way the hexagonal pattern can be replicated to almost any material's surface provided that the plasma parameters are set properly. The feature size is determined by the diameter of the nanospheres that, in principle, can be decreased to about 10 nm. Moreover, our technique can be easily scaled-up by using industrial RF sputterers. The operation of our technique was presented by nanopatterning Pt thin films. The etching time was fixed as 100 s in the experiments mentioned here. The effect of changing so-called DC wall potential (U_{DC}) and the pressure of the sputtering (Ar) gas (P_{Ar}) - is depicted in Fig. 1. Fig. 1(a) is the reference ('basic settings'), where $U_{DC}=1200$ V and $P_{Ar}=2.5 \cdot 10^{-2}$ mbar. In Fig. 1(b) and Fig. 1(c) U_{DC} is set to 1000 V, or 800 V, respectively, at fixed P_{Ar} and etching time. The effect of setting P_{Ar} to $2 \cdot 10^{-2}$ mbar (i.e. decreasing it by $20 \pm 1\%$) with the same U_{DC} and etching time is seen comparing Fig. 1(a) and Fig. 1(d). It can be concluded that lowering of U_{DC} yields in shallower pattern depth, but in turn, lowering P_{Ar} by 20% causes no remarkable effect. This result can be quantitatively verified by investigating the replicas of LB-film imperfections in the patterned Pt films (marked by the red circles in Fig. 1).

Moreover, versatility of our technique was demonstrated by fabricating ordered hexagonal nanopatterns in polycrystalline metal (Ti besides of Pt), single crystalline semiconductor (Si) and insulating oxides (AlO_x , SiO_x) and it worked well regardless of crystal structure and electrical properties. As an example, Fig. 2 shows X-TEM and plan view SEM image of the successfully nanopatterned AlO_x (Fig. 2(a) and Fig. 2(b)), and Si sample (Fig. 2(c) and Fig. 2(d)), respectively.

At the end of 2016, CoPt (L1₀) thin films were nanopatterned and the microstructural and magnetic properties will be investigated in a collaboration with the *Technical University of Tokyo*. We intend to show that an alternative implementation of Bit Patterned Magnetic Media is feasible by means of the technique described here.

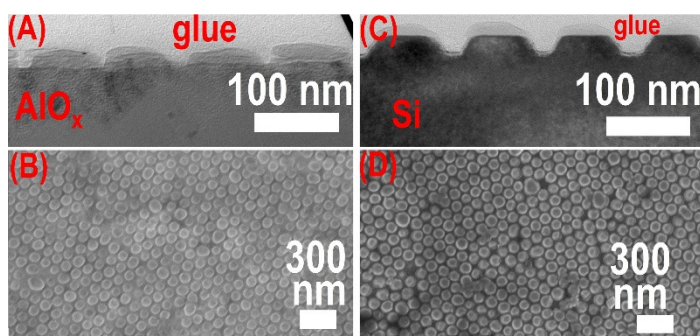


Figure 2: Typical images of AlO_x ((a): XTEM and (b): SEM image) and Si ((c): XTEM, (d): SEM) samples nanopatterned by our RF plasma etching technique

CHARACTERIZATION OF DEFECT STRUCTURE, MECHANICAL PROPERTIES AND STABILITY OF ELECTRODEPOSITED NANOCRYSTALLINE Ni FILMS

T. Kolonits, Zs. Czigány, P. Jenei, S. Zsurzsa, J. Gubicza, L. Péter, I. Bakonyi

The effect of various organic additives on the defect structure and mechanical properties of electrodeposited Ni films was investigated by X-ray diffraction (XRD) line profile analysis (eCMWP model) and transmission electron microscopy (TEM). The main task of the project is to investigate the effect of the additives on the grain structure and defect (dislocation and twin) density which influence the macroscopic properties and application of the layers.

The electrodeposited layers were deposited at room temperature at low current density onto various substrates (Al_2O_3 , Cu, Si). The basic electrolyte mainly contained nickel sulfate ($\text{NiSO}_4 \cdot 7 \text{H}_2\text{O}$) and boric acid (H_3BO_3).

XRD and TEM grain size and phase analysis was carried out to determine the microstructure (Fig. 1). Hardness, wear and friction tests were made to examine the mechanical properties. Heat treatment (near the melting point) was also applied to investigate the stability of the micro and macro properties.

According to our previous research in the film deposited without additives, a columnar structure was observed, textured into direction $\langle 220 \rangle$. Varying the additives in the bath and/or the substrate material, various microstructures were observed: textured (both in direction $\langle 220 \rangle$ or $\langle 200 \rangle$), non-textured, twinned, ultra-fine grained and nanocrystalline etc. Hardness and wear was related to the microstructure both before and after heat treatment. One of the additive-substrate combinations (trisodium-cytrate deposited on Cu substrate as cathode) showed outstanding hardness and thermal stability.

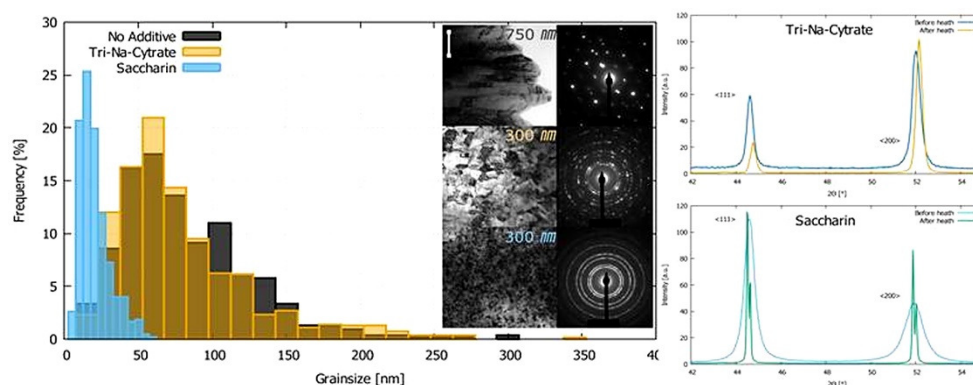


Figure 1: Grain size distribution of nanocrystalline Ni film deposited with trisodium-cytrate and saccharine additives determined by TEM (left). Trisodium-cytrate causes larger, textured grains compared to saccharine; but has a greater thermal stability as the corresponding XRD patterns show it (right).

EFFECT OF HIGH EFFICIENT ATTRITION MILLING ON 316L AUSTENITIC STEEL REINFORCED BY CERAMIC NANOPARTICLES

H. R. Ben Zine, K. Balázs, Cs. Balázs

The elaboration of Oxide Dispersion Strengthened (ODS) Steels is having an interest as a good candidate for nuclear applications due to its good properties at high temperatures (>700 °C). Powder Metallurgy (PM) technology is the most used process to elaborate ODS steels, the preparation of this last is playing very important effect on the final properties of the alloy. The aim of our work is to study the effect of attrition milling on the 316L stainless steel reinforced by yttria ceramic nanoparticles. During this work a combined wet milling in ethanol and dry milling process of steel powders together with fine yttria nanoparticles was proposed by high agitator rotation speed; 600 rpm.

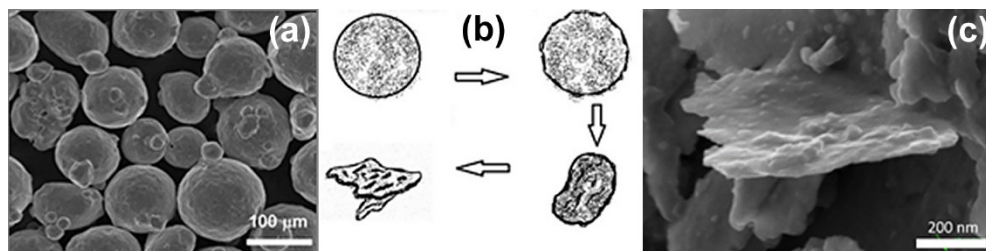


Figure 1: (a) 316L Starting powder. (b) Schematic view of changes of powder grain morphology; the shape transformation process. (c) Final powder grain shape after milling.

A high efficiency attritor mill (Unio Process, type 01-HD/HDDM) equipped with a stainless steel setup working at 600 rpm was employed consecutively for wet (5h) and dry milling (5h). The morphological characterization of starting austenitic steel powder was performed by scanning electron microscopy (Fig. 1(a)), the sample consisted of globular particles with average particles size of 50–100 μm. The powder structure after 1-hour milling showed considerable differences to the starting powder with globular grains. Their average size is lower. The Fig. 1(b) shows schematic draw of powder grain changes and the evolution of grain morphology during milling process (Fig. 1(c)). The morphological investigations demonstrated the existence of small grains in few micrometer ranges among globular grains and drastically change in morphology. The sample consisted of bimodal grains, on the one hand very small austenitic grains with lamellar structure and on the other hand of few 80 μm size globular particles. The average size of lamellar particles in one dimension is nanometer range in thickness, whereas their length is few micrometers.

NEW TYPE FUNCTIONAL ALLOY FILMS

F. Misják, B. R. Braeckman, Gy. Radnóczy, D. Depla

Multi-component or high-entropy alloys contain at least five different metals in near-equimolar concentrations. It is expected that the large mixing entropy favours the formation of simple solid solutions instead of intermetallic phases. Mainly face-centred-cubic (FCC) or body-centred-cubic phases are formed (Fig. 1). The phase formation depends on the alloy composition and the synthesis method. High entropy alloys processed by non-equilibrium methods such as splat quenching, ball milling and magnetron sputtering exhibit in most cases a single-phase structure. High entropy alloy films and coatings can have favourable functional properties like relatively high hardness and plasticity, good electrical or magnetic as well as anticorrosion properties making them suitable for different applications

Five component CoCrFeNiCu (HEA) films were deposited at room temperature onto SiO₂ covered Si substrates with a deposition rate of 10 nm/min, corresponding to a metallic flux of approximately 1.4×10^{15} at/cm²s. The average gaseous impurity flux provided by the base pressure in the vacuum chamber (5×10^{-4} Pa), corresponded to 1.42×10^{15} at/cm²s. Hence, the (HEA) film was deposited with an average impurity-to-metal flux ratio of about 1. In addition to the residual gas in the vacuum chamber the powder target is a second source of impurities.

The (HEA) powder target is likely to contain a fraction of oxygen impurities as the powder grains are covered by metal-oxide surface layers. Hence, the use of powder targets further increases the impurity-to-metal flux ratio [14]. In the present work, the structure formation mechanism of the CoCrFeNiCu (HEA) model system was investigated. TEM measurements established that the structure and morphology of the crystalline film corresponds zone III structure in the structure zone model of the thin film growth and the grain size is 2-5 nm. No texture is observed. With increasing film thickness weakly developed columnar grains could be detected and a slight increase of the crystallite size is also observed (Fig 1). HREM measurements confirmed that the films are dense, homogeneous, free of pores (Fig. 2). The morphological and texture properties confirm that the CoCrCuFeNi film grew in the impurity-controlled conditions which involve hindered growth of crystallites due to the formation of covering layers and repeated nucleation of the crystalline HEA phase in the thickness of the film. The nano-size grain structure (zone III type microstructure) and the lack of crystallographic texture are the consequence of this growth mechanism [Materials Surface Processing by Directed Energy Techniques. Amsterdam, Oxford, Elsevier, 2006. pp.443-474.], [Metallic Films for Electronic, Optical and Magnetic Applications: Structure, Processing and Properties. Cambridge, Elsevier, 2014. pp. 67-120.].

The formation of elongated in the growth direction grains and their increase in cross section close to the film surface indicates a remaining possibility of competing growth, characteristic of zone T. As a result, the main processes being active in the HEA film formation are: Nucleation and growth of the FCC HEA phase, the formation of a covering layer– presumably oxide-, repeated nucleation of the HEA phase on the surface of covering layer. Parallel to these the growing HEA crystallites can compete in growth among each other, preferably due to different surface capability or mechanism to incorporate oxygen. This process is leading to the V shape columnar like morphology of grains near the surface (Fig. 2).



Figure 1: Cross section TEM images of the CoCrFeNiCu (HEA) film: bright field image (top), dark field image (bottom). The diffraction pattern corresponds to a random FCC structure, no texture is detected.

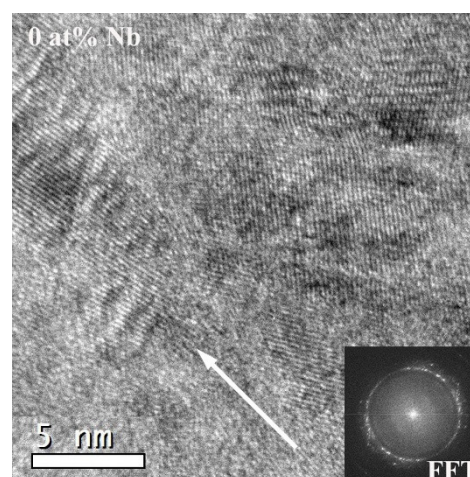


Figure 2: High resolution image of the HEA film. The arrow shows the growth direction. No second phase (crystalline or amorphous) is detected in the grain boundaries.

PROCESSING OF FAINT, DIFFUSE DIFFRACTION RINGS FROM AMORPHOUS MATERIALS

J. L. Lábár

Electron diffraction pattern (SAED) from amorphous materials is extremely faint. The intensity, plotted as a function of the length of the scattering vector is frequently a monotonically decreasing function (see Fig. 1). Furthermore, the width of the diffraction peaks (in the 1D representation, which is averaging by the azimuthal angle) also varies in a wide range in contrast to the narrower range observed for the narrower peaks of crystalline materials. That is why the methods (e.g. [Microsc. Microanal. 15, 20–29, 2009]) established for crystalline materials are not performing perfectly for amorphous patterns when center and elliptical distortion are to be determined.

We developed a new approach to process such patterns by applying the Levenberg-Marquardt (non-linear fitting) method to two distinct problems. In the first step two intervals are selected at the two sides of a “peak” in the 1D intensity distribution calculated for the entire angular range. The position of the peak is determined by fitting a background + peak composite function. In the second step the pattern is divided into sectors and the above fitting is performed in each sector. A peak-position vs. azimuthal angle function results and a combination of two trigonometrical functions is fitted to it. Shifting of the centre cause a $\cos(\alpha)$, while elliptical distortion a $\cos(2\alpha)$ type dependence. Amplitudes and phases of these functions provide magnitude and direction of shift and distortion.

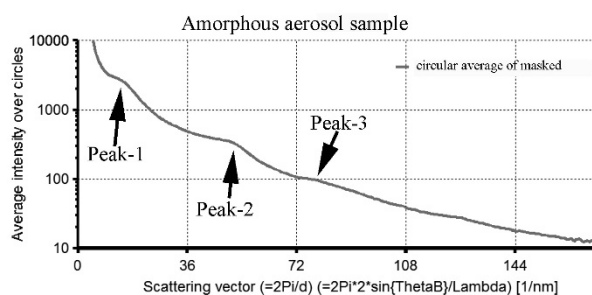


Figure 1: The intensity plotted as a function of the length of the scattering vector

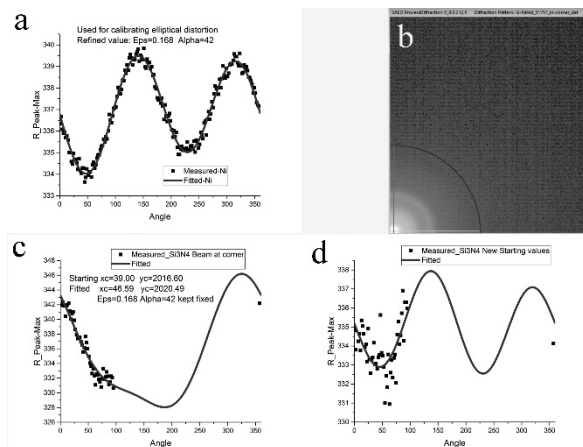


Figure 2: Calibration process of the distortion

If the direct beam is shifted to the corner of the pattern to protect the camera than only a fraction of the angular range is available from the measurement. In such cases we cannot obtain all parameters from a single pattern. The problem is circumvented by prior calibration of the distortion in a standard sample and fitting the shift of the pattern centre only, while keeping distortion fixed (Fig. 2). The procedure still remains robust and result in the same centre irrespective of the starting position (within a reasonable range), although the shape of the fitted functions is different (Fig. 2(c,d)).

HYDROGEL FILM FABRICATION FOR BIOSENSING

A. Saftics, B. Türk, S. Kurunczi, R. Horváth

Fabrication of a stable and reproducible surface with the required chemical functions is one of the major challenge in the development of label-free biosensors. Polysaccharide dextran interface layers are able to improve the sensitivity of biosensors, owing to the anti-fouling property and the high receptor immobilization capacity of the dextran chains.

Carboxymethyl-dextran (CMD) was synthesized in our laboratory from the native dextran. Grafting methods based on covalent coupling to aminosilane- and epoxysilane-functionalized surfaces were applied to obtain thin CMD layers. The carboxyl moiety of the CMD was coupled to the aminated surface by EDC-NHS reagents, while CMD coupling through epoxysilane molecules was performed without any additional reagents. The surface analysis following the grafting procedures consisted of x-ray photoelectron spectroscopy (XPS), attenuated total reflection infrared spectroscopy (ATR-IR), as well as atomic force microscopy (AFM), which proved the presence of the 1-2 nm thick CMD layer, and verified its covalent grafting to the surface. The *in situ* optical waveguide lightmode spectroscopy (OWLS) measurements were suitable to devise the structure of the interfacial dextran layers by the evaluation of the optogeometrical parameters. We found that the extent of the layer anisotropy was dependent both of the grafting procedure (using epoxysilane or aminosilane coatings) and the pH of the CMD solution applied for the grafting (Fig. 1). The apparent refractive index of the CMD layer was unrealistically higher than the reference values in the literature, which suggested parallel chain conformation to the surface. The developed methodologies allowed to design and fabricate nanometer scale ultrathin CMD layers with well-controlled surface structure, which are otherwise very difficult to characterize in aqueous environments using available instrumentation.

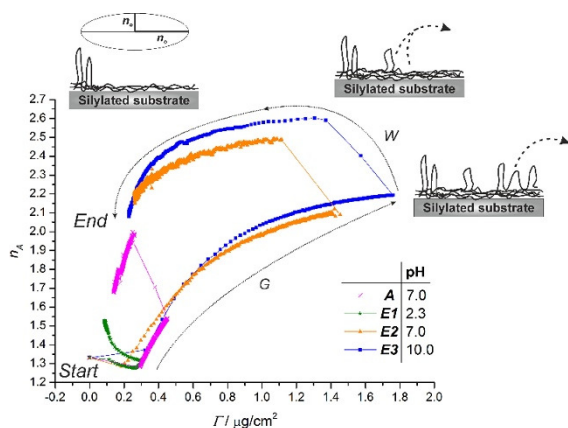


Figure 1: *In situ* OWLS measurements on the covalent grafting experiments of the CMD (n_A : apparent refractive index of the CMD layer; Γ : areal mass density of the deposited CMD; A, E: surface with aminosilane or epoxysilane coating, respectively; G, W: grafting or washing sections of the experiment).

ZNO NANOSTRUCTURE TEMPLATES AS A COST-EFFICIENT MASS-PRODUCIBLE ROUTE FOR THE DEVELOPMENT OF CELLULAR NETWORKS

E. Makarona, B. Péter, I. Székács, C. Tsamis, R. Horváth

The development of artificial surfaces which can regulate or trigger specific functions of living cells, and which are capable of inducing in vivo-like cell behaviours under in vitro conditions has been a long-sought goal over the past twenty years. In our work, an alternative, facile and cost-efficient method for mass-producible cellular templates is presented. The proposed methodology consists of a cost-efficient, two-step, all-wet technique capable of producing ZnO-based nanostructures on predefined patterns on a variety of substrates. ZnO—apart from the fact that it is a biocompatible material—was chosen because of its multifunctional nature which has rendered it a versatile material employed in a wide range of applications. Si, Si₃N₄, emulated microelectrode arrays and conventional glass cover slips were patterned at the micrometer scale and the patterns were filled with ZnO nanostructures. Using HeLa cells, we demonstrated that the fabricated nanotopographical features could promote guided cellular adhesion on the pre-defined micron-scale patterns only through nanomechanical cues without the need for further surface activation or modification (see Fig. 1). The suggested methodology is extremely promising for the creation of engineered cellular networks through purely nanomechanical cues.

One of the most important results of this study was a better understanding of the dynamics of selective cellular adhesion and the implication of time as a controlling factor that must be combined with nanomechano-sensation. Further studies are foreseen for the evolution of the method into a technology that can be readily transferred to mass-production and the development of real-life viable products.

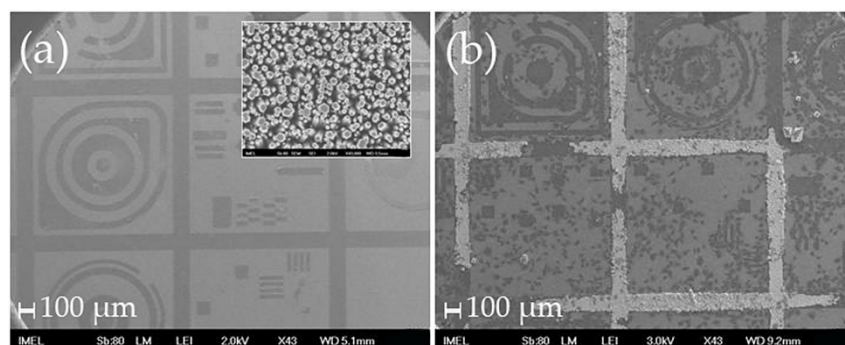


Figure 1: SEM images of (a): the Si wafer with larger patterns and flat areas (the darker areas contain the ZnO nanorods shown in the zoom-in inset image; scale bar: 100 nm); (b): the same samples with HeLa cells after 4 days in culture, where the cells mostly adhere onto the flat areas (the white areas are the nanorods that have been covered by salts from the nutrient medium that was not fully removed after washing).

SELF-ASSEMBLED, NANOSTRUCTURED COATINGS FOR WATER OXIDATION BY ALTERNATING DEPOSITION OF CU-BRANCHED PEPTIDE ELECTROCATALYSTS AND POLYELECTROLYTES

E. Farkas, D. Srankó, Zs. Kerner, B. Setner, Z. Szewczuk, W. Malinka, R. Horváth, L. Szyrwił, J. S. Pap

In the past few decades the importance of the LbL (Layer-by-Layer) technique has grown, especially to build up functional multilayers or surface-based nanodevices and surface modifications. The LbL method is based on the alternating exposure of a surface to oppositely charged polyelectrolytes. Those polymers are called polyelectrolytes (PEs), whose repeating units are ionic groups and have high molecular weight. The PLL (poly-L-lysine) and PAH (poly-(allylamine hydrochloride)) are positively charged PEs, these were used in our experiments. The advantages of the PEs have been taken to build heterogeneous catalytic layers with Cu-peptides on indium-tin-oxide (ITO) conducting OWLS chip surface, with the use of the principle of the LbL technique. The Cu-peptides were known to accelerate the half-reaction of water oxidation that has significance in envisioned water splitting systems to generate H₂ as renewable fuel. The peptide ligands bind to the metal in the equatorial positions at high pH and capable of stabilizing higher oxidation states occurring in catalysis. The applied complexes contain L-2,3-diaminopropionic acid (dap) linkers that provide branched structure with a glycine (Cu-3G) or a histidine (Cu-2GH) residue at the C-terminus.

Initially suitable polyelectrolyte pairs were sought to the Cu-peptides and Optical Waveguide Lightmode Spectroscopy (OWLS) was applied to monitor the build-up process of the nanocomposite multilayers in situ. The Cu-2GH paired with PAH and Cu-3G coupled with PLL were suitable for further studies. The layer-buildup mechanism is supposed to involve secondary binding forces beside the electrostatic interactions. Phosphate is also incorporated into the layers.

Optimization was also supported by electrochemical methods. Conditions of pH 9-10 and Cu-complex concentration of 0.1-0.5 mM were optimal for stable LbL formation. These layers show electrocatalytic activity at high positive (>1.1 V) potential and the measurement on EC-OWLS (OWLS with electrochemical function) shows, that the surface mass density is somewhat decreased after the alternating potential cycles, but the layers don't lose their activity (Fig. 1).

Other surface analyses included XPS (X-ray photoelectron spectroscopy) to detect the Cu(II) in an organic N-donor environment, and AFM that shows an inhomogeneous surface with nanoporous structure. The profilometric section demonstrates that the Cu-2GH multilayers are smoother and thinner, than that of Cu-3G.

In conclusion, with the use of OWLS/EC-OWLS it was possible to examine functional thin layers and define their properties. The Cu-peptide/PE film is electrochemically active stable, heterogeneous catalyst layers. This catalyst heterogenization method could lead to a cheaper, more economic and environmentally friendly technology.

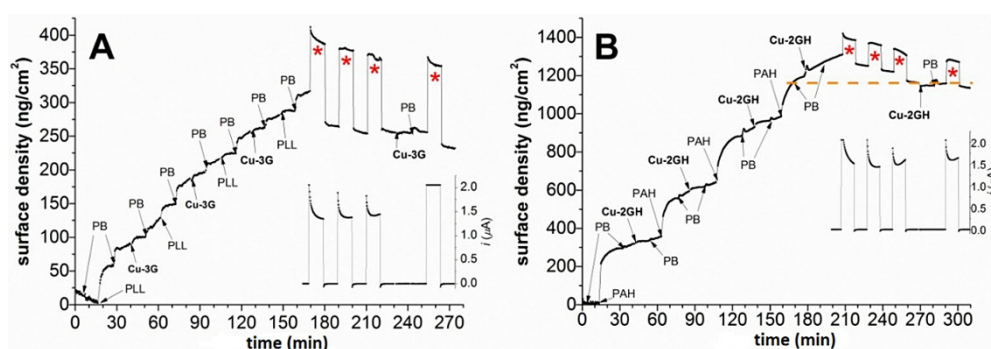


Figure 1: (A) three deposition cycles of PLL and Cu-3G (0.5 mM) in phosphate buffer (PB) (0.1 M) at pH = 10.12 and concomitant 3×10 min runs of CPE at 1.1 V vs. Ag/AgCl with intermittent breaks of 10 minutes and concomitant attempt to supply the electrolyzed surface with Cu-3G at an ITO-coated chip placed in an EC-OWLS cell; (B) the same sequence applied to PAH and Cu-2GH layers.

SELF-ASSEMBLY AND STRUCTURE OF FLAGELLIN-POLYELECTROLYTE COMPOSITE LAYERS: POLYELECTROLYTE INDUCED FLAGELLAR FILAMENT FORMATION DURING THE ALTERNATING DEPOSITION PROCESS

E. Farkas, D. Patkó, N. Q. Khánh, E. Tóth, F. Vonderviszt, R. Horváth

The simple and cost-effective bottom-up fabrication of complex functionalized nanostructures is extensively researched today. Here, the alternating deposition of the negatively charged protein flagellin and a positively charged polyelectrolyte are studied. The multilayer buildup was followed in situ using Optical Waveguide Lightmode Spectroscopy (OWLS) revealing the deposited surface mass density in real time during the alternating deposition process. The nanostructure of the assembled films was investigated by Atomic Force Microscopy (AFM) measurements. When flagellin was applied in its natural filamentous form no distinct multilayer buildup was observed, the filaments assembled mainly into bundles. In contrast, when thermally treated filament solution or pure flagellin monomer solution was used a systematic linearly growing buildup was seen, and thick, relatively smooth films were fabricated. The structural investigation (Fig. 1) revealed that the fabricated films are relatively smooth, what is in close connection with the assembling mechanism, having a tendency of filling up possible holes. We also concluded that the flagellin monomers assembled into nanofilaments inside the multilayer and even a single layer of polycation could induce the self-assembly of filaments, possibly by helping the adsorption of flagellin monomers close to each other. Both the filament formation and the multilayer buildup were completely absent when a truncated flagellin variant – missing the disordered terminal regions – was applied. Since these regions are necessary for filament formation, we conclude that the linearly growing nature of the layer is a clear consequence of filament formation.

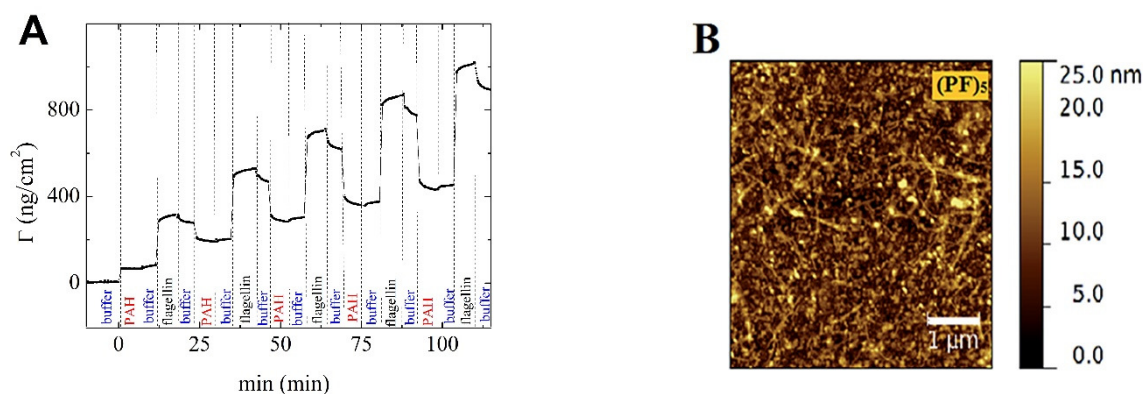


Figure 1: (A) Formation of 5 bilayer of flagellin and PAH polyelectrolyte monitored by OWLS. (B) AFM picture of 5 bilayer of flagellin and PAH polyelectrolyte

Therefore, this study first reveals a new type of linearly growing polyelectrolyte multilayer buildup mechanism, when one of the components induces the self-assembly of the oppositely charged component, creating a complex, stable and smooth filamentous nanostructured coating. These composite films can find diverse applications in nanotechnology and in biomedical sciences since the variable D3 domain of flagellin subunits can be easily modified to express enzymatic, fluorescent or molecular binding properties on the surfaces of the filaments. The present work therefore opens up novel routes in the bottom-up fabrication of complex nanostructured coatings.

CELL ADHESION MEASUREMENTS WITH A LABEL-FREE OPTICAL BIOSENSOR

N. Orgován, R. Ungai-Salánki, Sz. Lukácsi, N. Sándor, Zs. Bajtay, A. Erdei, B. Szabó, R. Horváth

Monocytes, dendritic cells (DCs), and macrophages (MFs) are closely related immune cells that differ in their main functions. To study the inherently and essentially dynamic aspects of these cells, dynamic cell adhesion assays were performed with a high-throughput label-free optical biosensor [Epic BenchTop (BT)] on surfaces coated with either fibrinogen (Fgn) or the biomimetic copolymer PLL-g-PEG-RGD [84]. We found that, all three cell types induced a larger biosensor signal on Fgn than on PLL-g-PEG-RGD.

The results obtained with evanescent-field-based label-free optical biosensor were compared with three different techniques in this study: the classical fluorescence reader-based adherence assay, the flow chamber technique, and the automated micropipette. The results obtained with the different techniques demonstrate that there are significant differences between the adhesion of the three cell types on Fgn. Monocytes were found to be the less adhesive than MFs and DCs. Furthermore, DCs adhered stronger than MFs; this is in accordance with the fact that DCs have larger expression levels of $\beta 2$ integrins than MFs (Fig. 1). Hence, it seems that the expression levels of $\beta 2$ integrins fundamentally influence the adhesion capacity of these immune cells.

These techniques confirmed the results obtained with the high-temporal-resolution Epic BT, but could only provide end-point data. In contrast, complex, non-monotonic cell adhesion kinetics measured by the high-throughput optical biosensor is expected to open a window on the hidden background of the immune cell-extracellular matrix interactions.

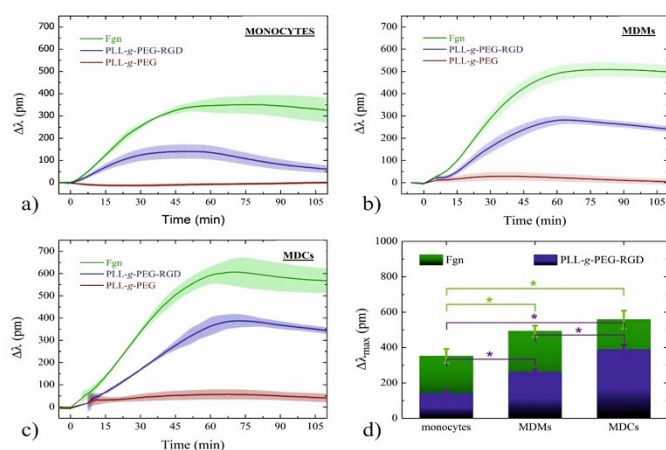


Figure 1: Time-dependent adherence of monocytes, monocyte-derived macrophages (MFs), and monocyte-derived dendritic cells (DCs) on PLL-g-PEG- and Fgn-coated surfaces, as was measured with the Epic BT in dynamic cell adhesion (DCA) assays. Representative kinetic profiles provoked by adhering and spreading monocytes, MFs, and DCs are shown in panels a), b), and c), respectively. PLL-g-PEG-coated surfaces were used as negative control. The background-corrected maximum biosensor signals induced by different cells on PLL-g-PEG-RGD- and Fgn-coated surfaces are shown in panel d). In all panels data are shown as means, error bars represent standard deviations. * indicates statistical significance with $p < 0.05$ (t-test).

LABEL-FREE OPTICAL BIOSENSOR FOR ON-LINE MONITORING THE INTEGRATED RESPONSE OF HUMAN B CELLS UPON THE ENGAGEMENT OF STIMULATORY AND INHIBITORY IMMUNE RECEPTORS

I. Kurucz, B. Péter, A. Prosz, I. Székács, R. Horváth, A. Erdei

The majority of current cell-based assays relies on the measurement of a single event at a predetermined time point in a specifically chosen signalling path-way, let it be second messenger release, reporter-gene production or target translocation. These measurements require the use of labelled compounds, sometimes the modification of cells to express the target in larger amount or to produce a reporter molecule to be able to monitor receptor engagement. The mentioned manipulations can be toxic for the cells and can interfere with normal cellular physiology of the target receptors or their environment and the applied fluorescence and coloured compounds may induce elevated background [Sensors and Actuators B, 240, 528–535 (2017)]. Consequently, functional cellular assays which can report from different signalling events in real time without the application of molecular engineering (in providing the suitable cellular partner) and without the use of labelling would be of high value for both theoretical and practical studies even if they are more complex and less specific than cell-based biochemical assays.

To be able to obtain holistic pictures about B cell responses to complex interlocking stimulations Epic BT optical biosensor was applied and set to establishing the method using human B cell lines, derived from Burkitt's lymphomas. We successfully immobilized non-adherent B cells on the surface of the biosensors, without the ligation of any specific receptors or adhesion molecules. This way we were able to demonstrate that engagement of the antigen specific B cell receptors (BCR) induced reproducible dynamic mass redistribution (DMR) inside the cells as a measure of receptor activation (see Fig. 1). The initiated DMR response proved to be specific, since only antibodies recognizing the BCR could generate the response; neither the assay-buffer, nor high concentration of indifferent proteins or non-specific antibodies had any effect. The measure of cell activation was sensitive, concentration dependent, and specifically and dose-dependently inhibited by the Syk inhibitor BAY 61-3606. The BCR-triggered DMR response was evoked from three human Epstein-Barr virus (EBV) negative B cell lines, but could not be elicited in two EBV-positive BL cell lines, where the presence of the EBV-derived LMP2A protein desensitizes the cells' response to the BCR-induced signalling.

Therefore, our work opens new avenues to study complex signalling events and to decipher interactions within the signalling network during B cell activation [Sensors and Actuators B, 240, 528–535 (2017)].

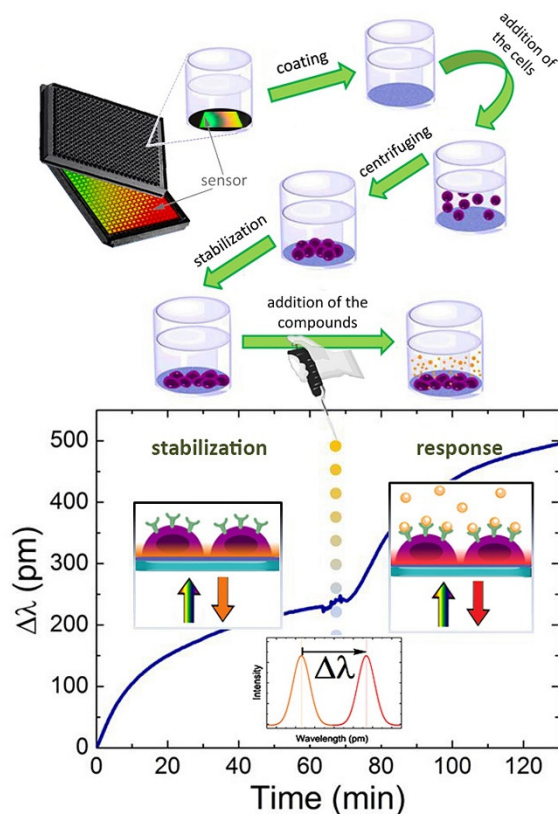


Figure 1: Experimental setup to perform real-time measurement of dynamic mass redistribution (DMR) using B-cell lines (A); and schematic illustration of the principle of DMR detection (B)

ANISOTROPIC INVASION AND ITS CONSEQUENCES

Gy. Szabó, L. Varga, M. Szabó

In the simplest spatial evolutionary games players are located at the sites of a square lattice, they play game with their four nearest neighbors and sometime they are allowed to adopt the strategy of a neighbor having higher income. For two-strategy evolutionary games the noisy imitations can result in anisotropic invasion velocities along the interface separating the territory of the two homogeneous strategy distributions denoted by black and white domains in Figs. 1 and 2.

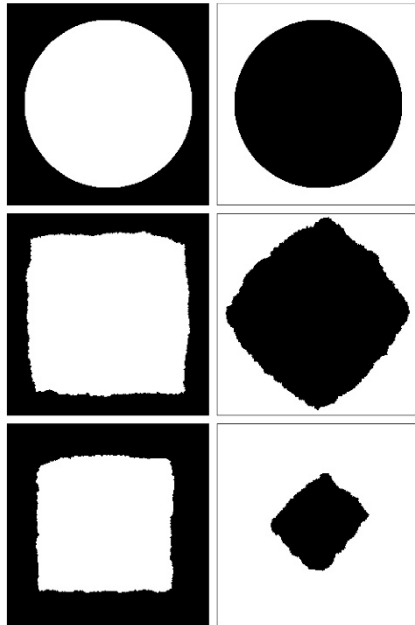


Figure 1: Evolution of white and black circular domains (from top to bottom the times are $t=0, 500,$ and 4000 MCS) for imitation at low noises on a square lattice

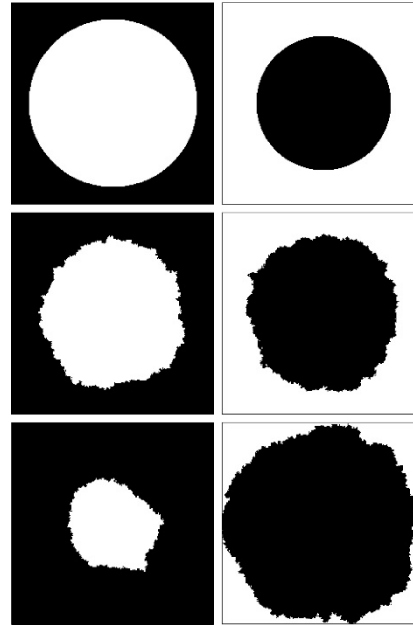


Figure 2: Evolution of circular white and black domains at a high noise level for the same payoff parameters used in Fig. 1.

In this system the pair interaction is composed of a coordination interaction of unit strength, and self- and cross-dependent payoff components with tunable strengths. For certain strengths of the tunable components the black domain can invade the territory of the white one along the horizontal and vertical interfaces. At the same time the opposite process (black domains invade the white's territories) can be observed for tilted (45°) interfaces. As a result, both the circular white and black islands shrink and vanish after forming square and diamond faceted territories for the same model parameters at low noises as illustrated in Fig. 1. This unusual feature is related to the advantage of cooperation when imitation controls the evolution.

At high noises the smooth interfaces become irregular that suppress the anisotropy of the invasion velocities and then the black territories always invade the white domains. The latter behaviour occurs typically in thermodynamic systems.

The above phenomenon has interesting consequences at low noise levels when the random initial state evolves into one of the homogeneous absorbing states. The selection of the final state is related to a percolation process. According to the continuous percolation theory if one of the phases percolates horizontally then it also will percolate vertically in the large size limit and the percolating phase can be considered as a sea in which the islands shrink and disappear at the end of evolution. In these regions of parameters both homogeneous absorbing phases can be realized in the final frozen state by choosing suitable portions of strategies in the initial state as it is illustrated in Fig. 3.

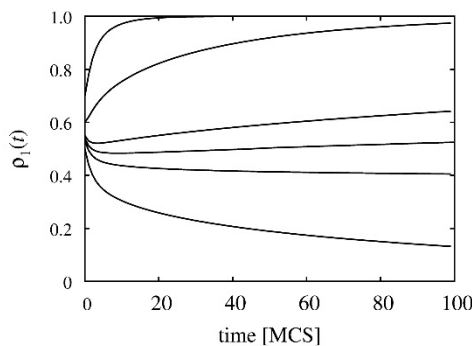


Figure 3: Frequency of white strategies versus time if the system is started from a random initial state with different portion of white strategies at $t=0$ for large sizes ($L=1000$)

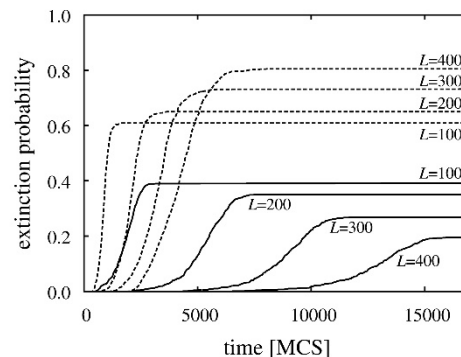


Figure 4: Extinction probability of the black (solid lines) and white (dashed lines) strategies as a function of time for different small system sizes indicated by the labels

Summarizing the essence, in contrary to the thermodynamic systems the present evolutionary games can develop into one of the two absorbing states with probabilities dependent on the size and initial composition. These features result in complex phase diagrams and technical difficulties in the numerical evaluation of the phase boundaries when tuning the model parameters.

MTDNA ANALYSIS OF 174 EURASIAN POPULATIONS USING A NEW ITERATIVE RANK-CORRELATION METHOD

Z. Juhász, H. Pamjav, T. Fehér, E. Németh, G. Bárány

In this study, we analysed 27-dimensional mtDNA haplogroup distributions of 174 Eurasian, North-African and American populations, including numerous ancient data as well. The main contribution of this work was the description of the haplogroup distribution of recent and ancient populations as compounds of certain hypothetical ancient core populations immediately or indirectly determining the migration processes in Eurasia for a long time. To identify these core populations, we developed a new iterative algorithm determining clusters of the 27 mtDNA haplogroups having strong rank-correlation among each other within a definite subset of the populations.

Based on this study, the current Eurasian populations can be considered as compounds of 3 early core populations regarding to maternal lineages. We wanted to show that a simultaneous analysis of ancient and recent data using a new iterative rank-correlation algorithm and the weighted SOC learning technique may reveal the most important and deterministic migration processes in the past. This technique allowed us to determine geographically, historically and linguistically well interpretable clusters of our dataset having a very specific, hardly classifiable structure. The method was validated using a 2-dimensional stepping-stone model.

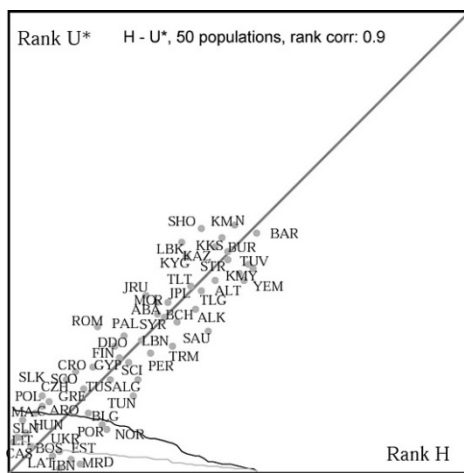


Figure 1: An example for iterative rank-correlation algorithm output. The 50-element subset of the 174 populations where the rank-correlation of haplogroups H and U* is 0.9. Point coordinates correspond to the rank values of the populations within the rank hierarchies of Hg-s H and U*

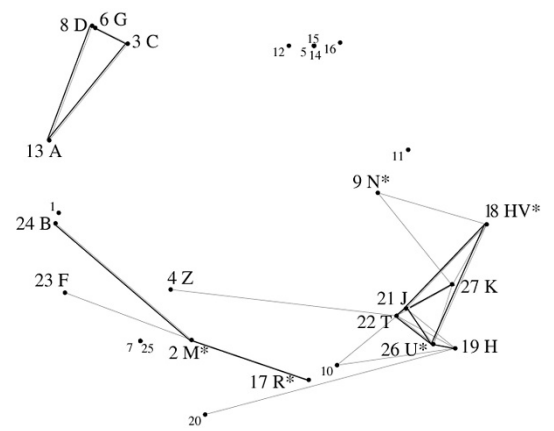


Figure 2: MDS map of (1-rank correlations) of 27 Hg-s. We found 3 disjunctive Correlating Hg-clusters (CHgC): 1. 18-HV*, 19-H, 21-J, 22-T, 26-U*, 27-K, (weaker links: 4-Z, etc.) – „Western” 2. 2-M, 17-R, 24-B (weaker link: 23-F) – „Eastern” 3. 3-C, 6-G, 8-D, 13-A – „Siberian”

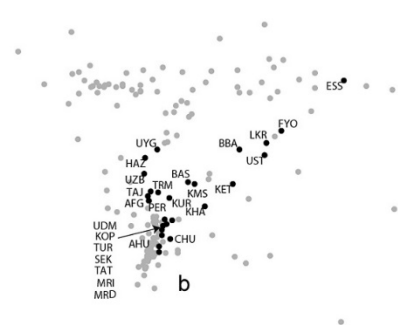
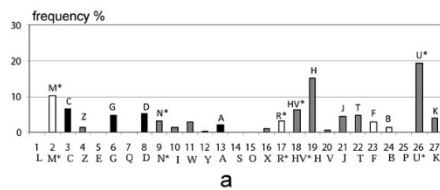


Figure 3: (a) The average of the haplogroup distributions constructing one of the most important clusters of our 174 populations, called S/5. Western, Siberian and Eastern haplogroups are denoted by grey, black and white columns. (b) MDS map of the 174 Hg-distributions, highlighting the members of Cluster S/5. 27 populations: UDMurt, KOmi, TURkish, SzEKler (Hungarian), TATar, MaRI, MoRDvin, CHUvash, KHAnty, Konda-ManSi, BAShkir, PERSian, AFGhan, UZBek, HAZara, UYGhur, KET, ESkimo. UST, BBA, LKR, FYO are ancient populations belonging to the Andronovo culture (2000 – 800 BC), AHU is an ancient Hungarian population (9th century).

ABBREVIATIONS

01-HD/HDDM	High efficiency attritor mill type
3U	Three-unit
7C2 diffractometer	Neutron diffractometer for liquids and disordered materials at the Laboratoire Leon Brillouin (LLB), Saclay, France
AAc	Acrylic acid
AB	Blood type group
ABAC	Oxygen close-packed stacking
AEKI	Institute for Atomic Energy Research
AEMI	Hungarian enterprise (Atomic Energy Engineering Ltd.)
AER	Atomic Energy Research
AES-1200	VVER-1200 Russian type reactor
AF	Antiferromagnetic
AFM	Atomic force microscopy
AG	Aktiengesellschaft (German pronunciation)
AGE-60	EU funded project
AHU	Ancient Hungarian population
ALADIN	Numerical weather prediction system, French acronym
ALD	Atomic layer deposition
ALLEGRO	Experimental Helium gas cooled fast reactor developed by the European V4G4
ALLIANCE	European Radioecology Alliance
AMEC	International association for measurement and evaluation of communication
ANCARA	Supercritical water loop
ÁNER	Refuelling neutron monitoring system (Hungarian acronym)
ASTM E-1921	Standard test method for determining of reference temperature
ASTRID	Advanced sodium technological reactor for industrial demonstration
ATHLET	Thermal-hydraulic computer code (Analysis of THERmal-hydraulics of LEaks and Transients)
ATOMKI	MTA Institute for Nuclear Research
ATR IR	Attenuated total reflection infrared spectroscopy
B4C	Boron-carbide
BAGIRA	New irradiation device at the BRR (Budapest Advanced Gas-cooled Irradiation Rig)
BCC	Body centred cubic
BCF	Boda Claystone Formation
BCR	B cell receptor
BDBA	Beyond design basis accident
BGE	Blender game engine
BIFROST	Extreme environment spectrometer at ESS
BISTRO	Reactor physical program code system
BME	Budapest University of Technology and Economics
BN-600	энергетический реактор на быстрых нейтронах – Fast neutron reactor, Russian acronym
BNC	Budapest Neutron Centre
BOD	Biological oxygen demand
BOR-60	быстрый опытный реактор –Experimental fast reactor, Russian acronym
BPM	Bit patterned media
BrightnESS	EU funded project in support of the European Spallation Source (ESS)
BRR	Budapest Research Reactor
BT	BenchTop
BW5	High energy x-ray diffractometer
BWER	Boiling water energetic reactor
BWR	Boiling water reactor
CCESC	Catalysis for clean energy and sustainable chemistry
CEA	Centre French Alternative Energies and Atomic Energy Commission
CEMS	Conversion electron spectroscopy
CERIC	Central European Research Infrastructure Consortium
CERN	Centre Européen pour la Recherche Nucléaire (French name of the European Organization for Nuclear Research)
CETS	Central European Training School
CFA	Confirmatory factor analysis
CFD	Computational fluid dynamics
CHANDA	EU funded project (CHallenges in Nuclear Data for the Safety of European Nuclear Facilities)
CIG	Career Integration Grant
CMC	Carboxymethylcellulose
CMD	Classical molecular dynamics

CNS	Cold neutron source
COBRA	Thermal-hydraulic code
COD	Chemical oxygen demand
CODEX	Core degradation experiment
CONCERT	EU H2020 project for the Integration of Radiation Protection Research
CONFIDENCE	Consortia of an European Joint Programme
CPE	Controlled potential electrolysis
CTAB	Cetyltrimethylammonium bromide
Cu-HCP	High conductivity phosphorous copper
CV	Cyclic voltammetry
CVD	Chemical vapour deposition
CZT detector	Cd-Zn-Te semiconductor medium resolution detector
DCA	Dynamic cell adhesion
DCL	DIGITAL Command Language
DCMS	Direct current magnetron sputtering
DESY	Deutsches Elektronen Synchrotron, Hamburg
DF	Discontinuity factor
DFT	Density functional theory
DGA	Diglycol amide
DLR	German Aerospace Centre (Deutsches Zentrum für Luft und Raumfahrt)
DLS	Dynamic light scattering
DMNs	Difficult-to-measure nuclides
DMR	Dynamic mass redistribution
DNA	Deoxyribonucleic acid
DNC	Delayed neutron counting
dpa	displacement per atom
DOSIS - 3D	Dose distribution inside the International Space Station - 3D
DRIE	Deep reactive ion etching
DRIFTS	Diffuse reflectance fourier transform infrared spectroscopy
DRM	Dry reforming
EASY-2003	European Activation System (interface program)
EBID	Electron beam induced deposition
EBV	Epstein-Barr virus
ECB	Ethanol-monochlorobenzene
ECCO	Reactor physical program code system
ECoG	Electrocorticographic
EDC	1-Ethyl-3-(3-dimethylaminopropyl)-carbodiimide
ECH	Electron-Cyclotron heating
EFDA	European Fusion Development Agreement
EIS	Electrochemical impedance spectroscopy
ELTE TTK	Eötvös Loránd University Faculty of Science (Hungarian acronym)
EMA	Effective medium approximation
EMI	Electromagnetic interference
ENIAC	FP7 program: Information and Communication Technologies' of the Specific Programme' Cooperation'
EPJ	European Physical Journal
EPMA	Electron probe micro-analyser
EPS	Environmental Protection Service
EQM	Engineering and qualification model
ERANOS	Reactor physical program code
ERC	European Research Council
ERIC	European Research Infrastructure Consortium
E-RIHS	EU funded project (European Research Infrastructure for Heritage Science)
ESA	European Space Agency
ESEO	European Student Earth Orbiter
ESNII	European Sustainable Nuclear Industrial Initiative (project)
ESPI	Energy sensitive pinhole imaging
ESS	European Spallation Source, Lund
EURADOS	European Radiation Dosimetry Group
EURAMED	Radiation protection in medicine
EVA	Extra-vehicular activity
FCC	Face centred cubic
FCT	Face centred tetragonal
FEM	Finite element method
FET	Field-effect transistor
FFT	Fast Fourier transform

FGR	Fission gas release
FIB	Focused ion beam
FL	Few-Layer
FM	Flight model
FRAPTRAN	Fuel Rod Analysis Program Transient
FRAT	Fuel Rod Analysis Toolbox
FRK	Polish Foundation for Cardiac Surgery Development (Fundacja Rozwoju Kardiologii)
FRL	Fuel and Reactor Materials Department, MTA EK
FRM II	Forschungs-Neutronenquelle Heinz Maier-Leibnitz, Munich
FSANS	Focused small angle neutron scattering instrument
FTIR	Fourier-transform infrared (spectroscopy)
FUMEX	FUel Modelling at EXtended burnup (research program organised by the IAEA)
FUROM	FUel ROd Model (program code system)
GC/MS	Gas chromatography-mass spectrometry
GCI	Grating coupled interferometry
GEN-IV	Generation IV
GEX	Corporation producing film-dosimeters
GF	Gel fraction
GFAP	Glial fibrillary acidic protein
GFR	Gas cooled fast reactor
GHG	Greenhouse gas
GM	General Motors
GNP	Graphene nanoplatelet
GRAS	Geant4 for Radiation in Space
GREMAN	Laboratory of the University of Tours
GRGDS	H-Gly-Arg-Gly-Asp-Ser-OH (pentapeptide sequence)
HAADF	High-angle annular dark-field imaging
HASYLAB	Hamburger Synchrotronstrahlungslabor (part of DESY)
HD	High definition
HEA	High Entropy Alloy
HELIOS	Reactor physical program code
HIP	Hot isostatic pressing
HIPD	High intensity powder diffractometer at LANSCE
HiPIMS	High Power Impulse Magnetron Sputtering
HLW	High-level radioactive waste
HOPG	Growth of MoS ₂ single and few-layer films on graphite
HORIZON	EU Research and Innovation programme available over 7 years (2014 to 2020)
HPLCMS/MS	High-performance liquid chromatography-tandem mass spectrometry
HR-EDS	High resolution energy dispersive spectrometry
HREM	High-resolution electron microscopy
HRP	Halden Reactor Project
HRS	Hyper-radiosensitivity
HRTEM	High resolution cross-sectional transmission electron microscopy
HSA	Human serum albumin
HV	Vicker hardness
HZDR	Helmholtz Zentrum Dresden Rossendorf
HZP	Hot zero power
IAEA	International Atomic Energy Agency
IAEA CRP	IAEA Coordinated Research Projects
IBMP	Institute for Biomedical Problems, Moscow
ICAPP 2016	2016 International Congress on Advances in Nuclear Power Plants, San Francisco
ICP-MS	Inductively coupled plasma mass spectrometry
ICT	Information communication technology
IEE SAS	Institute of Electrical Engineering Slovak Academy of Sciences
IFPE	International Fuel Performance Experiments
IISB	Fraunhofer Institute for Integrated Systems and Device Technology
ILL	Institut Laue-Langevin
IMEM	Institute of Materials for Electronics and Magnetism, Parma, Italy
IMST-CNR	Institute of Molecular Science and Technologies, Milano, Italy
INAA	Instrumental neutron activation analysis
INCITE	Intelligent catheters in advanced systems for interventions (research project)
INS	Infrared neural stimulation
INSTRON	A manufacturer of test equipment designed to evaluate the mechanical properties of materials and components, USA
IPERION CH	EU funded project (Integrated Platform for the European Research Infrastructure ON Cultural Heritage)

IPP	Max-Planck-Institut für Plasmaphysik, Garching
IQ	Installation qualification
IQNet	International network of partner certification bodies
IR	Infrared
IRR	Increased radioresistance
ISS	International Space Station
ITER	International Thermonuclear Reactor
ITO	Indium-tin-oxide
IVF	International Visegrád Fund
IWA	International Water Association
JEOL	Japan developer and manufacturer of electron microscopes and other scientific instruments
JPCS	Journal of Physics: Conference Series
JRA	Joint research activity
JRC	Joint Research Centre, (of the European Union)
KARATE	Reactor physical program code system
KEOP	Environment and Energy Operational Programme (Hungarian acronym)
KFKI	Former name of the research centre, nowadays the Campus name
KIT	Karlsruher Institut für Technologie
Kk	Pin-wise radial peaking factor
KMR	Central Hungarian Region (Hungarian acronym)
KOLA	Russian atomic power station
KP	Kelvin Probe
KRISS	Korea Research Institute of Standards and Science
LANSCÉ	Los Alamos Neutron Science Center
LDM	Low dimensional moderators
LDOS	Local density of states
LEL	Lower explosion limit
LET	Linear energy transfer
LH	Liquid hydrogen
LIBS	Laser induced breakdown spectroscopy
LiU	Linköping University, Sweden
LLB-Saclay	Laboratoire Léon Brillouin, Saclay, France
LNA	Locked nucleic acid
LOCA	Loss of coolant accident
LOD	Limit of detection
LPG	Liquefied petroleum gas
LPR-4	Tesla Linear electron accelerator
LSC	Liquid scintillation counting
MAT	Magnetic adaptive testing
MATPRO	Library of Materials Properties for Light-Water-Reactor Accident Analysis
MATTER	EU FP7 project (MATerial TESTING and Rules)
MC	Monte Carlo simulation
MCMP	Monte-Carlo Mapped Power
MCNP	Monte Carlo N-Particle Transport Code
MDS	Multidimensional scaling
MEA	Microelectrode array
MELODI	EU Strategic Research Agenda for low dose research
MEMS	Microelectromechanical system
MFA	Institute of Technical Physics and Materials Science (Hungarian acronym)
MLG	Multi-layered graphene
MMS	Microfluidic magnetic separation
MMT	Technical Support Activity for OAH
MOCVD	Metalorganic chemical vapour deposition
MONK	Reactor physical program code
MOS	Metal-oxide-semiconductor
MOX	Mixed oxide
MPH	Material property handbook
MTA EK	Hungarian Academy of Sciences Centre for Energy Research (Hungarian acronym)
MTS-6, MTS-7	⁶ Li and ⁷ Li enriched material in thermoluminescent dosimeter
MULTICELL	Reactor physical transport code
MVM	Hungarian Power Companies
NAA	Neutron activation analysis
NAL	Nuclear Analysis and Radiography Department, MTA EK
NCBJ	Polish National Centre for Nuclear Research (Narodowe Centrum Badań Jądrowych, Otwock-Świerk)
ND	Neutron diffraction

NDT&E	Independent Nondestructive Testing and Evaluation
NEMS	Nanoelectromechanical systems
NERIS	European Platform on Preparedness for Nuclear and Radiological Emergency Response and Recovery
NG	Neutron guide
NHS	N-hydroxysuccinimide
NII	Non-intrusive inspection
NIPS	Neutron-induced prompt gamma-ray spectroscopy
NIPS-NORMA station	A combined facility for neutron-based non-destructive element analysis and imaging at the Budapest Neutron Centre
NKFIH	National Research, Development and Research Office (Hungarian acronym)
NMI3-II	EU funded project: Neutron Scattering and Muon Spectroscopy Integrated Initiative
NMX	Macromolecular diffractometer
NNKP	National Nuclear Research Program
NNL	National Nuclear Laboratory, UK
NPC	Nanoparticle cluster
NPP	Nuclear Power Plant
NSD	Neutron Spectroscopy Department of the Wigner RCP
NT	Neutron tomography
NTC	Negative temperature coefficient
NUBIKI	Nuclear Safety Research Institute
NW	Nanowire
OAH	Hungarian Atomic Energy Authority (Hungarian acronym)
OAH-ANI-ABA	OAH project code
ODS	Oxide dispersion strengthened
OECD	Organisation for Economic Co-operation and Development
OECD NEA	Organisation for Economic Co-operation and Development, Nuclear Energy Agency
OER	Oxygen evolving reaction
OKI	National Public Health Institute
OM	Optical microscopy
OPC UA	Open Platform Communication Unified Architecture
OQ	Operational qualification
OTKA	Hungarian Scientific Research Fund (Hungarian acronym)
OWLS	Optical waveguide lightmode spectroscopy
PAH	Poly-(allylamine hydrochloride)
Paks NPP	Paks Nuclear Power Plant
PAZAR	Hungarian acronym for Noise Diagnostics System at Paks NPP
PAZAR-K	Signal evaluation software for PAZAR system
PCA	Principal component analysis
PCB	Printed circuit board
PCMI	Pellet cladding mechanical interaction
PD	Postdoc
PDMS	Polydimethylsiloxane
PDMS-b-PEO	Polydimethylsiloxane-b-poly(ethylene oxide)
PDP	Passive detector package
PE	Polyethylene
PECS	Plan for European Cooperating States
PEG-RGD	Poly(ethylene glycol)-Arg-Gly-Asp
PGAA	Prompt-gamma neutron activation analysis
PGAI	Prompt-gamma activation imaging
PIE	Post-irradiation examination
PILLE	Space-qualified thermoluminescent dosimeter
PIXE	Particle-induced X-ray emission or proton-induced X-ray emission
PLA	Poly(lactic acid)
PLL-g-PEG	Random graft co-polymer with a poly(L-lysine) backbone and poly(ethylene glycol) side-chains
PLOS	Public Library of Science
PM	Powder metallurgy
PORCA	Reactor physical program code
PP	Port plug
PQ	Performance qualification
PS	Photosensitizer
PSD	Diffractometer with position sensitive detector
PSI	Paul Scherrer Institute, Suisse
PTB	German National Metrology Institute, German acronym
PTFE	Polytetrafluoroethylene (Teflon)

PTR-32 HV	Counting Electronics
PVT	Poly-vinyl toluene
pXRF	Portable XRF spectrometer
PWR	Pressurized water reactor
QA	Quality assurance
QC	Quality control
QM	Quality Management
QMS	Quadrupole mass spectrometer
RAD	Static/dynamic thermal-neutron and X-ray imaging station at BNC
RADCUBE	A joint mission name of the ESA
RADEFF GOT	Goal Oriented Training Programme of European Fusion Development Agreement
RadMag	Instrument for measuring space radiation and magnetic field parameters
RAL	Reactor Analysis Department, MTA EK
RANC 2016	International Conference on Radioanalytical and Nuclear Chemistry
RBC	Red blood cells (Component of Blood)
RBS	Rutherford backscattering
RCP	Research Centre for Physics
RCS	Rod Control System
REMIX	REgenerated MIXture of U-Pu oxides
RER	Regional European projects of IAEA
RGD	Arg-Gly-Asp (peptide sequence)
RIA	Reactivity Initiated Accident
RING	Release of Iodine and Noble Gases
RMC method	Reverse Monte Carlo method
RMR	Reactivity Monitoring System (Hungarian acronym)
RMS	Root mean square
RPCS	Reactor Power Control System
RPV	Reactor Pressure Vessel
SAED	Selected area electron diffraction
SAFEMOST	Highly Safe GaN Metal-Oxide-Semiconductor Transistor Switch
SAFEST	EU funded project: Severe Accident Facilities for European Safety Targets
SANS	Small angle neutron scattering
SBF	Simulated body fluid
SBL	Nuclear Security Department, MTA EK
SBR	Signal-to-background ratio
SCALE	Reactor physical program code system
SCE	Saturated calomel electrode
SCIP	Studsвик Cladding Integrity Project
SDP	Secondary Dirac points
SE	Shielding effectiveness, or Spectroscopic ellipsometry
SEM	Scanning electron microscopy
SEM/EDX	Scanning electron microscopy coupled with energy dispersive X-ray spectroscopy
SEMILAB	Leading manufacturers of metrology solution materials
SERPENT	Reactor physical Monte Carlo code
SFAT	Spent Fuel Attribute Tester
SFR	Sodium cooled fast reactor
SI	Structural integrity
SIMTONIA	SIMulation TOols for Nuclear Industrial Applications
SINE2020	EU funded project: Science and Innovation with Neutrons in Europe in 2020
SINAC	Simulator software for Interactive modelling of environmental consequences of Nuclear Accidents
SMAD	Solvated metal atom deposition
SMD	Solvation model based on density model
SMEINST	H2020 program (Small and Medium-sized Enterprises Instrument)
SODAR	SOmic Detection and Ranging
SOFT	Symposium on Fusion Technology 2016
SOPRA	Leading manufacturers of metrology solution materials
SP3	Simplified spherical harmonics method of order 3
SPD	Set of passive detectors
SPENVIS	Space Environment Information System
SPND	Self powered neutron detector
SPR	Surface plasmon resonance
SPS	Spark plasma sintering
SR	Synchrotron radiation
SSNTD	Solid state nuclear track detector
STEM	Scanning transmission electron microscopy

STEP	Standard for the exchange of product data
STM	Scanning tunneling microscopy
STP	Standard Temperature and Pressure
STS	Scanning tunneling spectroscopy
SURE	ISS: a Unique REsearch Infrastructure
SVL	Radiation Protection Department, MTA EK
TECDOD	Technical documents of IAEA
TL	Thermoluminescent
TLD	Thermoluminescent dosimeter
TMDC	Transition metal dichalcogenide
TNA	Technology needs assessment project
TPD	Temperature-programmed desorption
TPO	Temperature programmed oxidation
TPR	Temperature programmed reduction
TRABCO	Hot channel program code
TRITEL	Three dimensional silicon detector telescope
TSKGO	Self-developed computer code for modelling telescope sipping and hermetical control examinations
TTX	Table Top Exercise
TU Delft	Delft University of Technology
TXRF	Transmission X-ray fluorescence
TZM	Titanium-Zirconium Molybdenum
ÚJV Rez	Czech Nuclear Research Institute in Rez (Ustav Jaderneho Vyzkumu)
ULOF	Unprotected loss of flow
UNA	Unlocked nucleic acid
UOX	Uranium dioxide
UTOP	Unprotected transient of overpower
UV	Ultraviolet
VARIANT	Reactor physical program code system
VERONA	Reactor core monitoring and the reactivity measurement system for VVER type NPPs
VF	Additional local improvement factor
VINCO	EU funded project: Visegrad Initiative for Nuclear Cooperation
VKSZ	National Research, Development and Innovation Office project
VPE	Vapor phase epitaxial
VUJE	Slovak Engineering Company in the field of Power Generation (Výskumný ústav jadrových elektrární)
VV Bolometer	Vacuum Vessel Bolometer
VVR	Water-Cooled Water-Moderated Reactor, Russian acronym
VVER	Water-Cooled Water-Moderated Energetic Reactor, Russian acronym
VVER-SCP	VVER with supercritical parameters of water coolant
VVER-SCP	VVER supercritical pressure
WDS	Wavelength dispersive analyser
WGFS	Working Group on Fuel Safety
Wigner FK	Wigner Research Centre for Physics
WIMS	Reactor physical program code
WPMAT EDDI	EU funded project: Work Package Materials, Engineering Data & Design Integration task
XAS	X-ray absorption spectrometry
XPS	X-ray photoelectron spectroscopy
XRD	X-ray diffraction
XRF	X-ray fluorescence analysis
XTEM	Cross sectional transmission electron microscope
ZGNR	Zigzag nanoribbon
ZIRLO	High performance fuel cladding Zr material, developed by Westinghouse

IMPRINT

Editors

*Katalin Gmélíng
Attila R. Imre
László Redler*

Lector

Ferenc Szlávik

Publisher

*Ákos Horváth
Tamás Belgya
MTACentre for Energy Research
H-1121, Budapest, Konkoly Thege M. út 29-33.
Hungary*

Design

Anikó Jécsai

Picture credits

*Centre for Energy Research,
Hungarian Academy of Sciences*

Accessibility

<http://www.energia.mta.hu/>

Contact

Centre for Energy Research, Hungarian Academy of Sciences
Location: KFKI Campus 29-33 Konkoly-Thege Miklós street 1121 Budapest, Hungary
Mailing address: 1525 Budapest 114., P.O. Box 49., Hungary
Phone: (+36 1) 395 91 59 **Fax:** (+36 1) 395 92 93
E-mail addresses: info@energia.mta.hu





Centre for Energy Research
Hungarian Academy of Sciences
Budapest 114, P.O. Box 49, H-1525, Hungary
Phone: +36 1 395 9159, Fax: +36 395 9293
www.energia.mta.hu